Quinoline carboxamides as modulators of Breast Cancer Resistance Protein (ABCG2):
Investigations on potency, selectivity, mechanism of action, cytotoxicity, stability and drug-like properties

Dissertation

zur Erlangung des Doktorgrades der Naturwissenschaften (Dr. rer. nat.)

der Fakultät für Chemie und Pharmazie

der Universität Regensburg

vorgelegt von

Stefanie Bauer

aus Passau

2014

Die vorliegende Arbeit entstand in der Zeit von Januar 2011 bis Februar 2014 unter der Anleitung von Herrn Prof. Dr. Armin Buschauer und Herrn Prof. Dr. Günther Bernhardt am Institut für Pharmazie der Naturwissenschaftlichen Fakultät für Chemie und Pharmazie der Universität Regensburg.

Das Promotionsgesuch wurde eingereicht im Februar 2014.

Tag der mündlichen Prüfung: 28.02.2014

Prüfungsausschuss: Prof. Dr. J. Heilmann   (Vorsitzender)

                       Prof. Dr. A. Buschauer (Erstgutachter)

                       Prof. Dr. G. Bernhardt (Zweitgutachter)

                       Prof. Dr. J. Wegener   (Prüfer)

Für
meine Eltern
und
meinen Verlobten
Mario

So eine Arbeit wird eigentlich nie fertig,
man muss sie für fertig erklären, wenn man nach
Zeit und Umständen das Mögliche getan hat.

Johann Wolfgang von Goethe (1749 - 1832)

Danksagung

Publications, Oral Presentations and Posters

Prior to submission of this thesis, results were published in part.

Publications:

C. Ochoa Puentes, P. Höcherl, M. Kühnle, S. Bauer, K. Bürger, G. Bernhardt , A. Buschauer, B. König (2011); *Solid phase synthesis of tariquidar-related modulators of ABC transporters preferring breast cancer resistance protein.* Bioorg. Med. Chem. Lett. 21 (12), 3654–3657.

C. Ochoa Puentes and S. Bauer, M. Kühnle, G. Bernhardt , A. Buschauer, B. König (2013); *Benzanilide – Biphenyl Replacement: A Bioisosteric Approach to Quinoline Carboxamide-type ABCG2 Modulators.* ACS Med. Chem. Lett. 4 (4), 393-396.

S. Bauer, C. Ochoa Puentes, Q. Sun, M. Bause, G. Bernhardt , B. König, A. Buschauer (2013); *Quinoline Carboxamide-Type ABCG2 Modulators: Indole and Quinoline Moieties as Anilide Replacements.* ChemMedChem 8, 1773-1778.

K. Pollinger, R. Hennig, S. Bauer, M. Breunig, J. Tessmar, A. Buschauer, R. Witzgall, A. Göpferich (2014); *Biodistribution of Quantum Dots in the Kidney After Intravenous Injection.* J. Nanosci. Nanotechnol. 14, 3313-3319.

Short lectures:

Joint Meeting of the Austrian and German Pharmaceutical Societies, University of Innsbruck, September 20-23, 2011
Overcoming ABCG2-mediated Drug Resistance with New ABCG2 Modulators Derived from Tariquidar

Bad Herrenalber Transporter- und Barriere-Tage, Bad Herrenalb, May 14-16, 2012
New Highly Potent and Selective Modulators of BCRP

Research Day of the Emil Fisher Graduate School of Pharmaceutical Sciences and Molecular Medicine, Institute of Pharmacy and Food Chemistry, University of Erlangen, July 7, 2013
Inhibition of the Efflux Transporter ABCG2: A Strategy to overcome the Blood-Brain Barrier and Chemoresistance

Poster presentations:

XXIInd International Symposium on Medicinal Chemistry, Berlin, September 2-6, 2012
and
Research Day of the Emil Fischer Graduate School of Pharmaceutical Sciences and Molecular Medicine, Institute of Pharmacy and Food Chemistry, University of Erlangen, July 19, 2012
N-Acylated anthranilic acid esters: Highly potent and selective modulators of Breast Cancer Resistance Protein (BCRP, ABCG2)

6th Summer School Medicinal Chemistry, University of Regensburg, September 26-28, 2012
Optimization of highly potent and selective ABCG2 transporter modulators with respect to solubility and chemical stability

Professional training:

04/2011	Fortbildung für Projektleiter und Beauftragte für Biologische Sicherheit (§15 und 17 Gentechniksicherheitsverordnung). *University of Regensburg, Germany*
03/2012	Radioanalytik - Umgang mit offenen radioaktiven Stoffen. *University of Regensburg, Germany*
03/2012 - 07/2012	Weiterbildung „Versuchstierkunde und Tierschutz" (Bestandteil des Nachweises der Sachkunde für den Umgang mit Versuchstieren innerhalb der EU, FELASA Kategorie B) *University of Regensburg, Germany*
06/2012 – 01/2014	Member of the Emil Fischer Graduate Programme *University of Regensburg & University of Erlangen, Germany*

Contents

Abbreviations

AB	antibody
ABCB1	ATP-binding cassette transporter, subfamily B, member 1
ABCC1	ATP-binding cassette transporter, subfamily C, member 1
ABCG2	ATP-binding cassette transporter, subfamily G, member 2
ADP	adenosine diphosphate
AM	acetoxymethylester
APS	ammonium peroxodisulfate
aq.	aqueous
ATCC	American Type Culture Collection
ADP	adenosine diphosphate
ATP	adenosine triphosphate
AUC	area under the concentration-time curve
BBB	blood-brain barrier
BCNU	1,3-bis(2-chloroethyl)-1-nitrosourea (carmustine)
BCRP	Breast Cancer Resistance Protein (= ABCG2 transporter)
BMDP	Brain Multidrug Resistance Protein
bp	base pair(s)
BSA	bovine serum albumin
CBAVD	Congenital bilateral aplasia of vas deferens
cDNA	copy DNA (desoxyribonucleic acid)
CHAPS	3-[(3-cholamidopropyl)dimethylammonio]-1-propanesulfonate
CHI	Chromatographic Hydrophobicity Index
CIN	Chromosome Instability
CLSM	Confocal Laser Scanning Microscopy
CNS	central nervous system
CPD	citrate-phosphate-dextrose
Da	Dalton
DAB	3,3'-diaminobenzidine
DJS	Dubin-Johnson Syndrom
DMEM	Dulbecco's Modified Eagle Medium
DMSO	dimethyl sulfoxide
DNA	desoxyribonucleic acid
Doxo	doxorubicin
DTT	Dithiothreitol
EC	endothelial cells
ECL	enhanced chemiluminescence
E. coli	Escherichia coli
EDTA	ethylene diamine tetraacetic acid
EGTA	ethylene glycol tetraacetic acid
EMEM	Eagle's Minimum Essential Medium
ESI	Electron-Spray-Ionization
Etp	etoposide
FACS	Fluorescence Activated Cell Sorter

FCS	fetal calf serum
FLAG	octapeptide epitope for the labelling of proteins
FLI	fluorescence in vivo imaging
FSC	forward scatter
FTC	fumitremorgin C
g	gravitation acceleration
GBM	Glioblastoma multiformae
GeoMean	geometric mean value
H33342	Hoechst 33342 dye
HDL	high density lipoprotein
HE	haematoxylin-eosin staining
HMEC	human microvascular endothelial cells
HPLC	high performance (pressure) liquid chromatography
HPLC-MS	high performance (pressure) liquid chromatography - mass spectrometry
HRP	horseradish peroxidase
HSA	human serum albumin
HUGO	Human Genome Nomenclature Committee / Human Genome Organization
IAM	Immobilized artifical membrane
IEP	Isoelectric point
IHC	Immunohistochemistry
I_{max}	maximal inhibitory effect
i.p.	intraperitoneal
IC_{50}	concentration of inhibitor required to give 50% inhibition of activity
IgG	immunoglobulin G
kb	kilobase
LB	lysogeny broth (for cultivation of E. *coli*)
logD	logarithm of the octanol/ water distribution coefficient as a function of pH
logP	logarithm of the octanol/ water partition coefficient
Luc2	luciferase2 enzyme
mAU	milli-absorbance units of peak area
MDR	multidrug resistance
MDR1	multidrug resistance protein 1 (= ABCB1 transporter)
MeCN	acetonitrile
Mito	mitoxantrone
MG	Masson-Goldner staining
MOPS	3-morpholinopropane-1-sulfonic acid
MRP1	Multidrug Resistance Associated Protein 1 (= ABCC1 transporter)
MTX	methotrexate
MWCO	Molecular Weight Cut Off
MXR	Mitoxantrone resistance protein (= ABCG2 transporter)
NBD	nucleotide binding domain
Pac	paclitaxel
PBCEC	porcine capillary endothelial cells
PBS	phosphate buffered saline
PBS-T	PBS supplemented with 0.1 % triton X-100

PCR	polymerase chain reaction
PE	phycoerythrin
PEG	polyethylene glycol
PFA	paraformaldehyde
P-gp	P-glycoprotein (= ABCB1 transporter)
pH	negative logarithm of the hydrogen ion concentration
PhA	pheophorbide a
PHHI	persistent hyperinsulinemic hypoglycemia of infancy
P_i	inorganic phosphate
PMSF	phenylmethylsulfonyl fluoride
PPB	plasma protein binding
psi	pounds per square inch (1 psi = 0.069 bar)
PXE	Pseudoxanthoma elasticum
RAMEB	randomly methylated-β-cyclodextrin
rcf	relative centrifugal force
RFI	relative fluorescence intensity
RFU	relative fluorescence unit
RP	reversed phase
rpm	revolutions per minute
rt	room temperature
S	signal peptide sequence
s.c.	subcutaneous
SDS	sodium dodecyl sulfate
SDS-PAGE	SDS polyacrylamide gel electrophoresis
SEM	standard error of the mean
Sf9	insect cell line of *Spodoptera frugiperda*
SOC	salt optimized + carbon broth (for transformation of E. *coli*)
SSC	sideward scatter
TAE	tris-acetat-EDTA buffer
TBS-T	Tris buffered saline Tween20 buffer
TEMED	N,N,N',N'-tetramethylethylenediamine
TEER	transendothelial electrical resistance
TFA	trifluoroacetic acid
TMD	transmembrane domain
TMEP	Tris-mannitol-EDTA-PMSF buffer
Topo	topotecan
Tris	tris(hydroxymethyl)aminomethane
Trp	tryptophan
Tyr	tyrosine
U	enzyme unit
UV	ultraviolet
Vbl	vinblastine
WB	Western blot
WHO	World Health Organization
wt	wildtype

Chapter 1

1   General introduction

1.1   The ABC protein superfamily

The ATP-binding cassette (ABC) protein superfamily is one of the largest transporter gene families in living organisms. So far, 48 genes encoding ABC proteins have been identified in humans.

The Transporter Classification (TC) Database, a classification system for membrane transport proteins, approved by the International Union of Biochemistry and Molecular Biology (IUBMB), divides the ABC family (TC# 3.A.1) into importers and exporters and subdivides the exporters into three evolutionarily independent distinct superfamilies [Wang et al., 2009]. These have been designated ABC1, ABC2 and ABC3 as they evolved along three different pathways of origin, arising from triplication of a primordial 2 transmembrane α-helical segment (TMS), duplication of a three-TMS-encoding genetic element or from a 4 TMS precursor yielding either eight- or ten-TMS proteins, respectively. Within the ABC superfamily there are dozens of subfamilies corresponding to their substrate specificities.

According to a standard nomenclature recommended by to the Human Genome Organization (HUGO), the ABC proteins are divided into seven subfamilies (ABCA-ABCG) based on their sequence homology and domain organization [Dean et al., 2001], in particular the monophyletic ATP hydrolyzing   constituents.   A   comprehensive   list   is   available   at http://www.genenames.org/genefamilies/ABC.

ABCB1 (P-glycoprotein, P-gp; MDR1), ABCC1 (multidrug resistance-associated protein 1, MRP1) and ABCG2 (Breast Cancer Resistance Protein, BCRP; mitoxantrone resistance protein, MXR) are the most intensely studied representatives of all ABC transporters and play a major role in the transport of drugs across biological barriers and the development of multidrug resistance (MDR) in cancer cells [Borst and Elferink, 2002].

1.2   Physiological and pharmacological functions of ABC transporters

The ABC efflux pumps use the energy of ATP hydrolysis to transport a huge variety of molecules against the concentration gradient across biological membranes [Deeley et al., 2006]. In our cellular defense system, the location of ABC transporters in the gastrointestinal tract represents the first defense mechanism against numerous ingested xenobiotics. As this also includes numerous orally administered drugs, ABC proteins, especially P-gp, play a major role in limiting the uptake and, thus, the bioavailability of drugs [Sarkadi et al., 2006]. ABC transporters are furthermore involved in limiting the access of various compounds to sensitive compartments like the testes, the placenta or the brain, thereby protecting these organs from toxic agents. Classically exemplified by ABCB1, ABCC1 and ABCG2, respectively, it became clear that these plasma membrane proteins are key players in protecting the organism from xenobiotics and toxines by preventing their uptake and procuring their elimination.

Mutations of ABC proteins are responsible for the appearance of diseases such as Dubin-Johnson syndrome (DJS; ABCC2), mucoviscidosis (ABCC7) or pseudoxanthoma elasticum (PXE; ABCC6) [Chassaing et al., 2005; Deeley et al., 2006; Gadsby et al., 2006; Burke et al., 2008]. Furthermore, the cholesterol efflux regulatory protein (CERP; ABCA1) mediates the transport of cholesterol and phospholipids from cells to HDL apolipoproteins, such as apoA-I [Oram et al., 2008]. Mutations of the ABCA1 protein led to hypoalphalipoproteinemia (Tangier disease), an inherited disorder characterized by a reduced circulation of HDL and a risk factor for cardiovascular disease [Negi et al., 2013].

1.2.1   Structures and cellular mechanisms of ABC transporters

In eukaryotes, the ABC full-transporter is supposed to encode four domains consisting of two cytosolic ATP-binding segments, also known as nucleotide-binding domains (NBDs) and two transmembrane domains (TMDs). Half-size transporters contain only one NBD and one TMD forming either homodimers or heterodimers to create a functional transporter and are found in both prokaryotes and eukaryotes. The TMDs contain 6 hydrophobic segments: membrane-spanning α-helices which form the TM channel and provide the specificity for the substrate (**Figure 1.1**).
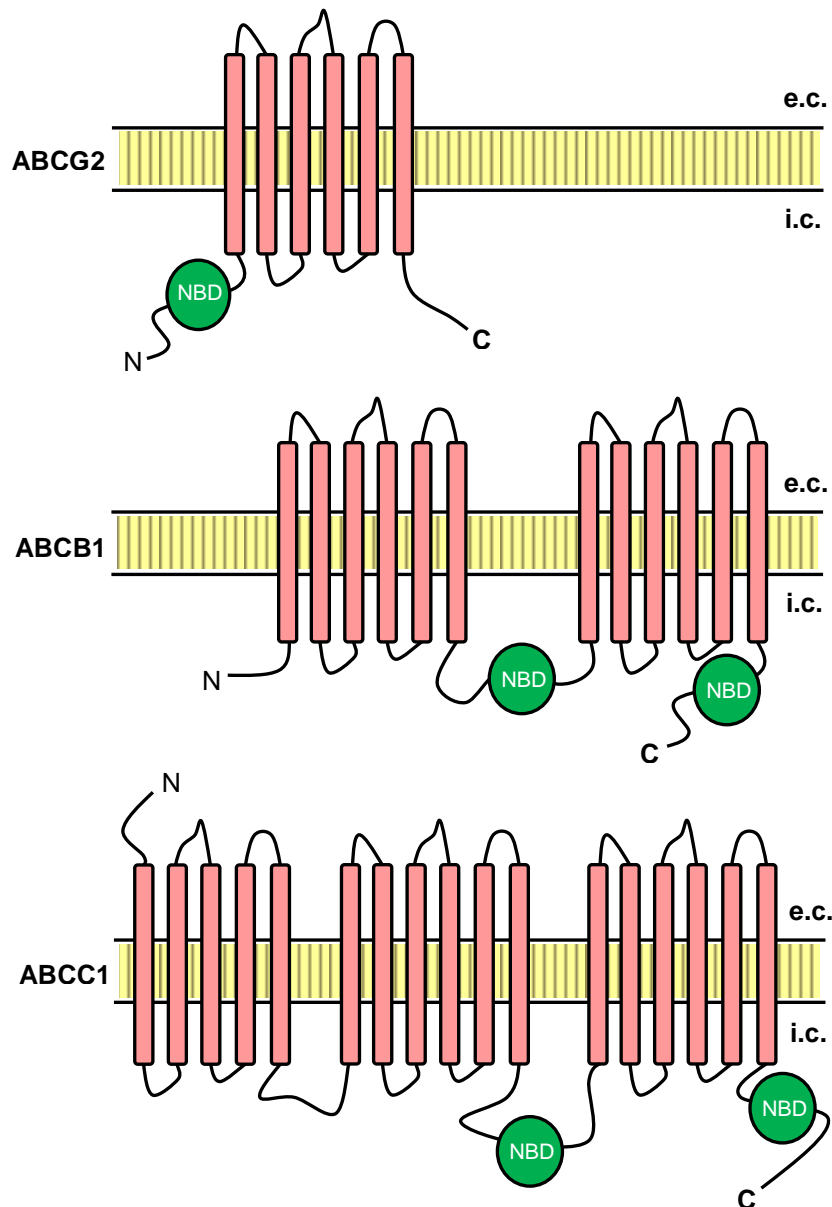
Figure 1.1: Topology and domain arrangement of the ABC transporters ABCG2, ABCB1 and ABCC1, respectively. ABCG2 is a half-size transporter and consists of six membrane-spanning segments and one NBD on the N-terminal side of the TMD. Both the ABCB1 and ABCC1 transporter comprise two ATP-binding sites. ABCC1 additionally contains a N-terminal domain composed of five transmembrane helices, the physiological relevance of which is widely unknown [Deeley et al., 2006]; illustration adapted from [Gillet et al., 2007] with alterations.

The ATP-binding domains contain three highly conserved motifs: Walker A and B motifs for nucleotide binding [Walker et al., 1982], separated by 90-120 amino acids and a signature 'C' motif located upstream of the Walker B site and unique to the ABC superfamily [Dean et al., 2001; Sharom, 2008].

Binding of a substrate by an ABC transporter induces a conformational change in the TMDs which is then transmitted to the NBDs forming a dimer responsible for ATP binding and hydrolysis as well as for substrate translocation [Higgins, 2001; Damas et al., 2011] with intracellular ADP and inorganic phosphate (P_i) as end products (**Figure 1.2**). Many fundamental questions concerning substrate

binding and the following translocation processes, including a detailed mechanism of ATP hydrolysis [Jones and George, 2013], are still unanswered. Latest findings, however, suggest that two ATPs are required for the formation of a NBD dimer [Zoghbi and Altenberg, 2014].
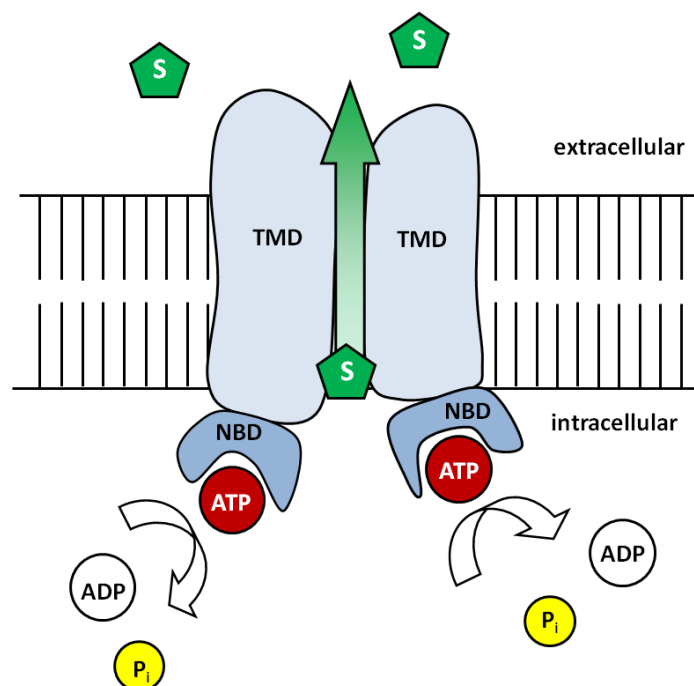
Figure 1.2: Schematic molecular mechanism of substrate binding and ATP hydrolysis by ABC transporters (export pumps); TMD = transmembrane domain, NBD = nucleotide-binding domain, S = substrate, ATP = adenosine triphosphate, ADP = adenosine diphosphate, P_i = inorganic phosphate.

1.2.2   ABC transporters and the phenomenon of multidrug resistance

Cancer chemotherapy is compromised by a phenomenon known as multidrug resistance (MDR), defined as the cross-resistance or insensitivity of cancer cells to numerous drugs which are often structurally or functionally unrelated [Ullah, 2008]. MDR is often the ultimate cause of failure of cytotoxic drugs in cancer chemotherapy. Many mechanisms of drug resistance, such as activation of detoxifying systems, evasion of the apoptotic control, changes in cellular repair mechanisms or activation of drug efflux pumps have been identified [Gillet and Gottesman, 2010]. Based on this knowledge, strategies to overcome drug resistance and to increase the efficacy of cancer chemotherapy have been developed. Thereby, the inhibition or modulation of cellular efflux pumps to reverse drug resistance has been subject of research for decades.

Despite the protective detoxifying function of ABC transporters, several complications arise in cancer therapy as the overexpression of ABC proteins directly leads to multidrug resistance. One of the most

important phenomena of MDR in cancer is an increased efflux of cytostatics from cancer cells mediated by transporters of the ABC protein family.

Stimulated by the identification of the MDR1 gene [Juliano and Ling, 1976], initially many clinical trials in cancer therapy focused on the ABCB1 transporter. P-gp expression was considered to be solely responsible for the phenomenon of MDR. However, during the last two decades it became clear that ABCB1 is not the only member of the ABC transporter family which is involved in the resistance against clinically relevant chemotherapeutics. After the discovery of MRP1 (ABCC1) and its affiliation to the ABC transporter family [Cole et al., 1992], additional proteins contributing to chemoresistance were identified, including the Breast Cancer Resistance Protein.

Table 1.1: List of selected human ABC genes, their physiological function and localization as well as anticancer drugs accepted as substrates by the corresponding efflux pump.[a]

HUGO nomen-clature	Synonyms, symbols	TC identification number	Localization	Examples of cytostatics as substrates	Function, involvement in human disease
ABCB1	MDR1, P-gp, PGY1	3.A.1.201.1	BBB, kidney, intestine, placenta	taxanes, epipodo-phyllotoxines, anthracyclines, vinca alkaloids	multidrug resistance
ABCB4	MDR3, PGY3, MDR2	3.A.1.201.3	liver	paclitaxel, vinblastine	progressive familial intrahepatic cholestasis (PFIC)
ABCC1	MRP1, GS-X	3.A.1.208.8	lung, testes, kidney	doxorubicin, etoposide, vincristine, methotrexate (MTX)	multidrug resistance
ABCC2	MRP2, cMOAT	3.A.1.208.2	liver, intestine, kidney	MTX, etoposide, doxorubicin, vincristine, cisplatin	multidrug resistance, Dubin-Johnson syndrome
ABCC6	MRP6, MLP1	3.A.1.208.10	kidney, liver		Pseudoxanthoma elasticum
ABCC7	CFTR, MRP7	3.A.1.202.1	exocrine tissues		cystic fibrosis (mucoviscidosis)
ABCG2	MXR, BCRP	3.A.1.204.2	placenta, breast, BBB, intestine	mitoxantrone, topotecan, anthracyclines	multidrug resistance

[a] with modifications according to: [Dean et al., 2001; Borst and Elferink, 2002; Gottesman et al., 2002; Deeley et al., 2006; Szakacs et al., 2008].

1.2.3 ABC Transporters expressed at the blood-brain barrier

The blood-brain barrier (BBB) is a diffusion barrier formed by endothelial cells between the blood circulation and the central nervous system (CNS). The BBB controls cerebral homeostasis, protects the CNS from environmental toxins and restricts the access of pharmacologically active compounds to the brain. Therefore, various transport and carrier systems are expressed at the BBB among which

ABC transporters play a crucial role in pharmacotherapy [Shen and Zhang, 2010; ElAli and Hermann, 2011] as they limit the brain uptake of numerous centrally active compounds [Begley, 2004].
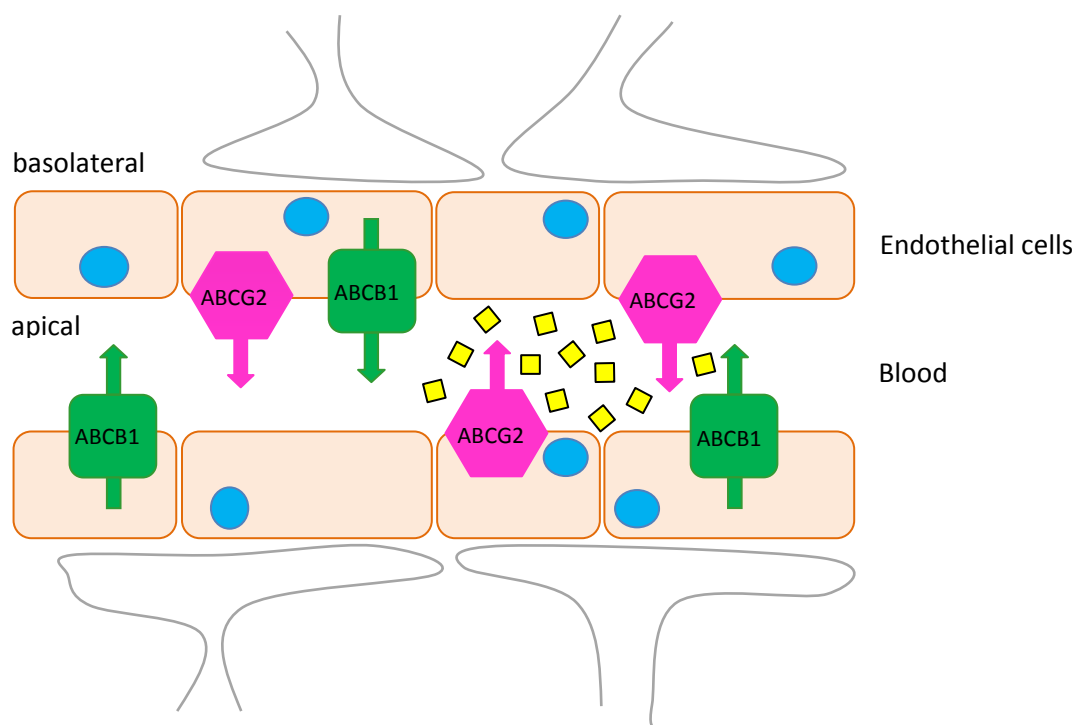
Figure 1.3: Schematic illustration of ABCB1 and ABCG2 transporter expression at the luminal membrane of brain capillary endothelial cells at the blood-brain barrier. ABCB1 and ABCG2 substrates (drugs) are pumped from the basolateral to the blood side of brain capillaries, resulting in a decreased uptake into the brain. Illustration adapted from [Shukla et al., 2011] with modifications.

Thereby, the chemotherapy of malignant central nervous system (CNS) tumors is compromised due to the expression of ABC proteins at the blood-brain barrier namely ABCB1 and ABCG2 [Cooray et al., 2002; Nies et al., 2004; Miller and Cannon, 2013], restricting the access of many potent cytostatics such as anthracyclines, epipodophyllotoxins or taxanes [Hermann and Bassetti, 2007] to the brain, provided that these compounds are substrates of the respective pumps.

The phenomenon of multidrug resistance is a major obstacle in the treatment of malignancies of the CNS. Strategies for drug delivery to the brain by circumventing these ABC transporters are of great importance.

By analogy with an approach described for ABCB1 [Fellner et al., 2002; Hubensack et al., 2008], co-administration of ABCG2 modulators forms an attractive strategy to overcome MDR tumors and to enhance the penetration of cytostatics into the brain to improve chemotherapy of malignancies in the CNS [Breedveld et al., 2006].

1.3   References

Begley, D. J. ABC transporters and the blood-brain barrier. *Curr. Pharm. Des.* **2004**, 10(12), 1295-1312.

Borst, P. and Elferink, R. O. Mammalian ABC transporters in health and disease. *Annu. Rev. Biochem.* **2002**, 71, 537-592.

Breedveld, P., Beijnen, J. H. and Schellens, J. H. Use of P-glycoprotein and BCRP inhibitors to improve oral bioavailability and CNS penetration of anticancer drugs. *Trends Pharmacol. Sci.* **2006**, 27(1), 17-24.

Burke, M. A., Mutharasan, R. K. and Ardehali, H. The sulfonylurea receptor, an atypical ATP-binding cassette protein, and its regulation of the KATP channel. *Circ. Res.* **2008**, 102(2), 164-176.

Chassaing, N., Martin, L., Calvas, P., et al. Pseudoxanthoma elasticum: a clinical, pathophysiological and genetic update including 11 novel ABCC6 mutations. *J. Med. Genet.* **2005**, 42(12), 881-892.

Cole, S. P., Bhardwaj, G., Gerlach, J. H., et al. Overexpression of a transporter gene in a multidrug-resistant human lung cancer cell line. *Science* **1992**, 258(5088), 1650-1654.

Cooray, H. C., Blackmore, C. G., Maskell, L., et al. Localisation of breast cancer resistance protein in microvessel endothelium of human brain. *Neuroreport* **2002**, 13(16), 2059-2063.

Damas, J. M., Oliveira, A. S., Baptista, A. M., et al. Structural consequences of ATP hydrolysis on the ABC transporter NBD dimer: molecular dynamics studies of HlyB. *Protein Sci.* **2011**, 20(7), 1220-1230.

Dean, M., Hamon, Y. and Chimini, G. The human ATP-binding cassette (ABC) transporter superfamily. *J. Lipid Res.* **2001**, 42(7), 1007-1017.

Deeley, R. G., Westlake, C. and Cole, S. P. Transmembrane transport of endo- and xenobiotics by mammalian ATP-binding cassette multidrug resistance proteins. *Physiol. Rev.* **2006**, 86(3), 849-899.

ElAli, A. and Hermann, D. M. ATP-binding cassette transporters and their roles in protecting the brain. *Neuroscientist* **2011**, 17(4), 423-436.

Fellner, S., Bauer, B., Miller, D. S., et al. Transport of paclitaxel (Taxol) across the blood-brain barrier in vitro and in vivo. *J. Clin. Invest.* **2002**, 110(9), 1309-1318.

Gadsby, D. C., Vergani, P. and Csanady, L. The ABC protein turned chloride channel whose failure causes cystic fibrosis. *Nature* **2006**, 440(7083), 477-483.

Gillet, J. P., Efferth, T. and Remacle, J. Chemotherapy-induced resistance by ATP-binding cassette transporter genes. *Biochim. Biophys. Acta.* **2007**, 1775(2), 237-262.

Gillet, J. P. and Gottesman, M. M. Mechanisms of multidrug resistance in cancer. *Methods Mol. Biol.* **2010**, 596, 47-76.

Gottesman, M. M., Fojo, T. and Bates, S. E. Multidrug resistance in cancer: role of ATP-dependent transporters. *Nat. Rev. Cancer* **2002**, 2(1), 48-58.

Hermann, D. M. and Bassetti, C. L. Implications of ATP-binding cassette transporters for brain pharmacotherapies. *Trends Pharmacol. Sci.* **2007**, 28(3), 128-134.

Higgins, C. F. ABC transporters: physiology, structure and mechanism--an overview. *Res. Microbiol.* **2001**, 152(3-4), 205-210.

Hubensack, M., Müller, C., Höcherl, P., et al. Effect of the ABCB1 modulators elacridar and tariquidar on the distribution of paclitaxel in nude mice. *J. Cancer Res. Clin. Oncol.* **2008**, 134(5), 597-607.

Jones, P. M. and George, A. M. Mechanism of the ABC transporter ATPase domains: catalytic models and the biochemical and biophysical record. *Crit. Rev. Biochem. Mol. Biol.* **2013**, 48(1), 39-50.

Juliano, R. L. and Ling, V. A surface glycoprotein modulating drug permeability in Chinese hamster ovary cell mutants. *Biochim. Biophys. Acta.* **1976**, 455(1), 152-162.

Miller, D. S. and Cannon, R. E. Signaling Pathways that Regulate Basal ABC Transporter Activity at the Blood-Brain Barrier. *Curr. Pharm. Des.* **2013**.

Negi, S. I., Brautbar, A., Virani, S. S., et al. A novel mutation in the ABCA1 gene causing an atypical phenotype of Tangier disease. *J. Clin. Lipidol.* **2013**, 7(1), 82-87.

Nies, A. T., Jedlitschky, G., Konig, J., et al. Expression and immunolocalization of the multidrug resistance proteins, MRP1-MRP6 (ABCC1-ABCC6), in human brain. *Neuroscience* **2004**, 129(2), 349-360.

Oram, J. F., Wolfbauer, G., Tang, C., et al. An amphipathic helical region of the N-terminal barrel of phospholipid transfer protein is critical for ABCA1-dependent cholesterol efflux. *J. Biol. Chem.* **2008**, 283(17), 11541-11549.

Sarkadi, B., Homolya, L., Szakacs, G., et al. Human multidrug resistance ABCB and ABCG transporters: participation in a chemoimmunity defense system. *Physiol. Rev.* **2006**, 86(4), 1179-1236.

Sharom, F. J. ABC multidrug transporters: structure, function and role in chemoresistance. *Pharmacogenomics* **2008**, 9(1), 105-127.

Shen, S. and Zhang, W. ABC transporters and drug efflux at the blood-brain barrier. *Rev. Neurosci.* **2010**, 21(1), 29-53.

Shukla, S., Ohnuma, S. and Ambudkar, S. V. Improving cancer chemotherapy with modulators of ABC drug transporters. *Curr. Drug Targets* **2011**, 12(5), 621-630.

Szakacs, G., Varadi, A., Ozvegy-Laczka, C., et al. The role of ABC transporters in drug absorption, distribution, metabolism, excretion and toxicity (ADME-Tox). *Drug. Discov. Today* **2008**, 13(9-10), 379-393.

Ullah, M. F. Cancer multidrug resistance (MDR): a major impediment to effective chemotherapy. *Asian Pac. J. Cancer Prev.* **2008**, 9(1), 1-6.

Walker, J. E., Saraste, M., Runswick, M. J., et al. Distantly related sequences in the alpha- and beta-subunits of ATP synthase, myosin, kinases and other ATP-requiring enzymes and a common nucleotide binding fold. *EMBO J.* **1982**, 1(8), 945-951.

Wang, B., Dukarevich, M., Sun, E. I., et al. Membrane porters of ATP-binding cassette transport s
    ystems are polyphyletic. *J. Membr. Biol.* **2009**, 231(1), 1-10.

Zoghbi, M. E. and Altenberg, G. A. ATP binding to two sites is necessary for dimerization of
    nucleotide-binding domains of ABC proteins. *Biochem. Biophys. Res. Commun.* **2014**, 443(1),
    97-102.

*C*hapter 2

2   Scope and Objectives

Previously, a series of new tariquidar analogs was synthesized, which were surprisingly identified as potent and selective ABCG2 modulators with compound UR-ME22-1 as the most promising representative [Kühnle et al., 2009]. Aiming at higher water solubility, compounds bearing triethylenglycol groups were prepared to improve efficacy [Ochoa-Puentes et al., 2011]. Indeed, the maximal response of this new class of 2nd generation modulators clearly increased, but unfortunately, by analogy with their precursors, in mouse plasma the compounds were enzymatically cleaved at the central core structure within 10 min.

In continuation of the work of Matthias Kühnle [Kühnle, 2010] and Peter Höcherl [Höcherl, 2010], one aim of this thesis was to obtain potent and stable ABCG2 modulators with regard to planned *in vivo* studies in orthotopic brain tumor xenograft models in nude mice. For this purpose, the chemical structure of the already characterized 1st and 2nd generation ABCG2 modulators was modified in close cooperation with the group of Prof. Dr. Burkhard König (Institute of Organic Chemistry, University of Regensburg).

To explore, if the new 3rd and 4th generation modulators meet the criteria of future tumor pharmacological studies, in this thesis bio-analytical and functional investigations had to be performed:

- Firstly, the ABCG2 potency and selectivity against other ABC transporters, i.e. ABCB1 and ABCC1, had to be tested *in vitro* in fluorescent based microplate assays using ABC transporter overexpressing cells. To broaden the spectrum of screening methods, alternative new assays in the 96-well plate format had to be established.

- Biopharmaceutical aspects, especially chemical stability, binding to plasma proteins (albumin) as well as potential cytotoxicity had to be considered.

- To get closer to the *in vivo* situation, selected ABCG2 modulators were tested in a blood-brain barrier model based on porcine brain capillary endothelial cells in cooperation with the group of Prof. Dr. H.-J. Galla (Institute of Biochemistry, University of Münster).

- To examine functional interactions of the newly developed modulators with the ABCG2 transporter, a colorimetric ATPase assay using membrane preparations from recombinant baculovirus infected Sf9 cells was aimed at. This assay type should give information whether the synthesized compounds act as ABCG2 transporter substrates or as inhibitors.

In view of the treatment of malignant brain tumors, different human brain tumor cell types were characterized with regard to chemosensitivity against established anti-cancer drugs, their growth kinetics and their ABC transporter expression as well as their tumorigenicity in subcutaneous tumor xenograft models.

2.1   References

Höcherl, P. New tariquidar-like ABCB1 modulators in cancer chemotherapy: Preclinical pharmacokinetic / pharmacodynamic investigations and computational studies. PhD thesis, University of Regensburg, Germany, 2010.

Kühnle, M. Experimental therapy and detection of glioblastoma: investigation of nanoparticles, ABCG2 modulators and optical imaging of intracerebral xenografts. PhD thesis, University of Regensburg, Germany, 2010.

Kühnle, M., Egger, M., Müller, C., et al. Potent and selective inhibitors of breast cancer resistance protein (ABCG2) derived from the p-glycoprotein (ABCB1) modulator tariquidar. *J. Med. Chem.* **2009**, 52(4), 1190-1197.

Ochoa-Puentes, C., Höcherl, P., Kühnle, M., et al. Solid phase synthesis of tariquidar-related modulators of ABC transporters preferring breast cancer resistance protein (ABCG2). *Bioorg. Med. Chem. Lett.* **2011**, 21(12), 3654-3657.

*C*hapter 3

3   Modulation of the Breast Cancer Resistance Protein (ABCG2)

3.1   Introduction

ATP-binding cassette (ABC) transporters prevent the entry of a broad variety of anti-cancer drugs into cells, which limits their therapeutic value. In cancer, the expression of ABC transporters such as ABCB1 (P-gp), ABCC1 (MRP1) or ABCG2 (BCRP) is associated with the phenomenon of multidrug resistance (MDR) [Gottesman et al., 2002; Han and Zhang, 2004]. Hence, chemotherapy of malignant brain tumors is compromised by efflux pumps expressed at the blood-brain barrier (BBB), especially by ABCB1 and ABCG2, as numerous cytostatics are substrates of these proteins (cf. Chapter 1).

3.1.1   The ABCG2 transporter

The human ABCG2 protein is a 655 amino acid polypeptide and, like all members of the ABCG subfamily, a half-size transporter forming homodimers in the plasma membrane [Sarkadi et al., 2004]. As ABCG2 is highly expressed at the placenta [Staud et al., 2006], the mammary gland, the intestine and at the blood-brain barrier [Cooray et al., 2002; Robey et al., 2007] it is thought to play an important role in normal tissues in protecting these organs from potentially toxic xenobiotics. Although its role in health is not fully clear, the protection of the fetus from toxic organic anions by excreting metabolites into the maternal circulation seems to be a major task of the ABCG2 transporter [St-Pierre et al., 2000; Fetsch et al., 2006].

Since ABCG2 was first described in drug-resistant cell lines [Chen et al., 1990; Doyle et al., 1998], various chemically unrelated cytoststatic agents have been demonstrated to be substrates of the protein, like the anthracenedione mitoxantrone, the camptothecin-derived aromatic topoisomerase I inhibitors topotecan and irinotecan as well as the anthracyclines daunorubicin and doxorubicin and many more [Bates et al., 2001; Doyle and Ross, 2003; Robey et al., 2007]. Overexpression of ABCG2

has also been shown to confer moderate resistance to etoposide and methotrexate, but not to cisplatin, paclitaxel or vinblastine [Jäger, 2009].

3.1.2   BCRP inhibitors

Co-administration of ABCG2 inhibitors and appropriate cytostatics might be useful to enable the drugs to cross the BBB and to overcome the treatment refractiveness of malignancies in the CNS by increasing the drug levels [Breedveld et al., 2006].

Compared to other ABC transporters like P-glycoprotein and MRP1, the number of reported ABCG2 inhibitors is still limited [Ahmed-Belkacem et al., 2006], although the list has grown during the last years: the diketopiperazine fumitremorgin C (FTC; **Figure 3.1**), isolated from *Aspergillus fumigatus*, was reported first [Rabindran et al., 2000], but neurotoxic effects banned the compound from *in vivo* studies. An analogue of the natural compound FTC, Ko143 [Allen et al., 2002], is known as one of the most potent and selective ABCG2 inhibitors. Elacridar (GF120918) [de Bruin et al., 1999], tariquidar (XR9576) [Kannan et al., 2011] and their common analog WK-X-34 [Jekerle et al., 2006; Jekerle et al., 2007] are potent dual ABCB1 and ABCG2 modulators.

Different flavonoids [Zhang et al., 2004; Zhang et al., 2005] and chromone derivatives [Valdameri et al., 2012; Winter et al., 2013] as well as methoxy-chalcones [Valdameri et al., 2012] were described as potent ABCG2 inhibitors. Previously, the same group identified resveratrol derivatives (methoxy-stilbenes) as specific inhibitors of ABCG2 [Valdameri et al., 2012].

A compound called YHO-13177 and its water-soluble diethylaminoacetate prodrug were recently shown to reverse BCRP-mediated drug resistance *in vitro* and *in vivo* [Yamazaki et al., 2011]. However, despite the increased trend in identifying ABCG2 inhibitors, little research has been conducted with a focus on a possible *in vivo* application.

Nevertheless, the co-adminstration of anticancer agents with BCRP inhibitors seems a promising concept to treat brain tumors by enhancing the drug delivery into the brain and will, hopefully, attract further attention in preclinical and clinical investigations.

During the last years, our group, in corporation with the Institute of Organic Chemistry (Prof. Dr. B. König, University of Regensburg), was able to identify highly potent inhibitors of ABCG2 by a consequent straight-forward synthesis strategy optimizing the structure-activity relationships of recently described BCRP modulators [Kühnle et al., 2009]. Our efforts resulted in a series of compounds among which are the most potent ABCG2 modulators reported so far [Ochoa-Puentes et al., 2011; Bauer et al., 2013; Ochoa-Puentes et al., 2013].

3.2   Objective

In continuation of the work of Matthias Kühnle [Egger, 2009; Kühnle, 2010] the development and *in vitro* characterization of potent and stable ABCG2 modulators was of major interest. With regard to structural optimization concerning chemical stability under physiological conditions, recently synthesized substances [Kühnle et al., 2009] were modified and further analogs were prepared. The compounds were characterized in view of their inhibitory potency against ABCG2, their toxicity and the extent of reverting ABCG2 mediated drug resistance. Additionally, the selectivity against ABCB1 and ABCC1 was investigated using a new established fluorescence based calcein-AM assay. The most potent inhibitors were investigated with respect to their chemical stability in mouse plasma by means of HPLC-MS analysis as an assessment for planed *in vivo* studies in nude mice.

3.3   Materials and methods

3.3.1   Drugs and chemicals

Hoechst 33342 (Invitrogen, Karlsruhe, Germany) was dissolved in sterile water to produce a 0.8 mM working solution. A stock solution of mitoxantrone was performed by diluting Novantron® (Wyeth Pharma, Münster, Germany) in 70% ethanol to a concentration of 2 mM. Pheophorbide a (PhA; Frontier Scientific, Logan, UT) was dissolved in DMSO to prepare a 200 µM working solution. Calcein-AM (4 mM in anhydrous DMSO) and pluronic F127 were obtained from Biotium (Hayward, CA, USA). Topotecan and vinblastine (vinblastine sulfate; both from Sigma, Munich, Germany) were diluted in 70% ethanol [100 µM] and stored at 4 °C.

Bovine serum albumin (BSA) and crystal violet were purchased from Serva (Heidelberg, Germany).

PBS (phosphate buffered saline) was made of 8.0 g/L NaCl, 1.0 g/L $Na_2HPO_4 \cdot 2\,H_2O$, 0.20 g/L KCl, 0.20 g/L KH_2PO_4 and 0.15 g/L $NaH_2PO_4 \cdot H_2O$. The pH-value was adjusted to 7.4 by using 1 M NaOH.

Loading buffer was made of 120 mM NaCl, 5 mM KCl, 2 mM $MgCl_2 \cdot 6\,H_2O$, 1.5 mM $CaCl_2 \cdot 2\,H_2O$, 25 mM HEPES (4-(2-hydroxyethyl)piperazine-1-ethanesulfonic acid), 10 mM glucose, pH 7.4.

A solution of 4% (m/v) paraformaldeyde (PFA) in PBS was made by stirring 2 g of PFA per 50 mL total solution while heating on a magnetic stirrer for approximately 60 min.

If not otherwise stated, chemicals (p.a. quality) were obtained from Merck (Darmstadt, Germany). Purified water (Milli-Q system, Millipore, Eschborn, Germany) was used throughout.

3.3.2   Test compounds

The ABC-transporter modulators were synthesized by Dr. Michael Egger [Egger, 2009], Dr. Cristian Ochoa-Puentes, Manuel Bause and Qui Sun in the workgroup of Prof. Dr. König (Institute of Organic Chemistry, University of Regensburg, Germany) and dissolved in DMSO to a concentration of 10 mM if possible. All stocks were stored at -20 °C.

In the following, the synthesized ABCG2 modulators are termed as 1st, 2nd, 3rd and 4th generation modulators, respectively, according to their structural characteristics.

Tariquidar was synthesized in our laboratory according to literature [Dodic et al., 1995; Roe et al., 1999] with slight modifications [Hubensack, 2005].

Fumitremorgin C (FTC; Merck, Darmstadt, Germany) was also dissolved in DMSO and diluted to a concentration of 1 mM as well as elacridar, a kind gift of GlaxoSmithKline (Munich, Germany). The FTC-analog Ko143 was a kind gift of Dr. A. H. Schinkel from the Netherlands Cancer Institute (Amsterdam, NL). Reversan was purchased from Tocris Bioscience (Bristol, UK) and diluted to a 3 mM working solution in DMSO.

Figure 3.1 gives an overview of the standard ABC transporter modulators. All synthesized ABCG2 modulators are summarized in **Tables 3.1-3.7**.
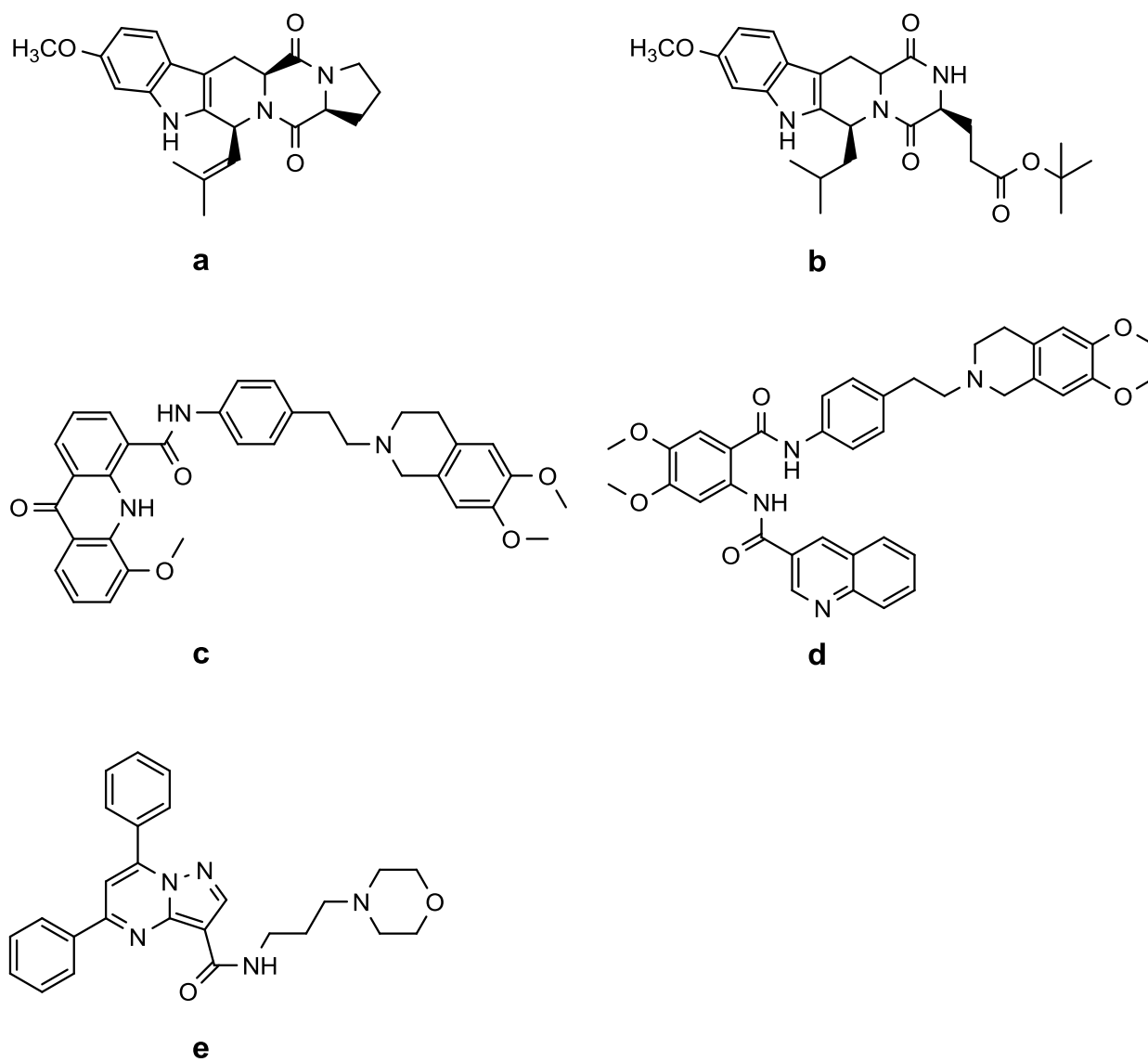
Figure 3.1: Structures of the ABCG2 modulators fumitremorgin C (**a**), its analog Ko143 (**b**), the dual ABCB1/ABCG2 inhibitors elacridar (**c**) and tariquidar (**d**) and the ABCC1 inhibitor reversan (**e**).

Table 3.1: Structures of the two most potent 1st generation ABCG2 modulators bearing an amide core [Kühnle et al., 2009].

no. (lab code)	Het
1 (UR-ME 1-4)	
2 (UR-ME 22-1)	
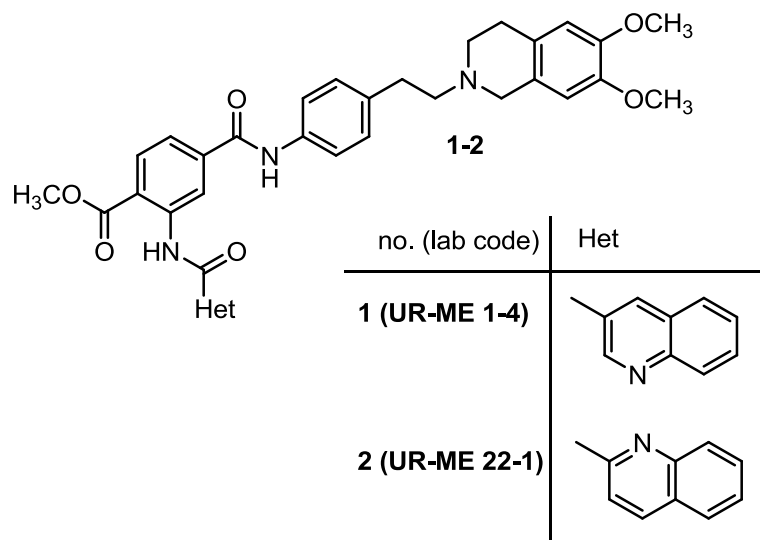
Table 3.2: Structures of 2nd generation ABCG2 modulators with variations of R^1 and R^2 [Ochoa-Puentes et al, 2011].
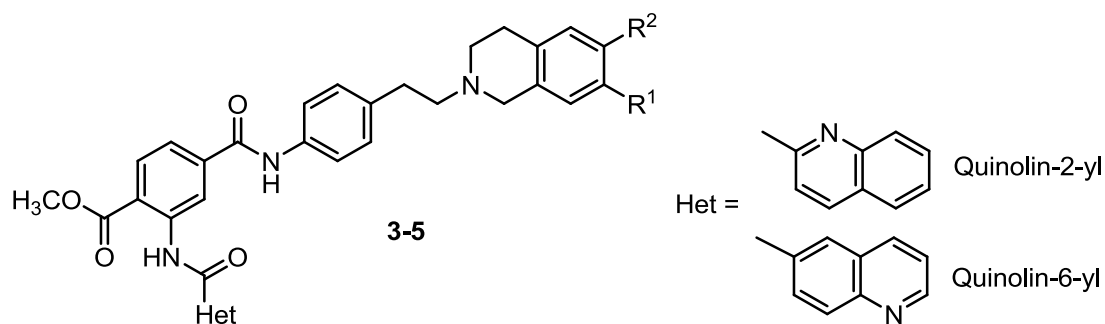
no. (lab code)	R^1	R^2	Het
3 (UR-COP77)	OCH_3	$O(CH_2CH_2O)_3CH_3$	Quinolin-2-yl
4 (UR-COP78)	$O(CH_2CH_2O)_3CH_3$	OCH_3	Quinolin-2-yl
5 (UR-COP134)	$O(CH_2CH_2O)_3CH_3$	OCH_3	Quinolin-6-yl
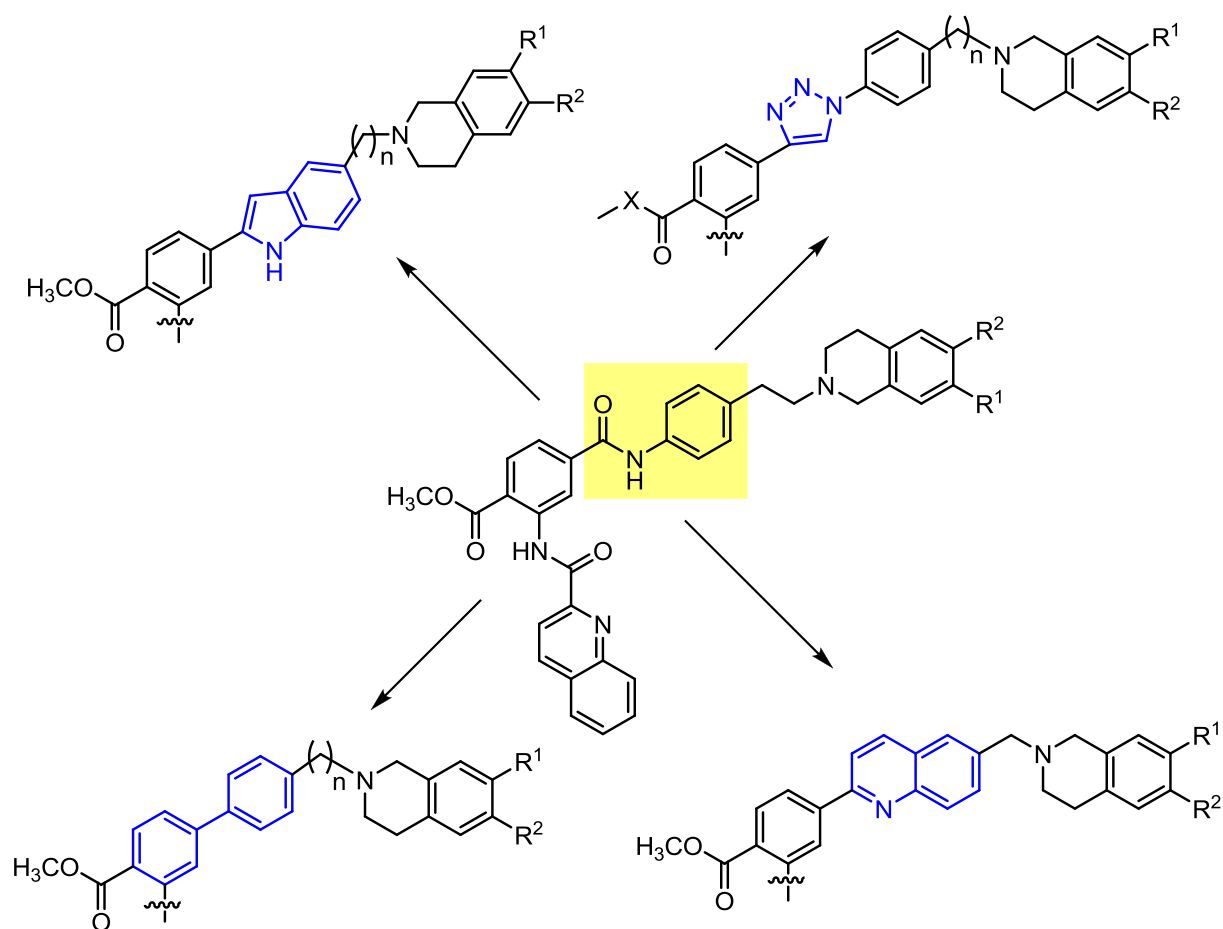
Figure 3.2: Replacement of the central benzamide moiety according to a bioisosteric approach by a biphenyl system, an indole, a quinoline and a trizole core, respectively: 3rd and 4th generation modulators.

Table 3.3: Structures of 3rd generation ABCG2 modulators: biphenyl series.
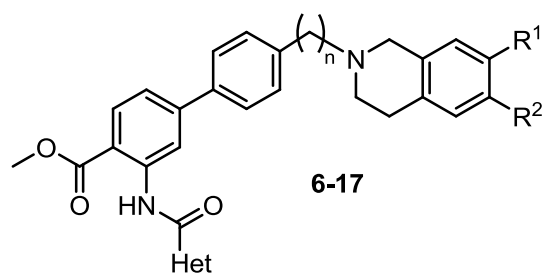
no. (lab code)	n	R^1	R^2	Het
6 (UR-COP142)	1	OCH$_3$	OCH$_3$	Quinolin-6-yl
7 (UR-COP145)	1	OCH$_3$	OCH$_3$	Quinolin-2-yl
8 (UR-COP147)	1	H	H	Quinolin-6-yl
9 (UR-COP153)	1	H	H	Quinolin-2-yl
10 (UR-COP154)	1	OCH$_3$	O(CH$_2$CH$_2$O)$_3$CH$_3$	Quinolin-2-yl
11 (UR-COP157)	1	OCH$_3$	O(CH$_2$CH$_2$O)$_3$CH$_3$	Quinolin-6-yl
12 (UR-COP228)	1	O(CH$_2$CH$_2$O)$_3$CH$_3$	OCH$_3$	Quinolin-2-yl
13 (UR-COP245)	2	OCH$_3$	OCH$_3$	Quinolin-2-yl
14 (UR-COP246)	2	H	H	Quinolin-2-yl
15 (UR-COP248)	2	O(CH$_2$CH$_2$O)$_3$CH$_3$	OCH$_3$	Quinolin-2-yl
16 (UR-COP258)	2	O(CH$_2$CH$_2$O)$_3$CH$_3$	O(CH$_2$CH$_2$O)$_3$CH$_3$	Quinolin-2-yl
17 (UR-COP270)	1	O(CH$_2$CH$_2$O)$_3$CH$_3$	O(CH$_2$CH$_2$O)$_3$CH$_3$	Quinolin-2-yl

Table 3.4: Structures of 3rd generation ABCG2 modulators: indole series.
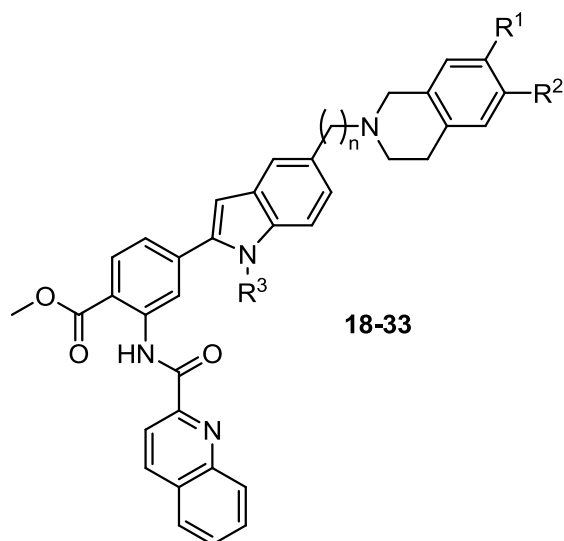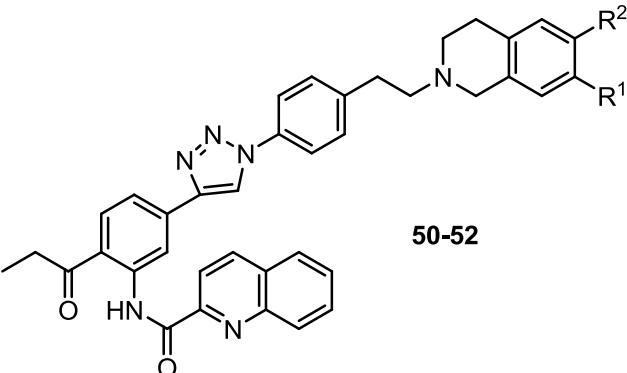
no. (lab code)	n	R^1	R^2	R^3
18 (UR-COP224)	1	OCH$_3$	OCH$_3$	CH$_3$SO$_2$
19 (UR-COP235)	2	H	H	CH$_3$SO$_2$
20 (UR-COP236)	2	OCH$_3$	OCH$_3$	CH$_3$SO$_2$
21 (UR-COP237)	2	O(CH$_2$CH$_2$O)$_3$CH$_3$	OCH$_3$	CH$_3$SO$_2$
22 (UR-COP238)	1	H	H	CH$_3$SO$_2$
23 (UR-COP239)	1	O(CH$_2$CH$_2$O)$_3$CH$_3$	OCH$_3$	CH$_3$SO$_2$
24 (UR-COP256)	1	O(CH$_2$CH$_2$O)$_3$CH$_3$	O(CH$_2$CH$_2$O)$_3$CH$_3$	CH$_3$SO$_2$
25 (UR-COP271)	2	O(CH$_2$CH$_2$O)$_3$CH$_3$	O(CH$_2$CH$_2$O)$_3$CH$_3$	CH$_3$SO$_2$
26 (UR-COP240)	1	H	H	H
27 (UR-COP251)	1	O(CH$_2$CH$_2$O)$_3$CH$_3$	OCH$_3$	H
28 (UR-COP254)	1	OCH$_3$	OCH$_3$	H
29 (UR-COP260)	1	O(CH$_2$CH$_2$O)$_3$CH$_3$	O(CH$_2$CH$_2$O)$_3$CH$_3$	H
30 (UR-COP264)	2	H	H	H
31 (UR-COP268)	2	OCH$_3$	OCH$_3$	H
32 (UR-COP269)	2	O(CH$_2$CH$_2$O)$_3$CH$_3$	OCH$_3$	H
33 (UR-COP272)	2	O(CH$_2$CH$_2$O)$_3$CH$_3$	O(CH$_2$CH$_2$O)$_3$CH$_3$	H

Table 3.5: Structures of 3$^{\text{rd}}$ generation ABCG2 modulators: triazole series.

34-40
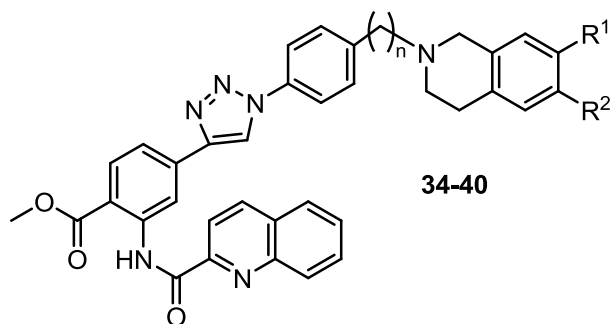
no. (lab code)	n	R^1	R^2
34 (UR-MB19-5)	2	OCH$_3$	OCH$_3$
35 (UR-MB81-2)	2	H	H
36 (UR-MB83-2)	2	O(CH$_2$CH$_2$O)$_3$CH$_3$	O(CH$_2$CH$_2$O)$_3$CH$_3$
37 (UR-MB84-3)	1	O(CH$_2$CH$_2$O)$_3$CH$_3$	OCH$_3$
38 (UR-MB86-2)	1	OCH$_3$	OCH$_3$
39 (UR-MB95-2)	2	O(CH$_2$CH$_2$O)$_3$CH$_3$	OCH$_3$
40 (UR-MB113-3)	2	OH	OCH$_3$

Table 3.6: Structures of 3rd generation ABCG2 modulators: quinoline series.
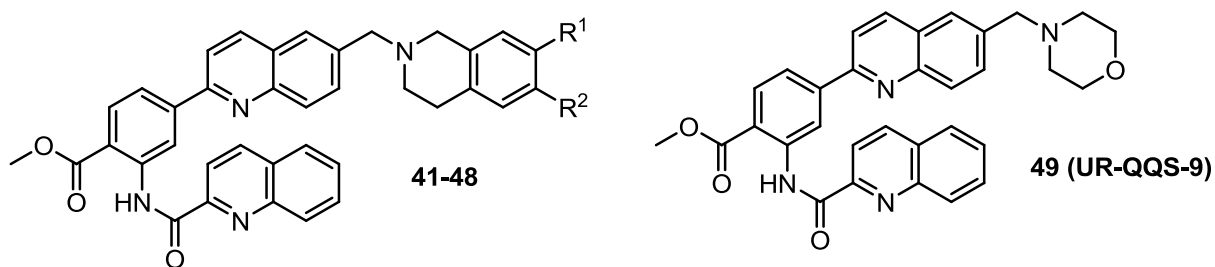
no. (lab code)	R^1	R^2
41 (UR-QQS-1)	O(CH$_2$CH$_2$O)$_3$CH$_3$	O(CH$_2$CH$_2$O)$_3$CH$_3$
42 (UR-QQS-2)	O(CH$_2$CH$_2$O)$_3$CH$_3$	OCH$_3$
43 (UR-QQS-3)	OCH$_3$	OCH$_3$
44 (UR-QQS-4)		OCH$_3$
45 (UR-QQS-5)		OCH$_3$
46 (UR-QQS-6)		OCH$_3$
47 (UR-QQS-7)		OCH$_3$
48 (UR-QQS-10)		OCH$_3$

Table 3.7: Structures of 4th generation ABCG2 modulators: triazole series containing a ketone.

no. (lab code)	R^1	R^2
50 (UR-MB107-6)	OH	OCH_3
51 (UR-MB108-4)	OCH_3	OCH_3
52 (UR-MB136-4)	$O(CH_2CH_2O)_3CH_3$	OCH_3

3.3.3   New fluorescent ABCG2 modulators

Selected compounds of the triazole series showed distinctive fluorescence, when diluted with MeCN/0.05% TFA (aq.) at a ratio of 70/30 for HPLC analysis. Fluorescence spectra were recorded with a LS50 B spectrofluorimeter from Perkin Elmer (Rodgau, Germany) at a scan rate of 240.

3.3.4   Cell culture

MCF-7/Topo cells, an ABCG2 overexpressing subclone of MCF-7 cells (ATCC® HTB-22™, a human breast adenocarcinoma cell line), were cultured in Eagle's Minimum Essential Medium (EMEM; Sigma, Munich, Germany) containing L-glutamine, 2.2 g/L $NaHCO_3$ and 110 mg/L sodium pyruvate (Serva, Heidelberg, Germany) supplemented with 10% fetal calf serum (FCS; Biochrom, Berlin, Germany) and selected as described [Hubensack, 2005]. Briefly: treatment of MCF-7 cells with increasing concentrations of topotecan (final concentration: 550 nM) over approximately 40 days yielded sufficient quantities of the ABCG2 transporter.

Human Kb-V1 cells, an ABCB1 overexpressing subclone [Kohno et al., 1988; Hubensack, 2005] of human Kb cells (ATCC® CCL-17™) were cultured in Dulbecco's Modified Eagle Medium (DMEM; Sigma, Munich, Germany) supplemented with 3.7 g/L $NaHCO_3$ and 110 mg/L sodium pyruvate (DMEM⁺⁺) in addition to 10% FCS and 330 nM vinblastine to maintain sufficient ABCB1 transporter expression.

MDCKII-MRP1 cells: MDCKII cells (Madin-Darby Canine Kidney cells, strain II; a dog epithelial cell line; ATCC® CRL-2936™), transfected with human ABCC1 [Bakos et al., 1998; Evers et al., 1998], were a

kind gift from Prof. Dr. P. Borst from the Netherland Cancer Institute (Amsterdam, NL). The cells were cultured in DMEM^{++} supplemented with 10% FCS. Trypsinization was performed at 37 °C (95% air, 5% CO_2) for 20-30 min using 0.1% trypsin / 0.04% EDTA (Roche Diagnostics, Mannheim, Germany).

The human glioblastoma cell line U-118 MG (ATCC$^®$ HTB-15™) was maintained in DMEM^{++} containing 10% FCS.

All cells were cultured in a water-saturated atmosphere (95% air, 5% CO_2) at 37 °C in 25-cm^2, 75-cm^2 or 175-cm^2 cell culture flasks purchased from Nunc (Wiesbaden, Germany), Greiner (Frickenhausen, Germany) or Sarstedt (Nümbrecht, Germany) and passaged every 3-7 days after trypsinization using 0.05% trypsin / 0.02% EDTA if not otherwise mentioned. Cell banking was performed according to the 'seed stock concept' [Hay, 1988]. Cells were routinely monitored for *mycoplasma* contamination by PCR (Venor® GeM, Minerva Biolabs GmbH, Berlin), and only *mycoplasma* negative cultures were used.

3.3.5   Cell based assays for the determination of ABC transporter modulation

All assays were performed in the microtiter plate format using 96-well plates (Greiner, Frickenhausen, Germany) and a GENios Pro microplate reader (TECAN Deutschland GmbH, Crailsheim, Germany) for fluorescence detection.

3.3.5.1 ABCG2 modulation: Hoechst 33342 and pheophorbide a microplate assays

The standard protocol was as follows (according to [Kühnle, 2010] with slight modifications):

MCF-7/Topo cells were seeded into 96-well plates at a density of 20,000-25,000 cells/well (total volume: 100 μL) and incubated over night (95% air, 5% CO_2) at 37 °C. The next day, the incubation medium was removed from the microplate. Afterwards, cells were incubated for 2 hours (37 °C, 5% CO_2) with loading suspension: EMEM, supplemented with 10% FCS, L-glutamine, 2.2 g/L $NaHCO_3$, 110 mg/L sodium pyruvate and 8 μM Hoechst 33342 (H33342) or 1 μM pheophorbide a (PhA) in combination with the test compounds at increasing concentrations (10 nM-100 μM). The structures of H33342 and PhA are shown in **Figure 3.3**.

Fumitremorgin C served as positive control at a final concentration of 10 μM, corresponding to 100% inhibition of H33342 and PhA efflux, respectively. The supernatants were discarded, and the cells were fixed for 20 min under light protection using 100 μL per well of a 4% paraformaldehyde solution. Finally, MCF-7/Topo cells were washed twice with 250 μL of PBS per well in order to get rid

of residual dye. Afterwards, cells were overlaid with 100 µL of PBS, and fluorescence was determined with a GENios Pro microplate reader.

Instrument settings were as follows: measurement mode: fluorescence top; excitation filter (Hoechst 33342): 340/35, excitation filter (pheophorbide a): 380/10; emission filter (Hoechst 33342): 485/20, emission filter (pheophorbide a): 670/25; number of reads: 10; integration time: 40 µs; lag time: 0 µs; mirror selection: automatic; plate definition file GRE96ft.pdf; multiple reads per well (Circle): 3x3; time between move and flash: 50 ms.

On each plate, the optimal gain was calculated by determination of the fluorescence intensity in the presence of the reference compound fumitremorgin C and the microtiter plates were stored at 4 °C until cell quantification. To consider unspecific toxic effects of the test compounds during the incubation phase, the obtained fluorescence values were normalized to the biomass in each well. For this purpose, the cells were stained with a 0.02% aqueous crystal violet solution (100 µL/well) for 20 min. Excess dye was removed by rinsing the microplates with water for 20 min. Crystal violet bound by the cells was extracted with 70% ethanol (180 µL/well) while shaking the microplates for 2-4 h. Subsequently, the absorbance as a parameter proportional to cell mass was measured at 590 nm with a TECAN plate reader. For normalization of the fluorescence intensities to the cell mass, fluorescence values were divided by the corresponding absorbances. All values were corrected with respect to the cellular uptake of the dye by diffusion (DMSO control value), and the data were referred to the maximal signal measured in the presence of the reference compound FTC at a concentration of 10 µM (100% inhibition).

Addition of the modulators at increasing concentrations led to sigmoidal concentration response curves in semilogarithmic plots. IC_{50} values were calculated using SigmaPlot 11.0 software (Systat Software GmbH, Erkrath, Germany) by fitting 'Four parameter logistic curve'. Errors were expressed as standard error of the mean (SEM).
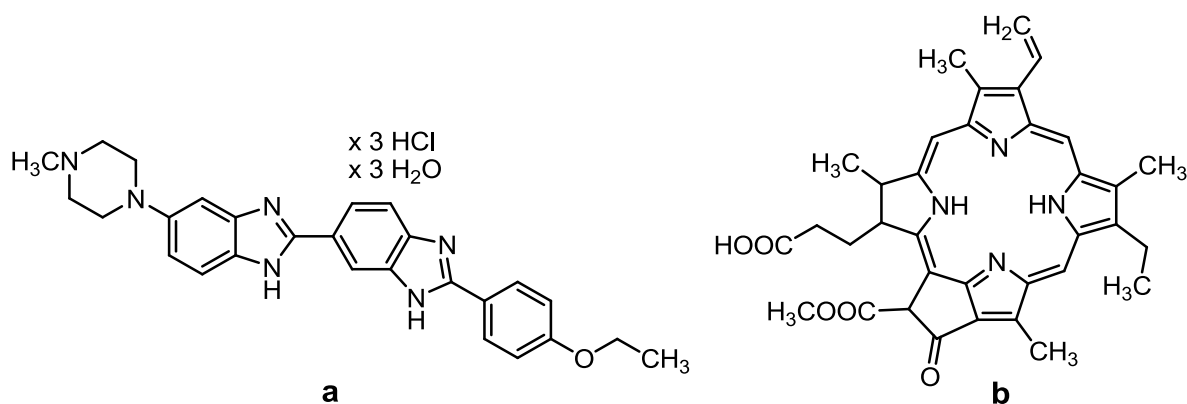
Figure 3.3: Chemical structures of the fluorescent BCRP substrates H33342 (**a**) and pheophorbide a (**b**).

3.3.5.2 Mitoxantrone microplate assay for the determination of ABCG2 modulation

Because of unfavourable fluorescent properties of some synthesized compounds and discrepencies between H33342 and PhA assay, another assay was established for the determination of BCRP modulation. With excitation and emission wavelengths far from those of the H33342 dye and the fluorescent modulators, mitoxantrone (**Figure 3.4**) was chosen as a fluorescent ABCG2 substrate, since a flow cytometric mitoxantrone assay protocol already existed [Kühnle, 2010].

In terms of comparability with the H33342 and the PhA assay the mitoxantrone assay was also established in the 96-well format.
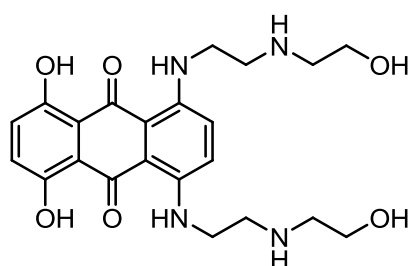
Figure 3.4: Structure of the antineoplastic agent mitoxantrone, which is a fluorescent substrate of ABCG2.

MCF-7/Topo cells were seeded into 96-well plates (density: 20,000 cells/well) and incubated over night (95% air, 5% CO_2) at 37 °C. The next day, the incubation medium was removed, and the cells were overlaid with loading suspension (EMEM, supplemented with 10% FCS, L-glutamine, 2.2 g/L $NaHCO_3$, 110 mg/L sodium pyruvate and 20 µM mitoxantrone in combination with the test compound at increasing concentrations) for 3 hours (37 °C, 5% CO_2).

Fumitremorgin C served as positive control at a final concentration of 10 µM corresponding to 100% ABCG2 inhibition. The supernatants were drained, and the cells were immediately washed twice with 250 µL of PBS (without fixation). Afterwards, cells were overlaid with 100 µL of PBS, and the relative fluorescence intensities were determined with the GENios Pro microplate reader. Time between washing and the measurement was kept as short as possible to avoid ABCG2-independent efflux of mitoxantrone.

Instrument settings were as follows: measurement mode: fluorescence top; excitation filter: 612/10; emission filter: 670/25; number of reads: 10; integration time: 40 µs; lag time: 0 µs; mirror selection: automatic; plate definition file: GRE96ft.pdf; multiple reads per well (Circle): 3x3; time between move and flash: 100 ms.

The following cell quantification procedure and the calculation of IC_{50} values were performed by analogy with the H33342 assay.

3.3.5.3 Calcein-AM efflux assay for the determination of ABCB1 modulation

The assay was performed as described elsewhere [Höcherl, 2010].

3.3.5.4 Calcein-AM efflux assay for the determination of ABCC1 modulation

MDCKII-MRP1 cells were seeded into flat-bottomed 96-well plates at a density of about 20,000 cells/well. On the following day, cells were washed with loading buffer in order to remove unspecific serum esterases. Afterwards, cells were incubated with loading suspension (loading buffer, 5 mg/mL BSA, 1.25 µL/mL pluronic F127 (20% (m/v) in DMSO)) containing 0.5 µM calcein-AM (**Figure 3.5**) and the test compound at increasing concentrations (10 nM-100 µM) for 60 min (37 °C / 5% CO_2). Reversan served as positive control at a final concentration of 30 µM corresponding to 100% ABCC1 inhibition. In general, test compounds were investigated as triplicates, controls as sextuplicates, respectively.

Subsequently, the loading suspension was discarded, and the cells were fixed with 4% PFA solution for 20 min. After three washing circles (loading buffer), fixed cells were overlaid with loading buffer, and relative fluorescence intensities were determined at 535/25 nm at the GENios Pro microplate reader after excitation at 485/20 nm. The following cell quantification procedure was performed by analogy with the H33342 assay. The obtained mean fluorescence intensities were related to the controls and plotted against the various concentrations of test compounds.

TECAN instrument settings: Measurement mode: fluorescence top; number of reads: 10; integration time: 40 µs; lag time: 0 µs; mirror selection: Dichroic 3 (e.g. Fl.); plate definition file: GRE96ft.pdf; multiple reads per well (Circle): 3x3; time between move and flash: 100 ms.
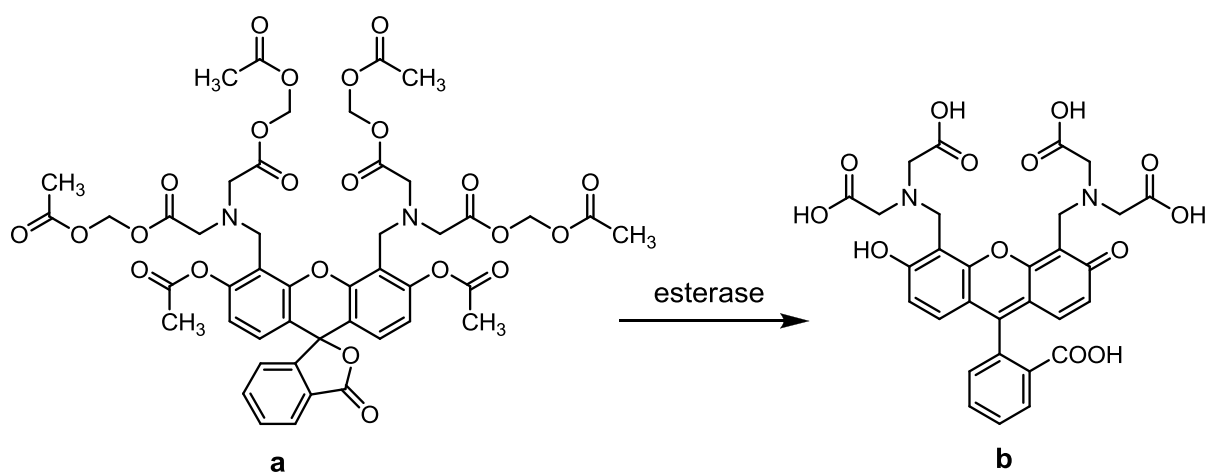
Figure 3.5: Structure of nonfluorescent calcein-AM (**a**), a substrate of ABCB1 and ABCC1, which is converted to green-fluorescent calcein (**b**) in live cells after acetoxymethyl ester hydrolysis by intracellular esterases.

3.3.6   Chemosensitivity assays

The assays were performed as described previously [Bernhardt et al., 1992] with slight modifications. In brief: 100 µL/well of a tumor cell suspension, yielding a density of 500 cells per well, were seeded into 96-well plates and incubated over night at 37 °C / 5% CO_2 in a water-saturated atmosphere.

The next day, fresh medium (100 µL/well) was added containing the 500-fold concentrated test compounds (16 wells per drug concentration) giving a final drug dilution of 1:1,000. On every plate, untreated cells (solvent DMSO in a dilution of 1:1,000) served as growth control (vehicle), cells treated with a reference cytostatic (e.g. vinblastine) as a positive control. Incubation of the cells was stopped after different periods of time by removal of medium and fixation with 2% (v/v) glutardialdehyde (in PBS). All plates were stored at 4 °C until the end of the experiment and stained simultaneously with 100 µL/well of a 0.02% (m/v) aqueous crystal violet solution for 20 min. Subsequently, the trays were rinsed with water for 20 min in order to remove residual dye. Cell-associated crystal violet was redissolved in 70% ethanol (180 µL/well) under shaking for 2-4 hours. Absorbance was measured at 580 nm using a GENios Pro microplate reader.

Drug effects were expressed as corrected T/C-values for each group according to equation 1,

$$\frac{T}{C}\,corr.\,(\%) = \frac{T-C_0}{C-C_0}\cdot 100 \qquad\qquad \text{(equation 1)}$$

where T is the mean absorbance of the treated cells, C the mean absorbance of the controls and C_0 the mean absorbance of the cells at the time (t=0) when the drug was added.

When the absorbance of treated cells T was less than that of the culture at t=0 (C_0), the extent of cell death was calculated according to the following formula:

$$cytocidal\,effect\,(\%) = \frac{C_0-T}{C_0}\cdot 100 \qquad \text{(equation 2)}$$

SigmaPlot analysis software 11.0 was used for the creation of growth curves.

3.3.7   Chemical stability of ABCG2 modulators in human and mouse plasma

With respect to future *in vivo* studies, selected candidates of potent ABCG2 modulators were investigated for their stability in human and mouse plasma.

For mouse plasma, blood of NMRI (nu/nu) mice was collected by cardiac puncture in deep anesthesia using heparin-coated syringes. Samples were immediately centrifuged at 4,500 g (Eppendorf

centrifuge 5415R, Eppendorf, Hamburg, Germany) for 7 min, and the supernatant was carefully removed. After pooling, the plasma was fractioned into small aliquots and stored at -80 °C. Human CPD (citrate-phosphate-dextrose) plasma was purchased from the Bavarian Red Cross (BRK; Regensburg, Germany).

3.3.7.1 Determination of the activity of unspecific esterases

The enzymatic activity of unspecific esterases in human and murine plasma samples was determined spectrophotometrically. Therfore, the development of the colored product o-nitrophenol, formed by enzymatic cleavage of the chromogenic substrate nitrophenyl butyrate, was determined as a function of time: 40 µL ortho-nitrophenylbutyrate (Fluka, Munich, Germany) were mixed with 1 mL of 0.1 M Na_2HPO_4 buffer (pH 7.2). After warming to 37 °C, 10 µL of murine or human plasma were added and UV absorbance was measured for 2 min at 414 nm using a Cary 100 UV-Vis spectrophotometer (Varian, Darmstadt, Germany). Absorbance was plotted against time, and the linear slope at the beginning of the reaction was determined and used for the calculation of the volume activity according to the following equation:

$$V_A = \frac{\frac{A \cdot V}{t}}{\varepsilon \cdot d \cdot v} \qquad\qquad \text{(equation 3)}$$

V_A = volume activity [U/mL]

A = absorbance of o-nitrophenol at 414 nm

t = time [min]

V = total volume [mL]

ε = molar absorption coefficient (o-nitrophenol) [L$\cdot$ mol^{-1} $\cdot$ cm^{-1}]

d = path length [cm]

v = plasma volume [mL]

3.3.7.2 Assay procedure

The test compounds were dissolved in DMSO at a concentration of 3 mM. A 1:50 dilution of the substances with mouse plasma was prepared in 1.5-mL polypropylene reaction vessels (Eppendorf, Hamburg, Germany). The samples were shortly vortexed and immediately incubated at 37 °C. After increasing periods of time, aliquots were taken, after the reaction had been stopped by addition of two volumes of ice-cold acetonitrile (MeCN). For quantitative precipitation of the denatured proteins, the samples were efficiently vortexed and stored at 4 °C for 30 min. Finally, samples were

centrifuged at 14,000 g for 5 min, and the supernatants were transferred to new Eppendorf reaction vials. For HPLC analysis, the samples were diluted (1:2) with MeCN and stored at -80 °C until measurement.

3.3.7.3   HPLC and HPLC-MS analysis

3.3.7.3.1   HPLC analysis

Subsequent RP-HPLC analysis was performed with a Waters (Eschborn, Germany) system composed of a 600S controller and pump, a Waters degasser, a temperature control module, a 717 plus autosampler and a 2487 UV detector. A Luna RP-18 (Phenomenex, Aschaffenburg, Germany) analytical column (3 μm, 150 mm x 4.6 mm) thermostatted at 30 °C was used with a flow rate of 1.0 mL/min.

Samples were thawn at room temperature, and 100 μL were injected. UV detection was performed at 210 nm. During recovery analysis, the applied gradient was as following:

MeCN/0.05% TFA (aq.): 0 min: 15/85, 25 min: 80/20, 26 min: 95/5, 36 min: 95/5, 37 min: 15/85, 45 min: 15/85.

3.3.7.3.2   HPLC-MS analysis

Determination of cleavage products was performed by HPLC-MS analysis using an Agilent 1100 (Agilent Technologies, Palo Alto, CA) HPLC system equipped with a Luna C_{18}, 3 μm, 100 mm x 2 mm column (Phenomenex, Aschaffenburg, Germany) at 40 °C. Gradient elution with water containing formic acid (0.1%) and MeCN (0 min: 3%, 15 min: 95%, 17 min: 95%, 17.5 min: 3%, 19 min: 3%) was performed at a flow rate of 0.4 mL/min with UV detection at 220 nm. The HPLC was coupled to a Finnigan ThermoQuest TSQ (Triple-Stage-Quadrupol) 7000 ESI mass spectrometer.

3.3.8   ABC transporter modulation in a blood-brain barrier model

To get closer to *in vivo* conditions at the BBB, selected compound were tested in an *in vitro* blood-brain barrier model (**Figure 3.6**) imitating the physiological situation using endothelial cells, expressing the brain multidrug resistance protein (BMDP), the porcine homolog to the human ABCG2 gene [Hoheisel et al., 1998; Franke et al., 1999; Franke et al., 2000]. Thereby, the transport of the ABCG2 substrate ^{3}H-daunorubicin across a 'membrane' (cell monolayer of primary cultured brain capillary endothelial cells) was measured in the presence of selected ABCG2 modulators. The experiments were performed by Sabine Hüwel at the Institute of Biochemistry (Prof. Dr. H.-J. Galla) at the University of Münster.
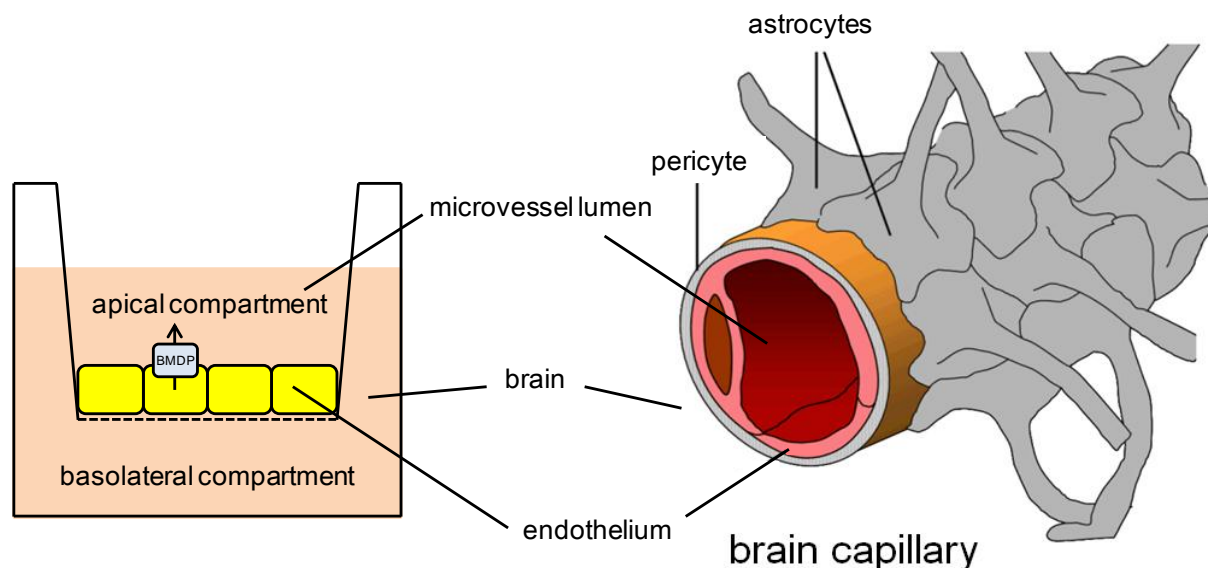
Figure 3.6: Simplified illustration comparing the *in vivo* situation at the BBB with the *in vitro* BBB model. The right panel shows a schematic cross-section through a brain capillary, the left panel shows the corresponding compartment in the experimental set-up of the transcellular transport model with a monolayer of porcine brain capillary endothelial cells expressing the brain multidrug resistance protein (BMDP). Illustration adapted from [Franke et al., 2000].

The transport assay protocol was as following [Eisenblätter et al., 2003]: the isolation of porcine capillary endothelial cells (PBCEC) has been described elsewhere [Franke et al., 2000]. DMEM/Ham's F12 medium (serum-free) containing L-glutamine (0.7 mM), penicillin/streptomycin (100 μg/mL), gentamicin (100 μg/mL) and hydrocortisone (550 nM) was used throughout with cells cultured on Transwell™ microporous polycarbonate filter membranes (0.4 μm pore size, 1 cm^2 growth area; Costar, Cambridge, MA) to prepare confluent cell monolayers. By supplementing the medium with hydrocortisone at physiological concentrations, the endothelial monolayer shows a transendothelial electrical resistance (TEER) of up to 1800 Ω/cm^2 similar to the situation *in vivo* and low paracellular permeabilities for sucrose [Levin, 1980; Crone and Olesen, 1982]. The barrier properties were quantified in terms of TEER determined by AC (alternating current) impedance analysis [Wegener et al., 2000] . The cells were incubated with the inhibitor at a specific concentration 60 min prior to the experiment, which was started by replacing the medium on both sides of the cell layer with fresh medium, containing 0.2 μM ^{3}H-daunorubicin (NEN Life Science Products; 5 Ci/mmol; 185 GBq/mmol) and the inhibitor at the corresponding concentration. After 0.5, 6, 12, 24, 36, 48 and 72 h, samples were taken from each compartment. The radioactivity at 0.5 h was set to 100% for each compartment. The tightness of the monolayer was monitored by the paracellular flux of ^{14}C-sucrose (Amersham Biosciences; 740 mCi/mmol; 27 GBq/mmol) from the apical to the basolateral compartment (2 μCi/mL or 1 μCi per filter). Three independent experiments were performed with three filters each.

3.4   Results and discussion

The following results were published in part [Bauer et al., 2013; Ochoa-Puentes et al., 2013]. Selected data, statements and figures are quoted with the permission of the corresponding journal.

3.4.1   Inhibition of ABCB1, ABCC1 and ABCG2

General procedure of ABC transporter inhibition assays:

In ABC transporter overexpressing cell lines, a fluorescent substrate of the corresponding ABC protein is not accumulated but extruded by the efflux pump. In combination with ABC modulators/inhibitors, the intracellular levels of the dyes increase resulting in higher fluorescence intensities, which can be directly referred to the extent of ABC transporter inhibition.

Intracellular fluorescence was monitored with a plate reader in a concentration-dependent manner. The relative fluorescent intensities allowed the construction of sigmoidal concentration response curves and the calculation of IC_{50} (respective concentration of the inhibitor required for half-maximal inhibition) and I_{max} values (inhibition by the highest concentration of the compound expressed in percent relative to the control compound).

The synthesized new compounds as well as the reference substances tariquidar, elacridar and Ko143 were investigated for ABCB1, ABCC1 and ABCG2 modulation in a concentration range from 10 nM to 100 µM. Precipitate formation in the loading suspension became visible for a number of modulators at final concentrations above 10 µM. These concentrations were not included in the calculation of IC_{50} and I_{max} values. Constructed concentration-response curves of selected ABCG2 modulators and the reference compounds are displayed in **Figures 3.7-3.8**.
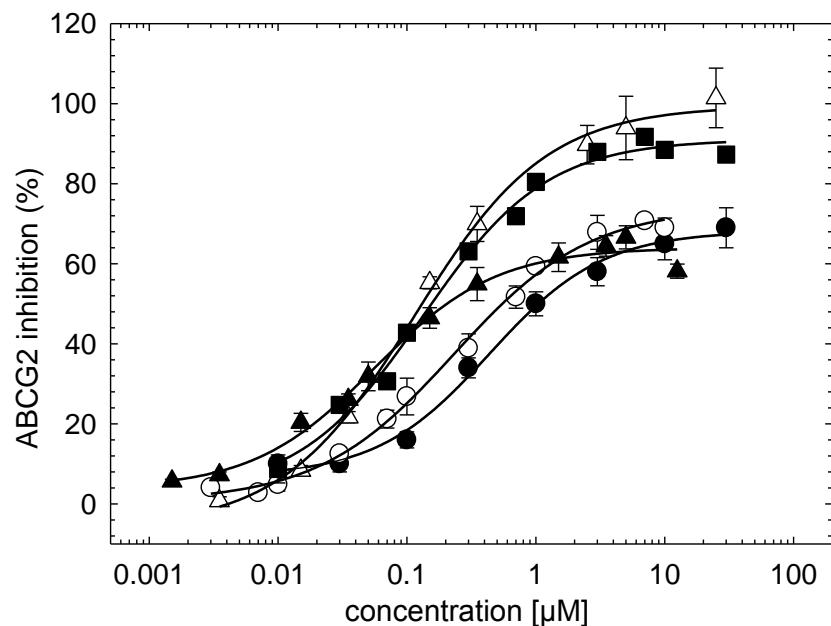
Figure 3.7: Inhibition of ABCG2 by the reference compounds tariquidar (*filled circles*), elacridar (*open circles*), Ko143 (*open triangles*) and compounds **2** (*filled triangles*) and **4** (*filled squares*).
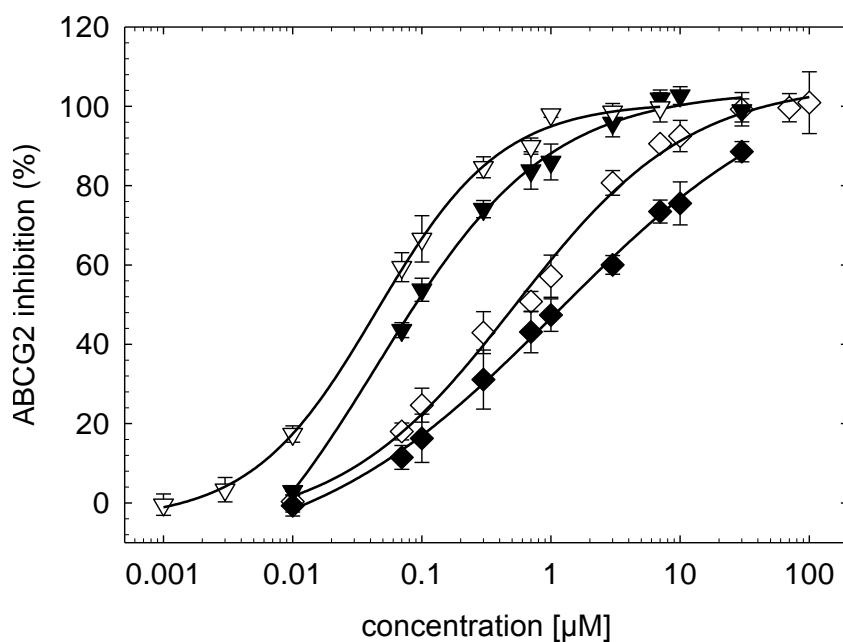
Figure 3.8: Inhibition of ABCG2 by 3rd and 4th generation modulators: **12** (*open diamonds*), **33** (*filled inverted triangles*), **42** (*filled diamonds*), and **52** (*open inverted triangles*), each representing the most potent compound of its series.

All results of the test compounds and the reference compounds regarding ABC transporter modulation are summarized in **Tables 3.8-3.13**. If not otherwise stated, mean values were calculated from two to three independent experiments performed in sextuplicate (ABCG2) or triplicate (ABCB1 and ABCC1). Maximal inhibitory effects are expressed as percental inhibition caused by the highest concentration of the compound tested (70 or 100 µM, respectively) relative to the control compound (100%). Compounds without an effect up to a concentration of 100 µM are designated as 'inactive'.

Table 3.8: Inhibition of ABCG2 and ABCB1 by compounds **1-5** and reference compounds.

Compound	ABCG2		ABCB1
	IC$_{50}$ [nM]^a	I$_{max}$ (%)	IC$_{50}$ [nM]^b
Fumitremorgin C	731 ± 92	100	n.d.
Ko143^c	117 ± 53	103 ± 7	inactive
Elacridar^c	127 ± 41	63 ± 7	193 ± 18^d
Tariquidar^c	526 ± 85	69 ± 5	223 ± 8^d
1 (UR-ME1-4)^c	104 ± 16	50 ± 1	9,450 ± 417^d
2 (UR-ME22-1)^c	65 ± 8	63 ± 2	>29,000^d
3 (UR-COP77)^e	183 ± 32	83 ± 5	>50,000
4 (UR-COP78)^e	130 ± 29	88 ± 3	>50,000
5 (UR-COP134)^e	508 ± 191	61 ± 4	>50,000

^{a} Mean values ± SEM calculated from two to three independent experiments performed in triplicate; ^{b} Calcein-AM micorplate assay (unless otherwise indicated); n.d.: not determined; ^{c} [Kühnle, 2010]; ^{d} data from flow cytometric calcein-AM assay; ^{e} [Ochoa-Puentes et al., 2011].

Table 3.9: Inhibition of ABCG2, ABCB1 and ABCC1 by 3rd generation modulators: biphenyl series, compounds **6-17**.

Compound	ABCG2		ABCB1		ABCC1
	IC$_{50}$ [nM]	I$_{max}$ (%)	IC$_{50}$ [nM]	I$_{max}$ (%)	IC$_{50}$ [nM]
6 (UR-COP142)	1,540 ± 110	92 ± 6	>10,000	119 ± 2	n.d.
7 (UR-COP145)	943 ± 79	87 ± 5	inactive		n.d.
8 (UR-COP147)	641 ± 175	94 ± 2	4,490 ± 160	100 ± 2	n.d.
9 (UR-COP153)	1,461 ± 169	85 ± 7	inactive		n.d.
10 (UR-COP154)	1,031 ± 170	114 ± 20	inactive		n.d.
11 (UR-COP157)	237 ± 65	67 ± 1	>18,000	105 ± 4	n.d.
12 (UR-COP228)	591 ± 87	109 ± 8	1230 ± 30	21 ± 8	n.d.
13 (UR-COP245)	3,214 ± 1,050	126 ± 15	inactive		n.d.
14 (UR-COP246)	1,100 ± 156	90 ± 2	inactive		n.d.
15 (UR-COP248)	760 ± 67	98 ± 6	5,420 ± 230	52 ± 5	n.d.
16 (UR-COP258)	544 ± 53	112 ± 19	5,990 ± 520	55 ± 6	n.d.
17 (UR-COP270)	839 ± 105	103 ± 3	4,430 ± 300	53 ± 7	inactive

Table 3.10: Inhibition of ABCG2, ABCB1 and ABCC1 by 3rd generation modulators: indole series, compounds **18-33**.

Compound	ABCG2		ABCB1		ABCC1
	IC$_{50}$ [nM]	I$_{max}$ (%)	IC$_{50}$ [nM]	I$_{max}$ (%)	IC$_{50}$ [nM]
18 (UR-COP224)	603 ± 204	56 ± 10	inactive		inactive
19 (UR-COP235)	1,264 ± 345	46 ± 2	inactive		inactive
20 (UR-COP236)	1,185 ± 272	50 ± 7	2,048 ± 47	17 ± 2	inactive
21 (UR-COP237)	683 ± 253	54 ± 4	1,076 ± 106	30 ± 7	inactive
22 (UR-COP238)	2,238 ± 202	22 ± 0	inactive		inactive
23 (UR-COP239)	639 ± 20	39 ± 2	1,068 ± 239	13 ± 4	inactive
24 (UR-COP256)	920 ± 145	49 ± 1	1,323 ± 368	28 ± 4	inactive
25 (UR-COP271)[a]	n.d.		n.d.		n.d.
26 (UR-COP240)	384 ± 47	98 ± 2	inactive		inactive
27 (UR-COP251)	140 ± 40	99 ± 6	1,341 ± 399	13 ± 4	inactive
28 (UR-COP254)	368 ± 63	97 ± 4	7,906 ± 595	15 ± 0	inactive
29 (UR-COP260)	132 ± 6	121 ± 19	3,940 ± 629	56 ± 10	inactive
30 (UR-COP264)	316 ± 83	96 ± 9	inactive		inactive
31 (UR-COP268)	160 ± 4	99 ± 1	inactive		inactive
32 (UR-COP269)	59 ± 11	101 ± 5	7,299 ± 910	14 ± 2	inactive
33 (UR-COP272)	46 ± 1	111 ± 9	3,570 ± 640	36 ± 4	inactive

[a] Insufficient stability excluded compound **25** from testing.

Table 3.11: Inhibition of ABCG2, ABCB1 and ABCC1 by 3rd generation modulators: triazole series, compounds **34-40**.

Compound	ABCG2		ABCB1		ABCC1
	IC$_{50}$ [nM]	I$_{max}$ (%)	IC$_{50}$ [nM]	I$_{max}$ (%)	IC$_{50}$ [nM]
34 (UR-MB19-5)	392 ± 40	92 ± 1	inactive		inactive
35 (UR-MB81-2)	426 ± 38	103 ± 1	inactive		inactive
36 (UR-MB83-2)	168 ± 81	96 ± 1	5,371 ± 1624	68 ± 1	inactive
37 (UR-MB84-3)	137 ± 4	88 ± 10	>35,000	34 ± 8	inactive
38 (UR-MB86-2)	371 ± 15	90 ± 2	>15,000	39 ± 4	inactive
39 (UR-MB95-2)	108 ± 24	97 ± 7	1,270 ± 313	91 ± 11	inactive
40 (UR-MB113-3)	145 ± 35	85 ± 6	inactive		inactive

Table 3.12: Inhibition of ABCG2, ABCB1 and ABCC1 by 3rd generation modulators: quinoline series, compounds **41-49**.

Compound	ABCG2		ABCB1		ABCC1
	IC$_{50}$ [nM]	I$_{max}$ (%)	IC$_{50}$ [nM]	I$_{max}$ (%)	IC$_{50}$ [nM]
41 (UR-QQS-1)	536 ± 160	77 ± 1	2,709 ± 158	41 ± 15	n.d.
42 (UR-QQS-2)	1,043 ± 53	107 ± 7	inactive		n.d.
43 (UR-QQS-3)	602 ± 44	60 ± 0	inactive		n.d.
44 (UR-QQS-4)	851 ± 93	81 ± 14	inactive		n.d.
45 (UR-QQS-5)	1,467 ± 568	70 ± 5	inactive		n.d.
46 (UR-QQS-6)	1,167 ± 214	61 ± 7	>15,000	25 ± 2	n.d.
47 (UR-QQS-7)	1,820 ± 861	75 ± 7	inactive		n.d.
48 (UR-QQS-10)	904 ± 45	58 ± 3	8,571 ± 211	21 ± 1	n.d.
49 (UR-QQS-9)	513 ± 101	53 ± 6	inactive		n.d.

Table 3.13: Inhibition of ABCG2, ABCB1 and ABCC1 by 4th generation modulators: triazole series bearing a ketone, compounds **50-52**.

Compound	ABCG2		ABCB1		ABCC1
	IC$_{50}$ [nM]	I$_{max}$ (%)	IC$_{50}$ [nM]	I$_{max}$ (%)	IC$_{50}$ [nM]
50 (UR-MB107-6)	48 ± 10	98 ± 11	inactive		inactive
51 (UR-MB108-4)	64 ± 3	95 ± 3	inactive		inactive
52 (UR-MB136-4)	55 ± 14	110 ± 17	2,551 ± 57	156 ± 2	inactive

Elacridar strongly inhibited the ABCG2 and the ABCB1 transporter, although without preference for one of the two targets, whereas tariquidar was about four times less potent at ABCG2, but almost equipotent with elacridar at ABCB1. The ABCG2 inhibitor Ko143, inactive at ABCB1, showed an IC$_{50}$ value of 117 nM with a maximal inhibitory effect comparable to that of fumitremorgin C. Compounds **1** and **2** were comparable to Ko143 regarding potency and selectivity, but produced a lower maximal response. Aiming at structural optimization of potent and selective ABCG2 inhibitors like **2**, compounds bearing triethyleneglycol ether groups at the tetrahydroisoquinoline moiety were synthesized (compounds **3-5**). Compounds **3** and **4** were comparable to UR-ME22-1 in potency, but considerably more efficient (maximal inhibition of 83% and 88% vs. 63%, relative to FTC). These results support the hypothesis that poor solubility of the ABCG2 modulators **1** and **2** in aqueous media is the factor limiting efficacy.

Compounds such as UR-COP78 (**4**) are highly potent and selective ABCG2 modulators, but prone to rapid enzymatic cleavage (cf. section 3.4.5.2) at the central benzanilide moiety. In search for more stable analogs, according to a bioisosteric approach, new series of potential modulators, bearing a

biphenyl, a quinoline, an indole and a triazole core, respectively, were prepared by conventional or solid phase synthesis.

All newly synthesized compounds showed a marked preference for ABCG2 inhibition.

Within the biphenyl series compounds **7**, **9**, **10**, **13** and **14** were completely inactive at the ABCB1 transporter, whereas the IC_{50} values of compounds **12** and **16** (~600 nM) were comparable to that of tariquidar, the maximal inhibitory effects were significantly higher, achieving 109% and 112%, respectively, relative to FTC. Except for **11**, all modulators show a maximal ABCG2 inhibition of 90% or higher. Compound **12**, the most potent - but not completely selective - BCRP modulator in this series, showed a maximum inhibition at the ABCB1 transporter of only 20%.

The potency of compounds **13-16**, bearing an ethylene linker, was not increased compared to that of the lower homolog **12**, suggesting that the distance between the tetrahydroisoquinoline core and the biphenyl motif may be varied within this class of ABCG2 modulators. Compounds **12** and **16**, indeed, showed higher IC_{50} values compared to all reference compounds, but, with respect to the maximal inhibitory effects, they were superior to tariquidar, elacridar, compounds **1-5** and comparable to Ko143.

Subsequent compounds of the indole, quinoline and triazole series, were designed with a quinoline-2-carboxamido substituent at the central benzamide.

Compounds **18-33** represent the indole series. Initial problems with deprotection during synthesis led to compounds **18-24**, the N-mesylated precursors of **25-33**. In general, the N-mesylated indoles showed higher IC_{50} values and lower maximal responses (~50%) compared to the unprotected analogs, suggesting that the unsubsituted NH-group of the indole core is essential for ABCG2 inhibition. Most of the indoles **25-33** inhibited the ABCG2 transporter at low nanomolar concentrations with maximal inhibitory effects of 100% or even surpassing that of FTC. Compounds **26**, **30** and **31** were selective for ABCG2, whereas the other compounds showed also activity at the P-glycoprotein with IC_{50} values in the micromolar range (e.g. selectivity ratio of compound **32**: 124 in favor of ABCG2). Compounds **29**, **32** and **33** were the most potent BCRP modulators of this series with IC_{50} values of 132 nM, 59 nM 46 nM, respectively, and maximal inhibitory effects higher than 100%. These indoles were superior to tariquidar, FTC and even to Ko143, the most potent ABCG2 transporter inhibitor reported so far. None of the compounds showed activity at the ABCC1 transporter. In general, the potencies of compounds with a methylene linker (n=1) at the indole core were comparable to those of compounds with an ethylene bridge (n=2).

Compounds **34-40** and **50-52** (triazole series) produced similar results with IC_{50} values in the low nanomolar range and potencies comparable to fumitremorgin C (100%). Together with **32** and **33**, compounds **50-52** are the most potent ABCG2 modulators reported so far.

Compounds **39** and **52** also showed distinct activity at the P-gp and work as potent dual ABCB1/ABCG2 transporter modulators with a maximal ABCB1 inhibition of 91% and 156% compared to tariquidar [1 µM], respectively.

The introduction of one or two triethylene glycol chains at the tetrahydroisoquinoline core in the series of 3rd generation modulators, in general, on the one hand increased the inhibitory activity compared to UR-ME22-1 (**2**), probably due to improved water solubility, on the other hand ABCG2 selectivity was decreased.

In another synthesis approach, a quinoline instead of an indole was introduced as a putative anilide bioisostere resulting in compounds **41-49**. Compounds **41** and **42**, bearing one or two triethylenglycol chains, respectively, were indeed the two most potent representatives of this series, but in general, the quinoline bearing compounds turned out to be hardly soluble and less potent compared to the indole series regarding ABCG2 modulation, suggesting that the extension of the indole ring system to a quinoline reduces ABCG2 inhibition.

Compounds **44-49** contain linkers with various basic heterocycles instead of a methoxy group or a triehylenglycol chain and were generally less potent and efficient in comparison to compounds of the indole and the triazole series.

3.4.2   **Fluorescence properties of selected ABCG2 modulators**

Besides modulators **38**, **51** and **52** only compounds **35** and **36** showed weak fluorescence (spectra not shown) in mobile phase with an emission maximum at 470 nm after excitation at 370 nm (**Figures 3.9-3.10**).
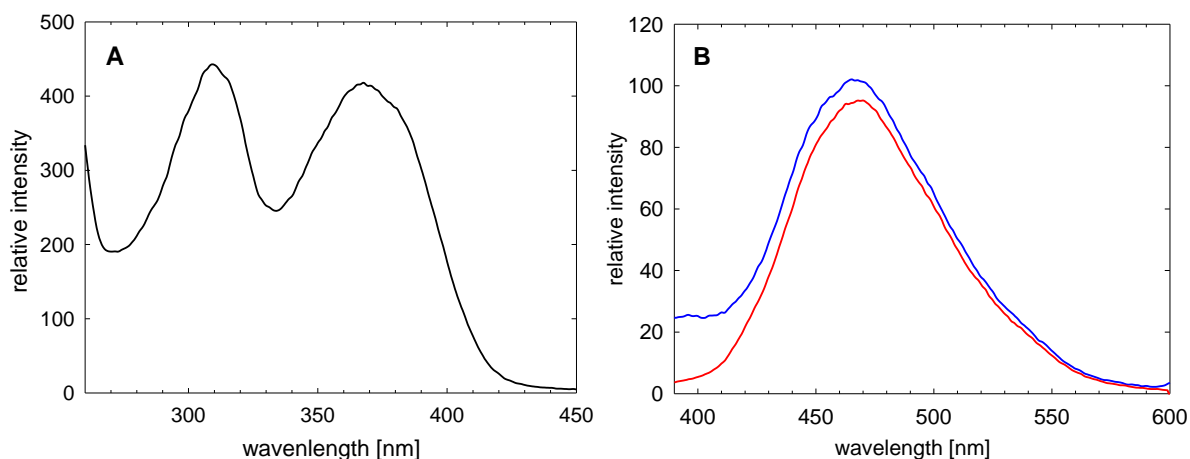
Figure 3.9: A) Excitation spectrum (λ_{em}: 480 nm; Ex Slit: 5; Em Slit: 10) of compound **51** [1 µM] in MeCN/0.05% TFA (aq.) at a ratio of 70/30; **B)** Emission spectrum (Ex Slit: 10, Em Slit: 5) of compound **51** [1 µM] after excitation at 310 nm (*blue*) and 370 nm (*red*), respectively.
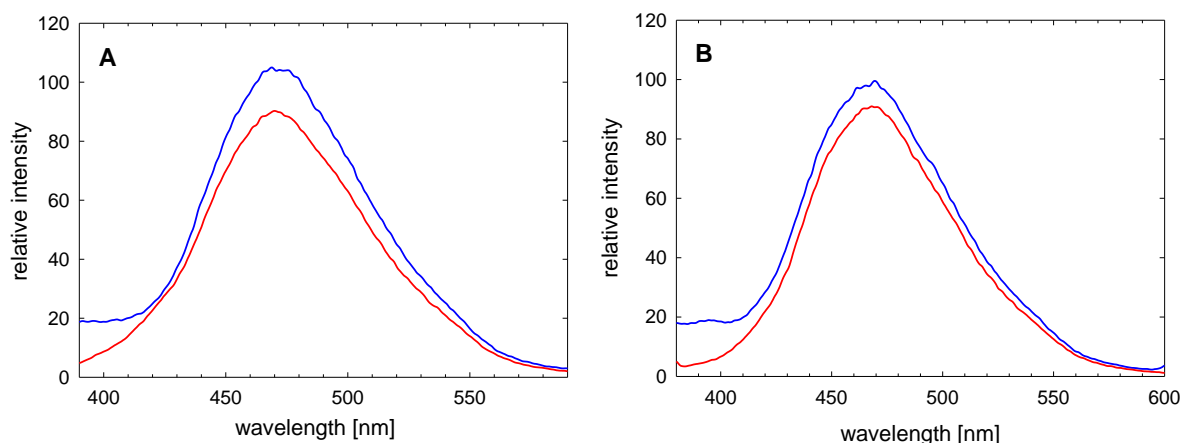
Figure 3.10: Emission spectra of compounds **38** (**A**) and **52** (**B**) [1 µM] in MeCN/0.05% TFA (aq.) at a ratio of 70/30 at two different excitation wavelengths: 310 nm (*blue*) and 370 nm (*red*); Ex Slit: 10, Em Slit: 5.

3.4.3   Alternative fluorescence based ABCG2 inhibition assays

Fluorescent ABC modulators like compounds **51** and **52** (λ_{ex}: 370 nm; λ_{em}: 480 nm) partially overlap with the excitation and emission spectra of the intercalated Hoechst 33342 dye (λ_{ex}: 340 nm, λ_{em}: 485 nm). To exclude that the fluorescence of these compounds interferes with the Hoechst assay, causing false positive results, a microplate assay was established, using mitoxantrone as a fluorescent ABCG2 substrate with spectral properties different from those of **51** and **52** and that of intercalated Hoechst 33342. Selected compounds were investigated in the Hoechst 33342, the mitoxantrone (λ_{ex}: 612 nm, λ_{em}: 670 nm) and additionally in the pheophorbide a (PhA; λ_{ex}: 380 nm, λ_{em}: 670 nm) microplate assay using MCF-7/Topo cells (**Table 3.14**).

If not otherwise stated, mean values and maximal inhibitory effects were calculated from two to three independent experiments performed in sextuplicate (Hoechst 33342 assay) or two experiments performed in triplicate (mitoxantrone and PhA assay).

Table 3.14: Inhibition of ABCG2 by selected modulators, determined in three different microplate assays using MCF-7/Topo cells. Fluorescent compounds are highlighted in blue.

Compound	H33342 Assay λ_{ex}: 340 nm; λ_{em}: 485 nm		Mitoxantrone Assay λ_{ex}: 612 nm; λ_{em}: 670 nm		PhA Assay λ_{ex}: 380 nm; λ_{em}: 670 nm	
	IC_{50} [nM]	I_{max} (%)	IC_{50} [nM]	I_{max} (%)	IC_{50} [nM]	I_{max} (%)
12	591 ± 94	109 ± 8	796 ± 146	94 ± 6	566 ± 74	65 ± 7
15	760 ± 67	98 ± 6	505 ± 13	89 ± 3	973 ± 87[a]	81 ± 2
26	384 ± 47	98 ± 2	275 ± 66	84 ± 2	710 ± 87[a]	71 ± 3
29	132 ± 6	121 ± 19	137 ± 4	100 ± 6	488 ± 56[a]	146 ± 5
31	160 ± 4	99 ± 1	151 ± 16	101 ± 9	278 ± 22[a]	125 ± 2
32	59 ± 11	101 ± 5	94 ± 33	99 ± 0	117 ± 34	103 ± 11
33	46 ± 1	111 ± 9	55 ± 13	104 ± 4	101 ± 11	90 ± 2
34	392 ± 40	92 ± 1	627 ± 127	88 ± 5	978 ± 67[a]	56 ± 1
38	371 ± 90	90 ± 2	426 ± 172	70 ± 6	856 ± 167	53 ± 7
40	145 ± 35	85 ± 6	251 ± 22	90 ± 2	141 ± 21	69 ± 6
51	64 ± 3	95 ± 3	49 ± 6	95 ± 2	480 ± 238	80 ± 2
52	55 ± 14	110 ± 17	115 ± 69	91 ± 12	94 ± 4	89 ± 0

[a] Mean values were calculated from a single experiment performed in triplicate.

As shown in **Table 3.14**, IC_{50} values as well as I_{max} values obtained in the Hoechst 33342 and the mitoxantrone assay are in a very good accordance. In general, the pheophorbide a assay yielded lowest activities with the exception of compounds **29, 31** and **32**. The fact that these compounds all belong to the indole series and are substituted at the tetrahydroisochinoline suggests that the different potencies and efficacies obtained in the PhA assay and the other two ABCG2 modulator assays are substrate dependent. Besides assay-dependent differences and variable extents of precipitation of the modulators, the low maximal inhibitory effects in the PhA assay may result from absorption of the excitation light for PhA by some of the compounds. **Figures 3.11-3.13** display the concentration-response curves for all compounds tested in the Hoechst 33342, the mitoxantrone and the pheophorbide a microplate assay, respectively.

Whereas compound **51** and **52** yielded almost identical results in the H33342 and the mitoxantrone assay (λ_{ex}: 380 nm; λ_{em}: 670 nm), compound **38** differs in the efficacy in the two assays.

As shown in **Figure 3.13** (**B**), the inhibition for compound **38** from the mitoxantrone assay does not deviate from that of the Hoechst assay up to a concentration of 1 µM. As **38** showed very poor solubility (even in DMSO), it is likely that precipitation was the cause of the discrepancies in the different ABCG2 assays.

In general, with the establishment of the mitoxantrone assay, a well-suited alternative test system in terms of ABCG2 inhibition was adjusted. As mitoxantrone fluorescence efflux assays in literature are mainly performed at the flow cytometer [Matsson et al., 2007], the here arranged assay in the 96-well format represents a comfortable alternative for the screening of a large variety of compounds.
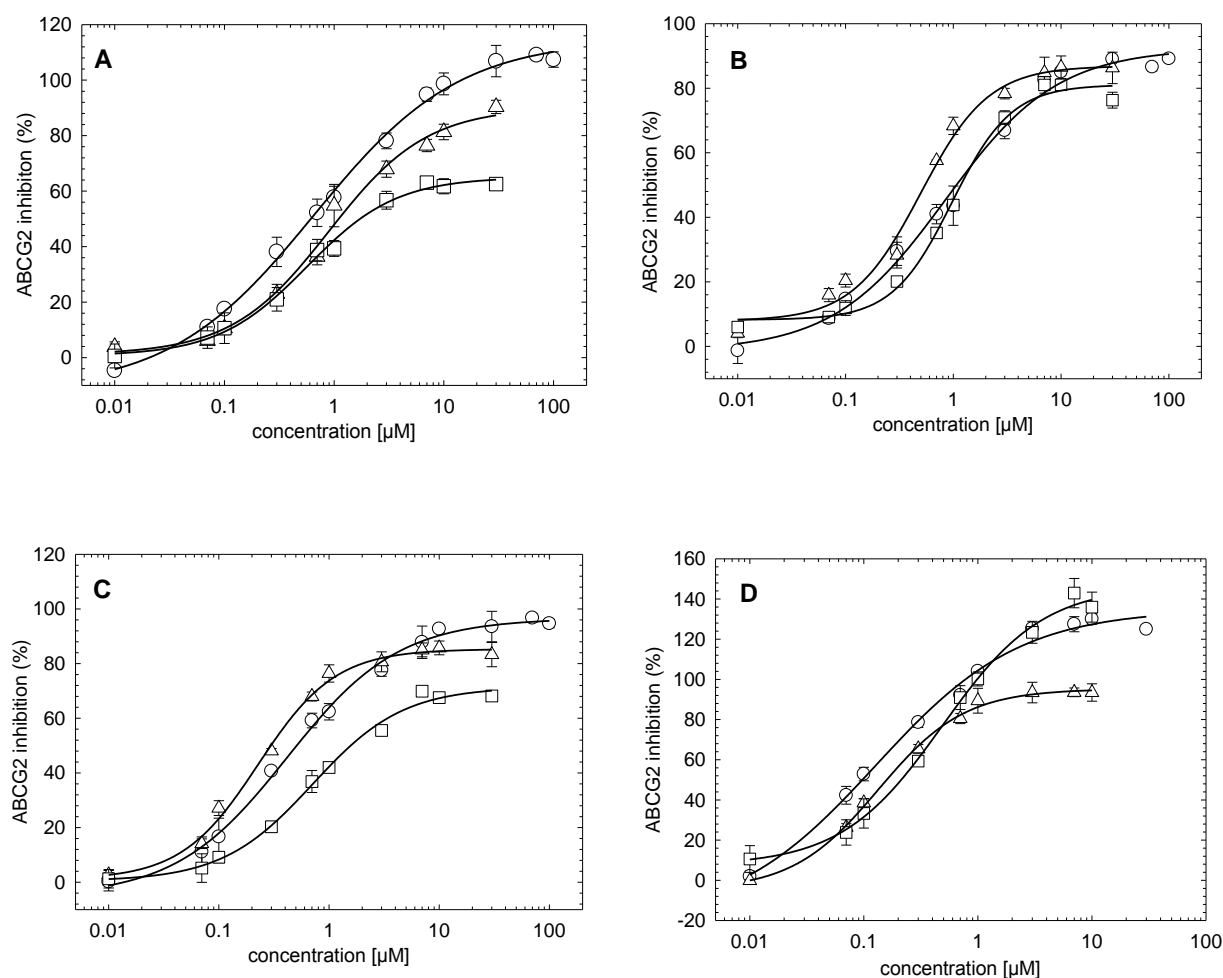
Figure 3.11: ABCG2 inhibition by compounds **12** (**A**), **15** (**B**), **26** (**C**) and **29** (**D**), respectively, in the Hoechst33342 (*open circles*), the mitoxantrone (*open triangles*) and the pheophorbide a (*open* squares) microplate assay.
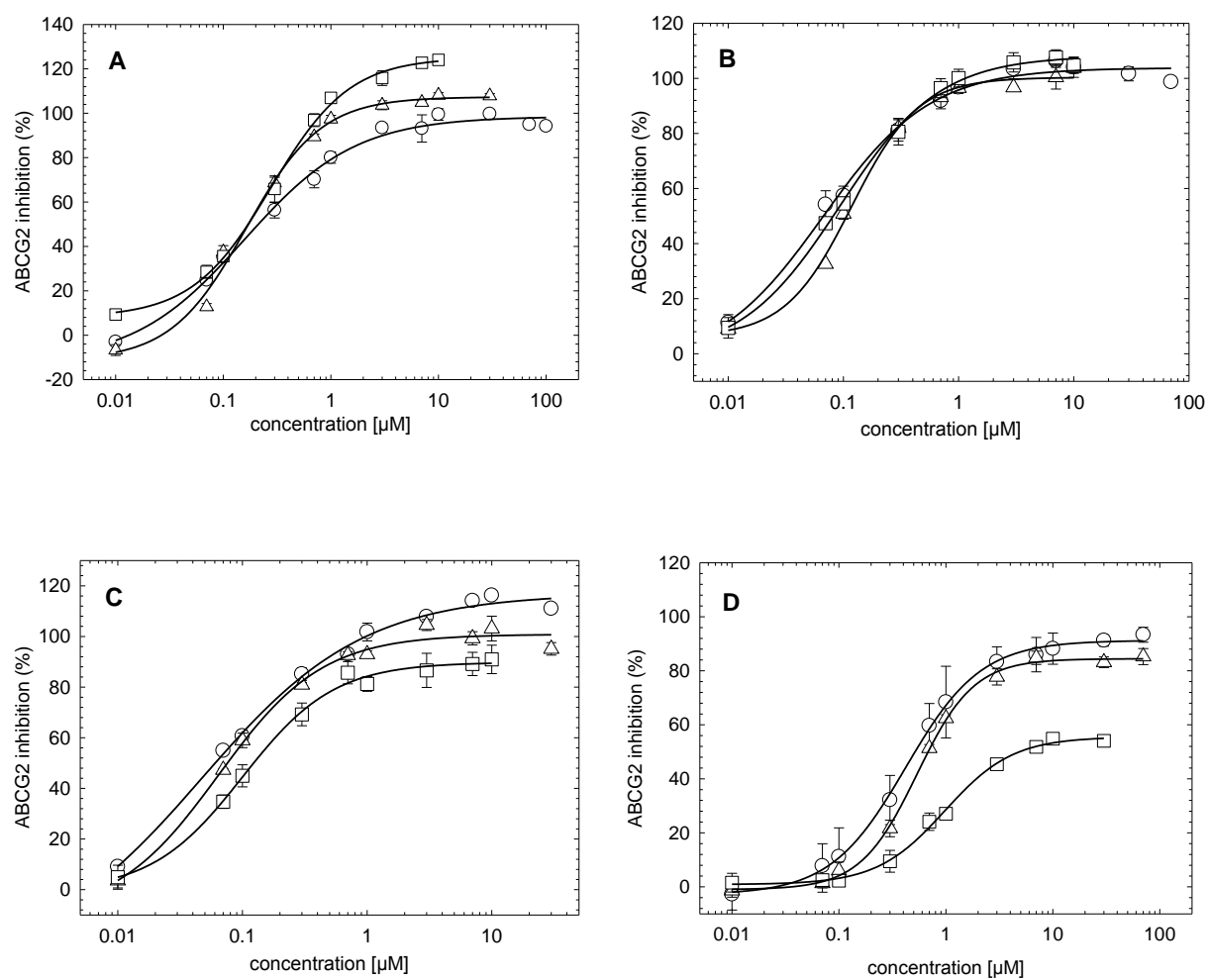
Figure 3.12: ABCG2 inhibition by compounds **31** (**A**), **32** (**B**), **33** (**C**) and **34** (**D**), respectively, in the Hoechst33342 (*open circles*), the mitoxantrone (*open triangles*) and the pheophorbide a (*open squares*) microplate assay.
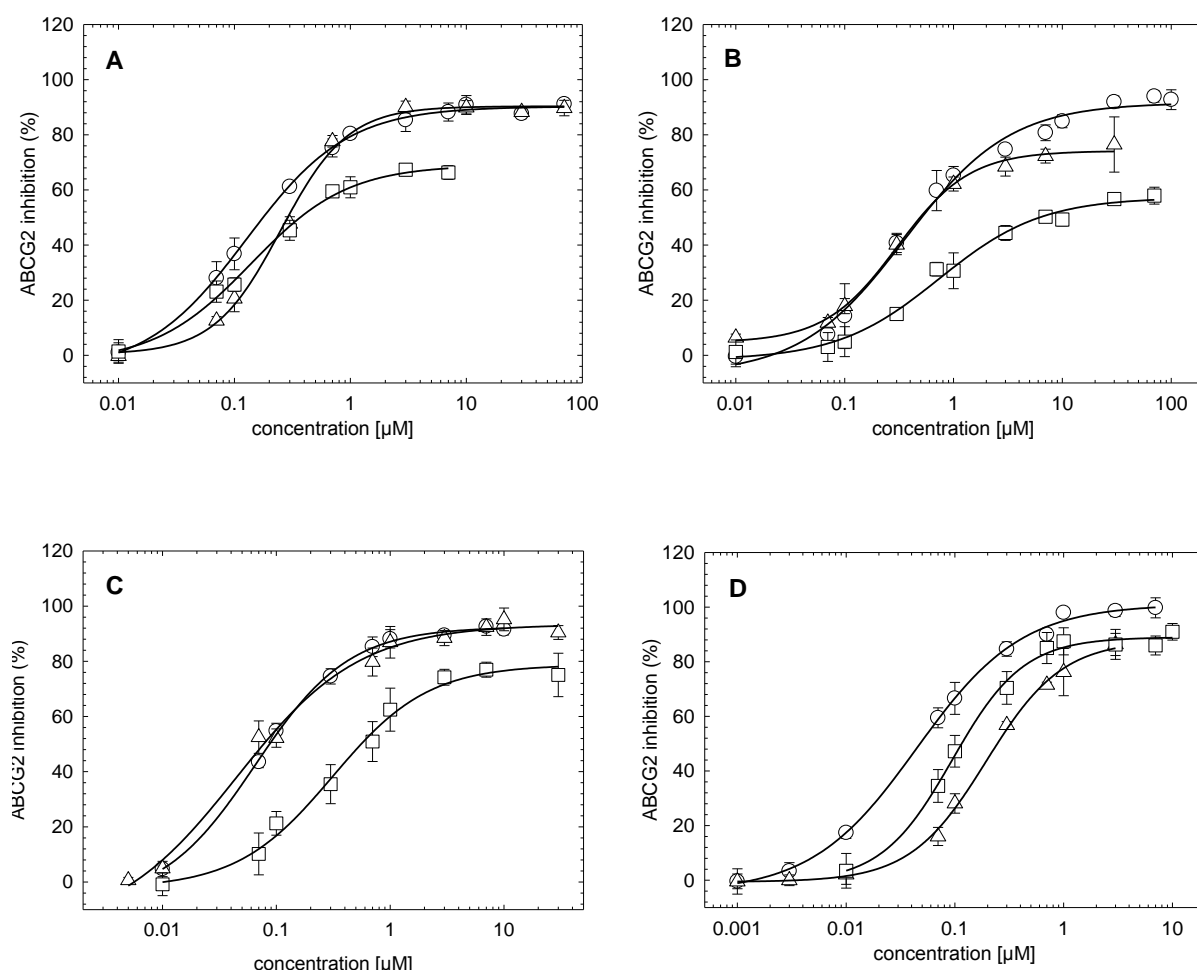
Figure 3.13: ABCG2 inhibition by **40** (**A**) and fluorescent compounds **38** (**B**), **51** (**C**) and **52** (**D**), respectively, in the Hoechst33342 (*open circles*), the mitoxantrone (*open triangles*) and the pheophorbide a (*open squares*) microplate assay.

3.4.4   Effect of co-administration of ABCG2 inhibitors with topotecan on the proliferation of MCF-7/Topo cells

To confirm ABCG2 transporter inhibition, resulting in a reversal of ABCG2 mediated drug resistance, the effect of the five most potent modulators (compounds **32**, **33**, **50-52**) on the proliferation of two cell lines was investigated using a kinetic crystal violet chemosensitivity assay (**Figures 3.14-3.18**). ABCG2-overexpressing MCF-7/Topo cells show resistance against the cytostatic drug topotecan, a known BCRP substrate, up to concentrations of 550 nM. The cells were incubated with topotecan alone and in combination with different concentrations of the new modulators. Considering potential cytotoxicity of the ABCG2 modulators, the cells were also treated with modulators alone.
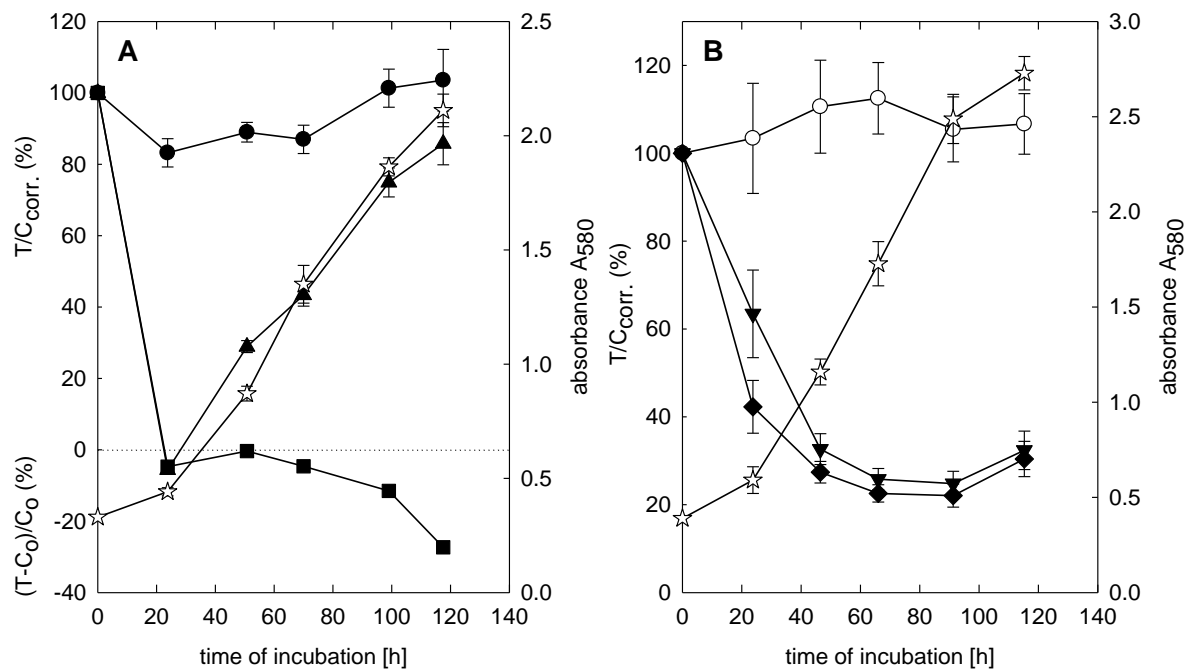
Figure 3.14: Effect of compound **32** (UR-COP269) alone (**A**) and in combination with topotecan (**B**) on proliferating MCF-7/Topo cells; vehicle (*open stars*); A) **32** [1 µM] (*filled circles*) and [5 µM] (*filled triangles*), positive control vinblastine [1 µM] (*filled squares*); **B**) topotecan [100 nM] (*open circles*), topotecan [100 nM] + **32** [100 nM] (*filled inverted triangles*), topotecan [100 nM] + **32** [500 nM] (*filled diamonds*).
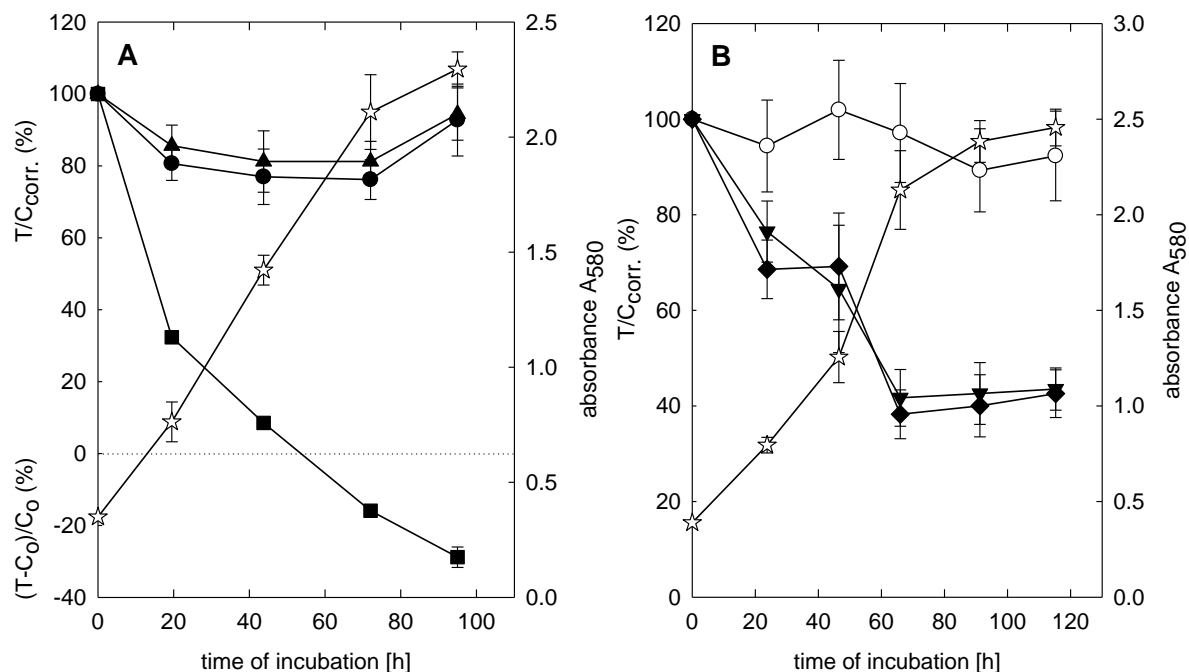
Figure 3.15: Effect of compound **33** (UR-COP272) alone (**A**) and in combination with topotecan (**B**) on proliferating MCF-7/Topo cells; vehicle (*open stars*); A) **33** [1 µM] (*filled circles*) and [5 µM] (*filled triangles*), positive control vinblastine [1 µM] (*filled squares*); **B**) topotecan [100 nM] (*open circles*), topotecan [100 nM] + **33** [100 nM] (*filled inverted triangles*), topotecan [100 nM] + **33** [500 nM] (*filled diamonds*).
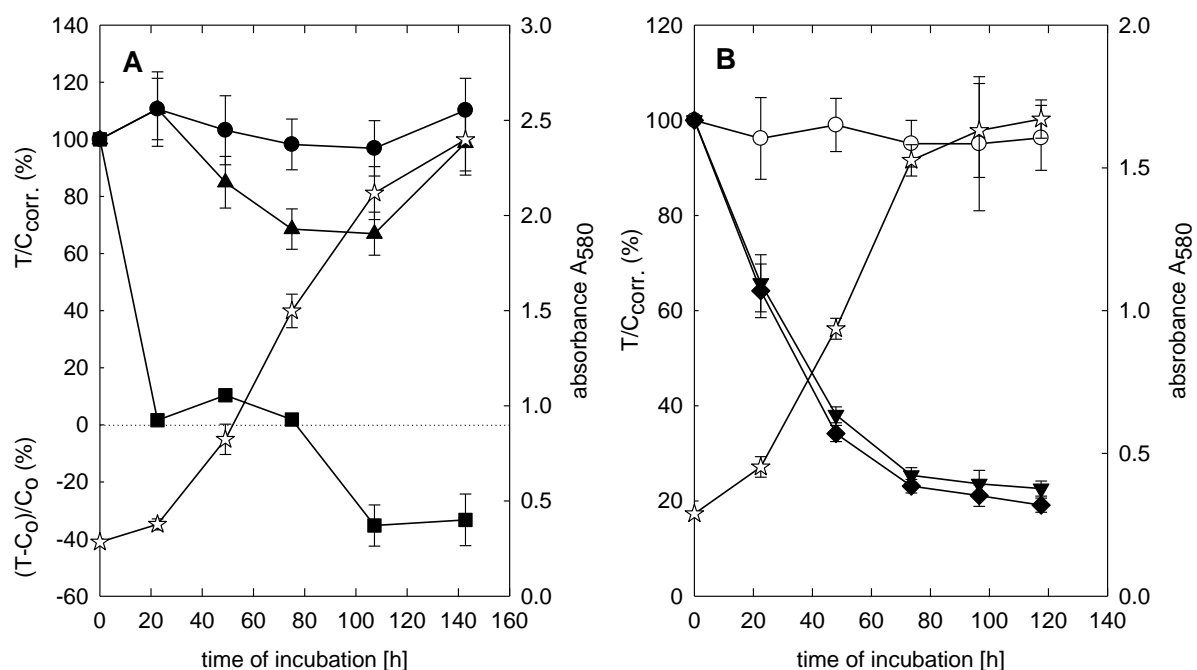
Figure 3.16: Effect of compound **50** (UR-MB107-6) alone (**A**) and in combination with topotecan (**B**) on proliferating MCF-7/Topo cells; vehicle (*open stars*); **A**) **50** [1 µM] (*filled circles*) and [5 µM] (*filled triangles*), positive control vinblastine [1 µM] (*filled squares*); **B**) topotecan [100 nM] (*open circles*), topotecan [100 nM] + **50** [100 nM] (*filled inverted triangles*), topotecan [100 nM] + **50** [500 nM] (*filled diamonds*).
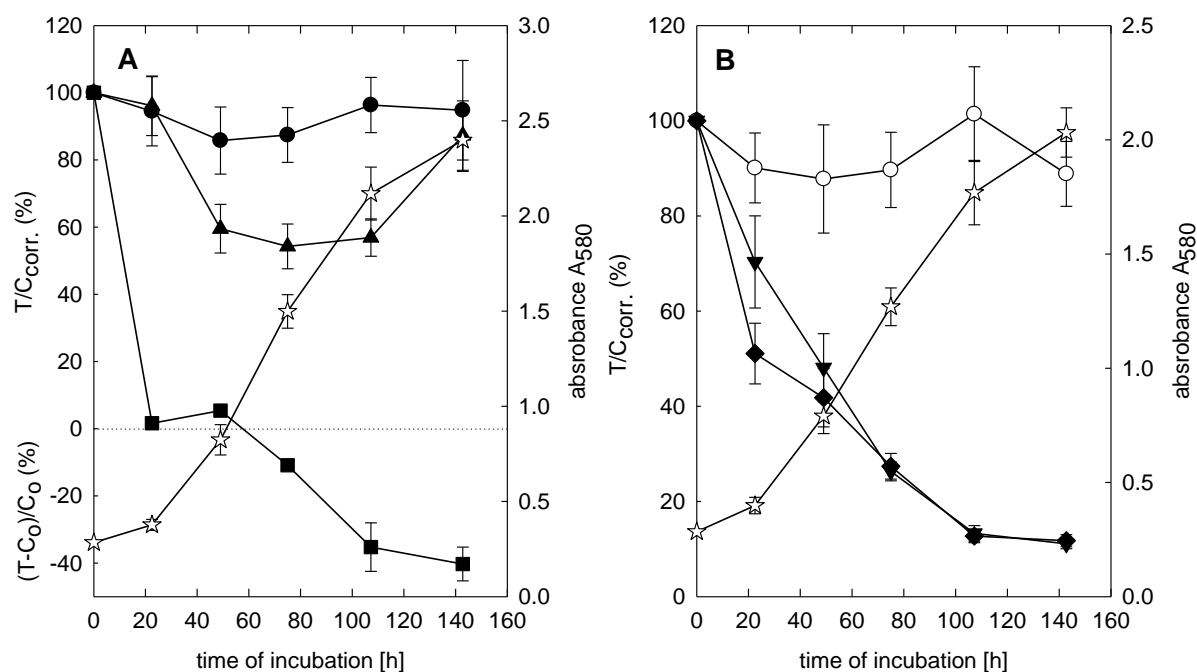
Figure 3.17: Effect of compound **51** (UR-MB108-4) alone (**A**) and in combination with topotecan (**B**) on proliferating MCF-7/Topo cells; vehicle (*open stars*); **A**) **51** [1 µM] (*filled circles*) and [5 µM] (*filled triangles*), positive control vinblastine [1 µM] (*filled squares*); **B**) topotecan [100 nM] (*open circles*), topotecan [100 nM] + **51** [100 nM] (*filled inverted triangles*), topotecan [100 nM] + **51** [500 nM] (*filled diamonds*).
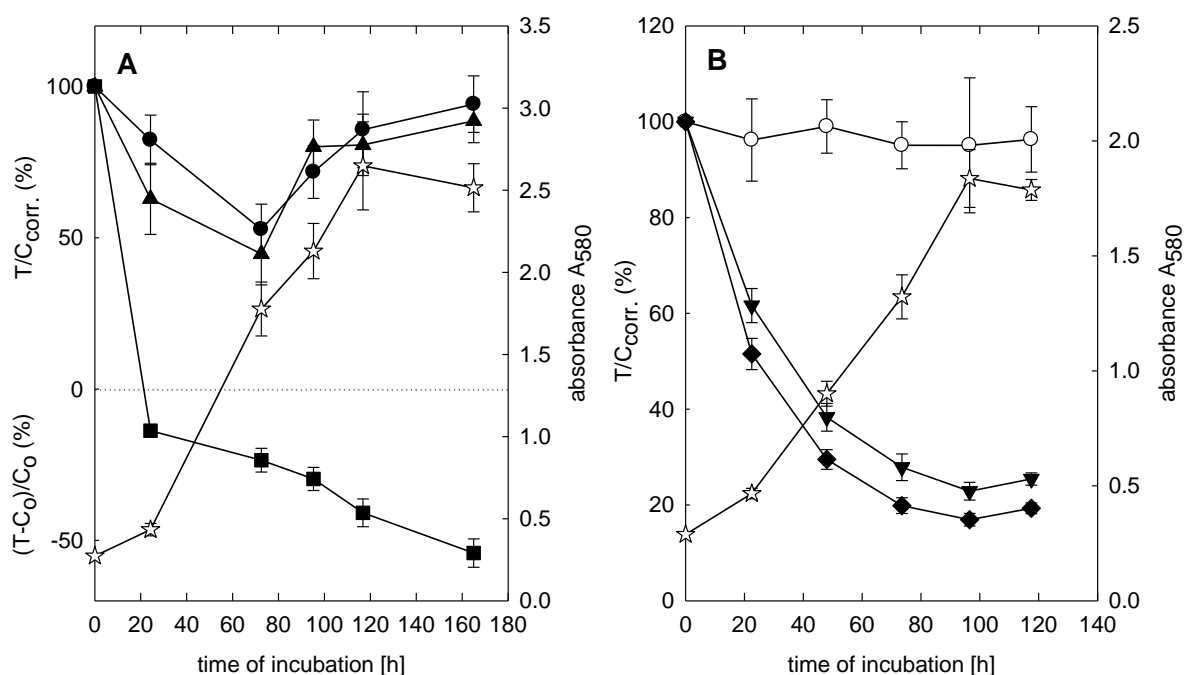
Figure 3.18: Effect of compound **52** (UR-MB136-4) alone (**A**) and in combination with topotecan (**B**) on proliferating MCF-7/Topo cells; vehicle (*open stars*); **A**) **52** [1 µM] (*filled circles*) and [5 µM] (*filled triangles*), positive control vinblastine [1 µM] (*filled squares*); **B**) topotecan [100 nM] (*open circles*), topotecan [100 nM] + **52** [100 nM] (*filled inverted triangles*), topotecan [100 nM] + **52** [500 nM] (*filled diamonds*).

The modulators alone did not affect the proliferation of MCF-7/Topo cells at high concentrations, i.e. 1 µM and 5 µM, respectively. Only compound **32** led to a temporary growth retardation [5 µM] 24 hours after addition of the compound.

The combination of topotecan at a nontoxic concentration of 100 nM with compounds **32** and **33**, respectively, resulted in a cytotoxic drug effect, even at a low modulator concentration of 100 nM. A higher concentration of the modulator did not increase cyctotoxicity. Compounds **50-52** caused a strong cytostatic effect on MCF-7/Topo cells in combination with topotecan.

In general, the combination with the cytostatic drug topotecan led to a total reversal of ABCG2 mediated drug resistance by all compounds tested.

As negative control, analogous experiments were performed using U-118 MG cells, which do not express the ABCG2 transporter. A nontoxic concentration of 10 nM topotecan in combination with different concentrations of the modulators did not influence cell proliferation at all (as an example shown for compound **32** in **Figure 3.19**).
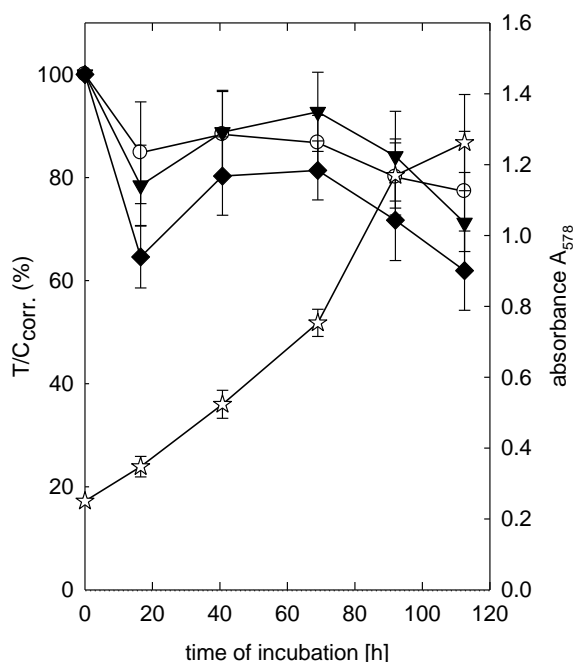
Figure 3.19: Effect of compound **32** (UR-COP269) in combination with topotecan on proliferating U-118 MG cells; vehicle (*open stars*), topo [10 nM] (*open circles*), topo [10 nM] + **32** [100 nM] (*filled inverted triangles*), topo [10 nM] + **32** [500 nM] (*filled diamonds*).

3.4.5 Chemical stability of selected ABCG2 transporter modulators under physiological conditions

As a prerequisite for planned *in vivo* studies, the most potent inhibitors were subjected to preliminary biopharmaceutical investigations with a focus on stability in mouse plasma. Because of the lack of drug like properties (rapid enzymatic cleavage in mouse plasma) of recently described and characterized 1st and 2nd generation modulators like compounds **1**, **2** and **4** [Kühnle, 2010; Ochoa-Puentes et al., 2011], the chemical structures of these target compounds were modified in a bioisosteric approach (replacement of the amide) with a main focus on stability resulting in a 3rd and 4th generation of modulators.

Bioisosteric replacements to create new molecules with improved biological properties to the parent compound are major objectives in successful structure-based drug design. Modification of a compound can attenuate toxicity and chemical stability, modify activity or alter pharmacokinetics. Whereas the classical bioisosteres involve structurally simple atoms or groups, nonclassical bioisosteres replace functional groups with a different number of atoms and/or different steric and electronic properties [Patani and LaVoie, 1996]. Classical bioisosterism comprises e.g. the replacement of hydrogen by fluorine classically exemplified by 5-fluoruracil derived from uracil or the isosteric substitution of an amino group for a hydroxyl group (folic acid and aminopterin).

Nonclassical bioisosterism includes the replacement of noncyclic structures with cyclic residues and vice versa or the replacement of functional groups [Lemke and Williams, 2012]. A successful story of bioisosteric replacement in drug discovery was shown for the angiotensin II receptor antagonist

losartan: With the replacement of the carboxylic acid residue of its lead structure by a tetrazol the oral bioavailabilty could significantly be improved [Herr, 2002; Dinges and Lamberth, 2012].

By analogy with the synthesis strategy described in this work, the replacement of a metabolic instable ester or amide with different heterocycles was shown previously [Eastwood et al., 2011; Monceaux et al., 2011]. Many other amide and ester isosteres are known including trifluoroethylamines (successfully shown for the cathepsin K inhibitor odanacatib [Gauthier et al., 2008]) and oxadiazolines [Sun et al., 2012] as well as isoxazole-ether scaffolds as acetyl group replacement of acetylcholine [Yu et al., 2012].

3.4.5.1   Chemical stability in culture medium and human CPD plasma

To investigate the stability of the new classes of modulators, the compounds were incubated in different media, including DMEM supplemented with 10% FCS as well as in murine and human plasma over a period of 24 hours. HPLC was used for analysis.

Compounds **7-10**, **12**, **19** and **34**, selected representatives of the biphenyl, indole and triazole series, respectively, were incubated at 37 °C in human plasma or DMEM + 10% FCS. All compounds were completely stable over a period of 24 hours in both media. Stabilities of compounds **12** and **19** after 24 h are displayed in **Figures 3.20-3.21**.
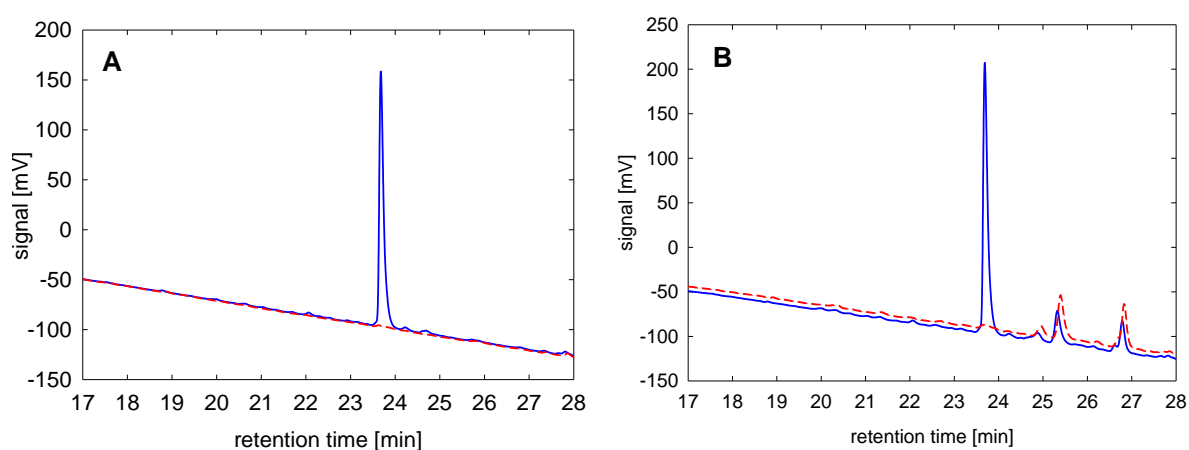
Figure 3.20: Chromatogram of a DMEM (+ 10% FCS) sample (**A**) and a human (CPD) plasma sample (**B**) containing compound **12** (final concentration: 3 μM) after 24 h of incubation at 37 °C; the respective chromatogram of a blank DMEM and plasma sample, processed by the same method, is shown as red dotted line.
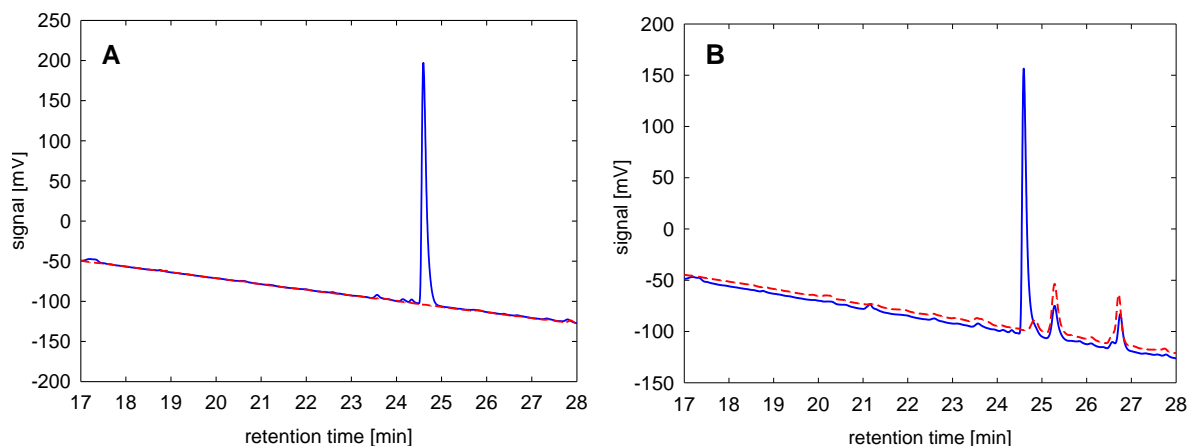
Figure 3.21: Chromatogram of a DMEM (+ 10% FCS) sample (**A**) and a human (CPD) plasma sample (**B**) containing compound **19** (final concentration: 3 μM) after 24 h of incubation at 37 °C; the respective chromatogram of a blank DMEM and plasma sample, processed by the same method, is shown as red dotted line.

3.4.5.2   Chemical stability in mouse plasma

As compounds **1**, **2** and **4** are prone to rapid enzymatic cleavage in mouse plasma at the central benzanilide moiety within 30 min (displayed in **Figure 3.22** for compound **4**) the new 3rd generation modulators were also investigated for their chemical stability in murine plasma.

Surprisingly, in mouse plasma, in all compounds of these new series of modulators the ester group is prone to enzymatic cleavage yielding the inactive carboxylic acid. However, hydrolysis of the ester occurs much slower than cleavage of the benzanilide of the 1st and 2nd generation modulators.

Regarding stability in murine plasma, all ester bearing indole-, biphenyl- and triazole-type modulators, respectively, have a half-life of about 24 h compared to 10 min in case of compounds **1**, **2** and **4**. Additionally, the quinoline carboxamide group was cleaved, though to a very small extent (as an example: see compound **12** in **Figure 3.24**).

Although the chemical stability in murine plasma was improved by the renunciation of the lable amide core, the results are not yet satisfactory. In search for completely stable ABCG2 modulators, the hydrolysis-sensitive ester group of the 3rd generation triazole series was replaced by a ketone (compounds **50-52**). These '4th generation modulators' were completely stable in murine plasma over a period of 24 h (**Figure 3.26**) and are therefore appropriate for *in vivo* investigations in nude mice.
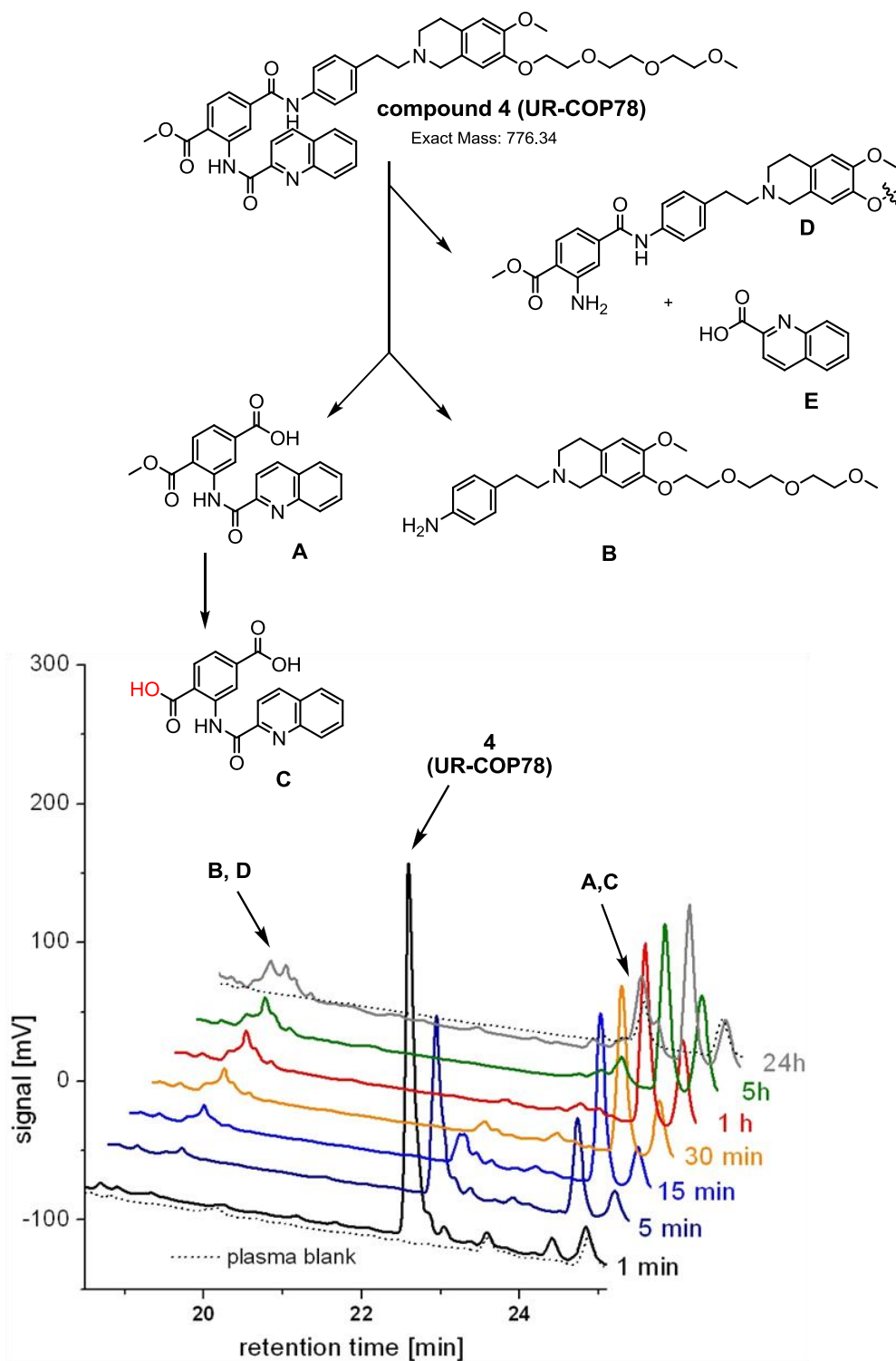
Figure 3.22: Enzymatic degradation of UR-COP78 (**4**), when incubated in mouse plasma over a period of 24 h at 37 °C: Complete decomposition to compounds **A** and **B** (main cleavage products) within 30 minutes. Additionally, the ester group and the quinoline carboxamide group were cleaved (HPLC analysis, UV detection at 210 nm). The cleavage products were identified by HPLC-MS analysis. Fragment E was only detectable by HPLC-MS-analysis (**Figure 3.23**)
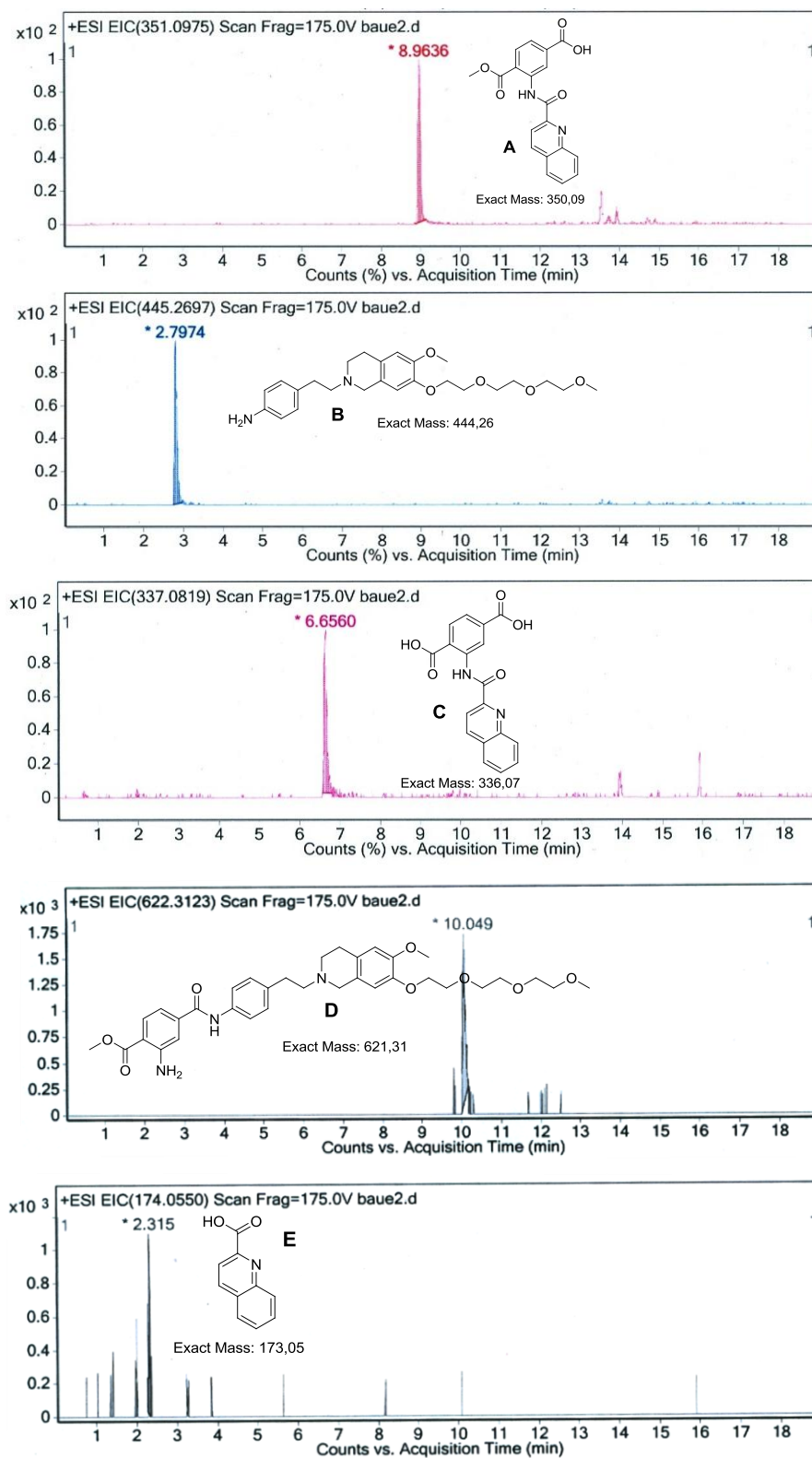
Figure 3.23: HPLC-MS analysis of compound **4** in mouse plasma: Detection of the cleavage products **A-E** in plasma of NMRI (nu/nu) mice, 24 h after incubation at 37 °C.
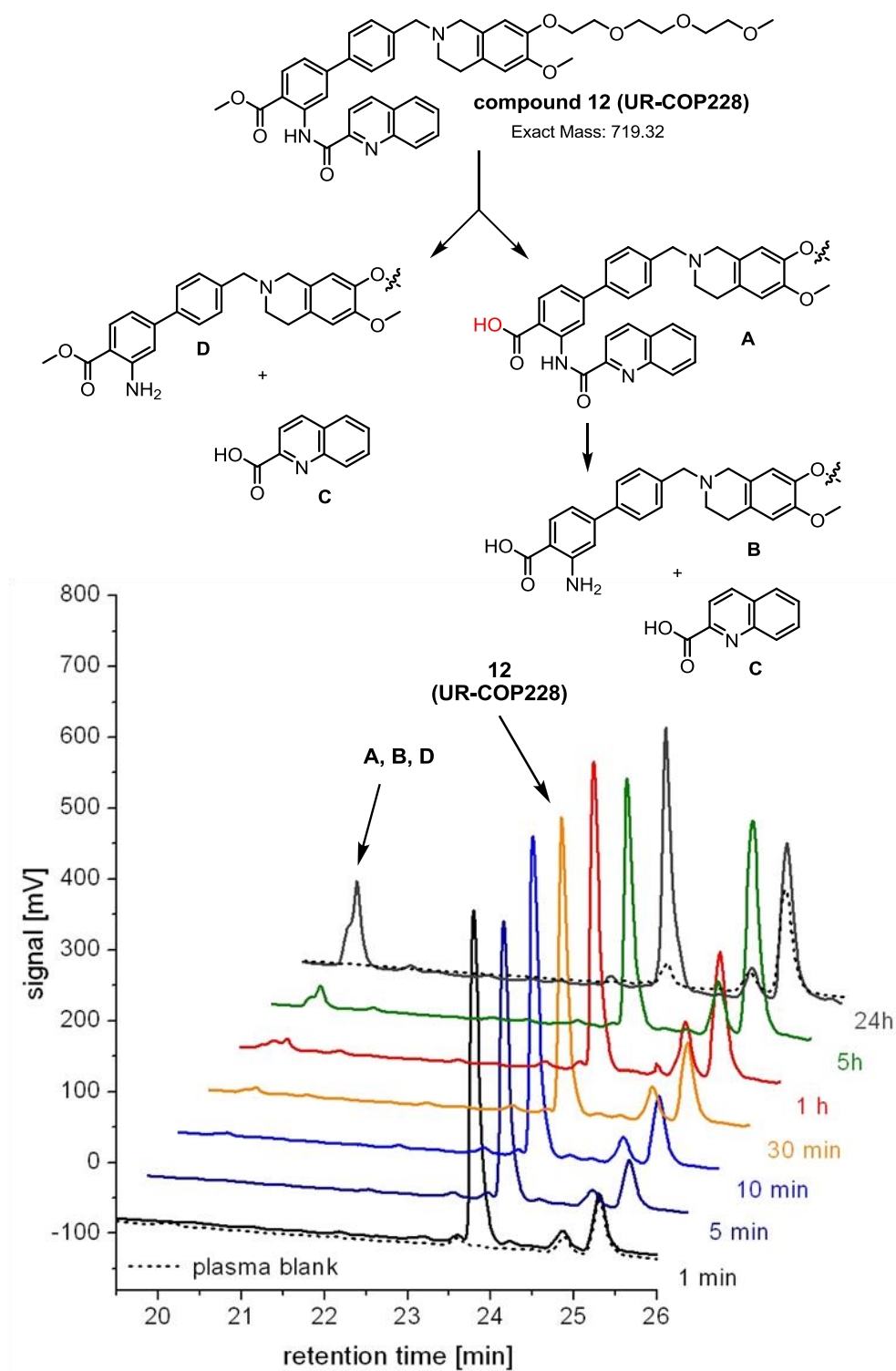
Figure 3.24: Enzymatic degradation of UR-COP228 (**12**), when incubated in mouse plasma over a period of 24 h at 37 °C. Main cleavage product: compound **A**, the inactive caboxylic acid after ester hydrolysis. Additional fragments appeard after degradation of the quinoline carboxamide group (HPLC analysis, UV detection at 210 nm). The cleavage products were identified by HPLC-MS analysis. Fragment C was only detectable by HPLC-MS-analysis (**Figure 3.25**)
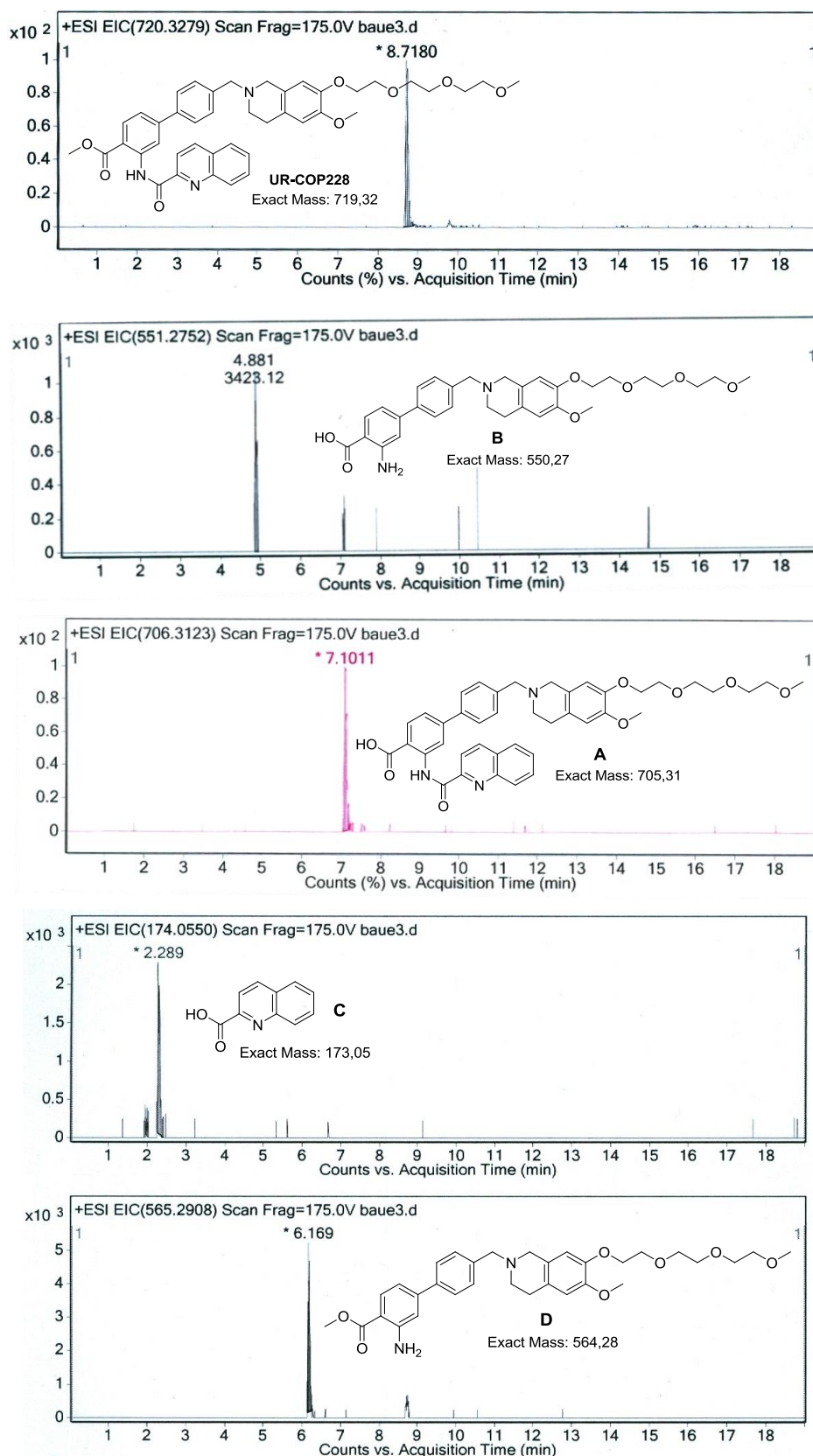
Figure 3.25: HPLC-MS analysis of compound **12** in mouse plasma: Detection of the cleavage products **A-D** in plasma of NMRI (nu/nu) mice, 24 h after incubation at 37 °C.

Figure 3.26: Chemical stability of compound **51** when incubated in mouse plasma over a period of 24 h at 37 °C (HPLC analysis, UV detection at 210 nm).

3.4.5.3   Esterase activity in human and murine plasma
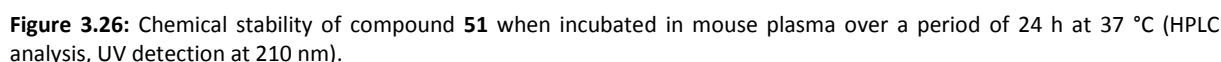
Because of the different stabilities of 3rd generation modulators after incubation for 24 h in human and murine plasma, respectively, the enzymatic activity of unspecific esterases was compared spectrophotometrically. Murine plasma showed a 1.5-fold higher esterase activity [6.04 ± 0.20 U/mL] in comparison to human CPD plasma [4.26 ± 0.26 U/mL] (Stefan Huber, personal communication). 3rd generation modulators bearing an ester group where therefore hydrolyzed in murine, but not in human plasma. There was no activity difference between CPD and heparinized human blood.

3.4.6   Effect of selected ABCG2 transporter modulators on the transport of Daunorubicin in a blood-brain barrier model

It was previously shown that the brain multidrug resistance protein (BMDP), the porcine homolog to the human ABCG2 gene, is highly expressed in porcine brain capillary endothelial cells (PBCEC) [Eisenblätter and Galla, 2002]. Thus, these cells can be used for transport studies in an established blood-brain-brain barrier model measuring the capability of BMDP to transport ³H-daunorubicin across a monolayer of PBCEC grown on porous filters in the presence of ABCG2 inhibitors. Daunorubicin was previously shown to be a substrate of the human homolog of BMDP [Doyle et al.,

1998]. PBCECs cultured on filter inserts, with the apical chamber corresponding to the blood and the basolateral chamber corresponding to the brain side *in vivo,* are morphologically polarized.

Tritium labeled daunorubicin was added to both compartments at identical concentrations. Upon addition of an ABCG2 inhibitor, the daunorubicin transport across the cell monolayer is hindered. The amount of daunorubicin which is transported from the basolateral to the apical compartment inversely correlates with the potency of an ABCG2 modulator.

The selective ABCG2 inhibitors fumitremorgin C (FTC), reference compound for ABCG2 inhibition in the used fluorescence-based microplate assays, and the two 1st generation modulators UR-ME4-1 (**1**) and UR-ME22-1 (**2**) were used for inhibition studies in the blood-brain barrier (BBB) model (**Figure 3.27**). Whereas at a concentration of 1 µM compounds **1** and **2** inhibit the transport of daunorubicin from the basolateral to the apical side of the PBCEC monolayer almost completely, FTC produced only moderate inhibition even at a concentration of 10 µM.
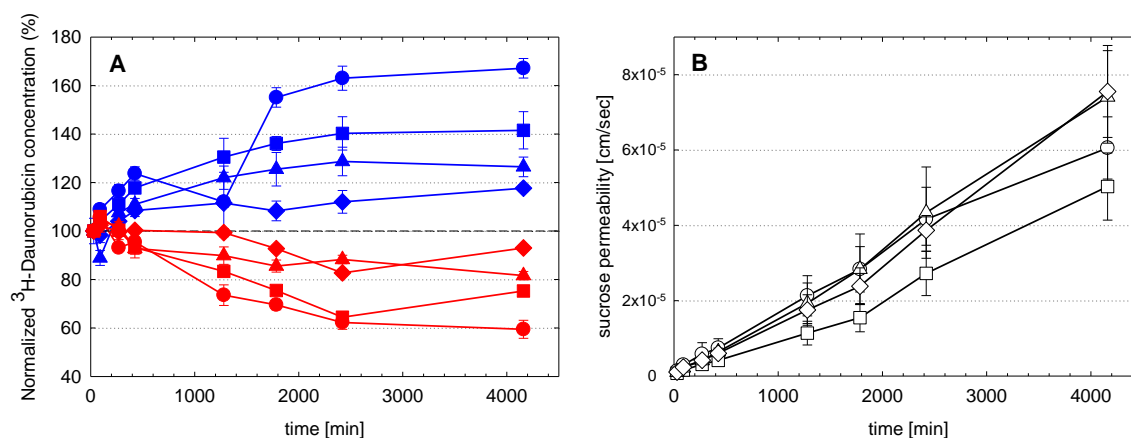
Figure 3.27:
A: Transendothelial transport of ^{3}H-daunorubicin across a PBCEC monolayer in presence of ABCG2 inhibitors: Fumitremorgin C [10 µM] (*squares*), compound **1** (UR-ME1-4) [1 µM] (*triangles*), compound **2** (UR-ME22-1) [1 µM] (*diamonds*), control (*circles*).
Concentrations of ^{3}H-daunorubicin were measured after 0.5, 6, 12, 24, 36, 48 and 72 h in each compartment (apical: blue; basolateral: red) and normalized to measurements at 0.5 h. The vertical bars for each data point represent the standard deviation of three replicate determinations. Transendothelial electrical resistance (n = 3): 1310 ± 379 Ωcm^{2}.
B: Corresponding tightness control of the endothelial cell monolayer in presence of ABCG2 inhibitors indicated by paracellular permeability of ^{14}C-sucrose.

In the Hoechst 33342 assay, the use of fetal calf serum (FCS) and the contained proteins may be beneficial for solubility properties of the ABCG2 modulators providing a reservoir in aqueous systems. Tests in the BBB model, however, were performed under serum-free conditions. Therefore, it is even more astonishing that compounds **1** and **2** were obviously superior to FTC [10 µM] in the BBB model at a concentration of 1 µM, whereas in the Hoechst 33342 they only reached 2/3 of the efficacy of FTC [10 µM] in the presence of FCS. The effective concentrations of free compounds may be much lower in the BBB model in comparison to the Hoechst 33342 assay.

Compounds **32** (UR-COP269) and **33** (UR-COP272) are among the most potent ABCG2 inhibitors known so far with IC_{50} values of 59 nM and 46 nM, respectively, and maximal inhibitory effects of over 100% (Hoechst33342 assay). Although comparable to compounds **1** and **2** in potency and clearly superior in efficacy (H33342 assay), the extent of daunorubicin transport inhibition was not as significant as for the aforementioned ABCG2 modulators in the blood-brain barrier model (**Figure 3.28**). In general, daunorubicin transport did not significantly change in presence of compounds **32** and **33**, respectively, at a concentration of 1 µM in comparison to the control. A concentration of 2 µM in case of **32** produced a moderate transport inhibition. The results for **33** [3 µM] are not reliable as sucrose permeability obviously increased when incubating the monolayer with this high modulator concentration.

Besides different grades of precipitation (water solubility) due to milieu differences between the Hoechst assay and the BBB model (buffer composition, pH value, hydrocortisone supplementation), species differences (human ABCG2 transporter in the H33342 assay vs. the porcine homolog in the BBB model) have to be considered for the inconsistent testing results in the two test system.
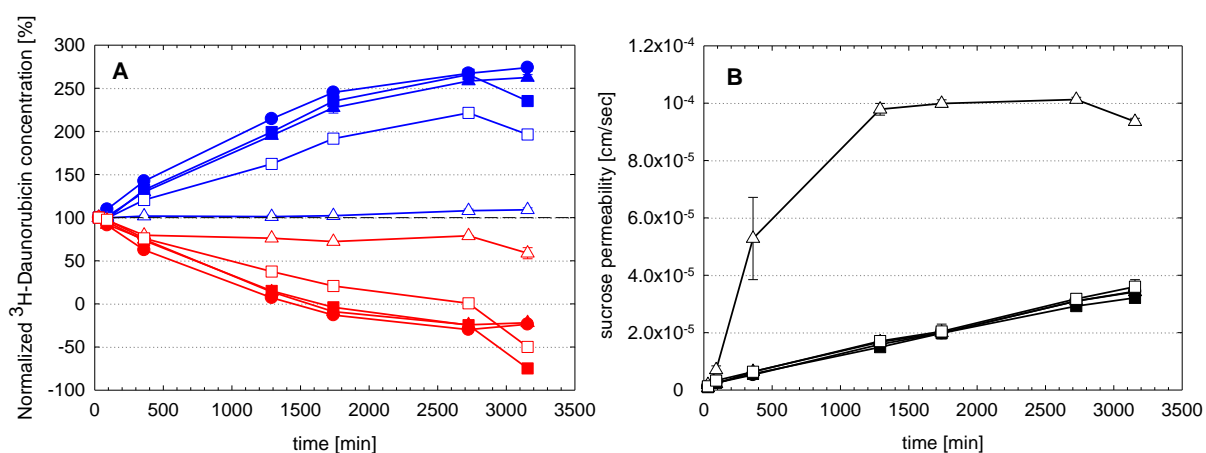
Figure 3.28:
A: Transendothelial transport of ^{3}H-daunorubicin across a PBCEC monolayer in presence of ABCG2 inhibitors: Compound **32** [1 µM] (*filled squares*) and [2 µM] (*open squares*), compound **33** [1 µM] (*filled triangles*) and [3 µM] (*open triangles*), control (*circles*).
Concentrations of ^{3}H-daunorubicin were measured after 0.5, 6, 12, 24, 36, 48 and 72 h in each compartment (apical: blue; basolateral: red) and normalized to measurements at 0.5 h. The vertical bars for each data point represent the standard deviation of three replicate determinations. Transendothelial electrical resistance (n = 3): 1617 ± 128 Ωcm^2.
B: Corresponding tightness control of the endothelial cell monolayer in presence of ABCG2 inhibitors indicated by paracellular permeability of ^{14}C-sucrose.

To elucidate, whether the synthesized modulators act as substrates or as inhibitors of the ABCG2 transporter, the BBB model experiment was performed as described above with a fixed concentration of the modulator on both sides of the monolayer. After different periods of time samples of each compartment were collected and changes in the modulator concentration on the two sides tried to be calculated by means of HPLC analysis. Unfortunately the concentration of the compounds in the samples was too low to be significantly quantified by HPLC analysis. The way of

detection was not sensitive enough as only UV detection was available for these classes of compounds.

3.5   Summary and conclusions

During this work, a series of about 50 new putative ABCG2 transporter modulators was synthesized in dependence on former described tariquidar analogs [Kühnle, 2010] with a major focus on the design of more stable, drug-like compounds.

Firstly, the problem of insufficient water solubility of the lead compound UR-ME22-1 (**2**) was attempted to be solved by the introduction of triethylenglycol chains resulting in a 2nd generation of ABCG2 modulators with compound **4** (IC$_{50}$ 130 nM, I$_{max}$ 88%) as most promising representative. The insertion of polyethylene glycol moieties led to a clearly increased efficacy.

Secondly, the instable benzamide moiety, point attack of esterases in mouse plasma, was replaced in a bioisosteric approach giving four new classes of 3rd generation modulators with a biphenyl system, an indole, a triazole and a quinoline, respectively, as central core structure.

Among these four new classes of BCRP modulators, compounds **29**, **32** and **33** bearing an indole are the most potent ones with IC$_{50}$ values in the H33342 assay of 132 nM, 59 nM and 46 nM, respectively, and maximal inhibitory effects of over 100% in comparison to the standard ABCG2 inhibitor fumitremorgin C. Stability tests in mouse plasma revealed that these 3rd generation modulators are neither immune against enzymatic degradation with the ester as new hydrolysis weak point.

In search for completely stable ABCG2 modulators, the synthesized structures were further improved replacing the hydrolysis-sensitive ester by a ketone giving compounds **50-52** which are stable in mouse plasma over a period of 24 hours. Additionally, together with **32** and **33**, compounds **50-52** turned out to be the most potent ABCG2 modulators reported so far.

The results were confirmed in a kinetic chemosensitivity assay where the incubation of topotecan resistant MCF-7/Topo cells with a combination of topotecan and the modulators led to a complete reversal of ABCG2-mediated drug resistance.

Because of coincident fluorescent properties of some compounds with the Hoechst 33342 dye, a second assay system was established using mitoxantrone as fluorescent substrate. Additionally, the selectivity against other ABC proteins was tested using an already existing calcein-AM assay for tests at the P-gp [Höcherl, 2010] and a new arranged microplate assay for inhibition tests at the ABCC1 transporter with reversan as standard compound.

Inconsistent results were obtained for the testing of compounds **1**, **2**, **32** and **33** in a porcine blood-brain barrier model. Although less efficient compared to FTC in the Hoechst 33342 assay, compounds **1** and **2** were clearly superior to the standard compound in the serum-free BBB model. The inhibitory effect of compounds **32** and **33** in the *in vitro* model was not as significant as for **1** and **2** although superior in the cell based microplate assay in both potency and efficacy.

The question rises whether species differences of the expressed ABCG2 transporters contributes to these results.

Subsequent projects with a major focus on the determination of the way of ABCG2 modulation are of major interest. The question has to be answered whether the synthesized compounds act as substrates or as inhibitors at the ABCG2 transporter. Therefore, different approaches are conceivable, either the use of radio-labeled ABCG2 modulators in the BBB model as a sensitive method or the testing of the compounds in an ATPase assay (see Chapter 6).

3.6   References

Ahmed-Belkacem, A., Pozza, A., Macalou, S., et al. Inhibitors of cancer cell multidrug resistance mediated by breast cancer resistance protein (BCRP/ABCG2). *Anti-Cancer Drugs* **2006**, 17(3), 239-243.

Allen, J. D., van Loevezijn, A., Lakhai, J. M., et al. Potent and specific inhibition of the breast cancer resistance protein multidrug transporter in vitro and in mouse intestine by a novel analogue of fumitremorgin C. *Mol. Cancer. Ther.* **2002**, 1(6), 417-425.

Bakos, E., Evers, R., Szakacs, G., et al. Functional multidrug resistance protein (MRP1) lacking the N-terminal transmembrane domain. *J. Biol. Chem.* **1998**, 273(48), 32167-32175.

Bates, S. E., Robey, R., Miyake, K., et al. The role of half-transporters in multidrug resistance. *J. Bioenerg. Biomembr.* **2001**, 33(6), 503-511.

Bauer, S., Ochoa-Puentes, C., Sun, Q., et al. Quinoline Carboxamide-Type ABCG2 Modulators: Indole and Quinoline Moieties as Anilide Replacements. *ChemMedChem* **2013**, 8, 1773-1778.

Bernhardt, G., Reile, H., Birnböck, H., et al. Standardized kinetic microassay to quantify differential chemosensitivity on the basis of proliferative activity. *J. Cancer Res. Clin. Oncol.* **1992**, 118(1), 35-43.

Breedveld, P., Beijnen, J. H. and Schellens, J. H. Use of P-glycoprotein and BCRP inhibitors to improve oral bioavailability and CNS penetration of anticancer drugs. *Trends Pharmacol. Sci.* **2006**, 27(1), 17-24.

Chen, Y. N., Mickley, L. A., Schwartz, A. M., et al. Characterization of adriamycin-resistant human breast cancer cells which display overexpression of a novel resistance-related membrane protein. *J. Biol. Chem.* **1990**, 265(17), 10073-10080.

Cooray, H. C., Blackmore, C. G., Maskell, L., et al. Localisation of breast cancer resistance protein in microvessel endothelium of human brain. *Neuroreport* **2002**, 13(16), 2059-2063.

Crone, C. and Olesen, S. P. Electrical resistance of brain microvascular endothelium. *Brain Res.* **1982**, 241(1), 49-55.

de Bruin, M., Miyake, K., Litman, T., et al. Reversal of resistance by GF120918 in cell lines expressing the ABC half-transporter, MXR. *Cancer Lett.* **1999**, 146(2), 117-126.

Dinges, J. and Lamberth, C. *Bioactive Heterocyclic Compound Classes*. Wiley-VCH Verlag GmbH & Co. KG, Weinheim, Germany, 2012.

Dodic, N., Dumaitre, B., Daugan, A., et al. Synthesis and activity against multidrug resistance in Chinese hamster ovary cells of new acridone-4-carboxamides. *J. Med. Chem.* **1995**, 38(13), 2418-2426.

Doyle, L. A. and Ross, D. D. Multidrug resistance mediated by the breast cancer resistance protein BCRP (ABCG2). *Oncogene* **2003**, 22(47), 7340-7358.

Doyle, L. A., Yang, W., Abruzzo, L. V., et al. A multidrug resistance transporter from human MCF-7 breast cancer cells. *Proc. Natl. Acad. Sci. U S A* **1998**, 95(26), 15665-15670.

Eastwood, P., Gonzalez, J., Gomez, E., et al. Indolin-2-one p38alpha inhibitors III: bioisosteric amide replacement. *Bioorg. Med. Chem. Lett.* **2011**, 21(21), 6253-6257.

Egger, M. Inhibition of ABC Transporters Associated with Multidrug Resistance. PhD thesis, University of Regensburg, Germany, 2009.

Eisenblätter, T. and Galla, H. J. A new multidrug resistance protein at the blood-brain barrier. *Biochem. Biophys. Res. Commun.* **2002**, 293(4), 1273-1278.

Eisenblätter, T., Hüwel, S. and Galla, H. J. Characterisation of the brain multidrug resistance protein (BMDP/ABCG2/BCRP) expressed at the blood-brain barrier. *Brain Res.* **2003**, 971(2), 221-231.

Evers, R., Kool, M., van Deemter, L., et al. Drug export activity of the human canalicular multispecific organic anion transporter in polarized kidney MDCK cells expressing cMOAT (MRP2) cDNA. *J. Clin. Invest.* **1998**, 101(7), 1310-1319.

Fellner, S., Bauer, B., Miller, D. S., et al. Transport of paclitaxel (Taxol) across the blood-brain barrier in vitro and in vivo. *J. Clin. Invest.* **2002**, 110(9), 1309-1318.

Fetsch, P. A., Abati, A., Litman, T., et al. Localization of the ABCG2 mitoxantrone resistance-associated protein in normal tissues. *Cancer Lett.* **2006**, 235(1), 84-92.

Franke, H., Galla, H. and Beuckmann, C. T. Primary cultures of brain microvessel endothelial cells: a valid and flexible model to study drug transport through the blood-brain barrier in vitro. *Brain Res. Protoc.* **2000**, 5(3), 248-256.

Franke, H., Galla, H. J. and Beuckmann, C. T. An improved low-permeability in vitro-model of the blood-brain barrier: transport studies on retinoids, sucrose, haloperidol, caffeine and mannitol. *Brain Res.* **1999**, 818(1), 65-71.

Gauthier, J. Y., Chauret, N., Cromlish, W., et al. The discovery of odanacatib (MK-0822), a selective inhibitor of cathepsin K. *Bioorg. Med. Chem. Lett.* **2008**, 18(3), 923-928.

Gottesman, M. M., Fojo, T. and Bates, S. E. Multidrug resistance in cancer: role of ATP-dependent transporters. *Nat. Rev. Cancer* **2002**, 2(1), 48-58.

Han, B. and Zhang, J. T. Multidrug resistance in cancer chemotherapy and xenobiotic protection mediated by the half ATP-binding cassette transporter ABCG2. *Curr. Med. Chem. Anticancer Agents* **2004**, 4(1), 31-42.

Herr, R. J. 5-Substituted-1H-tetrazoles as carboxylic acid isosteres: medicinal chemistry and synthetic methods. *Bioorg. Med. Chem.* **2002**, 10(11), 3379-3393.

Höcherl, P. New tariquidar-like ABCB1 modulators in cancer chemotherapy: Preclinical pharmacokinetic / pharmacodynamic investigations and computational studies. PhD thesis, University of Regensburg, Germany, 2010.

Hoheisel, D., Nitz, T., Franke, H., et al. Hydrocortisone reinforces the blood-brain properties in a serum free cell culture system. *Biochem. Biophys. Res. Commun.* **1998**, 247(2), 312-315.

Hubensack, M. Approaches to Overcome the Blood-Brain Barrier in the Chemotherapy of Primary and Secondary Brain Tumors: Modulation of P-glycoprotein 170 and Targeting of the Transferrin Receptor. PhD thesis, University of Regensburg, Germany, 2005.

Hubensack, M., Müller, C., Höcherl, P., et al. Effect of the ABCB1 modulators elacridar and tariquidar on the distribution of paclitaxel in nude mice. *J. Cancer Res. Clin. Oncol.* **2008**, 134(5), 597-607.

Jäger, W. Classical resistance mechanisms. *Int. J. Clin. Pharmacol. Ther.* **2009**, 47(1), 46-48.

Jekerle, V., Klinkhammer, W., Reilly, R. M., et al. Novel tetrahydroisoquinolin-ethyl-phenylamine based multidrug resistance inhibitors with broad-spectrum modulating properties. *Cancer Chemother. Pharmacol.* **2007**, 59(1), 61-69.

Jekerle, V., Klinkhammer, W., Scollard, D. A., et al. In vitro and in vivo evaluation of WK-X-34, a novel inhibitor of P-glycoprotein and BCRP, using radio imaging techniques. *Int. J. Cancer.* **2006**, 119(2), 414-422.

Kannan, P., Telu, S., Shukla, S., et al. The "Specific" P-Glycoprotein Inhibitor Tariquidar Is Also a Substrate and an Inhibitor for Breast Cancer Resistance Protein (BCRP/ABCG2). *ACS Chem. Neurosci.* **2011**, 2(2), 82-89.

Kohno, K., Kikuchi, J., Sato, S., et al. Vincristine-resistant human cancer KB cell line and increased expression of multidrug-resistance gene. *Jpn. J. Cancer Res.* **1988**, 79(11), 1238-1246.

Kühnle, M. Experimental therapy and detection of glioblastoma: investigation of nanoparticles, ABCG2 modulators and optical imaging of intracerebral xenografts. PhD thesis, University of Regensburg, Germany, 2010.

Kühnle, M., Egger, M., Müller, C., et al. Potent and selective inhibitors of breast cancer resistance protein (ABCG2) derived from the p-glycoprotein (ABCB1) modulator tariquidar. *J. Med. Chem.* **2009**, 52(4), 1190-1197.

Lemke, T. L. and Williams, D. A. *Foye's Medicinal Chemistry*. Lippincott Williams & Wilkin, 2012.

Levin, V. A. Relationship of octanol/water partition coefficient and molecular weight to rat brain capillary permeability. *J. Med. Chem.* **1980**, 23(6), 682-684.

Matsson, P., Englund, G., Ahlin, G., et al. A global drug inhibition pattern for the human ATP-binding cassette transporter breast cancer resistance protein (ABCG2). *J. Pharmacol. Exp. Ther.* **2007**, 323(1), 19-30.

Monceaux, C. J., Hirata-Fukae, C., Lam, P. C., et al. Triazole-linked reduced amide isosteres: an approach for the fragment-based drug discovery of anti-Alzheimer's BACE1 inhibitors. *Bioorg. Med. Chem. Lett.* **2011**, 21(13), 3992-3996.

Ochoa-Puentes, C., Bauer, S., Kühnle, M., et al. Benzanilide-Biphenyl Replacement: A Bioisosteric Approach to Quinoline Carboxamide-Type ABCG2 Modulators. *ACS Med. Chem. Lett.* **2013**, 4(4), 393-396.

Ochoa-Puentes, C., Höcherl, P., Kühnle, M., et al. Solid phase synthesis of tariquidar-related modulators of ABC transporters preferring breast cancer resistance protein (ABCG2). *Bioorg. Med. Chem. Lett.* **2011**, 21(12), 3654-3657.

Patani, G. A. and LaVoie, E. J. Bioisosterism: A Rational Approach in Drug Design. *Chem. Rev.* **1996**, 96(8), 3147-3176.

Rabindran, S. K., Ross, D. D., Doyle, L. A., et al. Fumitremorgin C reverses multidrug resistance in cells transfected with the breast cancer resistance protein. *Cancer Res.* **2000**, 60(1), 47-50.

Robey, R. W., Polgar, O., Deeken, J., et al. ABCG2: determining its relevance in clinical drug resistance. *Cancer Metastasis Rev.* **2007**, 26(1), 39-57.

Roe, M., Folkes, A., Ashworth, P., et al. Reversal of P-glycoprotein mediated multidrug resistance by novel anthranilamide derivatives. *Bioorg. Med. Chem. Lett.* **1999**, 9(4), 595-600.

Sarkadi, B., Ozvegy-Laczka, C., Nemet, K., et al. ABCG2 -- a transporter for all seasons. *FEBS. Lett.* **2004**, 567(1), 116-120.

St-Pierre, M. V., Serrano, M. A., Macias, R. I., et al. Expression of members of the multidrug resistance protein family in human term placenta. *Am. J. Physiol. Regul. Integr. Comp. Physiol.* **2000**, 279(4), R1495-1503.

Staud, F., Vackova, Z., Pospechova, K., et al. Expression and transport activity of breast cancer resistance protein (Bcrp/Abcg2) in dually perfused rat placenta and HRP-1 cell line. *J. Pharmacol. Exp. Ther.* **2006**, 319(1), 53-62.

Sun, Z. Y., Asberom, T., Bara, T., et al. Cyclic Hydroxyamidines as Amide Isosteres: Discovery of Oxadiazolines and Oxadiazines as Potent and Highly Efficacious gamma-Secretase Modulators in Vivo. *J. Med. Chem.* **2012**, 55(1), 489-502.

Valdameri, G., Gauthier, C., Terreux, R., et al. Investigation of chalcones as selective inhibitors of the breast cancer resistance protein: critical role of methoxylation in both inhibition potency and cytotoxicity. *J. Med. Chem.* **2012**, 55(7), 3193-3200.

Valdameri, G., Genoux-Bastide, E., Peres, B., et al. Substituted chromones as highly potent nontoxic inhibitors, specific for the breast cancer resistance protein. *J. Med. Chem.* **2012**, 55(2), 966-970.

Valdameri, G., Pereira Rangel, L., Spatafora, C., et al. Methoxy stilbenes as potent, specific, untransported, and noncytotoxic inhibitors of breast cancer resistance protein. *ACS Chem. Biol.* **2012**, 7(2), 322-330.

Wegener, J., Hakvoort, A. and Galla, H. J. Barrier function of porcine choroid plexus epithelial cells is modulated by cAMP-dependent pathways in vitro. *Brain Res.* **2000**, 853(1), 115-124.

Winter, E., Lecerf-Schmidt, F., Gozzi, G., et al. Structure-Activity Relationships of Chromone Derivatives toward the Mechanism of Interaction with and Inhibition of Breast Cancer Resistance Protein ABCG2. *J. Med. Chem.* **2013**, 56(24), 9849-9860.

Yamazaki, R., Nishiyama, Y., Furuta, T., et al. Novel acrylonitrile derivatives, YHO-13177 and YHO-13351, reverse BCRP/ABCG2-mediated drug resistance in vitro and in vivo. *Mol. Cancer. Ther.* **2011**, 10(7), 1252-1263.

Yu, L. F., Tuckmantel, W., Eaton, J. B., et al. Identification of novel alpha4beta2-nicotinic acetylcholine receptor (nAChR) agonists based on an isoxazole ether scaffold that demonstrate antidepressant-like activity. *J. Med. Chem.* **2012**, 55(2), 812-823.

Zhang, S., Wang, X., Sagawa, K., et al. Flavonoids chrysin and benzoflavone, potent breast cancer resistance protein inhibitors, have no significant effect on topotecan pharmacokinetics in rats or mdr1a/1b (-/-) mice. *Drug. Metab. Dispos.* **2005**, 33(3), 341-348.

Zhang, S., Yang, X. and Morris, M. E. Flavonoids are inhibitors of breast cancer resistance protein (ABCG2)-mediated transport. *Mol. Pharmacol.* **2004**, 65(5), 1208-1216.

*C*hapter *4*

4　Drug-like properties of new ABCG2 modulators

4.1　Introduction

4.1.1　Trends in medicinal chemistry and drug development

Nowadays, pharmaceutical companies mainly perform high-throughput screening to discover so called 'hits', which are subject of hit-to-lead processes to identify lead compounds for further optimization, aiming at the development of potential drug candidates. Computational methods as well as automated sample preparation and screening procedures led to drug libraries with an enormous number of new compounds. These techniques are used to improve chemical structures regarding biological activity to predict the compounds' physicochemical properties as well as drug absorption or oral bioavailability [Stegemann et al., 2007]. However, improving a compound's potency at the cost of solubility and bioavailability is a prominent negative trend in 'rational drug design' mainly resulting from higher H-bonding properties and increasing molecular weights attended by a enhanced lipophilicity, [Lipinski, 2000]. As a consequence, numerous compounds never pass clinical trials or become commercially available drugs.

4.1.2　The 'Rule of Five'

Lipinski's 'Rule of 5' is based on the drug-like properties of several thousand drugs [Lipinski et al., 2001] and a useful fingerpost or starting point in drug design and discovery with regard to bioavailability.

According to this rule, good absorption and permeation is more likely when:

1. There are not more than 5 H-bond donors (sum of OHs and NHs);
2. There are not more than 10 H-bond acceptors (sum of Os and Ns);
3. The molecular weight is ≤ 500 Da;
4. The log*P* is ≤ 5.

The 'Rule of 5' addresses all therapeutic areas. Nonetheless, there are occasional limitations. It should be modified for centrally active compounds [Pajouhesh and Lenz, 2005; Reichel, 2006] as CNS penetration is more likely if:

1. There are ≤ 3 H-bond donors;
2. There are ≤ 7 H-bond acceptors;
3. The molecular weight is < 400-500 Da;
4. The log*P* is ≤ 5.

Furthermore, it is limited, if there is a biological transporter involved. The commonly applied molecular weight cutoff of 500 Da per se, is not an excluding criterion regarding acceptable bioavailability [Veber et al., 2002], as shown for successful big drug molecules such as cyclosporine [Ptachcinski et al., 1986] or tacrolimus (FK506) [Venkataramanan et al., 1995].

4.1.3   Plasma protein binding

Besides the fulfillment of various physicochemical requirements, information about plasma protein binding (PPB) of drug candidates is key in drug development to enable estimates and extrapolations to *in vivo* kinetics as early as possible. Different methods for quantifying the binding of drugs to plasma proteins are available: equilibrium dialysis, ultrafiltration and ultracentrifugation are the most common ones. The results are usually expressed as %PPB (equation 4), where [D] is the free drug concentration and [DP] is the concentration of the drug protein complex:

$$\%PPB = 100 \cdot \frac{[DP] - [D]}{[DP]} \qquad \text{(equation 4)}$$

Based on binding experiments, actual concentrations of the free drug are calculated and used as a base for *in vivo* experiments. Information on PPB is also of great importance with regard to toxicity, because plasma proteins may act as reservoirs, and accumulation of drugs in tissues may substantially influence their plasma concentrations and retention times in the body.

The extent of drug distribution into tissues mainly depends on the degree of binding to the plasma proteins albumin, alpha-1-acid glycoprotein and lipoproteins. As only the free (unbound) drug is available for distribution in the body to get access to cellular targets, extensive PPB limits a drug's efficacy and influences its pharmacokinetics. On the other hand, drugs (mostly with relatively poor solubility), are often more easily transported *in vivo* when bound to plasma proteins.

Prominent clinical drugs with a high protein binding of over 90% are the antieptileptic drug phenytoin [Lund et al., 1972; Peterson et al., 1982], the anticoagulant warfarin [Mungall et al., 1984] or the anti-diabetic agent tolbutamide [Miners et al., 1982].

A further phenomenon observed in binding studies, is displacement of the drug from protein: interactions between two compounds can increase the free fraction of a drug highly bound to plasma proteins as the interacting drug displaces the substance of interest from its binding site. Drug displacement from PPB has to be regarded with suspicion due to potential clinically relevant interactions [Rolan, 1994] including unanticipated cross-reactions in terms of toxicity.

The phenomenon of poor water solubility and high lipophilicity is often associated with increased binding to proteins. However, for targeting the CNS, lipophilicity of compounds is favorable to overcome the endothelium of the blood-brain barrier [Waterhouse, 2003].

The discrepancies between solubility, plasma protein binding and BBB penetration of drug candidates pose a challenge even in case of 'drug-like' compounds, as the physico-chemical properties are not always predictive for adequate access to the brain and a corresponding biological activity in the CNS [Abbott et al., 2010].

To find candidates for future *in vivo* studies in nude mice, the characterization of the most potent ABCG2 modulators with respect to solubility and plasma protein binding is required. Attempts are described in this chapter.

4.2   Materials and methods

4.2.1   Drugs and chemicals

PBS was made of 8.0 g/L NaCl, 1.0 g/L $Na_2HPO_4 \cdot 2\ H_2O$, 0.20 g/L KCl, 0.20 g/L KH_2PO_4 and 0.15 g/L $NaH_2PO_4 \cdot H_2O$ (pH 7.4). Fetal calf serum (FCS) was obtained from Biochrom (Berlin, Germany) and Hoechst 33342 from Invitrogen (Karlsruhe, Germany). Fluorescence was measured with a LS50 B spectrometer from Perkin Elmer (Rodgau, Germany). If not otherwise stated, chemicals (p.a. quality) were obtained from Merck (Darmstadt, Germany). Milli-Q system (Millipore, Eschborn, Germany) was used for water purification.

4.2.2   Solubility

4.2.2.1   Comparison of solubilities in different media

As poor water solubility is a characteristic feature of the classes of ABCG2 modulators synthesized in our group, the solubility of representative examples, compounds **32**, **33**, **51**, and **52**, in DMSO was compared to the solubility in PBS (pH 7.4), determined by HPLC. Therefore, the same concentrations of the compound (0.5-20 µM) were prepared in DMSO and PBS, respectively. The samples were centrifuged (10 min, 16,000 g) with an Eppendorf centrifuge 5415R (Eppendorf, Hamburg, Germany) to separate undissolved compound, and the supernatants were filtered through Phenex™-RC 4 mm Syringe Filters 0.2 µm (Phenomenex, Aschaffenbug, Germany). As the compounds are readily soluble in DMSO, a linear calibration curve was calculated from the peak areas obtained for the samples diluted with DMSO, assuming that the compounds were completely dissolved. The peak areas for the corresponding centrifuged PBS samples were referred to the calibration line to calculate solute concentrations in buffer.

UV detection of compounds **32**, **51** and **52** was performed at 210 nm with a Waters (Eschborn, Germany) system using a 2487 UV detector (described in section 3.3.7.3) or a Merck-Hitachi HPLC system composed of a L-5000 controller, a 655A-12 pump, a 655A-40 autosampler, a F-1050 fluorescence spectrometer and a L-4250 UV-VIS detector on a Eurospher-100 C_{18} column (250 × 4 mm, 5 µm; Knauer, Berlin, Germany) at a flow rate of 0.8 mL/min under helium degassing and the following gradient: MeCN/0.05% TFA (aq.): 0 min: 60/40, 30 min: 95/5, 31 min: 95/5, 33 min: 95/5. UV detection for compound **33** was performed at 280 nm and fluorescence detection for compound **51** at 470 nm after excitation at 370 nm.

4.2.2.2 Fluorescence spectra of Hoechst 33342 after intercalation in DNA in the absence and presence of test compounds

All ABC transporter inhibition assays, described in Chapter 3, were performed either in culture medium supplemented with FCS or in buffer containing serum albumin. The question arose, why the newly synthesized compounds are so potent and efficient in these aqueous assay systems despite obviously limited water solubility. In this context it is of utmost importance to ensure that the measured increase in fluorescence in the assay, resulted from ABC transporter modulation and subsequent DNA intercalation of the dye (Hoechst 33342), but not from, cell-dependent interference between the Hoechst dye and the compounds. Therefore, compounds **33**, **34** and **51** were incubated without MCF-7/Topo cells in the presence and the absence of Hoechst 33342 on the basis of the protocol of the ABCG2 inhibition assay: the compounds were diluted in PBS containing 10% FCS and 8 µM of the Hoechst 33342 dye to a final concentration of 10 µM according to the standard procedure described in section 3.3.5.1. DNA (10 µg/mL), isolated from calf thymus, was added to the mixture to allow a DNA intercalation. DMSO served as negative control. The fluorescence spectrum of Hoechst 33342 in the presence of 1% (v/v) DMSO was compared with the spectra in the presence of the modulators.

4.2.3 Plasma protein binding studies

The binding of hydrophobic molecules to human serum albumin (HSA) or bovine serum albumin (BSA), an ortholog of HSA, has been extensively studied for years. Albumins are the most abundant proteins in the blood circulation (55% of all serum proteins) [Anderson and Anderson, 2002] and known to act as transporters for various drugs [Takehara et al., 2009]. To determine the extent of plasma protein binding of the newly synthesized modulators, the applicability of different methods was explored.

4.2.3.1 Ultrafiltration

Ultrafiltration was performed with Amicon Ultra-0.5 mL Centrifugal Filters (regenerated cellulose membrane, nominal molecular weight limit: 10 kDa) from Merck Millipore (Darmstadt, Germany) and Nanosep® Centrifugal Devices (modified polyethersulfone membrane) from Pall GmbH (Dreieich, Germany), respectively, at 16,000 g using an Eppendorf 5415R centrifuge.

4.2.3.2   Isothermal titration calorimetry

Isothermal titration calorimetry (ITC) is a widely used technique to study biological processes at the molecular level, especially to characterize binding affinities of ligands to a protein. Thereby, ITC measures small changes of temperature during the reaction and allows the simultaneous determination of thermodynamic parameters such as heat of binding (enthalpy; ΔH), number of binding sites (n) or the calculation of the binding constant K [Santos et al., 2007]. ITC experiments and the instrumental set-up (**Figure 4.1**) are described below.

The solution in the syringe containing the test compound was titrated into the sample cell (37 °C) with the protein solution. Every injection causes a change in heat, resulting in a change in temperature in the sample cell in comparison to the reference cell. The change in power, which was required to return the sample cell to 37 °C, was recorded with every injection till all binding sites of the protein in the sample cell were saturated (heat signal diminishes).

Isothermal titration calorimetry was carried out at the Institute of Organic Chemistry (Prof. Dr. B. König) using a VP-ITC Micro Calorimeter (MicroCal, Northhampton, MA). Selected synthesized modulators were used as titrants and were pipetted into a BSA solution (sample cell). To ensure that the established method and instrumental set-up worked, a standard compound was tested: propranolol hydrochloride (Sigma, Munich, Germany), soluble in water, was chosen as test compound because corresponding binding constants are extensively referenced in the literature. Therefore, a solution of 5 mM propranolol HCl (in PBS) was injected in 5 μL-steps into the sample cell containing a 1 mM protein (BSA) solution (in PBS).
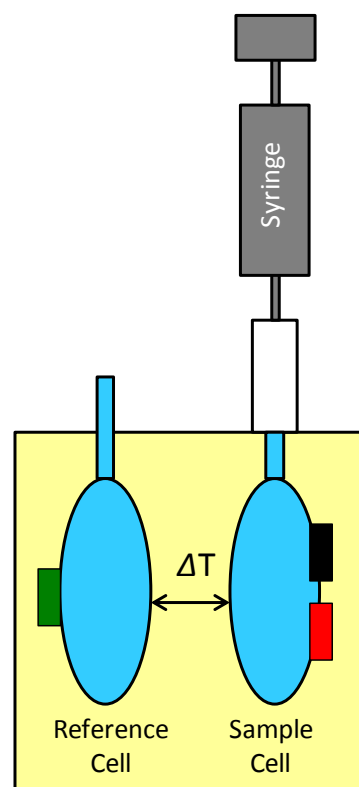
Figure 4.1: An ITC instrument consists of two identical cells surrounded by an adiabatic jacket (*yellow*). Reference heater (*green*), cell feedback heater (*black*) and calibration heater (*red*) detect temperature differences between the reference and the sample cell upon ligand titration into the sample cell containing the protein; illustration adapted from [Pierce et al., 1999].

4.2.3.3   Equilibrium dialysis

To evaluate the extent of protein binding, equilibrium dialysis was performed with DispoEquilibrium DIALYZERS and a Fast Micro-Equilibrium DIALYZER dialysis chamber (250 μL chamber; polycarbonate membrane, 0.01 μm pore size) from Harvard Apparatus (Holliston, MA, USA).
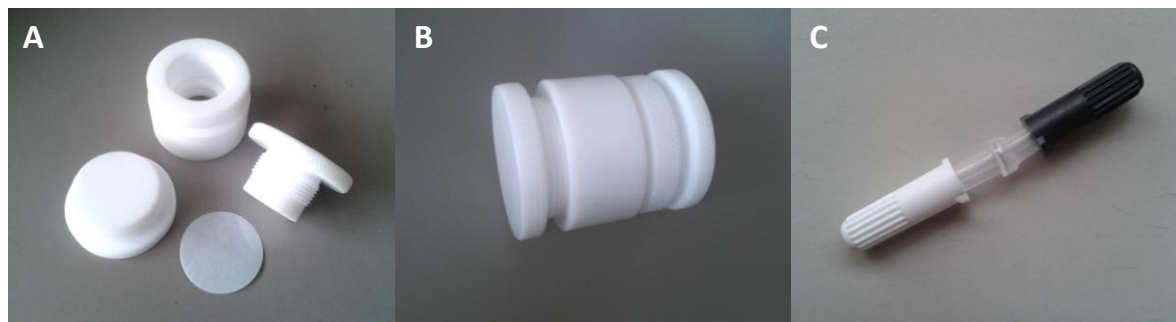
Figure 4.2: A, B) Fast Micro-Equilibrium DIALYZER dialysis chamber (250 µL); **C**) DispoEquilibrium DIALYZER; Harvard Apparatus (Holliston, MA).

The theory behind is as follows (according to 'Guide to Equilibrium Dialysis', Harvard Apparatus; http://www.nestgrp.com/pdf/Ap1/EqDialManual.pdf): two chambers are separated by a dialysis membrane with a defined molecular weight cut off (MWCO) such that the protein-bound compound is retained. A known concentration of a compound - small enough to pass freely through the membrane - is placed into one of the chambers (total volume: 250 µL). An equivalent volume of protein (BSA), dissolved in the same solvent at defined concentration is then placed in the other chamber. The compound diffuses across the membrane and either binds to the protein to a certain extent or remains free in solution. Diffusion across the membrane and binding continues until equilibrium has been reached. At equilibrium, the concentration of the free compound in solution is the same in both chambers and can be used to evaluate the binding characteristics of the sample.

To consider that the used compounds show sufficient solubility and cross the membrane, recovery studies were performed without protein with different synthesized modulators and quantified by HPLC. Recovery analysis was performed at 37 °C (water bath) under stirring for 4 h or overnight. For this purpose, compounds **4**, **50**, **51** and **52**, respectively, were dissolved at a concentration of 100 µM in PBS or PBS supplemented with various amounts of DMSO (5%, 10%, 15% or 20%).

4.2.3.4   Protein binding analysis via fluorescent spectroscopy

Fluorescence measurements were performed at the LS50 B spectrometer from Perkin Elmer at a scan rate of 240. Hellma® fluorescence cuvettes (SUPRASIL® quartz, semi Micro, pathlength 10 mm) and fatty acid/globulin free bovine serum albumin (BSA; ≥98% purity) were both purchased from Sigma (Munich, Germany). Fluorescence spectra were recorded after excitation at 280 nm (BSA) or 370 nm (fluorescent ABCG2 modulators).

4.2.3.5 HPLC-based methods to determine protein binding of selected ABCG2 modulators

Three representative ABCG2 modulators were kindly characterized in the laboratory of Origenis GmbH (Martinsried, Germany) by means of three different methods to estimate the extent of plasma protein binding.

The chromatographic hydrophobicity index (CHI) was calculated using a C_{18} column by converting retention times to volume percentage organic-phase concentrations. The CHI scale can be related to octanol/water partition coefficients (log$D$ values at pH 7.4) by taking the number of H-bond donor groups in the molecules into account.

Binding was measured on a column containing immobilized HSA, and membrane affinity was calculated via immobilized artifical membrane (IAM) HPLC analysis to model drug partitioning between an aqueous (mobile) phase and a cell membrane (IAM column). By all three methods, basically, the retention times of the compounds were measured (UV/VIS detection) and linearly ($y = a \cdot T_r + b$) converted into the corresponding parameter based on a calibration data set of thousands of compounds (Dr. M. Thormann, personal communication, 2013).

4.3 Results and discussion

4.3.1 Solubility of selected ABCG2 modulators

All investigations described in this chapter were severely compromised by poor water solubility of the synthesized ABCG2 modulators. To obtain at least a rough estimation of lipophilicity and solubility in water, different methods were applied.

4.3.1.1 Computational calculations

First calculations of the lipophilicity of selected ABCG2 modulators were performed with the ACD/Labs chemistry software 12.0 (Advanced Chemistry Development, Inc., Toronto, Canada).

Table 4.1: Computational predictions regarding water solubility of selected ABCG2 modulators.

Compd.	Molecular Weight [Da]	log$P$ [a]	log$D$ [b]	Solubility [c] [mg/L]
4	776.87	4.65	4.12	0.12
12	719.82	4.90	4.66	0.36
16	866.01	4.45	3.91	9.49
31	640.73	5.68	5.08	0.04
32	772.88	4.91	4.32	0. 44
33	891.02	3.66	3.08	14.00
40	654.71	4.98	4.56	0.95
50	652.74	4.90	4.48	1.28
51	666.77	5.42	5.05	0.47
52	798.93	4.65	4.28	4.12
42	770.87	4.76	4.69	0.08
47	721.84	5.75	3.52	1.97

[a] Octanol-water partition coefficient: ratio of a compound's concentration in octanol and water at equilibrium, expressed as its decadic logarithm log$P$; [b] distribution constant at pH 7.4; [c] solubility in water at pH 7.4.

4.3.1.2 Solubility in DMSO and PBS

Compounds **32**, **33**, **51**, and **52** were investigated for their solubility in PBS and DMSO by means of HPLC analysis. Compounds **32, 33** and **51** were neither detectable by UV absorbance in the supernatant of the centrifuged PBS samples at 210 nm (Waters HPLC system) or 280 nm (compound **33**; Merck HPLC system), respectively, nor by fluorescence detection (compound **51**; Merck HPLC system). Although the detection limit of the used UV detector and different spectral properties of the modulators have to be considered, these negative results reveal that compounds **32**, **33** and **51** are virtually insoluble in aqueous media. By contrast, compound **52** was detectable in PBS though at a very low concentration (**Figure 4.3**).
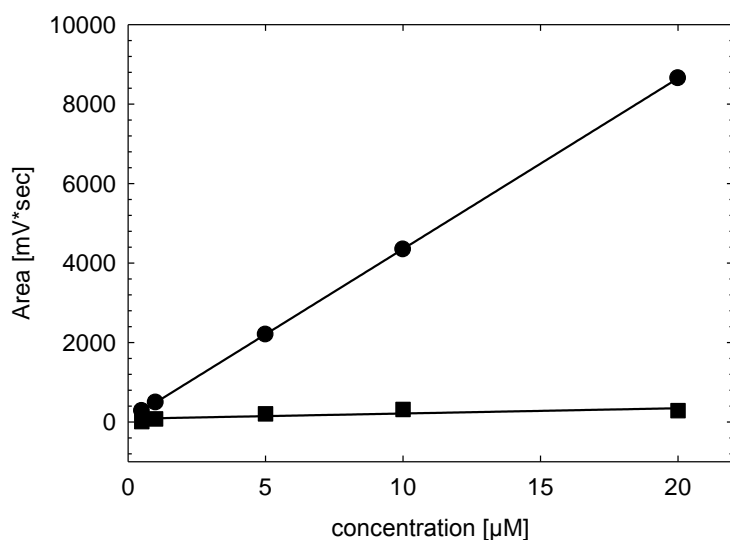
Figure 4.3: Main peak areas of compound **52** when diluted in DMSO (*circles*) or PBS (*squares*) at various concentrations obtained after RP-HPLC analysis performed with a Waters (Eschborn, Germany) HPLC system (UV detection at 210 nm); the applied gradient was as following: MeCN/0.05% TFA (aq.): 0 min: 15/85, 25 min: 80/20, 26 min: 95/5, 36 min: 95/5, 37 min: 15/85, 45 min: 15/85 at a constant flow rate of 1.0 mL/min.

The peak areas in the chromatograms of compound **52** for the centrifuged PBS samples were equivalent to the following free concentrations in buffer:

applied concentration [µM]	found concentration [µM]
0.50	-
1	0.04
5	0.34
10	0.60
20	0.53

Table 4.2: Found concentrations of compound **52** in PBS after centrifugation.

The highest concentration determined for compound **52** (0.6 µM) corresponds to a solubility of 0.48 mg/L in PBS. This value is ten times lower than the solubility calculated with ACD/Labs.

4.3.1.3 Fluorescence spectra of the Hoechst 33342 dye in the presence of different modulators

The fluorescence intensity of the Hoechst 33342 dye in presence of a modulator does not differ from the negative control (H33342 + DMSO) (**Figure 4.4**).

Fluorescence of the Hoechst 33342 dye is not affected by the combination with different modulators under Hoechst assay conditions, suggesting that the measured increase in fluorescence intensities in the Hoechst 33342 microplate assay, indeed, results from ABCG2 inhibition and subsequent DNA intercalation.

Hence, the modulators work in an aqueous assay system, despite low water solubility. It may be speculated that the synthesized compounds are actually much more potent than observed, i.e. lower concentrations suffice to reach a high ABCG2 inhibition, or they bind to protein in the medium (supplemented with FCS) and are thus brought into solution.
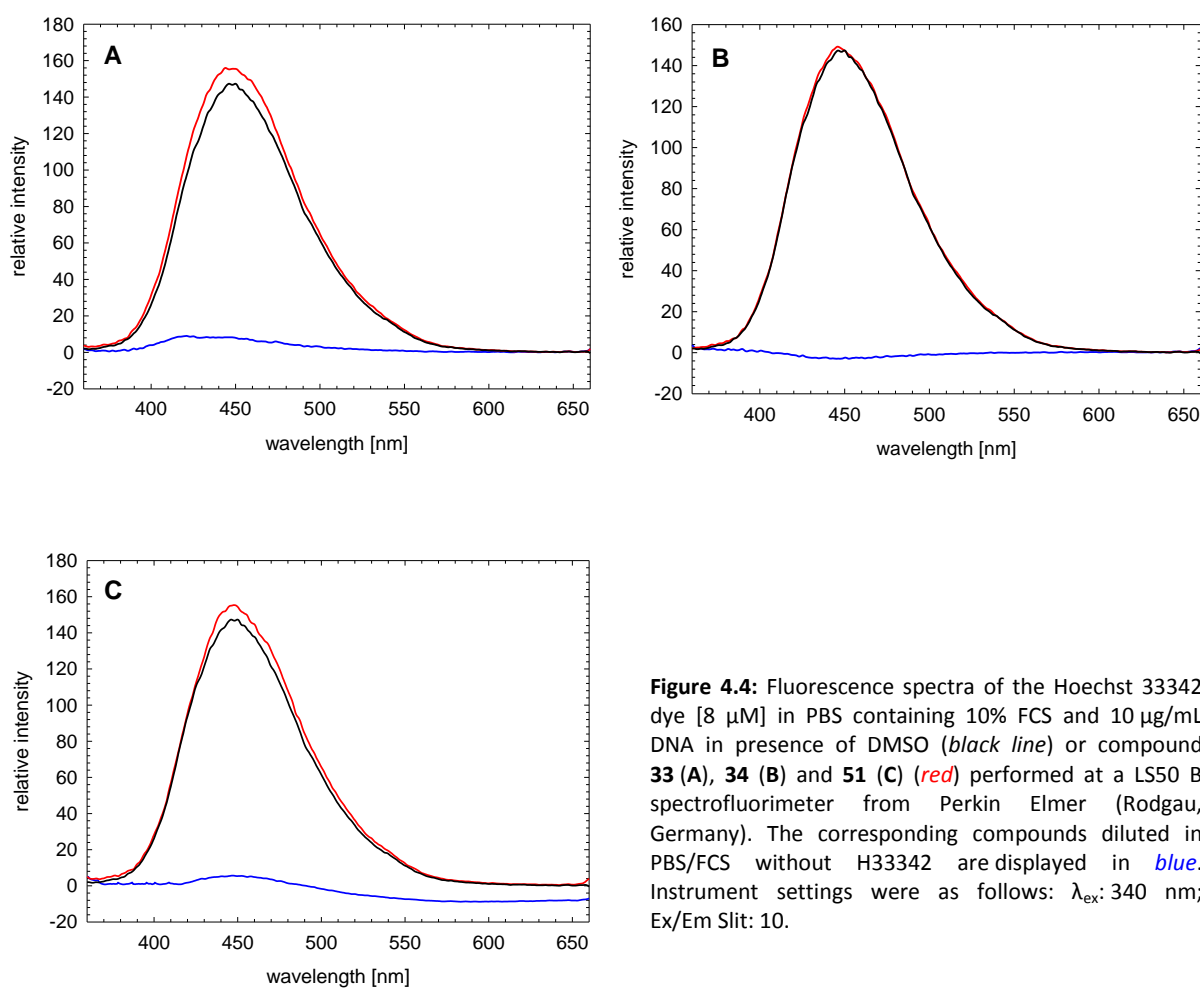
Figure 4.4: Fluorescence spectra of the Hoechst 33342 dye [8 µM] in PBS containing 10% FCS and 10 µg/mL DNA in presence of DMSO (*black line*) or compound **33** (**A**), **34** (**B**) and **51** (**C**) (*red*) performed at a LS50 B spectrofluorimeter from Perkin Elmer (Rodgau, Germany). The corresponding compounds diluted in PBS/FCS without H33342 are displayed in *blue*. Instrument settings were as follows: λ_{ex}: 340 nm; Ex/Em Slit: 10.

4.3.2   Extent of plasma protein binding

4.3.2.1   Ultrafiltration and ITC

Determination of plasma protein binding by ultrafiltration failed. Recovery studies revealed that the tested compounds completely adsorbed to the cellulose membranes.

Isothermal titration calorimetry was successfully performed for the test compound propranolol HCl (cf. **Figure 4.5**).
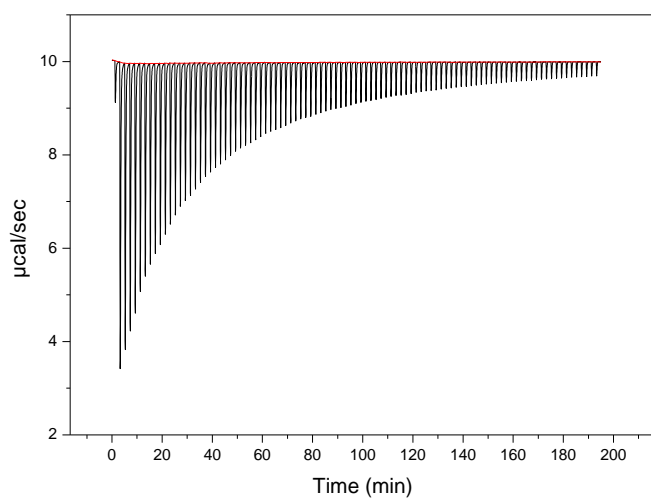
Figure 4.5: Titration thermogram of raw injection heats for titration of propranolol HCl [5 mM] into a BSA solution [1 mM].

In contrast, binding experiments via ITC were not successful with the synthesized ABCG2 modulators as these compounds are almost insoluble in water, and the composition of the solvent should be exactly the same for the titrant and the cell solution. Blank-experiments (negative control) with DMSO (titrant) as appropriate solvent for the synthesized compounds and BSA (in H_2O; sample cell) were performed prior to experiments, but produced unreliable results when the organic solvent was mixed with water. As DMSO causes protein precipitation and denaturation, pure DMSO is inappropriate as solvent for both titrant and BSA.

4.3.2.2   Equilibrium dialysis

Prior to PPB studies via equilibrium dialysis, recovery tests were performed with selected modulators. Compounds **4**, **50**, **51** and **52** were dissolved in PBS supplemented with DMSO (5%, 10%, 15% and 20%, respectively) and added to the sample chamber of the Fast Micro-Equilibrium DIALYZER. Unfortunately, after incubation over night at 37 °C, only compound **4** could be recovered to a small extent in PBS/DMSO at a ratio of at least 85/15 (HPLC analysis, UV detection at 210 nm), though, inadequate for PPB tests.

In general, all tested compounds were insoluble in pure PBS buffer. Likewise, DispoEquilibrium DIALYZERS were inappropriate for dialysis experiments as all tested compounds were adsorbed to the regenerated cellulose membrane.

4.3.2.3 Investigations on fluorescent modulators to determine protein binding

Intrinsic fluorescence of proteins is mainly due to the aromatic amino acids tryptophan (Trp) and (Tyr) (**Figure 4.6**), whereas the indole groups of Trp residues are the dominant source of emission.
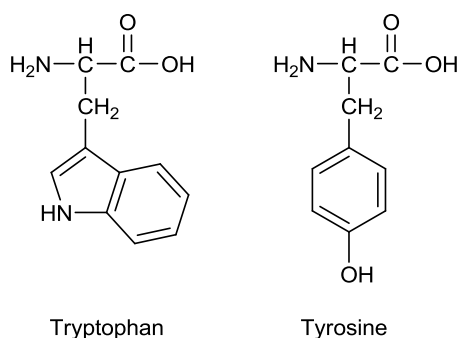
Figure 4.6: Chemical structures of the aromatic amino acids tryptophan and tyrosine.

Protein-protein association, protein unfolding as well as the binding of a ligand to a protein alters the sensitive microenvironment of Trp and its particular location within the protein thereby causing changes in the protein's tertiary and quaternary structure, resulting in changes in the fluorescence spectrum like maximum shifts to the red or the blue as well as intensity changes [Vivian and Callis, 2001].

Bovine serum albumin (66.2 kDa) contains 21 tyrosine and 2 tryptophan residues [Peters, 1985] that possess intrinsic fluorescence with Trp212, located in the core of the protein and Trp134 found on the surface of albumin. HSA, which shares 76% homology to BSA, contains only one Trp214 residue [Moriyama et al., 1996; Bujacz, 2012; Majorek et al., 2012; Patra et al., 2012].

Selected compounds of the triazole series described in Chapter 3, show distinctive fluorescence in organic solvents like chloroform (**Figure 4.7**). As fluorescent spectroscopy in protein analysis for investigations concerning protein binding and protein-ligand interactions is widely described in literature [Moriyama et al., 1996; Ladokhin, 2000; Takehara et al., 2009; Galecki et al., 2012], fluorescence may be used to determine the binding of the synthesized ABCG2 modulators to serum albumin.
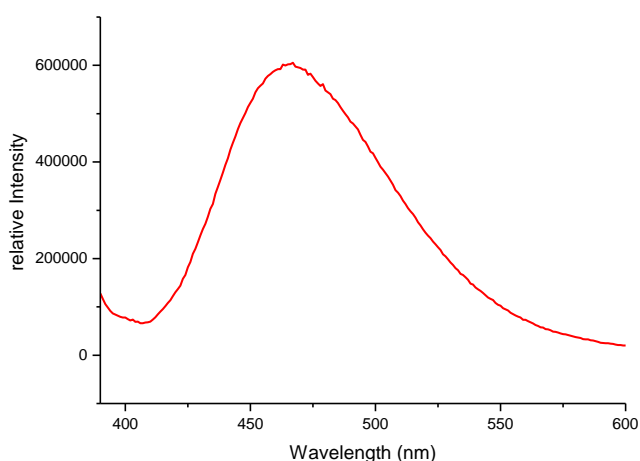
Figure 4.7: Emission spectrum of compound **34** in chloroform after excitation at 380 nm recorded at a Horiba 'Fluoromax 4' fluorescence spectrophotometer (HORIBA Jobin Yvon GmbH, Unterhaching, Germany) with Hellma® quartz cuvettes (1 cm); slit width: 10 nm.

Changes in either the fluorescence of the protein or the compounds upon binding can be exploited to study protein-ligand interactions. With excitation wavelengths between 370 and 380 nm and an emission around 470 nm, the fluorescence properties of the compounds do not interfere with those of serum albumin (λ_{ex}: 280 nm; λ_{em}: 350 nm).

Compound **52,** which is insoluble and therefore non-fluorescent in PBS (pH 7.4), shows weak fluorescence in DMSO (**Figure 4.8**). As described in Chapter 3, selected compounds show fluorescence under acidic HPLC conditions. With the addition of trifluoroacetic acid (TFA; Sigma, Munich, Germany) to the DMSO samples, the fluorescence intensity of **52** significantly increased (for further details also cf. section 4.3.3).
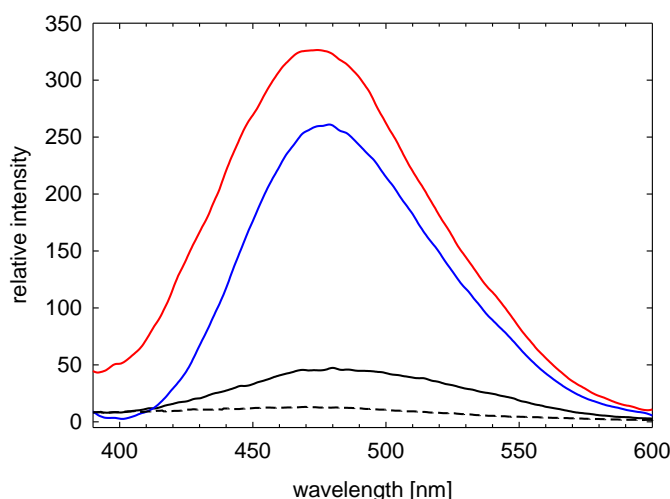
Figure 4.8: Fluorescence spectra of compound **52** [1 µM] after excitation at 370 nm in PBS (pH 7.4) (*black dotted line*), DMSO (*black*) and DMSO/TFA (aq.) at pH 5 (*blue*) and pH 3 (*red*); Ex/Em Slit: 5.

Due to insufficient solubility of fluorescent compounds in aqueous media, a minimum amount of 15% DMSO is required for spectroscopy. The pH dependent fluorescence of compound **52** at a concentration of 1 µM in PBS/DMSO (85/15) is shown in **Figure 4.9**.
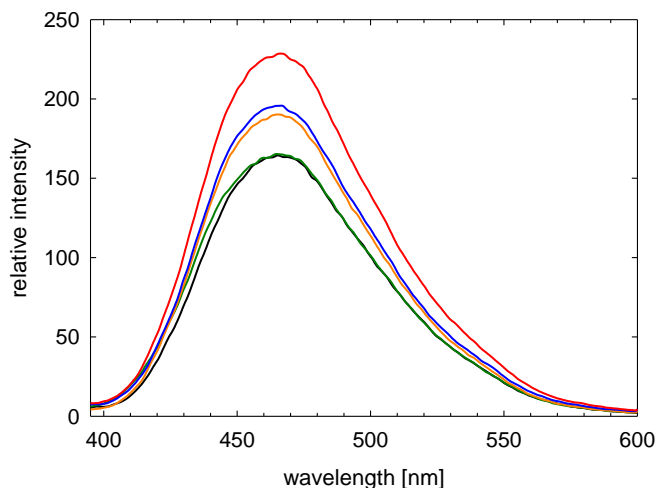
Figure 4.9: Fluorescence spectra of **52** [1 µM] in PBS/DMSO 85/15 at pH 6.5 (*gray*), pH 6.0 (*green*), pH 5.5 (*orange*), pH 5.0 (*blue*) and pH 3.0 (*red*), respectively; λ_{ex}: 370 nm; Ex/Em Slit: 10.

As fluorescence of albumin is affected by the local environment and thereby depending upon the solvent polarity, the effect of DMSO on the structural conformation of bovine serum albumin was estimated by monitoring the fluorescence properties of the protein.

Fluorescence spectra of BSA (λ_{ex}: 280 nm) dissolved in different PBS/DMSO combinations are shown in **Figure 4.10**: The fluorescence intensity decreased with increasing amounts of DMSO and a slight shift of the emission maximum from 350 nm (PBS) to 335 nm (PBS/DMSO 1:1) was visible.
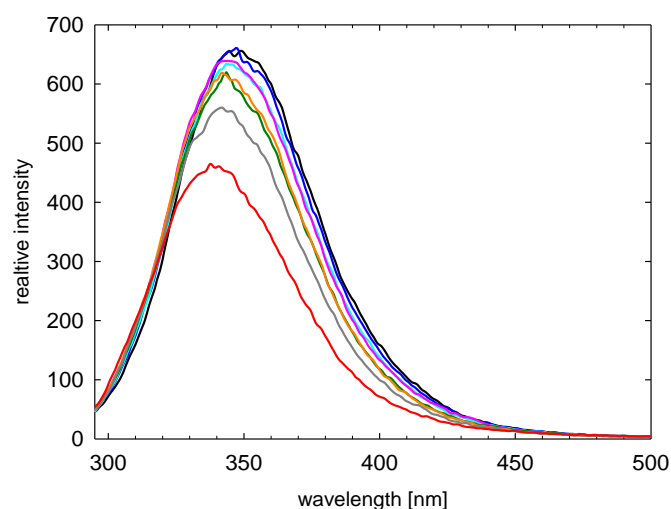
Figure 4.10: Fluorescence spectra of BSA [0.05 mg/mL] after excitation at 280 nm in different media: PBS (*black*) or PBS/DMSO: 95/5 (*dark blue*), 90/10 (*blue*), 85/15 (*pink*), 80/20 (*green*), 75/25 (*orange*), 70/30 (*gray*), 50/50 (*red*); Ex/Em Slit: 5.

In general, two contrary effects have to be considered influencing the fluorescent properties of albumin: by raising the percentage of DMSO, on the one hand, the polarity of the microenvironment of the protein (especially of the aromatic amino acid tryptophan) is drastically changed, and, on the other hand, an increasing DMSO concentration is assumed to denature and thereby unfold the protein. Precipitation also contributes to the decrease in fluorescence intensity so that a linear correlation between fluorescence intensities and the DMSO content cannot be hypothesized especially at a high DMSO content of 30% or 50%.

Similar results were recently published by Pabbathi et al. [Pabbathi et al., 2013]. The study revealed a doubling of the hydrodynamic radius of BSA in presence of 40% DMSO, suggesting complete unfolding of the protein.

A required amount of 15% DMSO due to solubility problems of ABCG2 modulators, indeed, hardly influenced the fluorescence properties of BSA (cf. **Figure 4.10**) suggesting that the native structure of BSA was retained under these conditions.

However, the attempt to quantify the extent of protein binding to BSA of the fluorescent compounds **51** and **52** in a mixture of PBS and DMSO at a ratio of 85:15 at pH 7 failed, due to lack of fluorescence emission at neutral pH. To guarantee sufficient fluorescence intensity of compounds **51** and **52**, protein binding investigations by means of fluorescent measurement have to be performed at pH values below 6.5 (**Figure 4.9**).

Moreover, the isoelectric point (IEP) of BSA is at pH 4.7 [Ge et al., 1998]. At pH 5 and below, acid-induced unfolding and denaturation of the protein occurs [Estey et al., 2006]. As shown in **Figure 4.11**, the fluorescence intensities of BSA are decreasing from pH 5.5 to pH 3 as a result of denaturation.
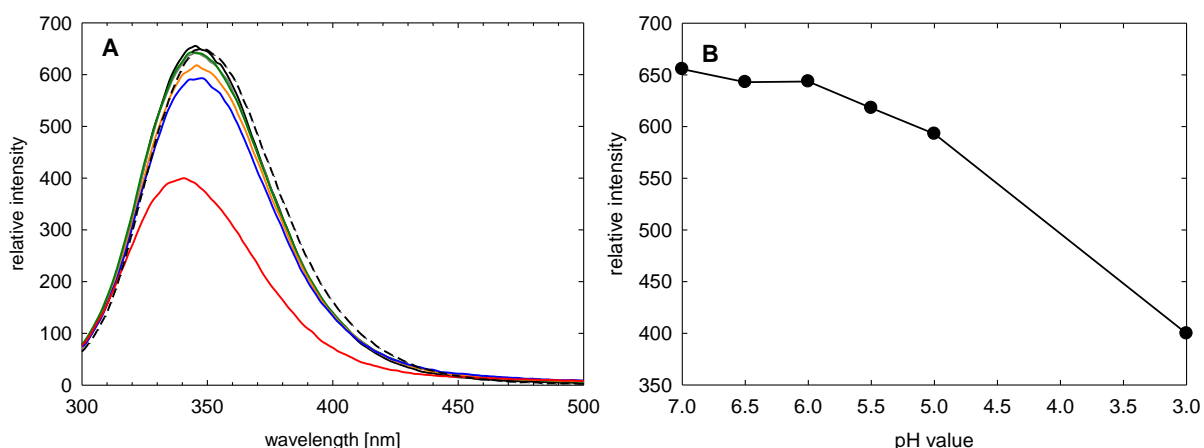
Figure 4.11: A) Fluorescence spectra of BSA [0.01 mg/mL] after excitation at 280 nm in PBS (pH 7; *black dotted line*) and in PBS/DMSO (85/15) at pH 7.0 (*black*), pH 6.5 (*gray*), pH 6.0 (*green*), pH 5.5 (*orange*), pH 5.0 (*blue*) and pH 3.0 (*red*), respectively; **B)** Maximal fluorescence intensities of BSA in PBS/DMSO 85/15 at 350 nm at descreasing pH value; Ex/Em Slit: 10.

Based on these results, a pH of 6.0 and a combination of PBS/DMSO at a ratio of 85/15 seems to be appropriate for fluorescence based binding experiments with compounds **51** and **52**, performed at the excitation and emission wavelengths of the modulators as sensitive changes in the fluorescence properties of BSA due to the use of DMSO may be mistaken for binding effects. **Figure 4.12** shows the fluorescence emission of compound **52** [1 µM] in the presence of bovine serum albumin at a molar ratio of 1/1.5 and 1/15 (BSA/ligand), respectively, over 60 minutes. The addition of BSA is

accompanied by an increase in the quantum yield of the fluorescent compound. Afterwards, the intensity continuously decreases within 30 minutes followed by a slight increase after 45 min to a constant value. The fluorescence intensity of compound **52** in presence of 0.1 mg/mL BSA halved within 1 h, whereas in presence of 1.0 mg/mL it was diminished to 70%. The effect of an increased quantum yield did not change significantly with different protein concentrations added.
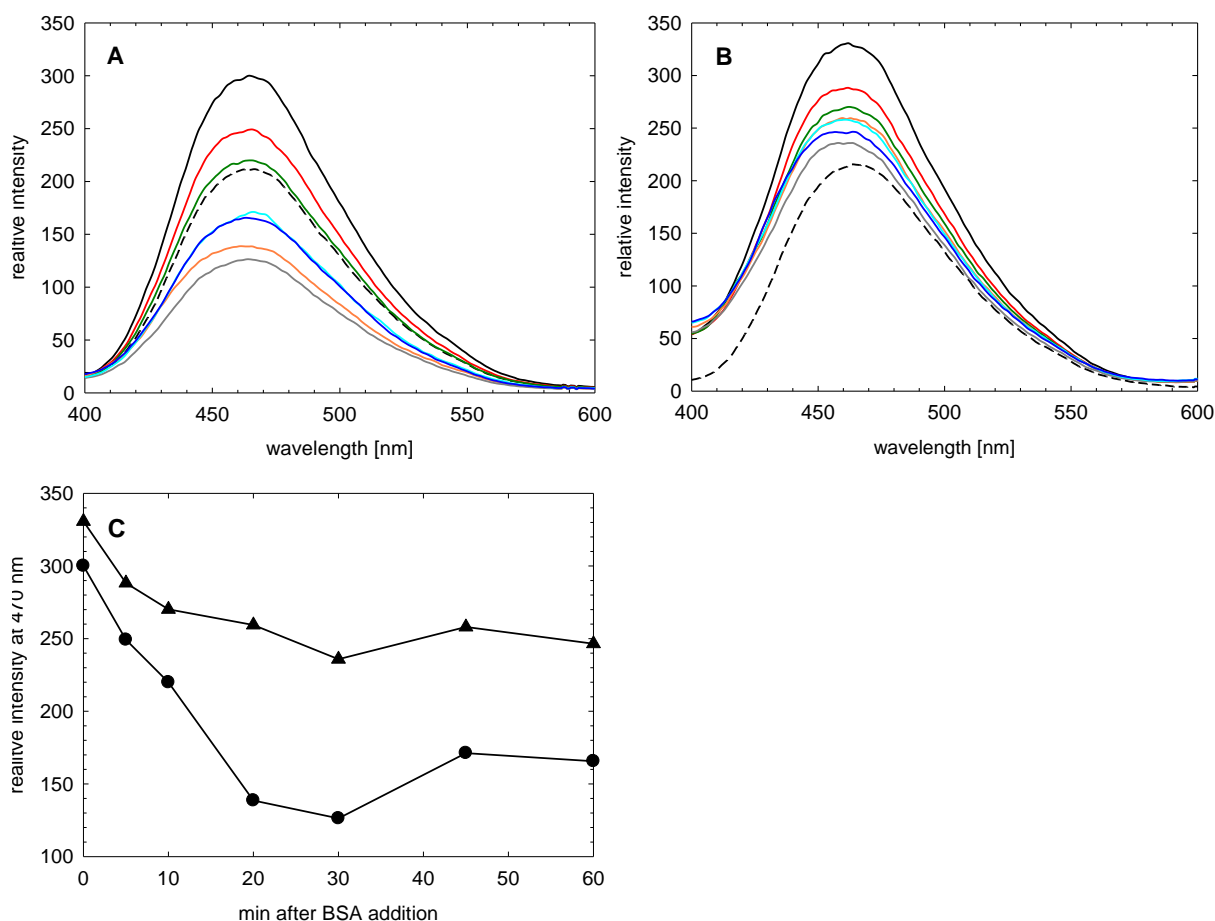
Figure 4.12: A,**B**) Fluorescence spectra of compound **52** [1 μM] after excitation at 370 nm in PBS/DMSO (85/15) at pH 6.0 alone (*black dotted line*) and in the same solvent in the presence of BSA [0.1 mg/mL] (**A**) or [1.0 mg/mL] (**B**) at different periods of time after BSA addition: 0 min (*black*), 5 min (*red*), 10 min (*green*), 20 min (*orange*), 30 min (*gray*), 45 min (*blue*), 60 min (*dark blue*); **C**) Maximal fluorescence intensities of **52** at 470 nm in PBS/DMSO containing 0.1 mg/mL (*filled circles*) and 1.0 mg/mL BSA (*filled trianlges*), respectively, as a function of time after protein addition; Ex/Em Slit: 10.

The gradient in fluorescence intensity over 60 min is difficult to interpret. It is conceivable that equilibrium between free and bound compound is reached after one hour. However, it cannot be ruled out that precipitation of the compound also contributes to the change in fluorescence meaning that an amount of 15% DMSO is insufficient to hold compound **52** permanently in solution.

In general, the estimation of %PPB by fluorescence measurements is impossible in case of compounds **51** and **52**, mainly due to the lack of emission at physiological pH in combination with precipitation, effects of DMSO on the structure and solubility of BSA.

4.3.2.4 Determination of lipophilicity parameters by HPLC

As all the aforementioned approaches for the estimation of protein binding failed, HPLC-based methods (experiments performed in cooperation with Origenis GmbH, Martinsried, Germany) were used to determine lipophilicity parameters for the prediction of PPB based on the work of Valko et. al. [Valko et al., 1997; Valko et al., 2000; Valko et al., 2003; Valko et al., 2011]. As displayed in **Table 4.3** compounds **31**, **32** and **51** (**Figure 4.13**) were estimated to bind to human serum albumin to almost 100%.

31 R = OCH$_3$
32 R = O(CH$_2$CH$_2$)$_3$CH$_3$
51
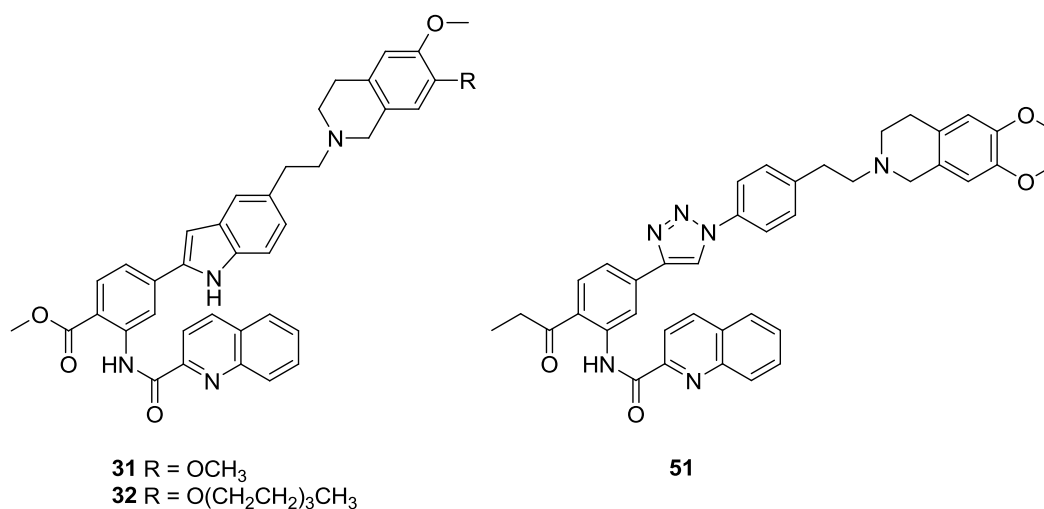
Figure 4.13: Chemical structures of ABCG2 modulators **31**, **32** and **51** with a molecular weight of 640, 772 and 666 Da, respectively.

Table 4.3: HSA binding affinities and chromatographically determined lipophilicity parameters of compounds **31**, **32** and **51**, respectively, each calculated in 2 independent experiments.

Cpd.	%PPB[a]	log$K$ (HSA)	logk_A (HSA)	Confid.[b] HSA	CHI[c]	log$d$	Confid.[b] log$d$	CHI IAM[d]	Confid.[b] IAM
31	98.37	1.78	4.96	1	123.61	3.59	2	74.50	1
	99.02	2.00	5.19	0				74.61	1
32	21.45	-0.56	2.62	1	105.03	3.17	0	57.19	1
	98.07	1.71	4.89	1				58.26	1
51	98.58	1.84	5.02	2	125.35	3.62	2	62.40	2
	98.33	1.77	4.95	1				62.57	1

[a] Calculated percental plasma protein binding; HPLC conditions: solvent A (5% (v/v) isopropanol in 50 mM ammonium acetate buffer; pH 7,4)/isopropanol (100%): 0 min: 100/0, 3.5 min: 0/30, 4.5 min: 0/30, 4.6 min: 100/0, 6 min: 100/0. [b] Confidence: 2 = without any doubt, 1 = likely, 0 = unlikely. [c] A C$_{18}$ column (40 °C) was used with an ammonium acetate buffer [50 mM; pH 7.4] + 5% (v/v) MeCN as solvent (solvent B) under the following gradient conditions: solvent B/MeCN: 0 min: 100/0, 3 min: 0/100, 4 min: 0/100, 4.2 min: 100/0, 6 min: 100/0. [d] IAM column at 40 °C with the following gradient: solvent B/MeCN: 0 min: 100/0, 5 min: 0/100, 5.5 min: 0/100, 6.5 min: 100/0, 8.2 min: 100/0.

The HSA binding values were derived from the gradient retention times and converted in its linear free energy-related log$K$ value using data from a calibration set of molecules:

$$\log K = \log \frac{\%PPB}{100 - \%PPB} \qquad \text{(equation 5)}$$

Percental value data and log$K$ values can be converted to binding affinity constant (logk_A) according to the following formula:

$$\log k_A = \log \frac{\%PPB}{100 - \%PPB} - \log [HSA] \qquad \text{(equation 6)}$$

k_A represents the binding affinity to HSA under the assumption that binding occurs exclusively to HSA, a binary complex is formed between the ligand and HSA, and the albumin concentration in plasma is around 0.0006 M ([HSA]) [Kratochwil et al., 2002; Borchardt et al., 2004].

Characterizing interactions of drugs via immobilized artificial membrane (IAM) chromatography is an efficient and time-saving method to obtain membrane interaction parameters of drugs, enabling the estimation of a compound's lipophilicity. With a calibration set of standard compounds, the gradient retention times can be converted to chromatographic hydrophobicity index (CHI) values (CHI IAM). As CHI correlates closely with traditional octanol-buffer distribution coefficient log$D$, CHI values were projected to a logarithmic scale by an intralaboratory equation that is more appropriate for a comparison (log$d$).

In general, the investigated ABCG2 modulators show very high protein (>98%) and membrane binding due to high lipophilicity.

4.3.3   pH-dependent fluorescence of ABCG2 modulators

As described in 4.3.2.3, selected ABCG2 modulators of the triazole series like compound **52** show an increase in fluorescence with decreasing pH values of the solvent.

A strong acid milieu of pH 1.5 even results in fluorescence emission in case of the biphenyl compound **12,** which is non-fluorescent in neutral milieu (**Figure 4.14**).

This fact suggests that the pH-dependent increase in fluorescence results from the protonation at the common quinoline substructure, thereby extending the conjugation of the π-electron system.
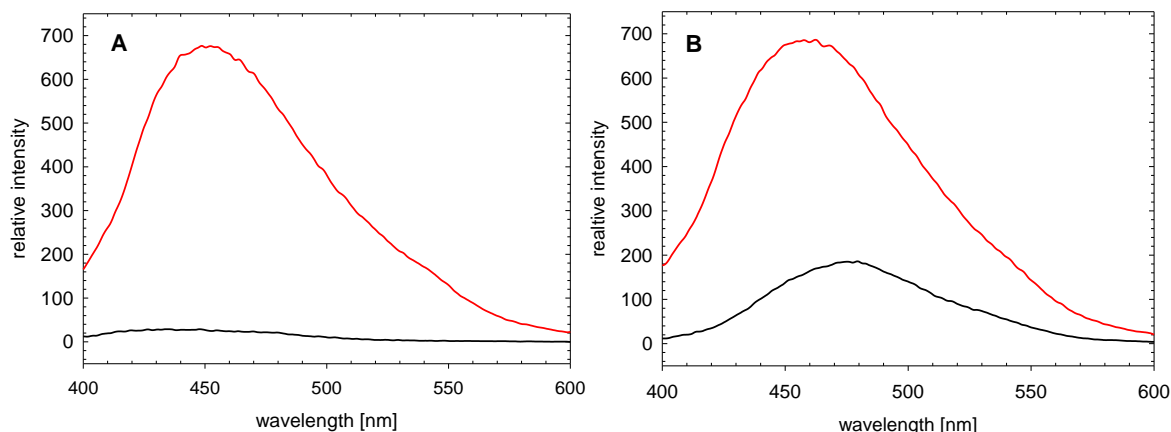
Figure 4.14: Fluorescence spectra of compounds **12** [1 µM] (**A**) and **52** [1 µM] (**B**) in DMSO (*black*) and DMSO/TFA (aq.) at pH 1.5 (*red*) after excitation at 370 nm; Ex/Em slit 10. In case of **52**, a slight shift of the emission maximum to the blue was visible with the addition of TFA.

ACD labs chemistry software identified the quinoline as a weak base with a pKa value around 1, whereas the 1,2,3-triazole substructure is not involved in an pH dependent fluorescence according to these calculations at pH 1.5 (**Figure 4.15**).

atom number	apparent pKa value
15	1.01
31	7.19

atom number	apparent pKa value
8	7.53
29	1.33
47	-1.72
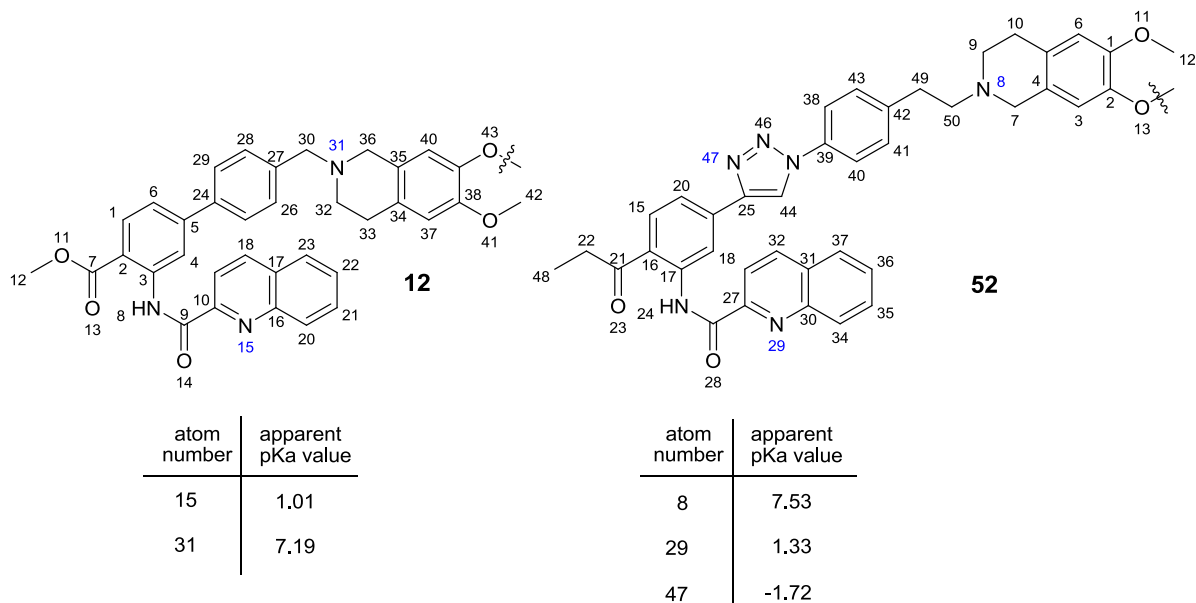
Figure 4.15: Calculated pKa values for compounds **12** and **52** by ACD/Labs chemistry software 12.0.

However, these pKa values have to be examined critically as they can strongly depend on the electronic charge distribution of the compound resulting in enormous differences in acidity between the ground and excited states [Marciniak et al., 1992] as is the case for six-membered aromatic nitrogen heterocyclic compounds, which are generally known to be more basic in the lowest excited state than in the ground state usually by at least five orders of magnitude [Schulman and Capomacchia, 1973].

Intramolecular proton transfer of organic compounds can result in drastic changes in their fluorescence properties. Detailed reaction dynamics and the influence of the microenvironment on the mechanism of reaction are often not completely understood.

The polymer photostabilizer Tinuvin P (2-(2'-hydroxy-5'-methylphenyl)benzotriazole), the photostability of which has been attributed to a very fast reversible intramolecular proton transfer, is shown in **Figure 4.16**. Keto-enol-like tautomers can be distinguished and different fluorescence properties (in various solvents) are due to different energy states: ground and excited states [Wiechmann et al., 1991].
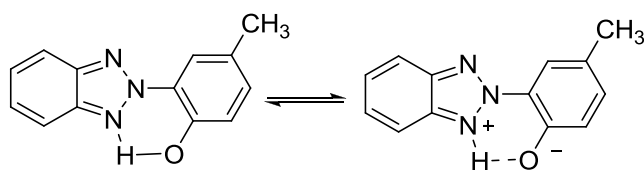
Figure 4.16: Keto- and enol-like tautomers of Tinuvin P.

Related results were obtained for 2-(2'-hydroxyphenyl)oxazole and 2-(2'-hydroxyphenyl)-4-methylthiazole [LeGourrierec et al., 1998].

A similiar pH- dependent tautomeric mechanism as well as solvent-dependent influences on the energy state in terms of fluorescence properties are also conceivable for the synthesized ABCG2 modulators both with the quinoline and the triazole substructre (**Figure 4.17**).
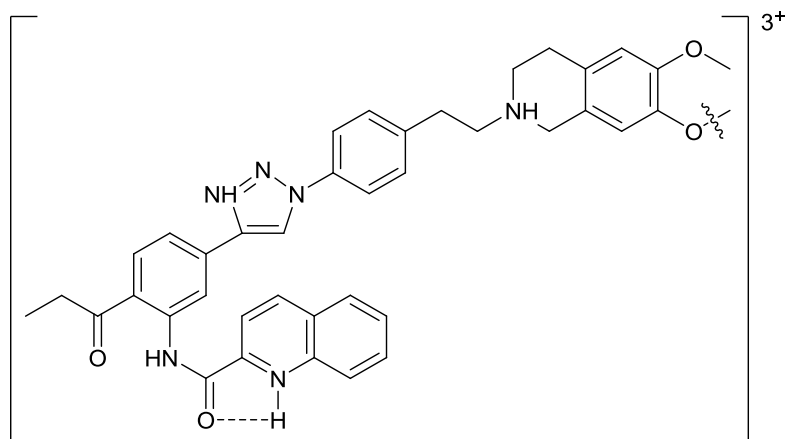
Figure 4.17: Hypothetical highly protonated form of compound **51.**

4.4   Summary and conclusions

The attempts to determine protein binding failed irrespective of the applied methods (equilibrium dialysis, ITC, ultracentrifugation, fluorescence spectroscopy). Very poor water solubility of the investigated ABCG2 modulators is the major reason for insufficient drug-like properties. High molecular weights (between 600 and 900 Da) and high log$P$ values usually result in poor absorption and permeation. In addition the extent of plasma protein binding is probably very high, as predicted on the basis of HPLC measurements. However, despite these unfavorable properties, the compounds show high potency in cell-based *in vitro* assays suggesting that they are either actually much more potent than calculated on the basis of the added concentration, i.e., the effective concentrations of free compounds are much lower, or the binding to proteins is beneficial to provide a reservoir of the compounds in the aqueous systems. It has to be further elucidated whether these ABCG2 modulators are suitable for *in vivo* studies in nude mice.

To come to more 'drug-like' compounds, the chemical structures have to be modified by introducing more hydrophilic moieties and/or by reducing the molecular weight.

4.5   References

Abbott, N. J., Patabendige, A. A., Dolman, D. E., et al. Structure and function of the blood-brain barrier. *Neurobiol. Dis.* **2010**, 37(1), 13-25.

Anderson, N. L. and Anderson, N. G. The human plasma proteome: history, character, and diagnostic prospects. *Mol. Cell. Proteomics* **2002**, 1(11), 845-867.

Borchardt, R. T., Kerns, E., Lipinski, C. A., et al. *Pharmaceutical Profiling in Drug Discovery for Lead Selection*. American Association of Pharmaceutical Scientists, Arlington, VA, 2004.

Bujacz, A. Structures of bovine, equine and leporine serum albumin. *Acta Crystallogr. D Biol. Crystallogr.* **2012**, 68(Pt 10), 1278-1289.

Estey, T., Kang, J., Schwendeman, S. P., et al. BSA degradation under acidic conditions: a model for protein instability during release from PLGA delivery systems. *J. Pharm. Sci.* **2006**, 95(7), 1626-1639.

Galecki, K., Despotovic, B., Galloway, C., et al. Binding of harmane to human and bovine serum albumin: fluorescence and phosphorescence study. *Biotechnol. Food Sci. 2012* **2012**, 76(1), 3-12.

Ge, S., Kojio, K., Takahara, A., et al. Bovine serum albumin adsorption onto immobilized organotrichlorosilane surface: influence of the phase separation on protein adsorption patterns. *J. Biomater. Sci. Polym. Ed.* **1998**, 9(2), 131-150.

Kratochwil, N. A., Huber, W., Muller, F., et al. Predicting plasma protein binding of drugs: a new approach. *Biochem. Pharmacol.* **2002**, 64(9), 1355-1374.

Ladokhin, A. S. *Fluorescence Spectroscopy in Peptide and Protein Analysis*. Encyclopedia of Analytical Chemistry, John Wiley & Sons Ltd. 2000, 5762 – 5779.

LeGourrierec, D., Kharlanov, V., Brown, R. G., et al. Excited-state intramolecular proton transfer (ESIPT) in 2-(2 '-hydroxyphenyl)pyridine and some carbon-bridged derivatives. *J Photoch Photobio A* **1998**, 117(3), 209-216.

Lipinski, C. A. Drug-like properties and the causes of poor solubility and poor permeability. *J. Pharmacol. Toxicol. Methods* **2000**, 44(1), 235-249.

Lipinski, C. A., Lombardo, F., Dominy, B. W., et al. Experimental and computational approaches to estimate solubility and permeability in drug discovery and development settings. *Adv. Drug Deliv. Rev.* **2001**, 46(1-3), 3-26.

Lund, L., Berlin, A. and Lunde, K. M. Plasma protein binding of diphenylhydantoin in patients with epilepsy. Agreement between the unbound fraction in plasma and the concentration in the cerebrospinal fluid. *Clin. Pharmacol. Ther.* **1972**, 13(2), 196-200.

Majorek, K. A., Porebski, P. J., Dayal, A., et al. Structural and immunologic characterization of bovine, horse, and rabbit serum albumins. *Mol. Immunol.* **2012**, 52(3-4), 174-182.

Marciniak, B., Kozubek, H. and Paszyc, S. Estimation of Pka* in the 1st Excited Singlet-State - a Physical-Chemistry Experiment That Explores Acid-Base Properties in the Excited-State. *J. Chem. Educ.* **1992**, 69(3), 247-249.

Miners, J. O., Foenander, T., Wanwimolruk, S., et al. The effect of sulphinpyrazone on oxidative drug metabolism in man: inhibition of tolbutamide elimination. *Eur. J. Clin. Pharmacol.* **1982**, 22(4), 321-326.

Moriyama, Y., Ohta, D., Hachiya, K., et al. Fluorescence behavior of tryptophan residues of bovine and human serum albumins in ionic surfactant solutions: a comparative study of the two and one tryptophan(s) of bovine and human albumins. *J. Protein Chem.* **1996**, 15(3), 265-272.

Mungall, D., Wong, Y. Y., Talbert, R. L., et al. Plasma protein binding of warfarin: methodological considerations. *J. Pharm. Sci.* **1984**, 73(7), 1000-1001.

Pabbathi, A., Patra, S. and Samanta, A. Structural transformation of bovine serum albumin induced by dimethyl sulfoxide and probed by fluorescence correlation spectroscopy and additional methods. *Chemphyschem* **2013**, 14(11), 2441-2449.

Pajouhesh, H. and Lenz, G. R. Medicinal chemical properties of successful central nervous system drugs. *NeuroRx.* **2005**, 2(4), 541-553.

Patra, S., Santhosh, K., Pabbathi, A., et al. Diffusion of organic dyes in bovine serum albumin solution studied by fluorescence correlation spectroscopy. *Rsc Adv.* **2012**, 2(14), 6079-6086.

Peters, T. Serum-Albumin. *Adv. Protein Chem.* **1985**, 37, 161-245.

Peterson, G. M., McLean, S., Aldous, S., et al. Plasma protein binding of phenytoin in 100 epileptic patients. *Br. J. Clin. Pharmacol.* **1982**, 14(2), 298-300.

Pierce, M. M., Raman, C. S. and Nall, B. T. Isothermal titration calorimetry of protein-protein interactions. *Methods* **1999**, 19(2), 213-221.

Ptachcinski, R. J., Venkataramanan, R. and Burckart, G. J. Clinical pharmacokinetics of cyclosporin. *Clin. Pharmacokinet.* **1986**, 11(2), 107-132.

Reichel, A. The role of blood-brain barrier studies in the pharmaceutical industry. *Curr. Drug Metab.* **2006**, 7(2), 183-203.

Rolan, P. E. Plasma protein binding displacement interactions-why are they still regarded as clinically important? *Br. J. Clin. Pharmacol.* **1994**, 37(2), 125-128.

Santos, H. A., Manzanares, J. A., Murtomaki, L., et al. Thermodynamic analysis of binding between drugs and glycosaminoglycans by isothermal titration calorimetry and fluorescence spectroscopy. *Eur. J. Pharm. Sci.* **2007**, 32(2), 105-114.

Schulman, S. G. and Capomacchia, A. C. Dual Fluorescence of Quinolinium Cation. *J. Am. Chem. Soc.* **1973**, 95(9), 2763-2766.

Stegemann, S., Leveiller, F., Franchi, D., et al. When poor solubility becomes an issue: From early stage to proof of concept. *Eur. J. Pharm. Sci.* **2007**, 31(5), 249-261.

Takehara, K., Yuki, K., Shirasawa, M., et al. Binding properties of hydrophobic molecules to human serum albumin studied by fluorescence titration. *Anal. Sci.* **2009**, 25(1), 115-120.

Valko, K., Bevan, C. and Reynolds, D. Chromatographic Hydrophobicity Index by Fast-Gradient RP-HPLC: A High-Throughput Alternative to log P/log D. *Anal. Chem.* **1997**, 69(11), 2022-2029.

Valko, K., Du, C. M., Bevan, C. D., et al. Rapid-gradient HPLC method for measuring drug interactions with immobilized artificial membrane: comparison with other lipophilicity measures. *J. Pharm. Sci.* **2000**, 89(8), 1085-1096.

Valko, K., Nunhuck, S., Bevan, C., et al. Fast gradient HPLC method to determine compounds binding to human serum albumin. Relationships with octanol/water and immobilized artificial membrane lipophilicity. *J. Pharm. Sci.* **2003**, 92(11), 2236-2248.

Valko, K. L., Nunhuck, S. B. and Hill, A. P. Estimating unbound volume of distribution and tissue binding by in vitro HPLC-based human serum albumin and immobilised artificial membrane-binding measurements. *J. Pharm. Sci.* **2011**, 100(3), 849-862.

Veber, D. F., Johnson, S. R., Cheng, H. Y., et al. Molecular properties that influence the oral bioavailability of drug candidates. *J. Med. Chem.* **2002**, 45(12), 2615-2623.

Venkataramanan, R., Swaminathan, A., Prasad, T., et al. Clinical pharmacokinetics of tacrolimus. *Clin. Pharmacokinet.* **1995**, 29(6), 404-430.

Vivian, J. T. and Callis, P. R. Mechanisms of tryptophan fluorescence shifts in proteins. *Biophys. J.* **2001**, 80(5), 2093-2109.

Waterhouse, R. N. Determination of lipophilicity and its use as a predictor of blood-brain barrier penetration of molecular imaging agents. *Mol. Imaging Biol.* **2003**, 5(6), 376-389.

Wiechmann, M., Port, H., Frey, W., et al. Time-Resolved Spectroscopy on Ultrafast Proton-Transfer in 2-(2'-Hydroxy-5'-Methylphenyl)Benzotriazole in Liquid and Polymer Environments. *J Phys Chem-Us* **1991**, 95(5), 1918-1923.

*C*hapter 5

5 Characterization of human brain tumor cell lines

5.1 Malignant brain tumors

5.1.1 Classification

According to the classification of central nervous system (CNS) malignancies recommended by the World Health Organization (WHO), brain tumors are grouped in tumor types and grades ranging from grade I (least malignant) to grade IV (most malignant) based on their histopathology [Louis et al., 2007]. Brain cancer can be categorized into primary brain tumors, originating from a brain cell type, and secondary tumors, i.e. brain metastases originating from malignancies in the periphery. 30% of all primary brain tumors are gliomas, descending from the glial (supportive) tissue [Dolecek et al., 2012]. Gliomas are grouped in several subtypes, including astrocytomas, ependymomas and oligodendrogliomas.

Glioblastoma multiforme (GBM) is the most common and aggressive form of all malignant primary brain tumors with a median survival time of only 15 months [Wen and Kesari, 2008]. It belongs to the group of astrocytic tumors and is classified as grade IV. About 15% of all brain tumors are GBM.

The aggressive and malignant medulloblastomas belong to the group of embryonal tumors and commonly occur in the cerebellum. Medulloblastomas and gliomas are the most common brain tumors in children (20% of childhood brain tumors) and carry the most malignant WHO designation (grade IV) [Huse and Holland, 2010; Cook and Freedman, 2012].

5.1.2 Incidence and mortality

As results of a project coordinated by the International Agency for Research on Cancer (IARC; Lyon, France) [Ferlay et al., 2013] the incidence and mortality data of different cancers in 40 European countries were presented for the year 2012. There were 3.45 million new cases of cancer and an

estimated number of 1.75 million deaths from cancer in Europe in 2012 with female breast, colorectal, prostate and lung cancer as the most common manifestations. The estimated number of new brain cancer cases in Europe was 57,100 with a concomitant mortality of 45,000.

Though new brain tumor incidences represent only 2% of all estimated new cancer cases, efficient treatment is urgently required, as the trend of new cases is rising (190,000 sufferers in the year 2002 worldwide, 238,000 in 2008) [Ferlay et al., 2010] and the five-year relative survival rates (percentage of people who are alive 5 years after their diagnosis) are still very low. Worldwide, every day about 650 people are diagnosed with a malignant brain tumor.

5.1.3   The blood-brain barrier and brain cancer therapy

The blood-brain barrier separates the brain and cerebrospinal fluid from the blood and is composed of high-density endothelial cells. As a regulatory barrier, it controls the entry and elimination of ions, neurotransmitters, macromolecules, neurotoxins or water soluble nutrients from and into the brain and, hence, sustains ionic homeostasis [Abbott et al., 2010]. Tight junctions are cell-cell junctional complexes in the apical region of cell membrane and form the intercellular barrier between the epithelial cells, thereby, almost completely obstructing paracellular diffusion under normal conditions [Stamatovic et al., 2008]. Transcellular pathways over the BBB include passive diffusion, adsorptive-mediated transcytosis and the active transport of molecules via various transporter-mediated shuttle systems (**Figure 5.1**).
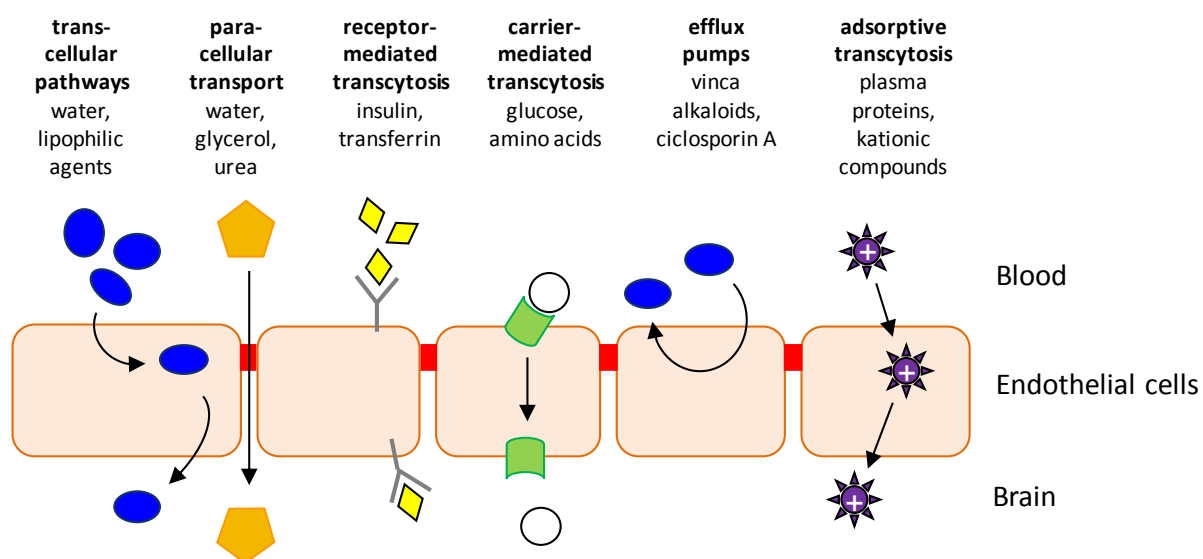
Figure 5.1: Schematic illustration of transport ways and mechanisms at the blood-brain barrier. Tight junctions are displayed in red.

The transporters expressed in the BBB comprise carrier-mediated, receptor-mediated and active efflux transporters [Pardridge, 2005] including organic anion and cation transporter systems [Sekine et al., 2000], nucleoside transporters and ABC efflux transporter like P-gp, BCRP and MRPs [Lee et al., 2001]. The BBB protects the CNS from xenobiotics including a large variety of pharmacotherapeutics. As a consequence, the medical treatment of CNS diseases like brain tumors is compromised. Several strategies were developed to overcome or bypass the BBB, aiming at improved therapies of CNS malignancies.

BCNU (1,3-bis(2-chloroethyl)-1-nitrosourea; carmustine), an alkylating agent of the group of nitrosoureas included in standard regimen for nearly 30 years [Walker and Hurwitz, 1970], as well as the DNA methylating agent temozolomide (Temodal®) are the drugs frequently used in systemic chemotherapy [Newlands et al., 1997; Stupp et al., 2005]. Promising strategies for an enhanced drug delivery into the brain have been developed, for instance, the therapeutic application of 'vectors' such as peptides [Rousselle et al., 2001] and viruses [Pertschuk et al., 2012; Robbins et al., 2012] or nanoparticles as carriers for the transport of packaged drugs to the brain [Martin-Banderas et al., 2011; Orthmann et al., 2012; Tosi et al., 2013].

Another field of current research in brain tumor treatment is the use of monoclonal antibodies. Since May 2009, bevacizumab (Avastin®) is approved by the Food and Drug Administration (FDA) for second-line treatment of glioblastoma in the USA [Cohen et al., 2009]. It is a recombinant humanized monoclonal antibody that binds to human vascular endothelial growth factor (VEGF) inhibiting intratumoral angiogenesis and, thereby, tumor growth and proliferation [Shih and Lindley, 2006].

Advances in chemotherapy also include more invasive approaches namely intracerebral (i.c.) and intracerebroventricular (i.c.v.) applications as well as the direct placement of the anticancer agent into the tumor cavity via convection enhanced delivery (CED) by means of a catheter or an implanted drug reservoir [Saito and Tominaga, 2012]. Biodegradable implants have been approved for the treatment of CNS tumors. The Gliadel® wafer, containing BCNU embedded in a polyanhydride matrix, is indicated in newly-diagnosed high-grade glioma and recurrent GBM patients. It is planted into the surgical cavity post surgery to release the cytostatic directly to the tumor site [Panigrahi et al., 2011]. In general, invasive methods mostly require a complex surgical intervention and are precarious not least because of unpredictable risks of infection, injury and long-term effects.

A better understanding of the pharmacology of brain tumors and the growth behavior and pathology of available human brain tumor cell lines *in vitro* is of major importance with respect to optimization of treatment therapies aiming at extending the average survival times and reducing the size and progression of malignant brain tumors. During this work, three different brain tumor cell lines were comprehensively characterized *in vitro* and partially *in vivo*.

5.2   Materials and methods

5.2.1   Drugs and chemicals

PBS (phosphate buffered saline) was made of 8.0 g/L NaCl, 1.0 g/L Na$_2$HPO$_4$ · 2 H$_2$O, 0.20 g/L KCl, 0.20 g/L KH$_2$PO$_4$ and 0.15 g/L NaH$_2$PO$_4$ · H$_2$O. The pH-value was adjusted to 7.4.

Bouin's solution (fixative for histopathology) was made of saturated picric acid, formaldehyde and glacial acetic acid in a ratio of 15:5:1. Giemsa solution for chromosomal staining was from AppliChem (Darmstadt, Germany) and Tris base as buffer constituent from usb (Cleveland, OH). The PerfectBlue™ Double gel system Twin S for SDS-PAGE (sodium dodecyl sulfate polyacrylamide gel electrophoresis) as well as the nitrocellulose membrane and the PerfectBlue™ 'Semi-Dry' electro blot apparatus for Western Blotting were obtained from Peqlab (Erlangen, Germany). Topotecan, etoposide, doxorubicin, methotrexate and vinblastine were purchased from Sigma (Munich, Germany). Paclitaxel (6 mg/mL; Bristol-Meyers Squibb, Wien, Austria) was obtained from the pharmacy of the University Hospital Regensburg. A solution of mitoxantrone (1 mM) was obtained by diluting Novantron® (Wyeth Pharma, Münster, Germany) in 70% ethanol.

If not otherwise stated, chemicals (p.a. quality) were obtained from Merck (Darmstadt, Germany) and antibodies from Santa Cruz Biotechnology (Heidelberg, Germany). Milli-Q system (Millipore, Eschborn, Germany) was used for the purification of water.

5.2.2   Cell lines and culture conditions

The human brain tumor cell lines SW 1783 (ATCC® HTB-13™; astrocytoma, grade III), Daoy (ATCC® HTB-186™; desmoplastic cerebellar medulloblastoma) and LN-18 (ATCC® CRL-2610™; glioblastoma grade IV) as well as the murine cell line P388D1 (ATCC® CCL-46™; murine lymphoid neoplasm with macrophage-like morphology) were cultured in Dulbecco's Modified Eagle Medium (DMEM; Sigma, Munich, Germany) supplemented with 10% FCS (fetal calf serum; Biochrom, Berlin, Germany), 3.7 g/L sodium hydrogen carbonate and 110 mg/L sodium pyruvate (Serva, Heidelberg, Germany).

Immortalized human microvascular endothelial cells (HMEC-1) [Ades et al., 1992] were kindly provided by Prof. Dr. J. Heilmann (Institute of Pharmaceutical Biology, University of Regensburg) and cultured in DMEM containing 15% FCS and 2 mM L-glutamine (Biochrom).

Cells were cultured in a water-saturated atmosphere (95% air, 5% CO$_2$) at 37 °C in 25-cm^2 or 75-cm^2 cell culture flasks purchased from Nunc (Wiesbaden, Germany), Greiner (Frickenhausen, Germany) and Sarstedt (Nümbrecht, Germany), respectively.

5.2.3   Cell staining

Microscopic slides were immersed in 200 mL 70% ethanol, containing 6 mL of concentrated HCl, for 24 h, washed with distilled water and dried. Dry coverslips were placed between filter papers and sterilized by autoclaving (121 °C, 15 psi) [Rooney and Czepulkowski, 1992].

Cells were seeded on the prepared slides for 1 day (5% CO_2, 37 °C), afterwards fixed for 1 h with Carnoy´s solution (ethanol/chloroform/glacial acetic acid 6:3:1) and stored in PBS containing 0.1% NaN_3. Sections were evaluated with a BH-2 microscope (Olympus, Hamburg, Germany) after Papanicolaou staining [Takahashi, 1987] using ScopePhoto 3.0 software.

5.2.4   Genetic stability - Karyology

The assay was performed as described previously [Jarzyna, 2007]: Cells were cultured on immersed and sterilized microscopic slides in Quadriperm 4-well lux-multiplates (Greiner) up to a confluency of 15-25% and afterwards overlaid with cell culture medium containing 0.5 µg/mL colcemide to arrest mitosis of the cells during metaphase.

After an incubation time of 3 h (37 °C, 5% CO_2), the medium was removed and a hypotonic potassium chloride solution (75 mM) preheated to 37 °C was carefully added to lyse the cells. After 30 min, an equal volume of ice-cold fixative (methanol/glacial acetic acid 3:1) was added and carefully removed at once. After two additional fixation steps on ice (last step: 10 min fixation) the fixative was removed and the slides were dried. Slides were stained for 8 min with a diluted Giemsa staining solution (10 mL filtered Giemsa solution, 90 mL of 25 mM KH_2PO_4, pH 6.8), thoroughly washed, dried and mounted with DePex (EMS, Hatfield, PA). Chromosome numbers of at least 50 cells in metaphase were determined per cell line with an Olympus BH-2 microscope using 40x and 100x Planapo oil immersion objectives (Zeiss, Jena, Germany).

5.2.5   Chemosensitivity against common cytostatic drugs and growth kinetics

The aforementioned human brain tumor cell lines were investigated for their chemosensitivity against common cytostatic drugs by means of a crystal violet assay as described in section 3.3.6.

In vitro growth behavior was determined in a similar manner: Cells were seeded in 96-well plates, fixed with glutardialdehyde after different times of incubation (37 °C, 5% CO_2) and stained with crystal violet. The absorbance, proportional to cell mass/number, was measured at 580 nm using a GENios Pro microplate reader (TECAN Deutschland GmbH, Crailsheim, Germany) and plotted on a

log-linear scale against the incubation time. The population doubling time was determined along the exponential phase of the curve.

5.2.6   Tumorigenicity and growth kinetics of subcutaneous tumors in nude mice

For tumor cell implantation into nude mice, human brain tumor cells were washed twice with 5 mL of pre-warmed serum-free culture medium and carefully harvested using a cell scratcher. After centrifugation at 1,000 rpm for 7 min at room temperature, using a Minifuge 1.0R (Heraeus Instruments GmbH, Hanau, Germany), the obtained cell pellet was resuspended in serum-free medium and the cell number was adjusted to a density of 1-3 x 10^6 cells per 100 µL by means of a Casy® 1 TTC cell counter (Schärfe System GmbH, Reutlingen, Germany) or a Neubauer counting chamber.

100 µL of the cell suspension were injected under the thoracic dermis of each mouse. Once a week, the bodyweight was controlled and the tumor diameters were monitored with a sliding caliper. To ensure tumor growth over various passages, 1 mm^3 tumor pieces were prepared from an excised non-necrotic tumor and again transplanted into nude mice by means of a trocar.

5.2.7   Histology

Solid tumors were prepared for histological staining by the following procedure:

After dissection, tumor tissue was fixed in Bouin´s solution and embedded in paraffin after dehydration with increasing concentrations of ethanol by a standard procedure (described in detail in [Müller, 2007]). Sections (6 µm) were cut by a Leica RM2255 microtome (Leica, Bensheim, Germany) and mounted on microscope slides. After deparaffinization with xylene and rehydration in decreasing concentrations of ethanol, slides were subsequently stained by the procedure of Masson-Goldner (MG) or with haematoxylin-eosin (HE) [Mulisch and Welch, 2010], dried and mounted with DePeX.

5.2.8   Induction of BCRP overexpression in brain tumor cells

To determine the ABCG2 transporter expression in the aforementioned human brain tumor cells Western Blot (WB) analysis of total cell lysates was performed. BCRP-positive cell types were further cultured and treated with topotecan at increasing concentrations over a period of approximately 10 weeks to amplify the transporter expression.

5.2.9 ABC transporter detection by Western Blot analysis

5.2.9.1 Cell lysis and protein quantification

Cell lines were lysed by physical disruption. Cells were harvested with a cell scratcher and washed three times with PBS. After centrifugation, the cell pellet was homogenized in PBS containing a protease inhibitor cocktail (SIGMA*FAST*™ Tablets; Sigma, Munich, Germany) followed by 5-6 repetitive freeze-thaw cycles in liquid nitrogen to disrupt the cells through ice crystal formation. After homogenization the protein content of each cell lysate was determined in a Bio-Rad Protein Assay (Bio-Rad Laboratories, Munich, Germany) based on the method of Bradford [Bradford, 1976] according to the standard procedure described in the manual. UV detection was performed with a Cary 100 UV-Vis spectrophotometer (Varian, Darmstadt, Germany).

5.2.9.2 SDS-PAGE and Western blot

Proteins were analyzed by SDS-PAGE. The basic procedure was that of Laemmli [Laemmli, 1970], using a 12% acrylamide resolving gel. The composition of all used buffers (in millipore water) was as follows:

Buffer A: 1.5 M Tris, 0.4% (m/v) SDS, pH 8.8

Buffer B: 0.5 M Tris, 0.4% (m/v) SDS, pH 6.8

Running buffer: 0.025 M Tris, 0.2 M glycine, 0.1% (m/v) SDS, pH 8.3

Blotting buffer: (always freshly prepared) 0.025 M Tris, 0.2 M glycine, 20% (v/v) methanol

TBS-T buffer: 0.02 M Tris, 0.14 M NaCl in millipore water (pH 7.6), 0.1% (v/v) Tween 20
                       (Carl Roth GmbH, Karlsruhe, Germany)

Sample buffer (6x): 0.15 M Tris, 1.0 M glycine, 0.6% (m/v) SDS, 9.0% (v/v) glycerol, 0.1% (m/v) bromophenol blue, 2% (v/v) β-mercaptoethanol, pH 6.8

Leammli buffer (6x): 0.38 M Tris, 12% (m/v) SDS, 60% (v/v) glycerol, 0.06% (m/v) bromophenol blue, 10 mM DTT

A 12% separation gel mixture for one gel contained 2.65 mL of millipore water, 2 mL of buffer A and 3.1 mL of acrylamide/bisacrylamide 30% solution (acrylamide/bisacrylamide 29/1; Sigma, Munich, Germany). Polymerization was started by addition of 3.5 μL of N,N,N',N'-tetramethylethylenediamine (TEMED; Serva, Heidelberg, Germany) and 35 μL of a 10% (m/v) ammonium peroxodisulfate solution (APS; Serva).

The mixture was filled into gel chambers (10 x 10 x 0.8 cm) and covered with a layer of water-saturated isobutyl alcohol. After complete polymerization (ca. 45 min) and discarding the

isobutyl alcohol layer, a stacking gel (3%) was poured on top of the separation gel. The stacking gel mixture contained 3.25 mL of millipore water, 1.25 mL of buffer B and 0.5 mL of acrylamide/bisacrylamide 30% solution. Polymerization was initiated as described above.

A defined amount of protein per cell lysate was mixed with 1/6 volume of Laemmli buffer (6x) or sample buffer (6x) and heated for 5 min at 100 °C before filling in the stacking gel pockets. Electrophoresis was performed in a PerfectBlue™ gel electrophoresis chambers filled with running buffer at 150 V for approximately 90 min.

The unstained protein marker peqGOLD Protein Marker I (14.4-116 kDa; Peqlab, Erlangen, Germany) or the Biotinylated Protein Ladder (9-200 kDa) with the Anti-biotin HRP-linked Antibody (1 : 1,000) from Cell Signaling Technology (Danvers, MA) were used.

WB was performed in a Perfect-Blue™ 'Semi-Dry' electro blot apparatus by placing the gels on top of a nitrocellulose membrane (0.2 μm) between 6 filter slides soaked in blotting buffer. The proteins were transferred to the membrane by blotting for 45 min at 250 mA. Then, the membrane was blocked by washing in 5% fat-free milk (in TBS-T buffer; block solution) for 2 h at room temperature or overnight at 4 °C. After three washing steps (5 min each) in TBS-T buffer, the primary antibody was incubated with the membrane for 2 h (rt) in block solution. After washing, the secondary antibody, conjugated with horseradish peroxidase, was diluted in block solution, added to the membrane and shaken at rt for 1 h. Immunoreactive bands were visualized via enhanced chemoluminescence (ECL) using the Pierce® ECL Western Blotting substrate kit (Thermo Scientific, Dreieich, Germany) according to the manufacturer's instructions.

Blots and gels were scanned using a GS-710 imaging densitometer (Bio-Rad Laboratories, Munich, Germany). Quantity One (Bio-Rad) software was used for band analysis.

A total protein content of 20 μg was blotted for each cell line. The primary rat monoclonal antibody ABCG2 (BXP-53) was used in a 1: 1,000 dilution, the secondary AB (goat anti-rat IgG-HRP) in a 1: 10,000 dilution.

5.2.10 ABC transporter detection by flow cytometry

To further characterize the ABC transporter expression, a flow cytometric FACS (fluorescence activated cell sorting) assay was performed. Confluent cells were trypsinized into a 1.5 mL Eppendorf reaction vessel, suspended in PBS and centrifuged at 1,000 g for 5 min. After resuspension in PBS supplemented with 10% FCS, cells were counted in a Casy® 1 TTC cell counter and the density was adjusted to a number of 2×10^6 cell/mL with PBS/FCS. Aliquots of 500 μL were taken and incubated with the primary antibody in an appropriate dilution. After 1 h of incubation at 4 °C under shaking,

three washing steps with PBS (1,000 g, 5 min each) followed. Cells were resuspended in a solution of 3% (m/v) BSA (bovine serum albumin) in PBS containing the phycoerythrin (PE)-conjugated secondary antibody and incubated for an additional hour in the dark. Then, cells were washed three times with PBS, resuspended in 500 µL BSA/PBS and measured at a FacsCalibur™ (Becton Dickinson, Heidelberg, Germany). Instrument settings were as follows:

FSC: E-1; SSC: 350, Fl-2, high flow. WinMDI 2.9 software was used for data analysis.

Antibodies and dilutions used for FACS analysis:

ABCB1:   Primary AB: Mdr (C-19) goat polyclonal antibody, 1:50

                       Secondary AB: rabbit anti-goat IgG-PE, 1:100

ABCC1:   Primary AB: MRP1 rabbit polyclonal antibody (abbiotec; Hoelzel Diagnostika GmbH, Köln, Germany), 1:30

                       Secondary AB: goat anti-rabbit IgG-PE (Rockland Inc.; Biomol GmbH, Hamburg, Germany), 1:100

ABCG2:   Primary AB: ABCG2 (BXP-53) rat monoclonal antibody, 1:50

                       Secondary AB: goat anti-rat IgG-PE, 1:100

5.3   Results and discussion

5.3.1   Morphology

Doay, LN-18 and SW 1783 cells, grown on tissue slides, were stained according to the method of Papanicolaou to illustrate plasma turquoise and nuclei blue (**Figures 5.2-5.4**).
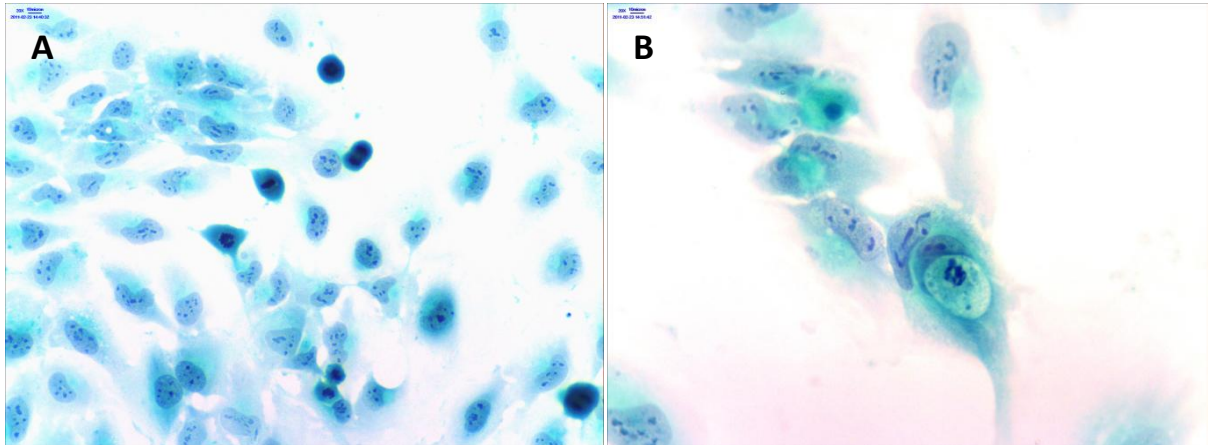
Figure 5.2: Microscopic images (Papanicolaou staining) of human Daoy cells (passage 7) with a high mitotic activity (**A**, objective: 20x); **B**) Magnification (objective: 40x) of highly malignant multi-nucleated cells.
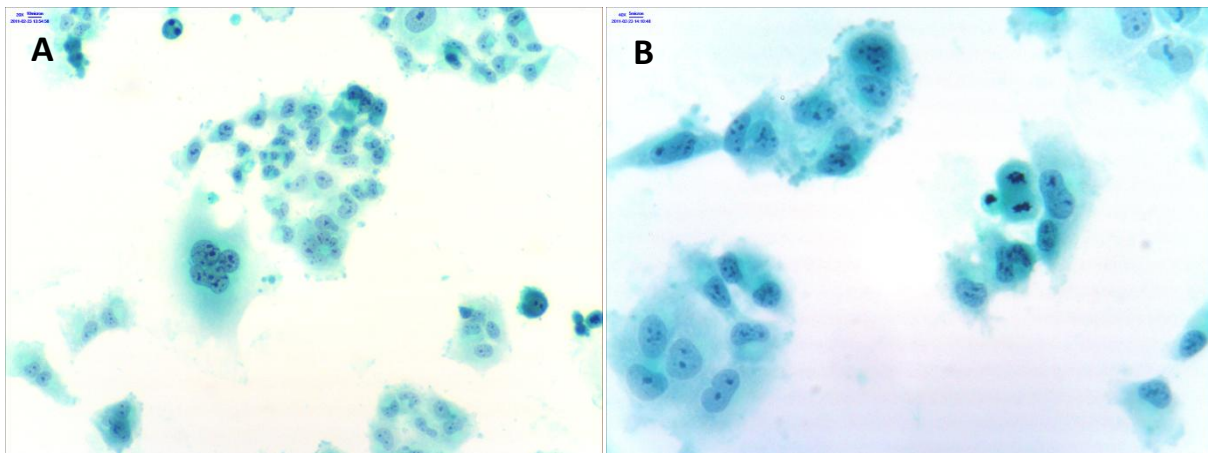
Figure 5.3: Microscopic images (Papanicolaou staining) of human LN-18 cells (passage 18); the cells show distinctive anisomorphism, an increased nucleoplasmatic ratio (**A**, objective: 20x) and multiple prominent nucleoli (**B**, lower left corner; objective: 40x).
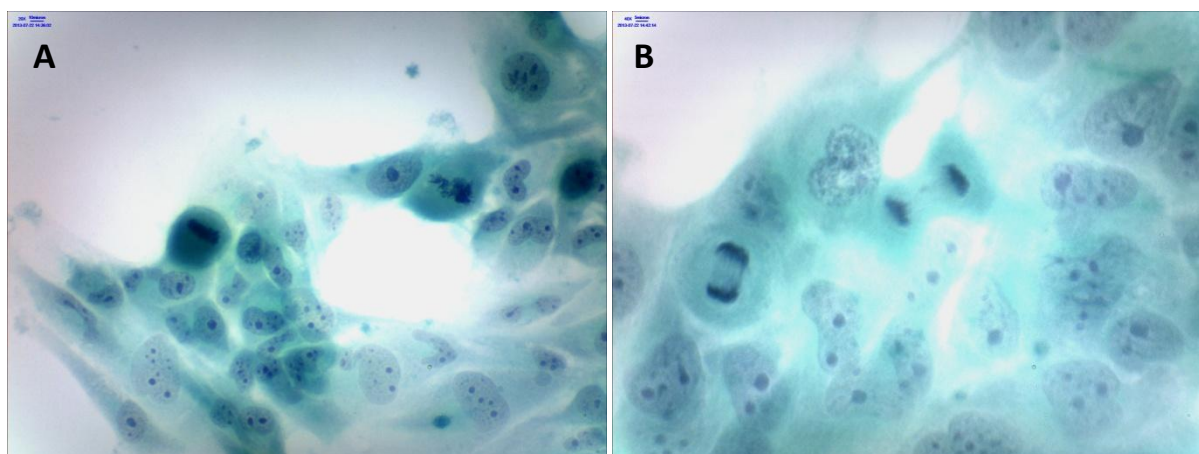
Figure 5.4: Microscopic images (Papanicolaou staining) of human SW 1783 cells (passage 42); highly anisomorphic cells (**A**, objective: 20x) with a high mitotic activity and multiple prominent nucleoli (**B**, objective: 40x).

5.3.2 *In vitro* growth of brain tumor cells

To evaluate growth characteristics like the doubling time or saturation density of the aforementioned brain tumor cell lines, growth curves were generated before starting any experiments. The growth of cells in culture is characterized by a *lag phase,* the time it takes for the cells to recover from subculture, attach and spread, a *log phase* in which an exponential increase in cell density arises and a *stationary phase* in which cell proliferation slows down due to the cell culture becoming confluent. The growth of Daoy (5th passage), LN-18 (7th passage) and SW 1783 (31st passage) cells over two weeks is shown in **Figure 5.5**.
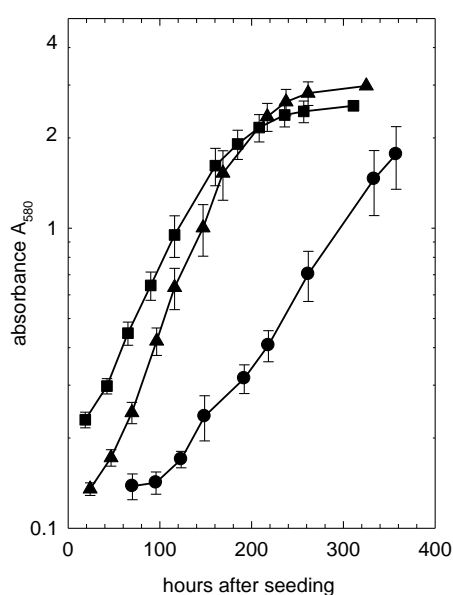
Figure 5.5: *In vitro* growth curves of LN-18 (*squares*), Daoy (*triangles*) and SW 1783 (*circles*) cells determined spectrophotometrically (UV detection, 580 nm).

The Daoy and LN-18 cell lines show similar growth rates with a mean doubling time of 40 h and 47 h, respectively. The SW1783 cell line shows the slowest proliferation kinetics with a mean doubling time of 64 h.

Doubling times of the three brain tumor cell lines did not significantly vary over different *in vitro* passages (data not shown) indicating that growth rates and chemosensitivities are independent of the utilized passage.

5.3.3   Aneuploidy

A prominent feature of cancer cells is an abnormal number of chromosomes (aneuploidy) caused by genomic instability inherent to most cancers. It occurs through chromosomal instability (CIN) by missegregation of whole chromosomes [Thompson and Compton, 2011]. CIN and aneuploidy are correlated with metastatic potential and contribute to resistance against chemotherapeutics in solid tumors [Kuukasjarvi et al., 1997; McClelland et al., 2009; Swanton et al., 2009].

Daoy, LN-18 and SW 1783 cells were investigated with regard to their chromosome distribution to evaluate their genetic stability and malignancy. Characteristic images obtained after cell preparation and Giemsa staining for the determination of the chromosomal number in the corresponding cell line are displayed in **Figure 5.6**.
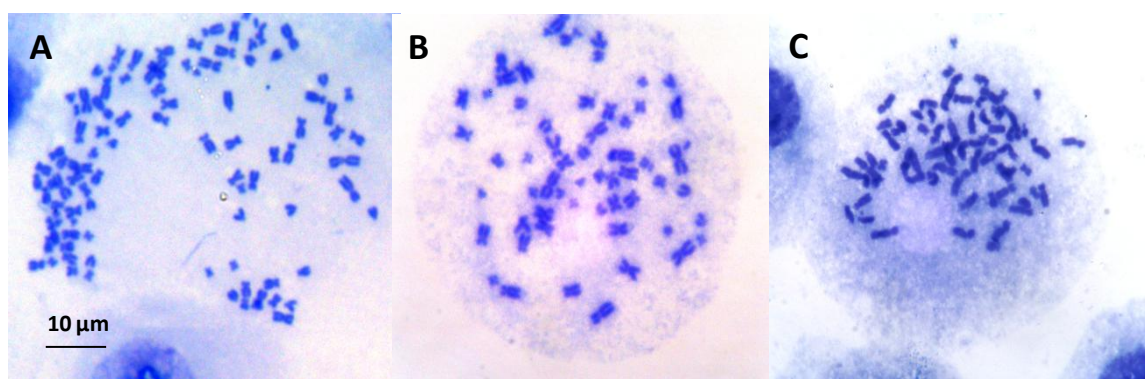
Figure 5.6: Metaphase chromosomes of Daoy (**A**), LN-18 (**B**) and SW 1783 cells (**C**) in the 7th, 18th and 81st passage, respectively, stained with Giemsa.

The number of chromosomes was plotted against the frequency in which the respective number was observed (**Figure 5.7**).
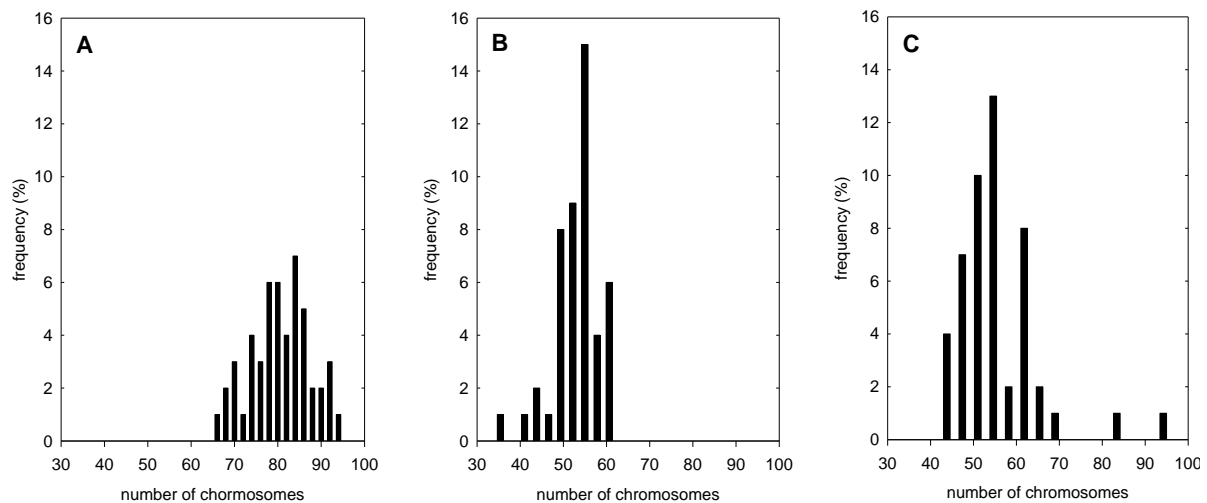
Figure 5.7: Chromosome distribution of human Daoy (**A**), LN-18 (**B**) and SW 1783 cells (**C**) in the 7th, 18th and 81st passage, respectively. For each passage the chromosomes of 50 well-spread metaphases were counted.

According to the information provided by the American Type Culture Collection (ATCC; Manassas, VA) the Daoy and SW 1783 cell lines are hypertetraploid with a modal chromosome number between 93 and 99. No karyotypical description was available for LN-18 cells. Whereas the obtained modal number of 84 for the Daoy cell line was in good greement withliterature, the main chromosome number of 56 determined for SW 1783 cells was different (**Table 5.1**). Unlike the Daoy cells, SW 1783 and LN-18 cells revealed a comparatively uniform chromosomal distribution.

Table 5.1: Karyology of the used human brain tumor cell lines

cell line	Passage	obtained modal chromosome number	range	modal chromosome number (ATCC)
Daoy	7	84	65 - 96	93 - 99
LN-18	18	54	34 - 60	-
SW 1783	81	56	42 - 96	96

For all three cell lines only minor changes in the chromosomal distribution were recognized over various *in vitro* passages (data not shown).

5.3.4   Chemosensitivity against cytostatic drugs

The cell lines Daoy, LN-18 and SW 1783 were tested for their chemosensitivity against selected anticancer drugs (**Figure 5.8**). The Daoy cell line was quite sensitive against all used cytostatics (**Figure 5.9**). Mitoxantrone, vinblastine or paclitaxel (10 nM each) and methotrexate or etoposide at a concentration of 1 µM yielded strong cytotoxic or cytocidal effects. Topotecan and doxorubicin caused a cytostatic drug effect at 10 nM.

The LN-18 (**Figure 5.10**) and SW 1783 cells (**Figure 5.11**) tolerated topotecan and doxorubicin at concentrations up to 10 nM. A concentration of 30 nM caused only a weak cytotoxic effect. Etoposide was well tolerated up to 1 µM by LN-18 cells and produced a weak toxic effect on SW 1783 cells.

The effects of all used anticancer drugs on the proliferation of the three cell lines are summarized in **Figure 5.12**. As topotecan, doxorubicin, mitoxantrone and etoposide were identified as ABCG2 substrates [Mo and Zhang, 2012], the results of the chemosensitivity studies suggest that both the LN-18 and SW 1783 cell line express the ABCG2 protein in the wildtype.
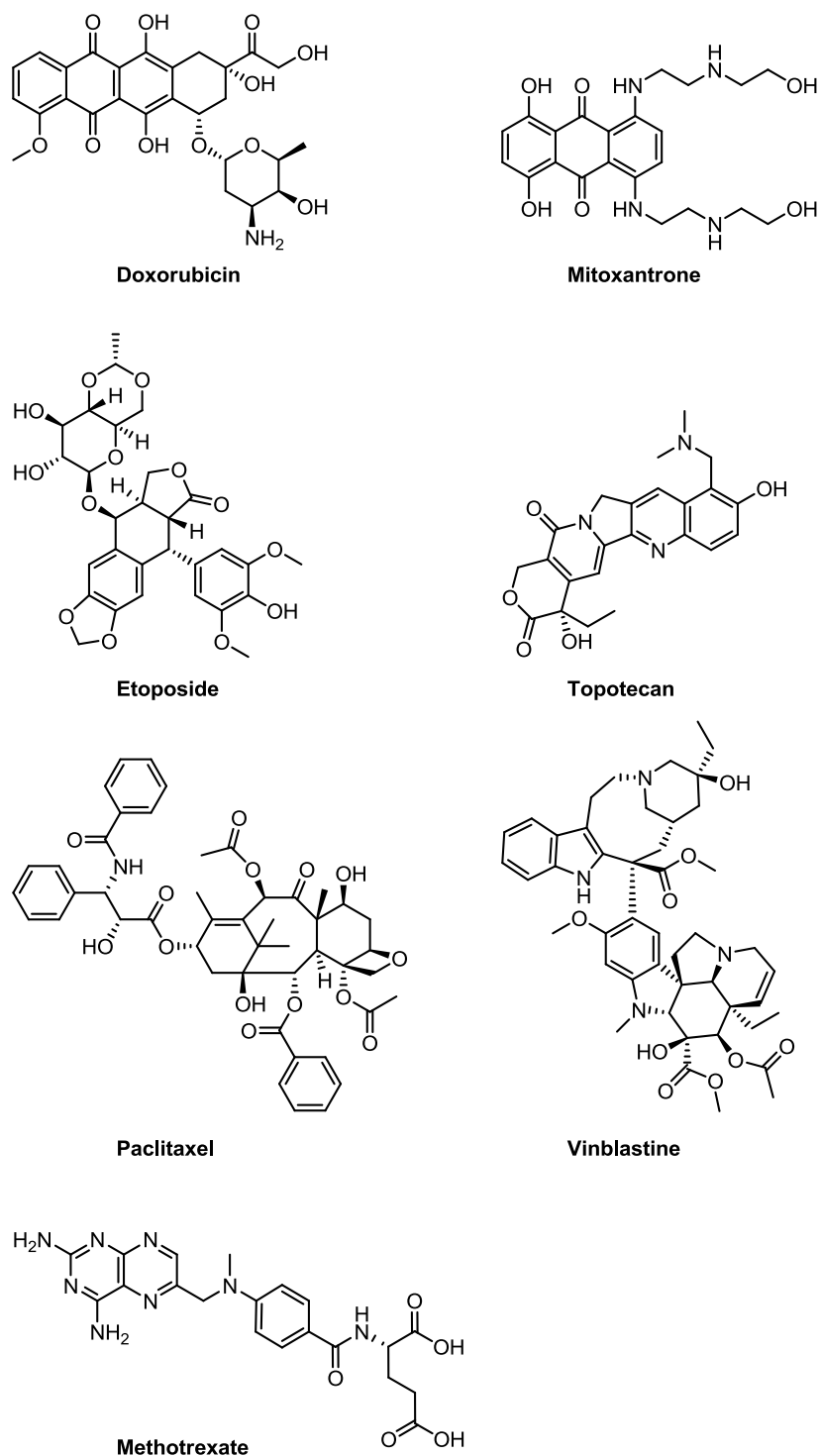
Figure 5.8: Chemical structures of anticancer drugs used for chemosensitivity studies: Doxorubicin (Doxo), Mitoxantrone (Mito), Etoposide (Etp), Topotecan (Topo), Paclitaxel (Pac), Vinblastine (Vbl), Methotrexate (MTX).
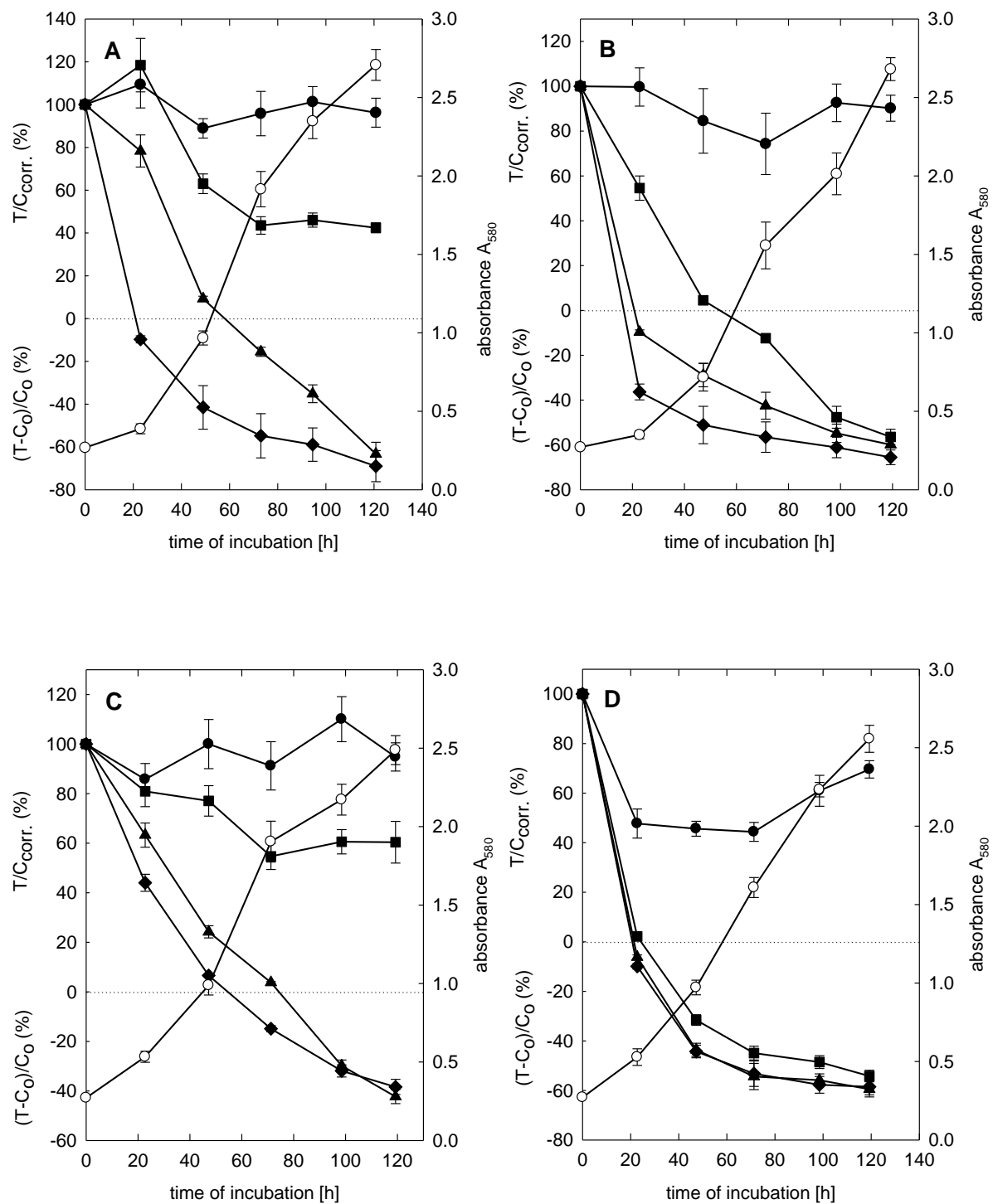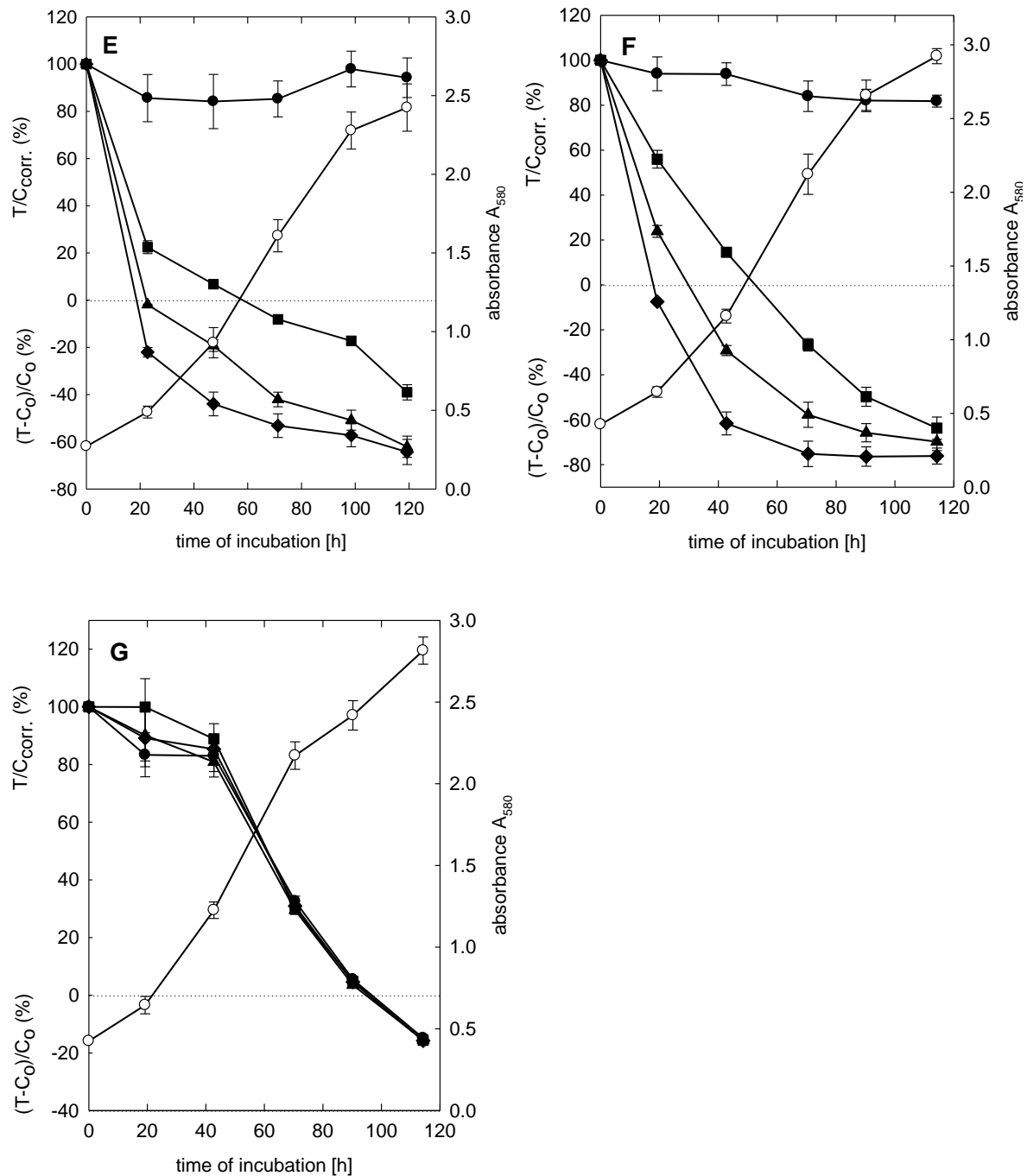
Figure 5.9: Chemosensitivity of Daoy cells against topotecan (**A**), mitoxantrone (**B**), doxorubicin (**C**), vinblastine (**D**) and paclitaxel (**E**) at the following concentrations: 1 nM (*filled circles*), 10 nM (*filled squares*), 30 nM (*filled triangles*), 100 nM (*filled diamonds*); **F**) Etoposide: 100 nM (*filled circles*), 1 μM (*filled squares*), 3 μM (*filled triangles*), 10 μM (*filled diamonds*); **G**) Methotrexate: 1 μM (*filled circles*), 10 μM (*filled squares*), 30 μM (*filled triangles*), 100 μM (*filled diamonds*); vehicle (*open circles*).
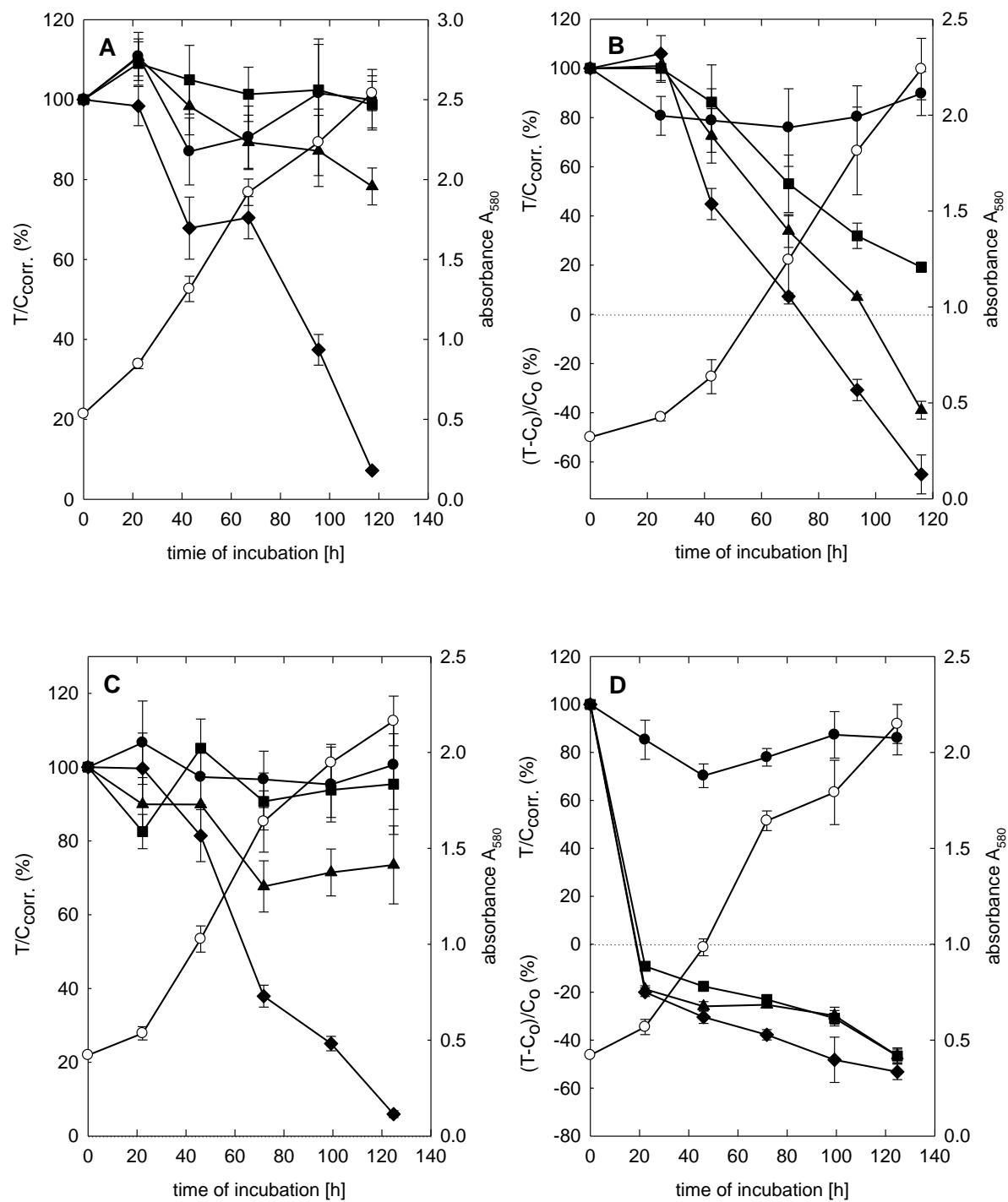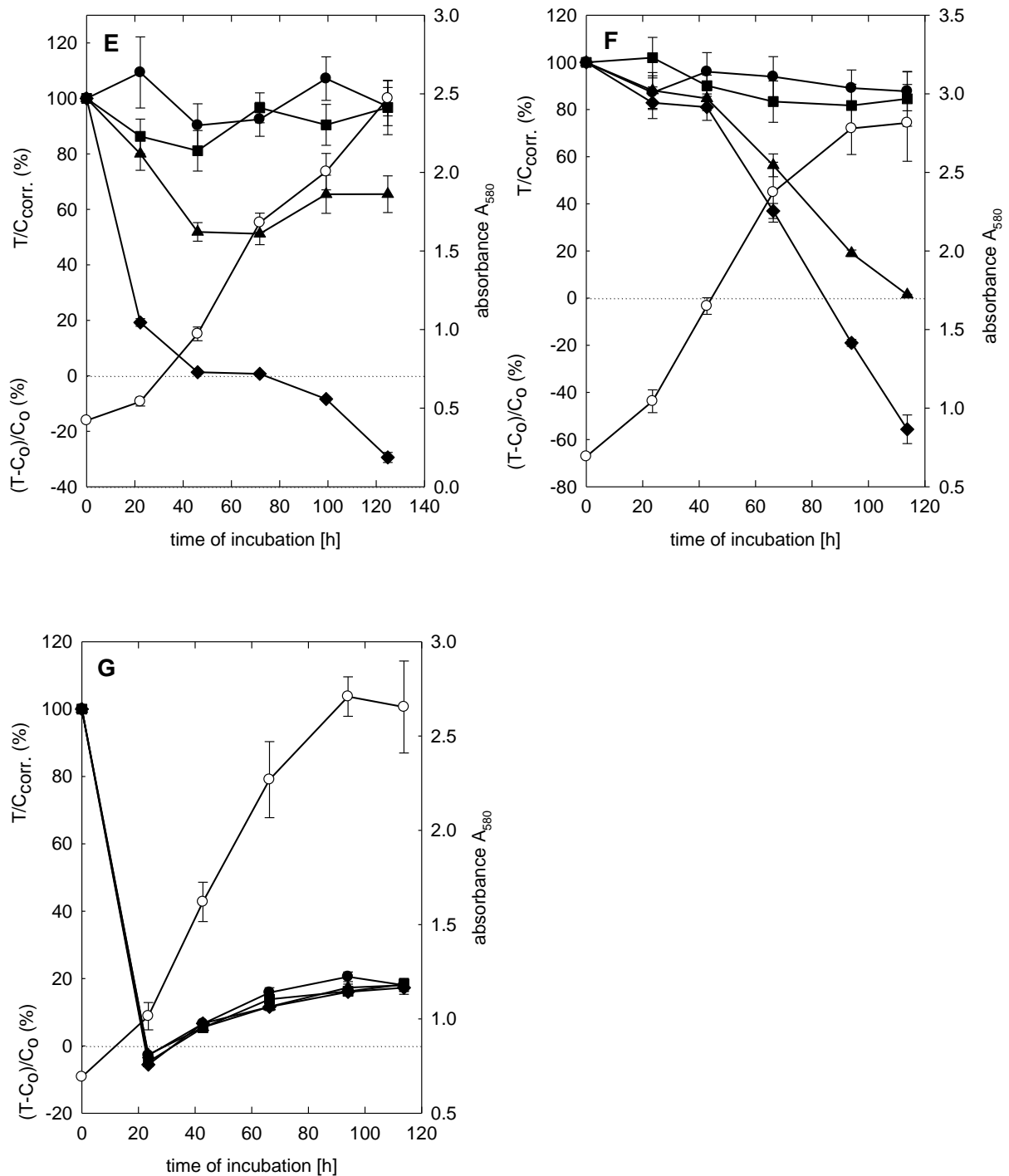
Figure 5.10: Chemosensitivity of LN-18 cells against topotecan (**A**), mitoxantrone (**B**), doxorubicin (**C**), vinblastine (**D**) and paclitaxel (**E**) at the following concentrations: 1 nM (*filled circles*), 10 nM (*filled squares*), 30 nM (*filled triangles*), 100 nM (*filled diamonds*); **F**) Etoposide: 100 nM (*filled circles*), 1 µM (*filled squares*), 3 µM (*filled triangles*), 10 µM (*filled diamonds*); **G**) Methotrexate: 1 µM (*filled circles*), 10 µM (*filled squares*), 30 µM (*filled triangles*), 100 µM (*filled diamonds*); vehicle (*open circles*).
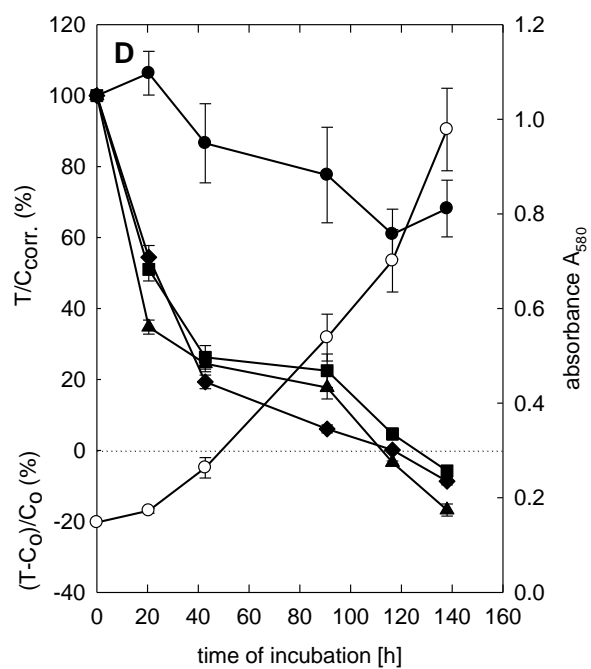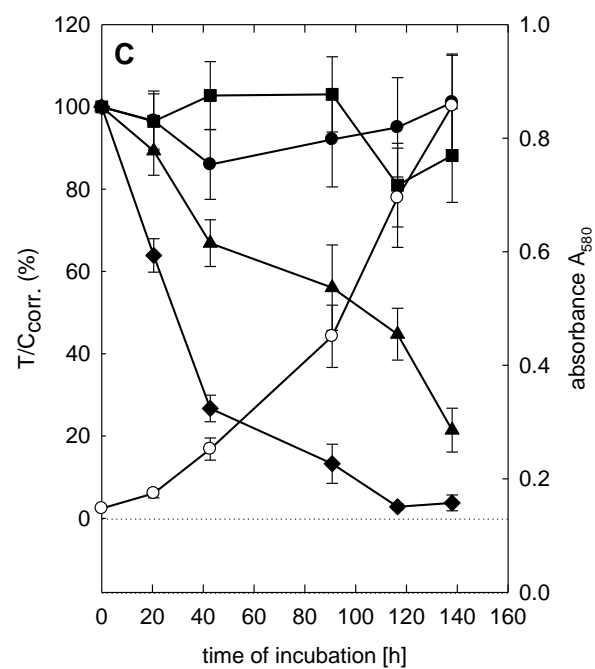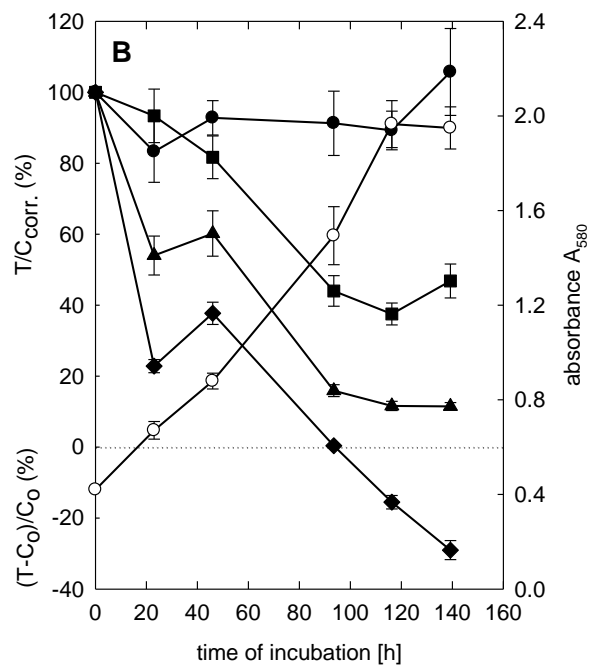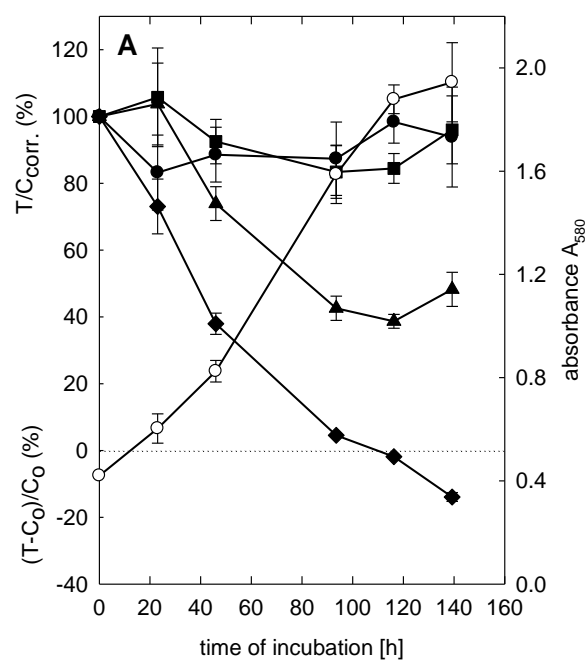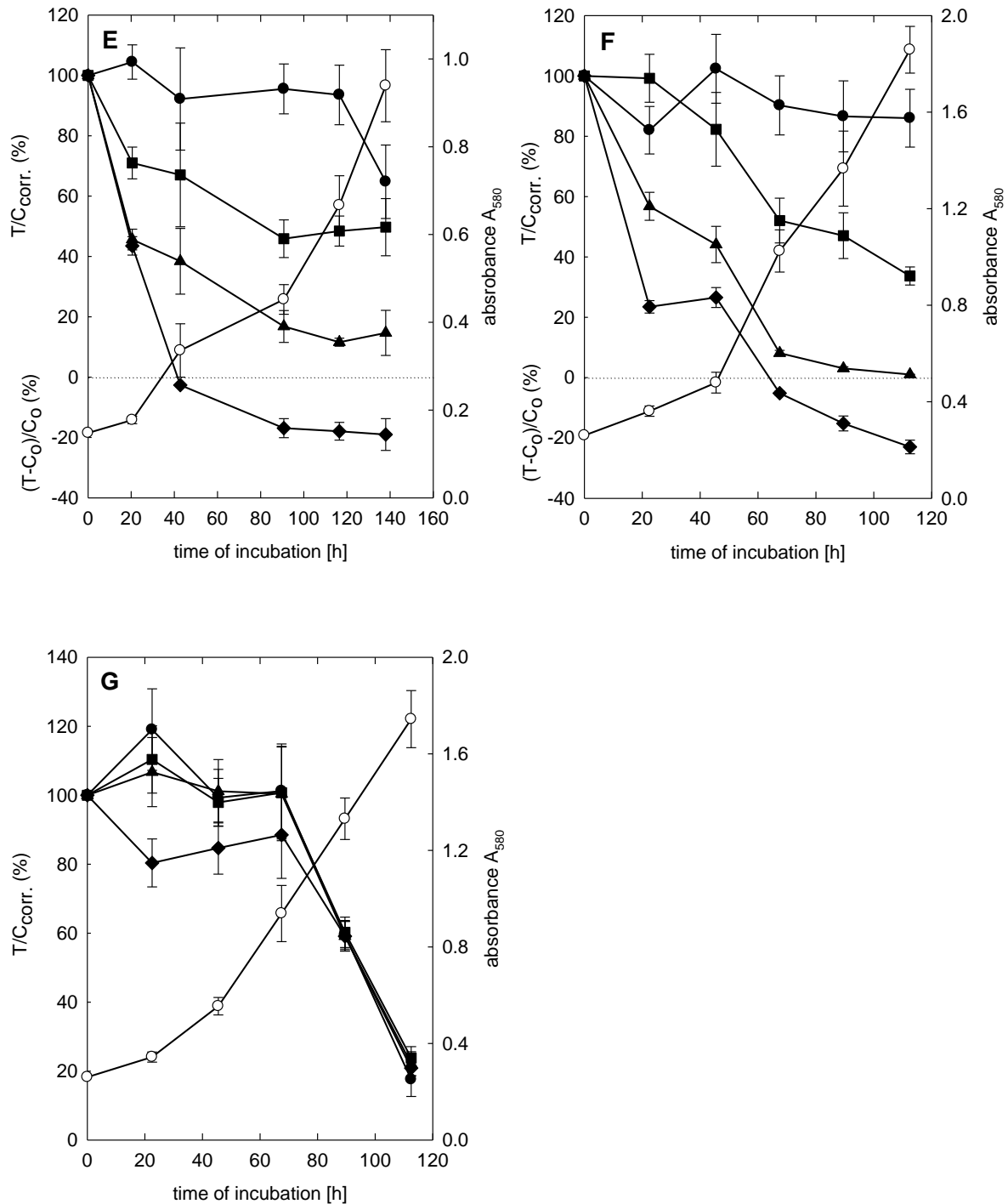
Figure 5.11: Chemosensitivity of SW 1783 cells against topotecan (**A**), mitoxantrone (**B**), doxorubicin (**C**), vinblastine (**D**) and paclitaxel (**E**) at the following concentrations: 1 nM (*filled circles*), 10 nM (*filled squares*), 30 nM (*filled triangles*), 100 nM (*filled diamonds*); **F**) Etoposide: 100 nM (*filled circles*), 1 µM (*filled squares*), 3 µM (*filled triangles*), 10 µM (*filled diamonds*); **G**) Methotrexate: 1 µM (*filled circles*), 10 µM (*filled squares*), 30 µM (*filled triangles*), 100 µM (*filled diamonds*); vehicle (*open circles*).

Drug	Conc.	Daoy	LN-18	SW 1783
Topo	1 nM	no effect	no effect	no effect
Topo	10 nM	cytostatic / cytotoxic	no effect	no effect
Topo	30 nM	cytocidal	weak cytotoxic	weak cytotoxic
Topo	100 nM	cytocidal	cytostatic / cytotoxic	cytocidal
Mito	1 nM	no effect	no effect	no effect
Mito	10 nM	cytocidal	weak cytotoxic	weak cytotoxic
Mito	30 nM	cytocidal	cytocidal	cytostatic / cytotoxic
Mito	100 nM	cytocidal	cytocidal	cytocidal
Doxo	1 nM	no effect	no effect	no effect
Doxo	10 nM	weak cytotoxic	no effect	no effect
Doxo	30 nM	cytocidal	weak cytotoxic	weak cytotoxic
Doxo	100 nM	cytocidal	cytostatic / cytotoxic	cytostatic / cytotoxic
Vbl	1 nM	weak cytotoxic	no effect	weak cytotoxic
Vbl	10 nM	cytocidal	cytocidal	cytocidal
Vbl	30 nM	cytocidal	cytocidal	cytocidal
Vbl	100 nM	cytocidal	cytocidal	cytocidal
Pac	1 nM	no effect	no effect	no effect
Pac	10 nM	cytocidal	no effect	weak cytotoxic
Pac	30 nM	cytocidal	weak cytotoxic	cytostatic / cytotoxic
Pac	100 nM	cytocidal	cytocidal	cytocidal
Etp	100 nM	no effect	no effect	no effect
Etp	1 µM	cytocidal	no effect	weak cytotoxic
Etp	3 µM	cytocidal	cytostatic / cytotoxic	cytostatic / cytotoxic
Etp	10 µM	cytocidal	cytocidal	cytocidal
MTX	1 µM	cytocidal	cytostatic / cytotoxic	cytostatic / cytotoxic
MTX	10 µM	cytocidal	cytostatic / cytotoxic	cytostatic / cytotoxic
MTX	30 µM	cytocidal	cytostatic / cytotoxic	cytostatic / cytotoxic
MTX	100 µM	cytocidal	cytostatic / cytotoxic	cytostatic / cytotoxic

Legend:
- no effect
- weak cytotoxic
- cytostatic / cytotoxic
- cytocidal

Figure 5.12: Summary of the different effects of the used anticancer drugs on the proliferation of Daoy, LN-18 and SW 1783 cells.

5.3.5 Characterization and growth kinetics of human brain tumor cell lines in a subcutaneous tumor model in nude mice

5.3.5.1 *In vivo* growth kinetics

With respect to their potential use in a new orthotopic brain tumor model, Daoy, LN-18 and SW 1783 cells were investigated *in vivo*. The cells were subcutaneously injected into nude NMRI (nu/nu) mice. Unfortunately, only the Daoy medulloblastoma cells were tumorigenic. **Figure 5.13** shows the *in vivo* growth kinetics of Daoy xenografts in consecutive passages when injected as cell suspension or implanted as solid tumor pieces.

In general, Daoy tumors were hardly supplied with blood resulting in a long phase of tumor formation (about 70 days) and a slow growth rate, especially in passages 0-2. Primarily in passage 3 the growth behavior changed. Take rates increased from 20% in passage 0 to 40-60% in the following passages. Nevertheless, the growth rates of Daoy tumors have not been reproducible till the end of this work. The body weight of animals was controlled as an indication of the general state of health. For future work tumor pieces were cryopreserved and afterwards stored in liquid nitrogen.
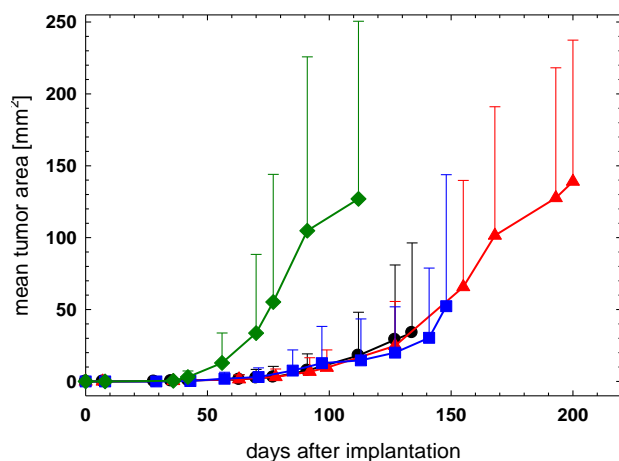
Figure 5.13: Growth curves of subcutaneous Daoy tumors over various passages after injection as cell suspension (passage 0; passage 25 in cell culture; *black circles*) or 1 mm³ tumor pieces (passages 1-3); passage 1: *red triangles*, passage 2: *blue squares*, passage 3: *green diamonds*.

5.3.5.2   Histology

Figure 5.14 shows the morphology of a human Daoy medulloblastoma tumor grown in nude mice after Masson-Goldner (MG) and haematoxylin-eosin (HE) staining. MG staining works with three different stains allowing a differentiated visualization of tissues: Cell nuclei are displayed in dark brown, cytoplasm and muscle fibers in red, connective tissue in green.

Attributes like anisomorphism and multiple prominent nucleoli highlight the malignant character of the Daoy cell line. Mitotic activity, however, is low, resulting in a very slow *in vivo* growth.
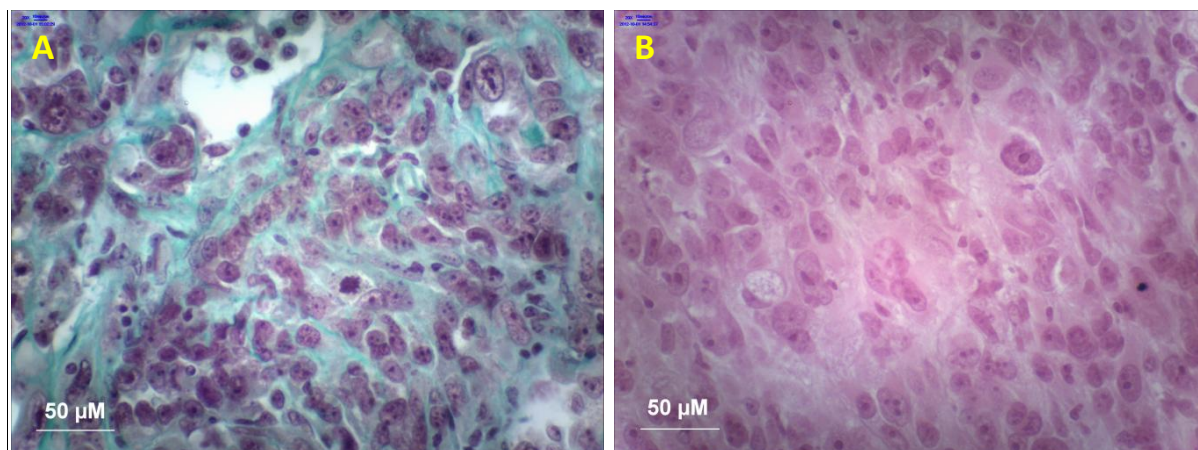
Figure 5.14: MG (**A**) and HE (**B**) staining of a subcutaneous Daoy tumor (passage 0), 150 days after implantation (BH-2 microscope, Olympus; objective 20x).

5.3.6   Investigations on ABCG2 induced cell lines

5.3.6.1   Western Blot analysis of wildtype and induced cell lines

Western Blot (WB) analysis and chemosensitivity tests (cf. section 5.3.4) revealed that LN-18 and SW 1783 cells express the ABCG2 protein in the wildtype (**Figure 5.15**, lanes **b** and **c**). Besides these two cell lines, additionally, Daoy and P388D1 cells were treated with increasing topotecan

concentrations to yield sufficient ABCG2 transporter expression. Induction of BCRP overexpression was monitored via WB analysis at different times after starting the topotecan treatment.
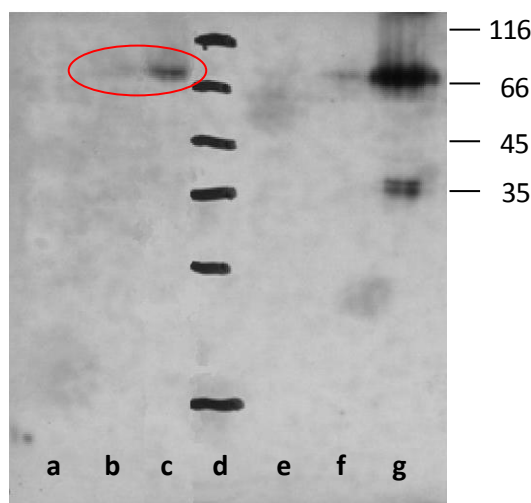
Figure 5.15: Immunological detection of ABCG2 expressed in various tumor cell lines. 20 µg of protein per cell lysate were loaded on each lane. **a**: Daoy; **b**: LN-18; **c**: SW 1783; **d**: peqGold Protein Marker I; **e**: P388D1; **f**: P388D1/Topo (350 nM); **g**: MCF-7/Topo (550 nM); numbers on the right designate masses of marker proteins in kDa.

After 10 weeks of treatment with topotecan up to a final concentration of 800 nM and 400 nM, respectively, LN-18 and SW 1783 cells (in the following designated as LN-18/Topo and SW 1783/Topo cells) show ABCG2 transporter expression (**Figure 5.16**) comparable to the standard cell line MCF-7/Topo. The predicted molecular weight of the ABCG2 transporter monomer is 72 kDa. Band analysis was performed with Quantity One (Bio-Rad) software and revealed a band of ~70 kDa for MCF-7Topo cells (positive control) as well as for induced SW 1783 and LN-18 cells (**Figure 5.16**, lanes **d** and **g**). Some diffuse bands were found at ~35 kDa, probably resulting from unspecific antibody binding or proteolysis of the target BCRP protein.

To have access to a murine ABCG2 transporter system with regard to investigations in animal models, the induction of ABCG2 was explored in the mouse cell line P388D1. However, although topotecan concentrations as high as 1 µM were tolerated, there was no induction of ABCG2 transporter expression detectable (**Figure 5.16**, lane **b**). By contrast, the Daoy cell line did not tolerate ascending topotecan concentrations beyond a concentration of 30 nM.
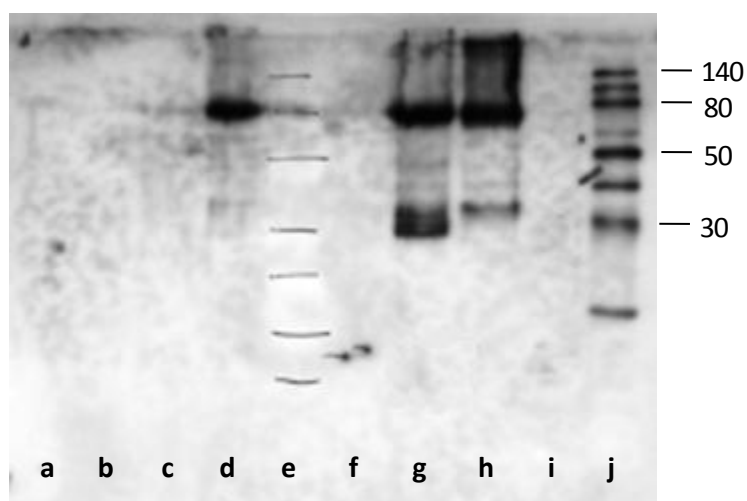
Figure 5.16: Immunological detection of ABCG2 in tumor cell lines 10 weeks after starting BCRP induction by incubation with topotecan. 20 µg of protein per cell lysate were loaded on each lane. **a**: Daoy/Topo (30 nM); **b**: P388D1/Topo (1 µM); **c**: SW 1783; **d**: SW 1783/Topo (400 nM); **e**: peqGold Protein Marker I; **f**: LN-18; **g**: LN-18/Topo (800 nM); **h**: MCF-7/Topo (550 nM); **i**: Kb-V1 (ABCG2-negative control); **j**: Biotinylated Protein Ladder (9-200 kDa, Cell Signaling); numbers on the right designate masses of marker proteins in kDa.

For a rough estimation of the expression level in the newly induced cell lines in comparison to the standard MCF-7/Topo cell line, the specular optical densities (OD) of the bands around 70 kDa were calculated after calibration by the Quantity One software for the GS-710 Imaging Densitometer (**Table 5.2**). The three topotecan treated cells types seemed to express the ABCG2 protein to a similar extent.

Table 5.2: Comparison of Western Blot band analysis for induced cell lines.

lane	cell line	calculated MW [kDa]	band OD
d	SW 1783/Topo (400 nM)	69.24	2.07
g	LN-18/Topo (800 nM)	68.36	2.15
h	MCF-7/Topo (550 nM)	70.02	2.00

5.3.6.2   Determination of ABCG2 overexpression by flow cytometry

In addition to the Western Blot analysis, an indirect flow cytometric FACS assay was performed to compare the ABCG2 transporter expression in LN-18 and SW 1783 wildtype cells to the expression in the corresponding topotecan treated cells. By analogy with the Western Blot analysis, an increased ABCG2 transporter expression was determined for LN-18/Topo (**Figure 5.17**) and SW 1783/Topo cells (**Figure 5.18**) compared to the wt cells. The quantification was based on the differences between the corresponding geometrical mean (GeoMean) values. Autofluorescence and the fluorescence of the cells under treatment with the secondary antibody alone were used as negative controls.
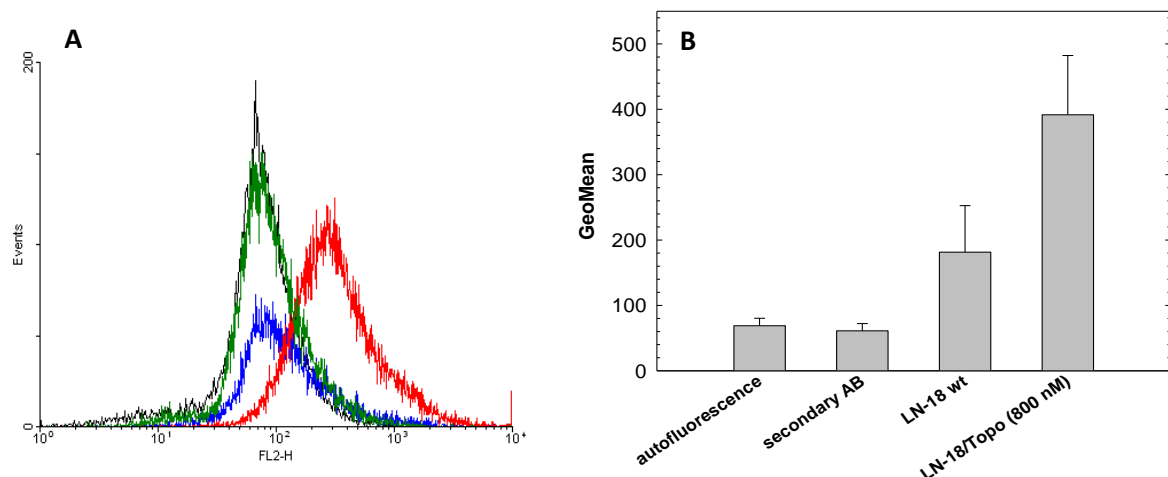
Figure 5.17: A) ABCG2 transporter expression determined by flow cytometric analysis on human LN-18 wildtype (*blue)* and LN-18/Topo (800 nM) cells (*red*); autofluorescense (*black*), secondary antibody (*green*). **B**) GeoMean values (+ SEM) of LN-18 wild type and topotecan induced cells calculated from 2 independent experiments.

Only for SW 1783 cells, marginal non-specific binding of the secondary antibody (goat anti-rat IgG-PE) was detectable. The GeoMean value of LN-18 cells was doubled by the treatment with topotecan, whereas the GeoMean of SW 1783/Topo cells was three times as high as for the wildtype cells. The induced SW 1783 cells contained a subpopulation, which was not further influenced by the treatment with topotecan (**Figure 5.18** (**A**), red graph).
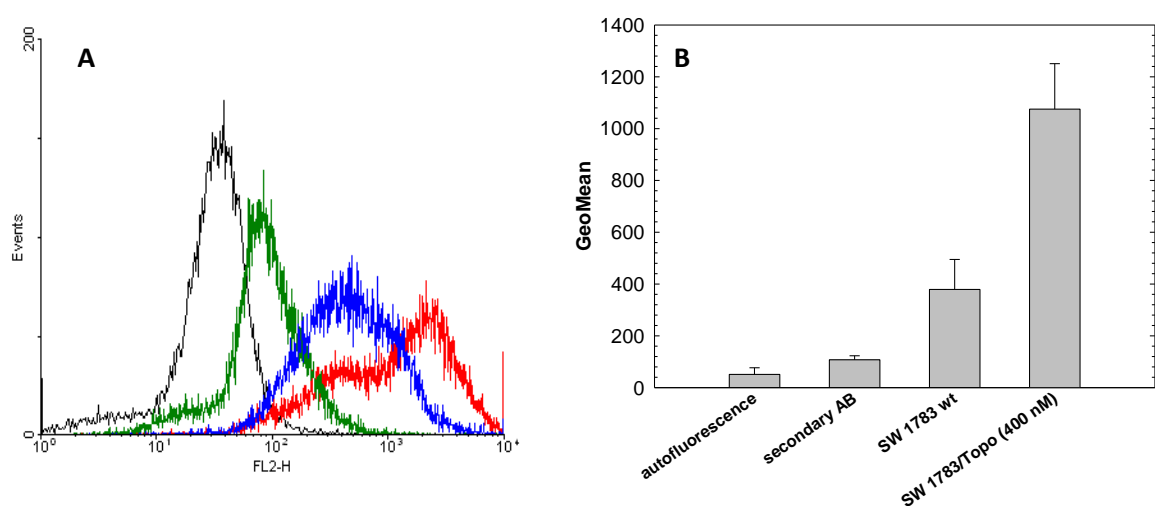
Figure 5.18: A) Graphical illustration of ABCG2 transporter expression via flow cytometric analysis in human SW 1783 wildtype (*blue*) and in SW 1783/Topo (400 nM) cells (*red)*; autofluorescense (*black*), secondary antibody (*green*). **B**) GeoMean values (+ SEM) of SW 1783 wild type and topotecan induced cells calculated from 2 independent experiments.

5.3.6.3   Hoechst 33342 assay using ABCG2 induced cancer cells

The Hoechst 33342 assay was performed with the ABCG2 overexpressing brain tumor cells to determine the transporter inhibition by a selection of synthesized modulators according to the

standard procedure described for MCF-7/Topo cells in section 3.3.5.1 using fumitremorgin C as the reference substance.

Table 5.3: Inhibition of ABCG2 by selected modulators in the Hoechst 33342 assay using three different BCRP overexpressing cell lines.

Compound	MCF-7/Topo[a]		SW 1783/Topo[b]		LN-18/Topo[b]	
	IC$_{50}$ [nM]	I$_{max}$ (%)	IC$_{50}$ [nM]	I$_{max}$ (%)	IC$_{50}$ [nM]	I$_{max}$ (%)
FTC	731 ± 92	100	842 ± 101	114 ± 19	1,129 ± 203	113 ± 12
12 (UR-COP228)	591 ± 87	109 ± 8	625 ± 52	117 ± 12	633 ± 255	105 ± 2
32 (UR-COP269)	59 ± 11	101 ± 5	68 ± 21	108 ± 6	71 ± 18	104 ± 13
33 (UR-COP272)	46 ± 1	111 ± 9	40 ± 9	112 ± 22	60 ± 16	109 ± 10
36 (UR-MB83-2)	168 ± 81	96 ± 1	173 ± 98	105 ± 18	257 ± 174	86 ± 9
41 (UR-MB108-4)	64 ± 3	95 ± 3	48 ± 10	101 ± 2	120 ± 42	103 ± 9

[a] Mean values (+ SEM) were calculated from two to three independent experiments performed in sextuplicate; [b] Mean values (+ SEM) were calculated from two independent experiments performed in triplicate.

As shown in **Table 5.3** and displayed in **Figure 5.19** for compounds **32** and **33**, the obtained IC$_{50}$ values and the maximal inhibitory effects are almost identical in the Hoechst 33342 assay, independent from the used cells. Therefore, these three cell lines are considered to be useful for the study of ABCG2 modulators in the H33342 assay.
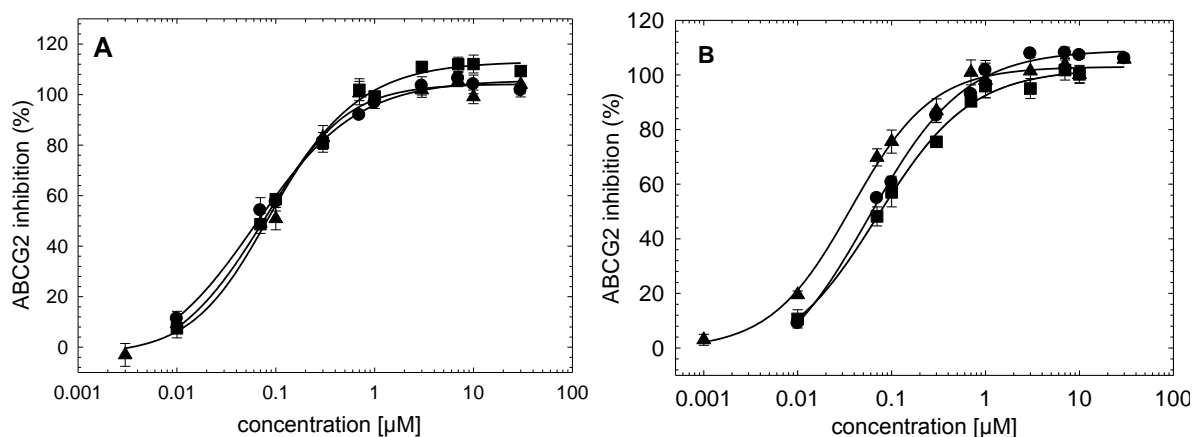
Figure 5.19: Inhibition of ABCG2 by compounds **32** (**A**) and **33** (**B**) using MCF-7/Topo (*filled circles*), SW 1783/Topo (*filled triangles*) and LN-18/Topo cells (*filled squares*).

5.3.6.4   Chemosensitivity of LN-18/Topo cells against selected cytostatics

The effect of mitoxantrone, doxorubicin (ABCG2 substrates) and vinblastine on the proliferation of ABCG2 overexpressing LN-18/Topo cells were investigated by means of a kinetic chemosensitivity assay. The results of the drug effects on wildtype (cf. section 5.3.4) and ABCG2 induced LN-18 cells are shown in **Figure 5.20** and **Figure 5.21**.

The treatment of LN-18 wildtype cells with mitoxantrone at concentrations of 30 nM and 100 nM, respectively, caused a strong cytocidal drug effect. LN-18/Topo cells, however, were resistant against this ABCG2 substrate at concentrations up to 100 nM.

In case of doxorubicin, a moderate substrate of BCRP, the differences between the effects on the two cell types were less significant as for mitoxantrone. Nevertheless, a high concentration of 100 nM resulted in a strong cytotoxic effect on LN-18 wt cells and only in a weak toxic effect on the ABCG2 induced cells.

As expected, the chemosensitivity against vinblastine (P-gp substrate) did not differ between the wildtype and LN-18/Topo cells (data not shown).
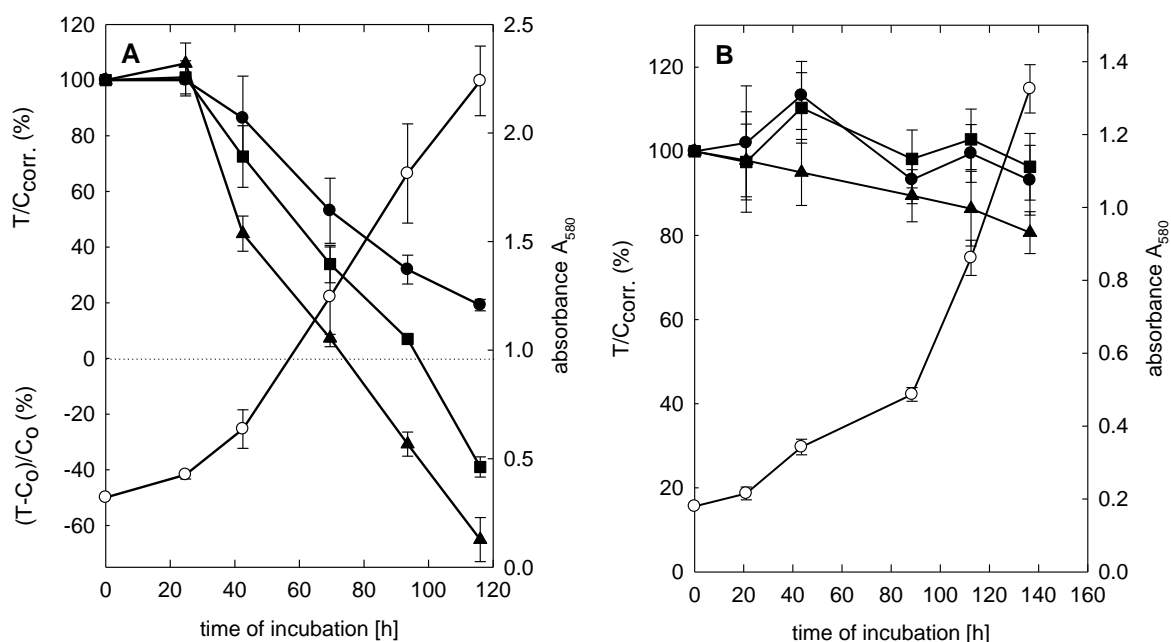
Figure 5.20: Chemosensitivity of LN-18 wt (**A**) and LN-18/Topo (**B**) cells against mitoxantrone at the following concentrations: 10 nM (*filled circles*), 30 nM (*filled squares*), 100 nM (*filled triangles*); vehicle (*open circles*).
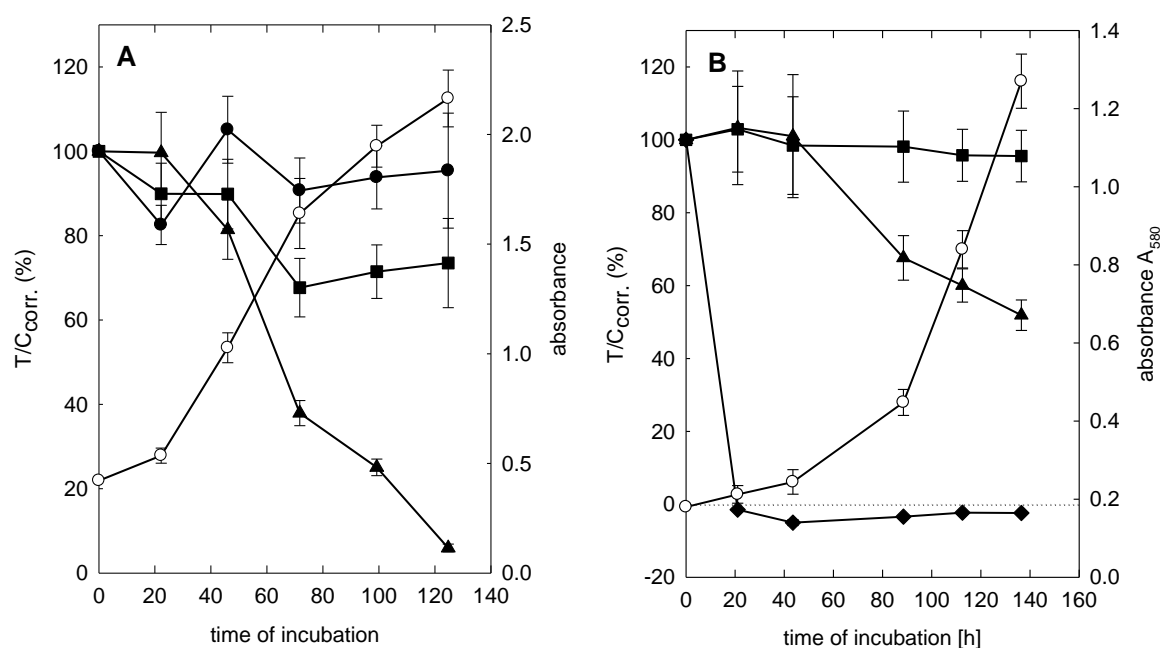
Figure 5.21: Chemosensitivity of LN-18 wt (**A**) and LN-18/Topo (**B**) cells against doxorubicin at the following concentrations: 10 nM (*filled circles*), 30 nM (*filled squares*), 100 nM (*filled triangles*); 300 nM (*filled diamonds*); vehicle (*open circles*).

5.3.7   ABC transporter expression in HMEC-1 cells

Immortalized human microvascular endothelial cells (HMEC-1) were investigated for ABCB1, ABCG2 and ABCC1 expression by means of a FACS assay as described in section 5.2.10 (GeoMean values cf. **Table 5.4**). The endothelial cells (EC) revealed moderate expression of MRP1 (ABCC1) and ABCG2, whereas P-gp (ABCB1) was not detected.

The test for ABC transporter expression via flow cytometric analysis was performed only once due to a very slow *in vitro* growth of the cells. The results have to be confirmed by additional experiments, nevertheless they are in a good agreement with recently published data [Eilers et al., 2008]. Eilers et al. monitored the expression of ABC transporters in primary EC from different human tissues, including dermal microvascular endothelial cells. The authors report on a significant ABCC1 transporter expression in all investigated ECs, whereas P-gp levels were lowest for microvessel derived ECs.

	ABCB1	ABCC1	ABCG2
autofluorescence	72.4	72.1	72.6
sec. AB	122.0	79.0	89.9
prim. + sec. AB	118.4	147.0	129.3

Table 5.4: GeoMean values for ABC transporter expression in HMEC-1 cells determined by flow cytometry. Background fluorescence of HMEC-1 cells and non-specific binding of the secondary antibody were detected and used as negative controls.
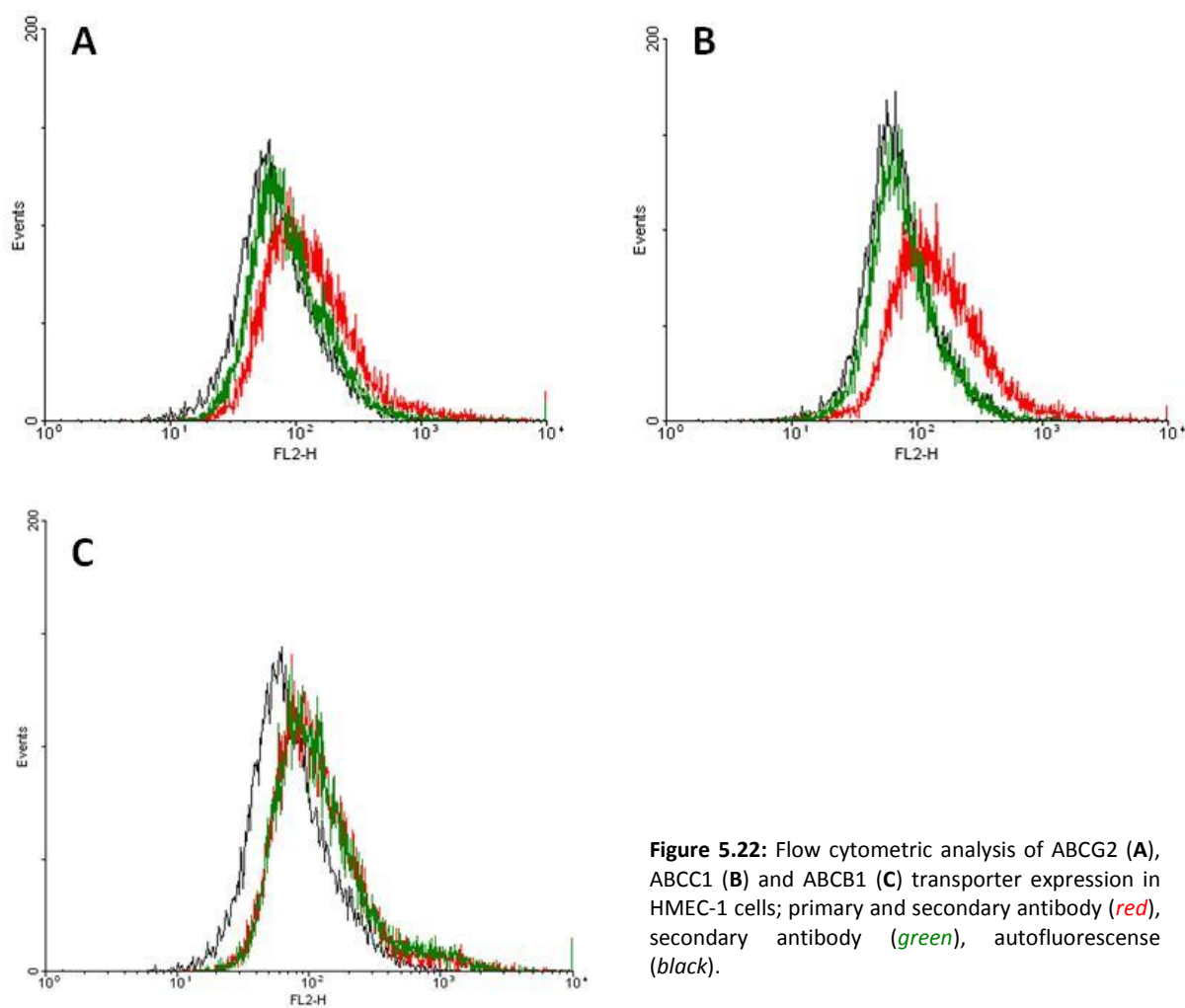
Figure 5.22: Flow cytometric analysis of ABCG2 (**A**), ABCC1 (**B**) and ABCB1 (**C**) transporter expression in HMEC-1 cells; primary and secondary antibody (*red*), secondary antibody (*green*), autofluorescense (*black*).

5.4   Summary

The malignant brain tumor cells Daoy, LN-18 and SW 1783 were investigated with regard to their morphology, *in vitro* growth kinetics, chemosensitivity against anticancer drugs, chromosome distribution and ABC transporter expression. All cell lines show pronounced features of high malignancy and genetic instability. Chemotoxicity studies revealed a high sensitivity of the Daoy cell line against almost all used cytotstatics whereas LN-18 and SW 1783 cells were at least partially resistant, for instance, against topotecan, doxorubicin and etoposide. Western Blot analysis and chemosensitivity tests indicated a slight ABCG2 transporter expression in LN-18 and SW 1783 wildtype cells. Treatment of these cells with increasing concentrations of topotecan yielded two BCRP overexpressing cell lines which are comparable to the standard MCF-7/Topo cell line and are therefore suitable for the use in *in vitro* assays.

The Daoy medulloblastoma cells were successfully established as subcutaneously growing tumors in nude mice, whereas LN-18 and SW 1783 cells were not tumorigenic under the same conditions. Results of FACS investigations on HMEC-1 cells suggest expression of the ABCC1 transporter in these endothelial cells.

5.5   References

Abbott, N. J., Patabendige, A. A., Dolman, D. E., et al. Structure and function of the blood-brain barrier. *Neurobiol. Dis.* **2010**, 37(1), 13-25.

Ades, E. W., Candal, F. J., Swerlick, R. A., et al. HMEC-1: establishment of an immortalized human microvascular endothelial cell line. *J. Invest. Dermatol.* **1992**, 99(6), 683-690.

Bradford, M. M. A rapid and sensitive method for the quantitation of microgram quantities of protein utilizing the principle of protein-dye binding. *Anal. Biochem.* **1976**, 72, 248-254.

Cohen, M. H., Shen, Y. L., Keegan, P., et al. FDA drug approval summary: bevacizumab (Avastin) as treatment of recurrent glioblastoma multiforme. *Oncologist* **2009**, 14(11), 1131-1138.

Cook, L. J. and Freedman, J. *Brain Tumors*. The Rosen Publishing Group, Inc., New York, USA, 2012.

Dolecek, T. A., Propp, J. M., Stroup, N. E., et al. CBTRUS statistical report: primary brain and central nervous system tumors diagnosed in the United States in 2005-2009. *Neuro Oncol.* **2012**, 14 Suppl 5, v1-49.

Eilers, M., Roy, U. and Mondal, D. MRP (ABCC) transporters-mediated efflux of anti-HIV drugs, saquinavir and zidovudine, from human endothelial cells. *Exp. Biol. Med. (Maywood)* **2008**, 233(9), 1149-1160.

Ferlay, J., Shin, H. R., Bray, F., et al. Estimates of worldwide burden of cancer in 2008: GLOBOCAN 2008. *Int. J. Cancer.* **2010**, 127(12), 2893-2917.

Ferlay, J., Steliarova-Foucher, E., Lortet-Tieulent, J., et al. Cancer incidence and mortality patterns in Europe: estimates for 40 countries in 2012. *Eur. J. Cancer* **2013**, 49(6), 1374-1403.

Huse, J. T. and Holland, E. C. Targeting brain cancer: advances in the molecular pathology of malignant glioma and medulloblastoma. *Nat. Rev. Cancer* **2010**, 10(5), 319-331.

Jarzyna, P. Preclinical investigations on the effect of the human hyaluronidase Hyal-1 on growth and metastasis of human colon carcinoma. PhD thesis, University of Regensburg, Germany, 2007.

Kuukasjarvi, T., Karhu, R., Tanner, M., et al. Genetic heterogeneity and clonal evolution underlying development of asynchronous metastasis in human breast cancer. *Cancer Res.* **1997**, 57(8), 1597-1604.

Laemmli, U. K. Cleavage of structural proteins during the assembly of the head of bacteriophage T4. *Nature* **1970**, 227(5259), 680-685.

Lee, G., Dallas, S., Hong, M., et al. Drug transporters in the central nervous system: brain barriers and brain parenchyma considerations. *Pharmacol. Rev.* **2001**, 53(4), 569-596.

Louis, D. N., Ohgaki, H., Wiestler, O. D., et al. The 2007 WHO classification of tumours of the central nervous system. *Acta Neuropathol.* **2007**, 114(2), 97-109.

Martin-Banderas, L., Holgado, M. A., Venero, J. L., et al. Nanostructures for drug delivery to the brain. *Curr. Med. Chem.* **2011**, 18(34), 5303-5321.

McClelland, S. E., Burrell, R. A. and Swanton, C. Chromosomal instability: a composite phenotype that influences sensitivity to chemotherapy. *Cell Cycle* **2009**, 8(20), 3262-3266.

Mo, W. and Zhang, J. T. Human ABCG2: structure, function, and its role in multidrug resistance. *Int. J. Biochem. Mol. Biol.* **2012**, 3(1), 1-27.

Mulisch, M. and Welch, U. *Romeis Mikroskopische Technik*. Spektrum Akademischer Verlag, Heidelberg, Germany, 2010.

Müller, C. New approaches to the therapy of glioblastoma: investigations on RNA interference, kinesin Eg5 and ABCB1/ABCG2 inhibition. PhD thesis, University of Regensburg, Germany, 2007.

Newlands, E. S., Stevens, M. F., Wedge, S. R., et al. Temozolomide: a review of its discovery, chemical properties, pre-clinical development and clinical trials. *Cancer Treat. Rev.* **1997**, 23(1), 35-61.

Orthmann, A., Zeisig, R., Suss, R., et al. Treatment of experimental brain metastasis with MTO-liposomes: impact of fluidity and LRP-targeting on the therapeutic result. *Pharm. Res.* **2012**, 29(7), 1949-1959.

Panigrahi, M., Das, P. K. and Parikh, P. M. Brain tumor and Gliadel wafer treatment. *Indian J. Cancer* **2011**, 48(1), 11-17.

Pardridge, W. M. The blood-brain barrier and neurotherapeutics. *NeuroRx.* **2005**, 2(1), 1-2.

Pertschuk, D., Cloughesy, T. F., Chang, S. M., et al. Ascending dose trials of the safety and tolerability of Toca 511, a retroviral replicating vector encoding cytosine deaminase, in patients with recurrent high-grade glioma. *J. Clin. Oncol.* **2012**, 30(15).

Robbins, J. M., Dickinson, P. J., York, D., et al. Evaluation of Delivery of Retroviral Replicating Vector, Toca 511, in Spontaneous Canine Brain Tumor. *Neuro Oncol.* **2012**, 14, 48-48.

Rooney, D. E. and Czepulkowski, B. H. *Human Cytogenetics - A Practical Approach*. Oxford University Press, USA, 1992.

Rousselle, C., Smirnova, M., Clair, P., et al. Enhanced delivery of doxorubicin into the brain via a peptide-vector-mediated strategy: saturation kinetics and specificity. *J. Pharmacol. Exp. Ther.* **2001**, 296(1), 124-131.

Saito, R. and Tominaga, T. Convection-enhanced delivery: from mechanisms to clinical drug delivery for diseases of the central nervous system. *Neurol. Med. Chir. (Tokyo)* **2012**, 52(8), 531-538.

Sekine, T., Cha, S. H. and Endou, H. The multispecific organic anion transporter (OAT) family. *Pflugers Arch.* **2000**, 440(3), 337-350.

Shih, T. and Lindley, C. Bevacizumab: an angiogenesis inhibitor for the treatment of solid malignancies. *Clin. Ther.* **2006**, 28(11), 1779-1802.

Stamatovic, S. M., Keep, R. F. and Andjelkovic, A. V. Brain endothelial cell-cell junctions: how to "open" the blood brain barrier. *Curr. Neuropharmacol.* **2008**, 6(3), 179-192.

Stupp, R., Mason, W. P., van den Bent, M. J., et al. Radiotherapy plus concomitant and adjuvant temozolomide for glioblastoma. *N. Engl. J. Med.* **2005**, 352(10), 987-996.

Swanton, C., Nicke, B., Schuett, M., et al. Chromosomal instability determines taxane response. *Proc. Natl. Acad. Sci. U S A* **2009**, 106(21), 8671-8676.

Takahashi, M. *Farbatlas der onkologischen Zytologie*. Perimed-Fachbuch-Verlag-Ges., Erlangen, Germany, 1987.

Thompson, S. L. and Compton, D. A. Chromosomes and cancer cells. *Chromosome Res.* **2011**, 19, 433-444.

Tosi, G., Bortot, B., Ruozi, B., et al. Potential Use of Polymeric Nanoparticles for Drug Delivery Across the Blood-Brain Barrier. *Curr. Med. Chem.* **2013**, 20(17), 2212-2225.

Walker, M. D. and Hurwitz, B. S. BCNU (1,3-bis(2-chloroethyl)-1-nitrosourea; NSC-409962) in the treatment of malignant brain tumor--a preliminary report. *Cancer Chemother. Rep.* **1970**, 54(4), 263-271.

Wen, P. Y. and Kesari, S. Malignant gliomas in adults. *N. Engl. J. Med.* **2008**, 359(5), 492-507.

C*hapter 6*

6   Towards an ATPase assay for the human ABCG2 transporter

6.1   Introduction

ABC transporter-mediated drug transport across membranes against a concentration gradient is driven by energy provided by the hydrolysis of ATP. Generated inorganic phosphate (P_i) is proportional to the ATPase activity of the transporter and can, in principle, be quantified by a colorimetric assay on cell membranes. Membrane preparations of recombinant baculovirus infected Sf9 cells are widely used to investigate the interaction of compounds with different members of the ABC transporter family [Germann et al., 1990; Sarkadi et al., 1992]. Activation as well as inhibition of ABC transporters can be investigated by measuring ATPase activity: Compounds that stimulate ATPase activity are generally considered substrates of the transporter whereas inhibitors decrease stimulated activity.

An ABCG2 ATPase assay harbors the potential of providing information on the mechanism of action of the synthesized ABCG2 modulators described in Chapter 3.

In the present work, an ATPase assay for the human ABCG2 transporter was established using membrane preparations of Sf9 insect cells. The gene encoding ABCG2 was cloned into the pVL1392 vector, expressed in Sf9 cells and an experimental protocol for the ATPase assay was set up.

6.2   Materials and Methods

6.2.1   Materials

The pcDNA5/FRT-ABCG2 and pcDNA5/FRT-ABCB1 plasmids were a kind gift of Prof. Dr. Deanna Kroetz (Departments of Biopharmaceutical Sciences and Pharmaceutical Chemistry, University of California, San Francisco, CA). Phusion® High-Fidelity DNA Polymerase (2 U/µL) and the

corresponding HF Buffer (5x), deoxynucleotide solution mix (dNTPs), the restriction enzymes *Xba*I and *Not*I-HF™, Antarctic Phosphatase, purified BSA (100x) and NEBuffer 4 for digestion, 6x Loading Dye, 100 bp DNA Ladder, 2-log DNA Ladder (0.1-10.0 kb) as well as T4 DNA Ligase (6 Weiss U/µL) and T4 DNA Ligase Reaction Buffer (10x) were all purchased from New England Biolabs (NEB; Ipswich, MA). All used primers were from Eurofins MWG Synthesis GmbH (Ebersberg, Germany). Melting temperatures (Tm) of the primers for estimating annealing temperatures were calculated using the online Tm Calculator of Thermo Scientific (www.thermoscientificbio.com/webtools/tmc/).

Agarose and gel chambers of the perfectBlue™ Mini S gel system were obtained from Peqlab (Erlangen, Germany). QIAquick Gel Extraction, QIAquick PCR Purification, QIAprep Spin Miniprep and QIAGEN Plasmid Maxi Kits were from QIAGEN (Hilden, Germany).

TAE buffer was made of 48.4 g/L Tris base (usb, Cleveland, OH), 11.42 mL glacial acetic acid and 20 mL EDTA solution (0.5 M, pH 8.0) in 1000 mL purified water. Ampicillin was obtained from Sigma (Munich, Germany).

PCR reactions were performed in a Mastercycle gradient Thermocycler (Eppendorf, Hamburg, Germany) and sequencing was performed by Entelechon (Bad Abbach, Germany) or Eurofins MWG Synthesis GmbH.

RIPA buffer for cell lysis was made of 20 mM Tris, 200 mM NaCl, 1 mM EDTA, 1% (v/v) Triton X-100, 5 mM K_2HPO_4. The pH was adjusted to 7.8 and 100 mL of buffer were supplemented with a protease inhibitor tablet (SIGMA*FAST*™ Tablets; Sigma).

All used antibodies were from Santa Cruz Biotechnology (Heidelberg, Germany).

3-Morpholinopropane-1-sulfonic acid (MOPS), sodium orthovanadate and EGTA for ATPase reaction buffer were purchased from Sigma. If not otherwise stated, chemicals (p.a. quality) were from Merck (Darmstadt, Germany). Purified water (Milli-Q system, Millipore, Eschborn, Germany) was used.

6.2.2   Transformation of *E. coli*

LB and recovery (SOC) media, selective agar plates and competent bacteria *E. coli* (TOP10 strain) were prepared as described before [Pop, 2010].

For chemical transformation, 200 µL of a suspension of competent *E. coli* cells were thawed on ice and approximately 1 ng of the plasmid DNA of interest was added prior to incubation on ice (30 min). Cells were heat-shocked (42 °C) for 90 sec and subsequently put on ice for 2 min. 1 mL of pre-warmed SOC medium was added and the bacteria were incubated for 45 min at 37 °C under shaking (200 rpm). The suspension was centrifuged for 5 min at 2,300 g. The bacterial pellet was resuspended in 20-50 µL of the residual medium and plated on ampicillin-containing (100 µg/mL)

agar plates for selection, as the used vectors included an ampicillin resistance gene. Plates were incubated overnight at 37 °C. Resistant colonies were picked the next day and used for overnight cultures in LB medium supplemented with 100 µg/mL ampicillin (amp-LB medium).

6.2.3   General procedures for preparation of plasmid DNA

6.2.3.1   Mini- and Maxi-Prep

For quick purification of up to 20 µg of high-copy plasmid DNA from 5 mL overnight culture of *E. coli* (in amp-LB medium), QIAprep Spin Miniprep Kit was used according to the manual for microcentrifugation.

For large scale preparations of DNA, 250 mL of amp-LB medium were inoculated with 250 µL of bacterial overnight culture suspension. QIAGEN Plasmid Maxi Kit was used for pure DNA isolation according to the manufacturer's instructions.

Usually, a 1:20 dilution of Mini-Prep or Maxi-Prep DNA was prepared and DNA concentration was determined at a BioPhotometer (Eppendorf; Hamburg, Germany).

6.2.3.2   Restriction enzyme digestion and dephosphorylation of plasmid ends

For restriction enzyme analysis of plasmid DNA and the subcloning of PCR products, the enzymes *Not*I-HF™ (20 U/µL) and *Xba*I (20 U/µL) were used. Double digestion was performed in a final volume of 50 µL of millipore water containing 5 µL NEBuffer 4 (10x), 0.5 µL BSA (100x), 1 µL of each enzyme and 2 µg of DNA or pVL1392 Baculovirus Transfer Vector (5 µg in 50 µL; BD Biosciences, Heidelberg, Germany) for 2 h at 37 °C in an Eppendorf reaction vessel. Enzymes were heat-inactivated for additional 20 min at 65 °C.

In order to avoid self-ligation, the DNA ends of the digested pVL1392 vector were dephosphorylated by incubating for 1 h at 37 °C with 1/10 volume of Antarctic Phosphatase (10x) followed by 5 min heat-inactivation at 65 °C.

6.2.3.3   Agarose gel electrophoresis

Agarose gels (1% or 3%) were prepared by dissolving 0.5 g or 1.5 g of agarose under heating and stirring in 50 mL of TAE buffer in a microwave. To visualize DNA, 1 µL of an ethidium bromide (Janssen Chimica; Beerse, Belgium) solution (10 mg/mL) was added. Gelling of the warm agarose solution was performed in a gel chamber for 30 min using a comb as placeholder to create gel pockets.

For analytical gels usually 5 µL of DNA products mixed with 1 µL of 6x DNA loading dye were applied. For quantitative gels after restriction enzyme digestion volumes up to 50 µL were pipetted into gels with larger pockets.

The 2-log DNA ladder (0.1-10.0 kb; 7-10 µL of) was used as reference to estimate the length of PCR or digestion products. Electrophoresis (in TAE buffer) was performed at 150 V (ca. 90 min) until the track dye has moved 2/3 of the gel length. After removing the gel tray from the electrophoresis chamber, DNA bands were visualized by illumination with UV light at 254 nm (Gel Doc 2000; Bio-Rad Laboratories, Munich, Germany) using Quantity One (Bio-Rad) software for data analysis.

6.2.3.4 Purification of PCR products and recovery of DNA fragments from agarose gels

DNA from PCRs was desalted and the polymerase was removed with the QIAquick PCR Purification Kit. DNA fragments after restriction enzyme digestion were first separated by agarose gel electrophoresis. Afterwards, bands with the correct sizes were excised from the gel under UV light (λ_{ex}: 254 nm) and extracted with the QIAquick Gel Extraction kit according to the manual.

6.2.4 Preparation of the S-ABCG2 construct via sequential overlap extension PCR

Primers were designed to provide two different PCR products, the signal peptide sequence (ATG AAG ACG ATC ATC GCC CTG AGC TAC ATC TTC TGC CTG GTA TTC GCC), a domain of 48 bp necessary for a correct transporter expression in Sf9 cells, and the ABCG2 template, with a region of common sequence. The two overlapping fragments were fused in a subsequent PCR amplification to obtain the extended ABCG2 template (**Figure 6.1**).

In PCR 1a, the DNA sequence of the signal peptide (S) was amplified. A plasmid containing the signal peptide sequence and the FLAG (F) epitope was used as template with the sense primer SF_NotIfor encoding the *Not*I restriction site followed by the first 18 bp of the signal peptide and the antisense primer Signal_rev comprising the final part (18 bp) of the signal peptide sequence.

In PCR 1b the cDNA of the ABCG2 receptor was amplified using the pcDNA5/FRT-ABCG2 vector as template. PCR 1b was performed with the sense primer ABCG2_for encoding the final 18 bp of the signal peptide followed by the initial 23 bp of the ABCG2 receptor and the antisense primer ABCG2_XbaI_rev comprising 31 bp of the C-terminal sequence of the ABCG2 receptor and the *Xba*I restriction site.

Due to their terminal complementarity, PCR products 1a and 1b, templates for PCR 2, will overlap and subsequently be extended.
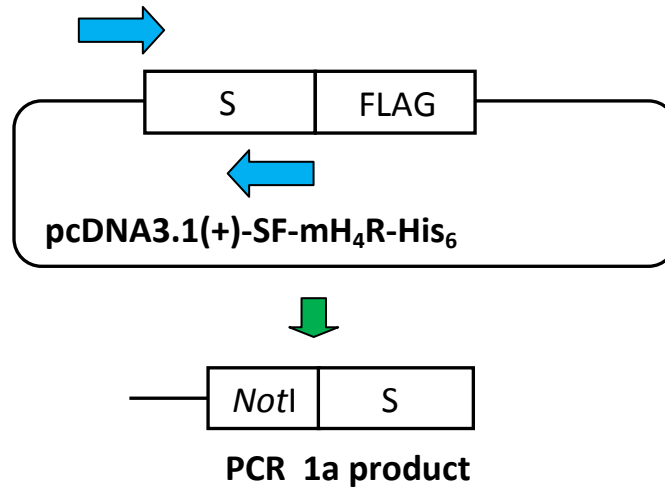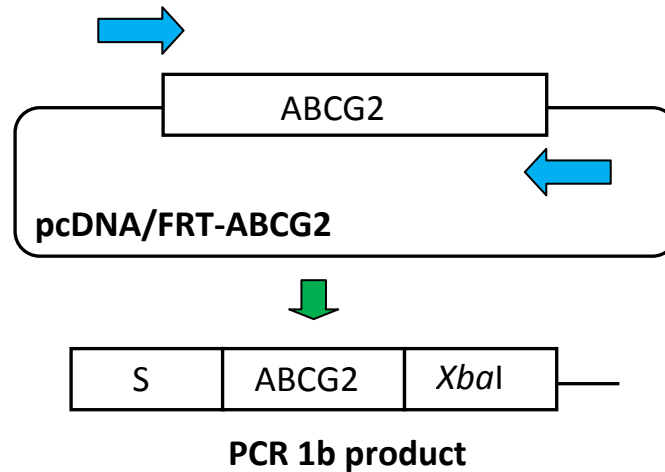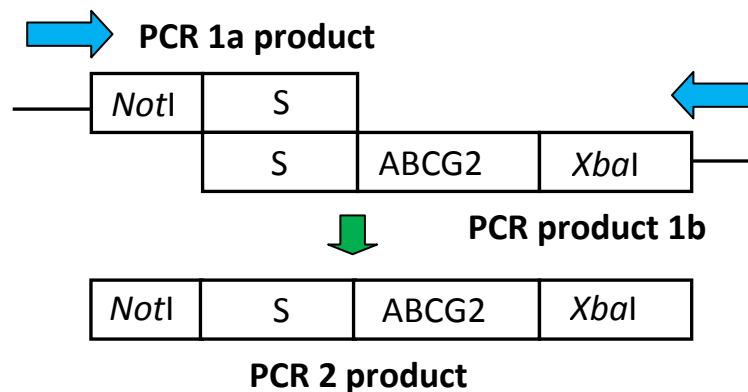
Figure 6.1: Strategy for the construction of the S-ABCG2 insert via overlap extension PCR. In separate PCR reactions (PCR 1a and 1b), two fragments of the target sequence are amplified. PCR 1a product contains the complete signal peptide sequence (**S**), whereas PCR 1b product comprises the complete sequence of the ABCG2 transporter and the final 18 bp of the signal peptide. In PCR 2 the two intermediate products with terminal complementarity form a new template DNA, annealing at the overlapping 18 bp of the signal peptide sequence. Primers are displayed as blue arrows.

6.2.4.1   PCR 1a for the S-ABCG2 construct

The template pcDNA3.1(+)-SF-mH$_4$R-His$_6$ containing the signal peptide sequence was kindly provided by Dr. Uwe Nordemann (Institute of Pharmacy, University of Regensburg).

sense primer SF_NotIfor: 5'- AGC TGC GGC CGC ATG AAG ACG ATC ATC GCC - 3'

                                                              *Not*I   signal peptide

antisense primer Signal_rev: 5'- GGC GAA TAC CAG GCA GAA - 3'

The PCR reaction mixture contained 1 ng template DNA, 0.5 µL (1 U) of Phusion® High–Fidelity DNA polymerase, 10 µL of 5x HF buffer, 1 µL dNTP Mix (10 mM), primers (0.5 µM each) and water up to a volume of 50 µL.

PCR reaction was performed with a gradient at 3 different annealing temperatures:

(1)	initial denaturation	98 °C, 30 sec
(2)	denaturation	98 °C, 10 sec
(3)	annealing	55 °C, 60 °C or 65 °C, 15 sec
(4)	extension	72 °C, 5 sec
(5)	final extension	72 °C, 5 min
(6)	hold	4 °C

Steps 2-4 were repeated 30 times.

Figure 6.2: Agarose gel (3%) electrophoresis of PCR 1a product; numbers indicate the sizes of the bands in base pairs (bp); Lanes **a-c** represent PCR products at 3 different annealing temperatures: 55 °C (**a**), 60 °C (**b**), 65°C (**c**).

Figure 6.2 shows the expected product (60 bp) of PCR 1a on a 3% agarose gel. All three annealing temperatures (lanes **a-c**) are suitable for this PCR reaction with a preference for 55 °C. The PCR product (lane **a**) was purified using the QIAquick PCR Purification Kit without further separation from possible side products. The DNA concentration was determined.

6.2.4.2 PCR 1b for the S-ABCG2 construct

PCR reaction mixture was the same as described for PCR 1a. 1 ng of the pcDNA5/FRT-ABCG2 vector was used as template.

sense primer ABCG2_for:

5'- TTC TGC CTG GTA TTC GCC ATG TCT TCC AGT AAT GTC GAA GT - 3'

      signal peptide   ABCG2

antisense primer ABCG2_XbaI_rev:

5'- ATA TCT AGA TTA AGA ATA TTT TTT AAG AAA TAA CAA TTT C - 3'

      *Xba*I   ABCG2

PCR reaction was performed with a gradient at 3 different annealing temperatures:

	(1) initial denaturation	98 °C, 30 s
	(2) denaturation	98 °C, 10 s
	(3) annealing	52 °C, 57 °C or 62 °C, 15 sec
	(4) extension	72 °C, 40 s
	(5) final extension	72 °C, 5 min
	(6) hold	4 °C

Steps 2-4 were repeated 30 times.

Figure 6.3 shows the expected ABCG2 construct (1992 bp) of PCR 1b on a 1% agarose gel. All three annealing temperatures (lanes **a**-**c**) are appropriate for this PCR reaction. The PCR product (lane **a**) was purified using the QIAquick PCR Purification Kit without further separation. The DNA concentration was determined.
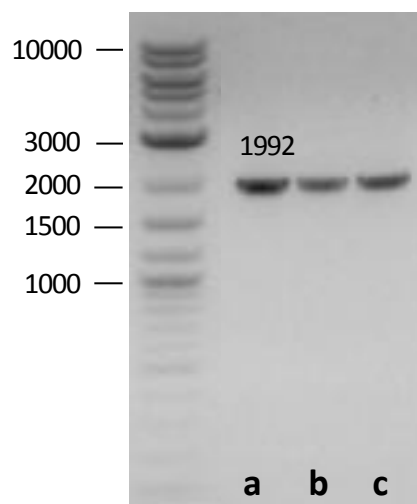
Figure 6.3: Agarose gel (1%) electrophoresis of PCR 1b product; lanes **a-c** indicate the 3 different annealing temperatures: 52 °C (**a**); 57 °C (**b**); 62°C (**c**).

6.2.4.3 PCR 2 for the S-ABCG2 construct

The annealed products of PCR 1a and PCR 1b served as template for the amplification of the new insert S-ABCG2 flanked by the restriction sites *Not*I (5' end) and *Xba*I (3' end) in PCR 2.
The sense primer NotI_for (5'- AGC TGC GGC CGC - 3') encoding the *Not*I restriction site was used.
ABCG2_XbaI_rev from PCR 1b served as antisense primer.

Due to the extremely different base pair lengths of PCR products 1a (60 bp) and 1b (1992 bp) three different PCR reactions were performed varying the ratio of concentrations of template 1a and 1b. **Figure 6.4** shows the results of PCR 2 fusing PCR 1a product with product 1b. The template concentrations of PCR reactions shown in lanes **a** and **b** were calculated according the DNA length ratio of the PCR products. All other reagents were used as described above in a total volume of 50 μL under cycling conditions according to PCR 1b with an annealing temperature of 57 °C. QIAquick PCR Purification Kit was used for purification.
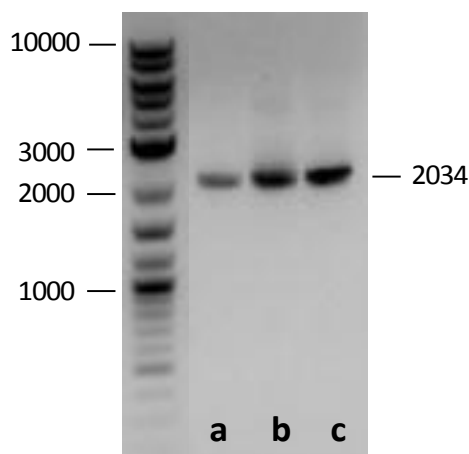
Figure 6.4: Agarose gel (1%) electrophoresis of PCR product 2 (2034 bp); lanes **a-c** indicate 3 different ratios: **a**: 0.03 ng (PCR 1a product) + 1 ng (PCR 1b product), **b**: 0.3 ng (1a) + 10 ng (1b), **c**: 1 ng (1a) + 10 ng (1b).

6.2.5   Preparation of the S-ABCB1 construct

Overlap extension PCR performed in the same way as for the S-ABCG2 construct was not successful for the ABCB1 transporter. In a second approach, the signal peptide sequence was completely inserted in the sense primer, flanked by the *Not*I restriciton site and the first 19 bp of the ABCB1 transporter (ordered as unmodified DNA oligo from Eurofins MWG Synthesis GmbH). ABCB1_XbaI_rev served as antisense primer comprising the *Xba*I restriction site and the final 17 bp of the ABCB1 transporter.

sense primer ABCB1_for(+S):

5'- AGC TGC GGC CGC ATG AAG ACG ATC ATC GCC CTG AGC TAC ATC TTC TGC CTG GTA TTC GCC ATG GAT CTT GAA GGG GAC C - 3'

antisense primer ABCB1_XbaI_rev:
5'- ATA TCT AGA TCA CTG GCG CTT TGT TC - 3'
         *Xba*I   ABCB1

Two different PCR strategies were chosen:

1. PCR 3a reaction was performed with a gradient at 3 different annealing temperatures:

   (1) initial denaturation   98 °C, 30 s

   (2) denaturation   98 °C, 10 s

   (3) annealing   57 °C, 62 °C or 67 °C, 15 s

   (4) extension   72 °C, 2 min

   (5) final extension   72 °C, 5 min

   (6) hold   4 °C

   Steps 2-4 were repeated 30 times.

2. Due to the length and the associated high melting temperature of the sense primer ABCB1_for(+S), additionally, PCR 3b reaction was performed in two cycles with an initial low and a following high annealing temperature:

   (1) initial denaturation   98 °C, 30 s

   (2) denaturation   98 °C, 10 s

   (3) annealing   60 °C, 15 s

   (4) extension   72 °C, 2 min

   Steps 2-4 were repeated 5 times.

   (5) denaturation   98 °C, 10 s

   (6) annealing   70 °C, 15 s

   (7) extension   72 °C, 2 min

   Steps 5-7 were repeated 25 times.

   (8) Final extension   72 °C, 5 min

   (9) hold   4 °C
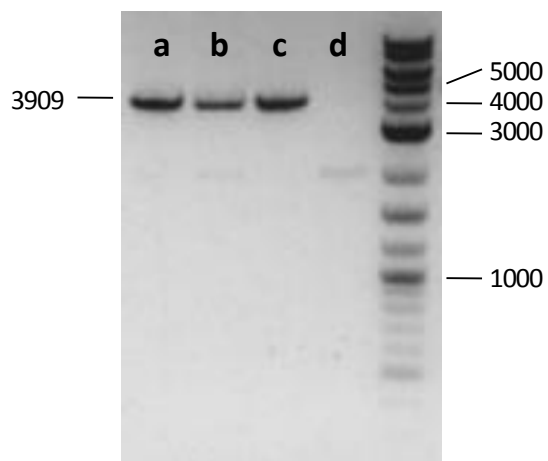
Figure 6.5: Agarose gel (1%) electrophoresis of PCR products 3a and 3b; lanes **a-c** indicate PCR 3a at three different annealing temperatures: 57 °C (**a**), 62 °C (**b**), 67°C (**c**); lane **d** indicates PCR 3b.

Figure 6.5 shows the expected product (3909 bp) of PCR 3a and PCR 3b on a 1% agarose gel. All three annealing temperatures of PCR 3a (lanes **a-c**) are suitable for this PCR reaction with a preference for 57 °C. PCR 3b (lane **d**) with the two different annealing cycles did not give the desired product. PCR product of lane **a** was purified and the DNA concentration was determined.

6.2.6   Subcloning of the S-ABCB1 and the S-ABCG2 construct into pVL1392 vector

For Sf9 cell line transfection, the S-ABCB1 and the S-ABCG2 fragment, respectively, were each subcloned into the pVL1392 plasmid in its multiple cloning site with the *Xba*I and *Not*I restriction sites (**Figure 6.6**) giving the pVL1392/S-ABCB1 and pVL1392/S-ABCG2 plasmid, respectively.
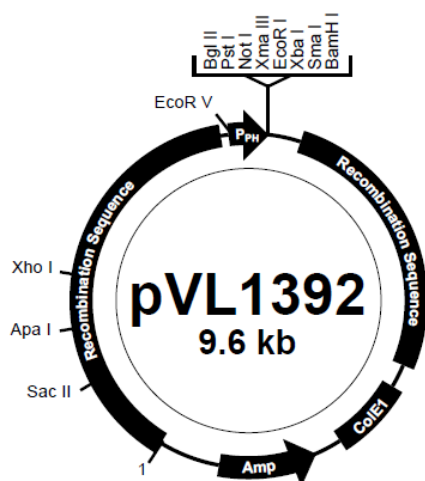
Figure 6.6: Vector map of pVL1392 vector (adopted from manual provided by BD biosciences).

Digestion of ABC transporter fragments and the pVL1392 transfer vector was prepared as described in section 6.2.3.2. The corresponding agarose gel electrophoresis is illustrated in **Figure 6.7**.
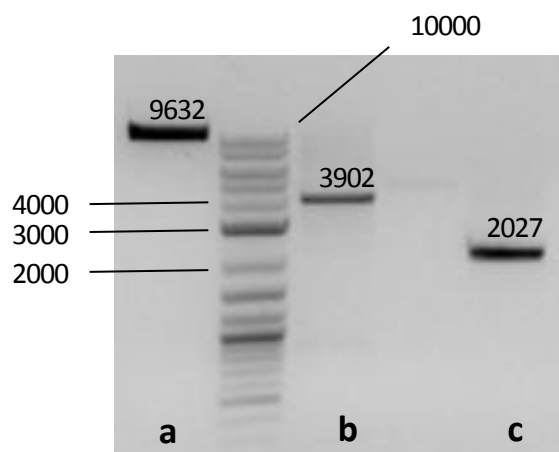
Figure 6.7: Agarose gel (1%) electrophoresis of digestion products: pVL1392 vector (**a**), S-ABCB1 fragment (**b**), S-ABCG2 fragment (**c**).

After gel electrophoresis and gel extraction (cf. sections 6.2.3.3 and 6.2.3.4), ligation was performed at 16 °C overnight in a 20 µL reaction mixture containing 1 µL T4 DNA Ligase and 2 µL of T4 DNA Ligase Reaction Buffer (10x) as well as the pVL1392 transfer vector (50 ng) and the insert in a molar ratio of 1:3 (vector to insert). The next day the samples were stored at -20 °C. After transformation of competent *E. coli*, Mini-Preps were prepared with colonies picked from ampicillin-containing agar plates, and a positive clone was chosen for Maxi-Prep.

Plasmid DNA was sequenced using the standard primers pVL1392for and pVL1392rev.

6.2.7 Sf9 insect cell culture and generation of recombinant baculoviruses

Sf9 insect cell culture and generation of recombinant baculoviruses has been described recently [Brunskole, 2011]. Sf9 cells (ATCC® CRL-1711™) were cultured in 250 or 500 mL disposable Erlenmeyer flasks at 28 °C under rotation at 150 rpm in Insect Xpress medium supplemented with 5 % (v/v) fetal calf serum. Recombinant baculoviruses encoding the S-ABCG2 construct were generated in Sf9 insect cells using the BaculoGold™ transfection kit (BD Biosciences, Heidelberg, Germany) according to manufacturer's protocol.

After initial transduction, high-titer virus stocks were generated by two sequential virus amplifications: in the first amplification, 50 mL cell suspension (density: 2.0×10^6 cells/mL) were infected with 1 mL of the supernatant fluid from the initial transduction. Cells were cultured for one week in a 125 mL Erlenmeyer flask, resulting in death of the cell population. As a control for infectious viruses, 3 mL of this culture were transferred into a 25 cm^2 flask and kept at 28 °C in parallel. The supernatant was harvested and stored under light protection at 4 °C.

In a second amplification, cells were cultured at a density of 3.0×10^6 cells/mL (total volume: 100 mL), infected with 5 mL of the supernatant fluid from the first amplification and cultured for two days. After 48 hours the supernatant was harvested. Cells showed signs of infection (altered morphology, viral inclusion bodies), but the majority of cells was still intact. The supernatant fluid from the second amplification step was stored under protection from light at 4 °C and used as high-titer virus stock to infect Sf9 cells. All supernatants were routinely filtered through Millex® filters (0.22 µm pore size; Merck Millipore, Darmstadt, Germany) to avoid bacterial or fungal contamination.

6.2.8 Recombinant transporter expression in pVL1392/S-ABCG2-infected Sf9 cells

6.2.8.1 Immunological detection of ABCG2 expression

To ensure an optimal accumulation of the desired ABCG2 protein, an ideal Sf9 infection time has to be determined. Cells were seeded at a density of 0.75×10^6 cells/mL, infected with high-titer baculovirus stock (1:500) and cultured. Cell aliquots were harvested at different times after infection (24-96 h) followed by three washing and centrifugation steps with PBS at 4 °C for 10 min (3,000 g) using a Minifuge 1.0R (Heraeus Instruments GmbH; Hanau, Germany). To monitor the expression of ABCG2 in pVL1392/S-ABCG2-infected Sf9 cells, total cell lysates were analyzed by immunoblotting.

6.2.8.1.1 Sf9 cell lysis

Cell lysis of ABCG2-infected Sf9 cells was performed by homogenizing the harvested cells in RIPA buffer. After incubation for 20 min on ice in an Eppendorf reaction vessel, the cell suspension was centrifuged (10 min, 4° C, 16,000 g) and the supernatant containing the proteins was frozen at -80 °C after addition of 10% (v/v) glycerol.

6.2.8.1.2 SDS-Page and Western Blotting

SDS-PAGE and WB analysis as well as the determination of the protein content of all cell lysates were performed as described in section 5.2.9. The primary rat monoclonal antibody ABCG2 (BXP-53) was used in a 1:1,000 dilution, the secondary AB (goat anti-rat IgG-HRP) in a 1:10,000 dilution.

For molecular weight control, the prestained protein marker peqGOLD Protein Marker III (20-122 kDa; Peqlab, Erlangen, Germany) or the Biotinylated Protein Ladder (9-200 kDa) from Cell Signaling Technology (Danvers, MA, USA) were used (secondary Anti-biotin, HRP-linked AB 1:1,000), respectively.

Western Blot analysis was similarly performed for ABCG2 membrane preparations.

6.2.8.2 Membrane preparation

For membrane preparation, 200 mL cultures with 3.0×10^6 cells/mL were infected 1:500 with S-ABCG2 high-titer virus stock, cultured and harvested 48 hours after infection by centrifugation at 4 °C (170 g, 10 min). The cell pellet was resuspended in 100 mL Tris-mannitol buffer (50 mM Tris, 300 mM mannitol, 0.5 mM phenylmethylsulfonyl fluoride (PMSF); pH 7) and again centrifuged.

For membrane preparation the cell pellet was lysed and homogenized (25 strokes) in TMEP (50 mM Tris, 50 mM mannitol, 1 mM EDTA, 10 µg/mL leupeptin, 10 µg/mL benzamidine, 0.5 mM PMSF, 2 mM DTT; pH 7) by means of a glass-Teflon tissue homogenizer. Buffers were used as described elsewhere [Sarkadi et al., 1992] with slight modifications. The use of protease inhibitors is recommended especially in insect cells, as the yields of recombinant proteins can significantly decrease due to high proteolytic activity [Gotoh et al., 2001].

After centrifugation for 10 min at 500 g to get rid of nuclei and unbroken cells, the supernatant, containing the membranes, was carefully removed and centrifuged at 100,000 g for 1 h in a Kontron TGA-45 ultracentrifuge (Kontron Instruments, Munich, Germany). The spun down membranes were resuspended in TMEP and homogenized by a 20 mL syringe in 15 strokes. Protein quantification was performed by the method of Bradford in a Bio-Rad Protein Assay (Bio-Rad Laboratories, Munich, Germany) according to the manual. Membrane aliquots at a protein concentration of 1.5-2.0 mg/mL were stored at -80 °C until use. All steps during membrane preparation were performed at 4 °C. Please confer to section 6.3.3.3.2 for a second modified membrane preparation protocol.

6.2.9　ATPase assay for the human BCRP

6.2.9.1　Principle

Determining the ATPase activity in membranes of Sf9 insect cells expressing the ABCG2 transporter may provide insight into the mechanism of action of modulators. The ATPase activity correlates with the liberation of inorganic phosphate (P_i), resulting from ATP hydrolysis when a substrate is transported. Inorganic P_i reacts with ammonium molybdate to form a complex, in the presence of the reducing agent ascorbic acid producing an intensively blue colored heteropoly complex (molybdenum blue), which can then be determined spectrophotometrically (**Figure 6.8**). The obtained absorbance is proportional to ATPase activity.
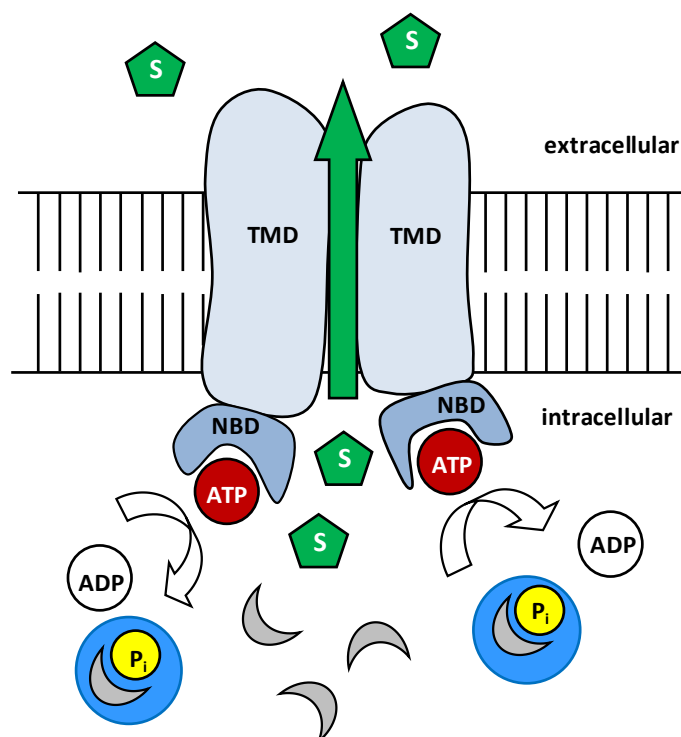
Figure 6.8: Principle of an ATPase assay: Substrate binding and subsequent ATP hydrolysis results in the release of ADP and inorganic phosphate. P_i forms a complex with ammonium molybdate (gray sickles) which results in an intensive blue color after reduction; TMD = transmembrane domain, NBD = nucleotide-binding domain, S = substrate; ATP = adenosine triphosphate; ADP = adenosine diphosphate; P_i = inorganic phosphate.

6.2.9.2   ATPase assay protocol

The ATPase assay protocol was established in the 96-well plate format according to the manual provided by GenoMembrane (http://www.genomembrane.com/ATPase_assay_Ver.6.5.n.pdf; Yokohama, Japan) based on the work of Sarkadi [Sarkadi et al., 1992].

6.2.9.2.1   Reagents and buffers

- MOPS-Tris buffer [100 mM] contained 20.93 g/L 3-morpholinopropane-1-sulfonic acid. The pH of 7.0 was adjusted with 1.7 M Tris (37 °C).

- Reaction buffer was made of 50 mM MOPS-Tris, 50 mM KCl, 5 mM sodium azide, 2 mM DTT (AppliChem; Darmstadt, Germany), 1 mM ouabain and 2 mM EGTA. Aliquots were stored at -20 °C.

- For a 100 mM orthovanadate solution, 0.368 g of sodium orthovanadate were dissolved in 16 mL millipore water, the pH was adjusted to 10 with 1 N HCl or 1 N NaOH and the solution was heated (100 °C) for 10 min. When cooled down, the solution was filled up to 20 mL. Reaction buffer was used to prepare a 12 mM working solution (also cf. section 6.3.3.1).

- 200 mM MgATP solution was made by dissolving 2.21 g of Na_2ATP (Boehringer; Mannheim, Germany) in 10 mL $MgCl_2$ solution [400 mM]. The pH was adjusted to 7.0 with

1.7 M Tris (37 °C) and the solution was filled up to 20 mL with millipore water. Aliquots of 1 mL were stored at -20 °C. A 12 mM working solution was made in reaction buffer.

- For the <u>indicator solution</u> (always freshly prepared), one part of a solution containing 15 mM zinc acetate and 35 mM ammonium molybdate were mixed with 4 parts of a 5% (m/v) ascorbic acid solution (pH 5.0 with 10 N NaOH)

- <u>Phosphate standards</u> (0, 0.05, 0.1, 0.25, 0.5, 1.0, 1.5 and 2.0 mM) were obtained by diluting a 1 M NaH_2PO_4 stock solution with reaction buffer. Small portions were stored at -20 °C.

- Reactions were stopped with a 10% (m/v) <u>SDS solution</u> (Sigma).

- <u>Test compounds</u> (in DMSO) were dissolved in reaction buffer to 3-fold concentrated stock solutions.

MgATP (instead of Na_2ATP) is essential for the assay system as ABCG2 drug transport requires the presence of magnesium ions [Litman et al., 2000; Özvegy et al., 2001]. It is furthermore linked to a drug-stimulated, vanadate-sensitive ATPase activity [Sarkadi et al., 1992; Telbisz et al., 2007]. Vanadate, an analog of inorganic phosphate, is a known inhibitor of many ATPases, including ATPase activities of ABC transporter [Senior et al., 1995; Chen et al., 2001]. Vanadate-sensitive ATPase activity (resulting from ABC transporter activity) can thereby be calculated by subtracting vanadate-insensitive from total ATPase activity.

6.2.9.2.2   Instrumental set-up

The ATPase assay for the human ABCG2 transporter was established in the 96-well plate format with absorbance detection at the GENios Pro microplate reader (TECAN Deutschland GmbH; Crailsheim, Germany). The optimal detection wavelength of the formed phosphomolybdate complex had to be determined. Therefore, 5 mL of indicator solution were mixed with 50 mg NaH_2PO_4. After 20 min the absorbance spectrum of the obtained colored complex was detected at a Cary 100 UV-Vis spectrophotometer (Varian; Darmstadt, Germany).

Additionally, the linearity of the absorbance of the phosphate standards after complexation and reduction was tested prior to any experiments at the above determined optimal wavelength. 60 µL per standard were incubated with 30 µL of 10% SDS and 200 µL coloring solution for 20 min under shaking (400 rpm) at 37 °C at a Grant-bio PHMP Thermoshaker for microplates (Grant Instruments; Cambrigdeshire, UK) and absorbance was measured at the microplate reader.

6.2.9.2.3 Assay procedure

The activity of the ABCG2 transporter is measured as vanadate-sensitive ATPase activity in the presence of inhibitors or stimulating agents (substrates) in membranes of ABCG2 expressing Sf9 cells as described earlier [Sarkadi et al., 1992; Glavinas et al., 2007].

The assay was performed on ice in the 96-well plate format on the basis of the manual provided by Geno Membrane:

Membranes were thawed on ice and carefully homogenized with a pipette. Phosphate standards are part of every plate to calculate a calibration plot for phosphate (60 µL/well of each phosphate standard performed in doublet). In the remaining wells, membranes (10 µL/well) were loaded with either 20 µL of the 3-fold concentrated test compound solutions or 3% (v/v) DMSO (in reaction buffer) for the negative and background control (8 wells each), respectively. The background control, measures the inorganic phosphate derived from the reaction buffer and was immediately stopped with a 10% (m/v) SDS solution (30 µL/well) prior to ATPase reaction. The negative control indicates the basal ATPase activity of the ABCG2 transporter in the absence of a substrate.

Four wells of each compound concentration and each negative control were overlaid with 10 µL of the 12 mM o-vanadate solution, the remaining wells with the corresponding volume of reaction buffer. The plate was shaken to mix the solutions and incubated for 3 min at 37 °C.

Subsequently, the reaction was started by the addition of 20 µL of 12 mM MgATP (except for phosphate standards). After an incubation time of 1 h (37 °C) under shaking the reaction was stopped by adding 30 µL/well of 10% SDS (except for thebackground control). Indicator solution was added (200 µL/well) and after further 30 min of incubation at 37 °C, absorbance of the obtained phosphomolybdate complex was determined in each well at 830 nm at the GENios Pro microplate reader when the temperature of the microplate had cooled down.

Instrument settings were as follows: Measurement mode: absorbance; number of reads: 10; plate definition file GRE96ft.pdf; time between move and flash: 100 ms. All values were corrected to the background control and the amount of inorganic phosphate generated in each well was calculated from the correlation equation obtained from phosphate standards on each plate. Data obtained under the treatment with orthovanadate were subtracted from the data gained in the absence of vanadate to obtain phosphate liberation resulting from ABCG2 activity. This amount of phosphate was divided by the incubation time and the protein content per well (corresponding to the used membrane preparation) to give the desired vanadate-sensitive ATPase activity [nmol P_i/min/mg protein].

For the investigation of ABCG2 inhibitors, the assay was performed as described with the exception that ATPase activity was stimulated with topotecan [100 µM]. Furthermore, topotecan served as

positive control on each plate and was used to determine the degree of inhibition caused by the highest compound concentration tested. The final DMSO content did not exceed 1% (v/v).

6.3   Results and discussion

The presentation of the results is focused on the ABCG2 protein.

6.3.1   Results of DNA sequencing

Plasmid DNA was sequenced using the standard primers pVL1392for and pVL1392rev. For the plasmid containing the S-ABCG2 construct with nearly 2000 bp, corresponding to about half of the length of the ABCB1 transporter, a complete Primer Walking DNA Sequencing was performed by Entelechon (Bad Abbach, Germany). The result confirmed an error-free ABCG2 sequence when compared to the NCBI database (**Figures 6.9-6.10**; data not completely displayed).

```
Seq_1   57    GCCGGCTCCCATCGTGACCTCCAGCCGCAGCGCCTCCCACGCCGGCCGCCGCGCGAGGGG   116
              |||   |       || || |||| || ||          ||      |||| | |
Seq_2   59    ATCGGGCGCGGATCAGATCTGCAGCGGCCGCATGAAGA-CGATCATCGCCCTGAGCTAC-   116


Seq_1   117   AGCGCTCGGGCGCGCCGGGTGTGGTTGGGGGAAGGGGTTGTGCCGCGCGCGGGCTGCGTG   176
              ||   ||   |           |
Seq_2   117   --ATCTTCTGCCTGGTATTCGCC-------------------------------------   137

                                            *  *  *

Seq_1   477   AGATAAAAACTCTCCAGATGTCTTCCAGTAATGTCGAAGTTTTTATCCCAGTGTCACAAG   536
                              ||||||||||||||||||||||||||||||||||||||||||||
Seq_2   138   ----------------ATGTCTTCCAGTAATGTCGAAGTTTTTATCCCAGTGTCACAAG   180


Seq_1   537   GAAACACCAATGGCTTCCCCGCGACAGCTTCCAATGACCTGAAGGCATTTACTGAAGGAG   596
              ||||||||||||||||||||||||||||||||||||||||||||||||||||||||||||
Seq_2   181   GAAACACCAATGGCTTCCCCGCGACAGCTTCCAATGACCTGAAGGCATTTACTGAAGGAG   240


Seq_1   597   CTGTGTTAAGTTTTCATAACATCTGCTATCGAGTAAAACTGAAGAGTGGCTTTCTACCTT   656
              ||||||||||||||||||||||||||||||||||||||||||||||||||||||||||||
Seq_2   241   CTGTGTTAAGTTTTCATAACATCTGCTATCGAGTAAAACTGAAGAGTGGCTTTCTACCTT   300


Seq_1   657   GTCGAAAACCAGTTGAGAAAGAAATATTATCGAATATCAATGGGATCATGAAACCTGGTC   716
              ||||||||||||||||||||||||||||||||||||||||||||||||||||||||||||
Seq_2   301   GTCGAAAACCAGTTGAGAAAGAAATATTATCGAATATCAATGGGATCATGAAACCTGGTC   360


Seq_1   717   TCAACGCCATCCTGGGACCCACAGGTGGAGGCAAATCTTCGTTATTAGATGTCTTAGCTG   776
              ||||||||||||||||||||||||||||||||||||||||||||||||||||||||||||
Seq_2   361   TCAACGCCATCCTGGGACCCACAGGTGGAGGCAAATCTTCGTTATTAGATGTCTTAGCTG   420


Seq_1   777   CAAGGAAAGATCCAAGTGGATTATCTGGAGATGTTCTGATAAATGGAGCACCGCGACCTG   836
              ||||||||||||||||||||||||||||||||||||||||||||||||||||||||||||
Seq_2   421   CAAGGAAAGATCCAAGTGGATTATCTGGAGATGTTCTGATAAATGGAGCACCGCGACCTG   480


Seq_1   837   CCAATTTCAAATGTAATTCAGGTTACGTGGTACAAGATGATGTTGTGATGGGCACTCTGA   896
              ||||||||||||||||||||||||||||||||||||||||||||||||||||||||||||
Seq_2   481   CCAATTTCAAATGTAATTCAGGTTACGTGGTACAAGATGATGTTGTGATGGGCACTCTGA   540


Seq_1   897   CGGTGAGAGAAAACTTACAGTTCTCAGCAGCTCTTCGGCTTGCAACAACTATGACGAATC   956
              ||||||||||||||||||||||||||||||||||||||||||||||||||||||||||||
Seq_2   541   CGGTGAGAGAAAACTTACAGTTCTCAGCAGCTCTTCGGCTTGCAACAACTATGACGAATC   600


Seq_1   957   ATGAAAAAAACGAACGGATTAACAGGGTCATTCAAGAGTTAGGTCTGGATAAAGTGGCAG   1016
              ||||||||||||||||||||||||||||||||||||||||||||||||||||||||||||
Seq_2   601   ATGAAAAAAACGAACGGATTAACAGGGTCATTCAAGAGTTAGGTCTGGATAAAGTGGCAG   660


Seq_1   1017  ACTCCAAGGTTGGAACTCAGTTTATCCGTGGTGTGTCTGGAGGAGAAAGAAAAAGGACTA   1076
              ||||||||||||||||||||||||||||||||||||||||||||||||||||||||||||
Seq_2   661   ACTCCAAGGTTGGAACTCAGTTTATCCGTGGTGTGTCTGGAGGAGAAAGAAAAAGGACTA   720


Seq_1   1077  GTATAGGAATGGAGCTTATCACTGATCCTTCCATCTTGTTCTTGGATGAGCCTACAACTG   1136
              |||||||||||||||||||||||
Seq_2   721   GTATAGGAATGGAGCTTATCA---------------------------------------   741


Seq_1   1137  GCTTAGACTCAAGCACAGCAAATGCTGTCCTTTTGCTCCTGAAAAGGATGTCTAAGCAGG   1196
Seq_2   742   ------------------------------------------------------------   741
```

Figure 6.9: Annealing of the N-terminal domain of the ABCG2 transporter (1965 base pairs) from NCBI database with the nucleotide sequence, obtained by sequencing (*blue*; 604 base pairs) using primer pVL1392for. The encoding region of the ABCG2 transporter from NCBI database is shown in *red* (start codon is underlined). The signal peptide sequence, obtained in sequencing is shown in *green*.

```
Seq_1  1981  GTTAGGATTGAAGCCAAAGGCAGATGCCTTCTTCGTTATGATGTTTACCCTTATGATGGT  2040
                                                         ||||||||||||||
Seq_2   530  ---------------------------------------------CCCTTATGATGGT  518


Seq_1  2041  GGCTTATTCAGCCAGTTCCATGGCACTGGCCATAGCAGCAGGTCAGAGTGTGGTTTCTGT  2100
             ||||||||||||||||||||||||||||||||||||||||||||||||||||||||||||
Seq_2   517  GGCTTATTCAGCCAGTTCCATGGCACTGGCCATAGCAGCAGGTCAGAGTGTGGTTTCTGT  458


Seq_1  2101  AGCAACACTTCTCATGACCATCTGTTTTGTGTTTATGATGATTTTTTCAGGTCTGTTGGT  2160
             ||||||||||||||||||||||||||||||||||||||||||||||||||||||||||||
Seq_2   457  AGCAACACTTCTCATGACCATCTGTTTTGTGTTTATGATGATTTTTTCAGGTCTGTTGGT  398


Seq_1  2161  CAATCTCACAACCATTGCATCTTGGCTGTCATGGCTTCAGTACTTCAGCATTCCACGATA  2220
             ||||||||||||||||||||||||||||||||||||||||||||||||||||||||||||
Seq_2   397  CAATCTCACAACCATTGCATCTTGGCTGTCATGGCTTCAGTACTTCAGCATTCCACGATA  338


Seq_1  2221  TGGATTTACGGCTTTGCAGCATAATGAATTTTTGGGACAAAACTTCTGCCCAGGACTCAA  2280
             ||||||||||||||||||||||||||||||||||||||||||||||||||||||||||||
Seq_2   337  TGGATTTACGGCTTTGCAGCATAATGAATTTTTGGGACAAAACTTCTGCCCAGGACTCAA  278


Seq_1  2281  TGCAACAGGAAACAATCCTTGTAACTATGCAACATGTACTGGCGAAGAATATTTGGTAAA  2340
             ||||||||||||||||||||||||||||||||||||||||||||||||||||||||||||
Seq_2   277  TGCAACAGGAAACAATCCTTGTAACTATGCAACATGTACTGGCGAAGAATATTTGGTAAA  218


Seq_1  2341  GCAGGGCATCGATCTCTCACCCTGGGGCTTGTGGAAGAATCACGTGGCCTTGGCTTGTAT  2400
             ||||||||||||||||||||||||||||||||||||||||||||||||||||||||||||
Seq_2   217  GCAGGGCATCGATCTCTCACCCTGGGGCTTGTGGAAGAATCACGTGGCCTTGGCTTGTAT  158


Seq_1  2401  GATTGTTATTTTCCTCACAATTGCCTACCTGAAATTGTTATTTCTTAAAAAATATTCTTA  2460
             ||||||||||||||||||||||||||||||||||||||||||||||||||||||||||||
Seq_2   157  GATTGTTATTTTCCTCACAATTGCCTACCTGAAATTGTTATTTCTTAAAAAATATTCTTA  98


Seq_1  2461  AATTTCCCCTTAATTCAGTATGATTTATCCTCACATAAAAAAGAAGCACTTTGATTGAAG  2520
             |
Seq_2    97  A------------------------------------------------------------  97
```

Figure 6.10: Annealing of the C-terminal domain of the ABCG2 transporter from NCBI database with the nucleotide sequence, obtained by sequencing (*blue*; anti-parallel; 434 base pairs) using primer pVL1392rev. The encoding region of the ABCG2 transporter from NCBI database is shown in *red* (stop codon is underlined).

6.3.2   ABCG2 expression in Sf9 cells

6.3.2.1 Infection time

The timing of harvesting the Sf9 cells after ABCG2-baculovirus infection seems to be critical. As shown in a recently published work, size and morphology of Sf9 cells change dramatically during infection: The membrane integrity was disrupted at later stages (>72 h) as numerous pores were observed by means of scanning electron microscopy [Saito et al., 2006; Saito et al., 2009]. Membrane vesicles prepared from such porous cells are useless. Western blot analysis (total cell lysate) of pVL1392/S-ABCG2-infected Sf9 cells revealed an optimal transporter expression after 48 h (**Figure 6.11**).
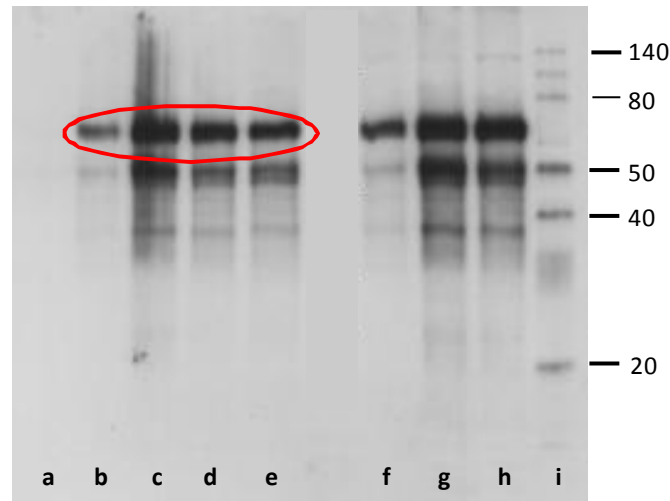
Figure 6.11: Expression of the ABCG2 gene product in Sf9 cells. Western blot analysis of total cell lysates prepared from Sf9 wt cells (**a**) and pVL1392/S-ABCG2-infected Sf9 cells at different times after infection: 24 h (**b**), 48 h (**c**), 72 h (**d**), 96 h (**e**); 10 µg protein were loaded on lanes **a-e**; lanes **f-h** correspond to lanes **b-d** except for loading with 20 µg protein; **i**) Biotinylated Protein Ladder (9-200 kDa; Cell Signaling); the sizes of molecular weight standards are indicated in kDa.

Closer examination of the Western blot with the Quantity One (Bio-Rad) software unfortunately revealed a main band (presumably a doublet) at 63-67 kDa (expected molecular weight of the glycosylated ABCG2 transporter monomer: 72 kDa). Additionally, some diffuse bands were visible probably resulting from proteolytic cleavage of the target ABCG2 protein into lower molecular weight products when expressed in Sf9 cells.

To confirm this lower molecular mass of the ABCG2 transporter in insect cells, the expression of BCRP in membrane preparations was compared to that in MCF-7/Topo cells (ABCG2 overexpressing subclone of human MCF-7 cells). Immunoblot analysis (**Figure 6.12**) showed that ABCG2 expressed in Sf9 cells migrates as a double band of lower apparent molecular mass (63 kDa and 66 kDa) than the ABCG2 protein of MCF-7/Topo cells (a wide band at 74 kDa). This phenomenon was previously reported by other groups [Özvegy et al., 2001; Pozza et al., 2006; Pozza et al., 2009].
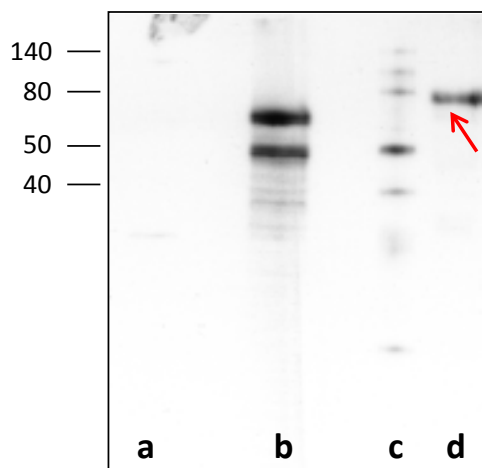
Figure 6.12: Immunoblot detection of the ABCG2 transporter expressed in Sf9 membrane preparations and MCF-7/Topo cells, respectively (10 µg of protein); **a**) Sf9 wt membrane, **b**) Sf9 ABCG2-membrane, **c**) Biotinylated Protein Ladder (9-200 kDa; Cell Signaling), **d**) MCF-7/Topo cells. Red arrow indicates the ABCG2 transporter (72 kDa) expressed in human MCF-7/Topo cells. Immunoblot analysis revealed an approximately 5-fold higher expression level of the lower ABCG2 homolog (doublet protein bands) compared to the ABCG2 monomer in MCF-7/Topo cells. BXP-53 (1:1,000) was used as primary AB.

The high extent of proteolysis of the ABCG2 transporter in Sf9 cells is remarkable. To check whether the formation of the ABCG2 homolog at lower molecular mass and the proteolytic effect in Sf9 cells depends on the time of infection and the dilution of the virus stocks, Sf9 membane preparations were made 24, 48 and 72 h after infection, each charged 1:100 and 1:500 with S-ABCG2 high titer virus stock, respectively (**Figure 6.13**).

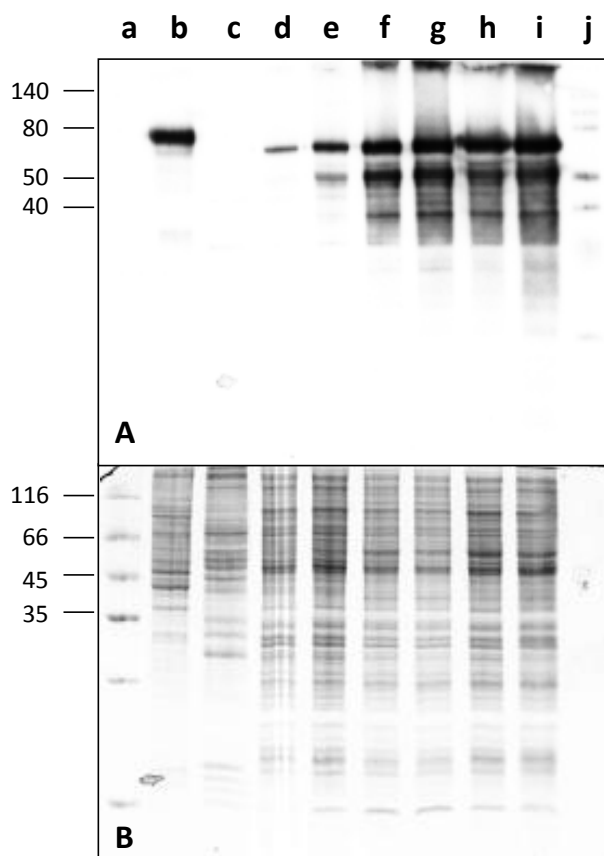**Figure 6.13: A**) Immunoblot analysis of ABCG2 protein expression in Sf9 membrane preparations and MCF-7/Topo cells, respectively; **B**) corresponding Coomassie blue-stained gel.
Cells were harvested at various times after infection (lanes **d-i**) with different dilutions of ABCG2 high titer virus stock (stated in brackets): **a**) peqGold protein marker I (14-116 kDa; Peqlab); **b**) MCF-7/Topo cells; **c**) Sf9 wt membrane; Sf9 ABCG2 membrane: **d**) 24 h (1:500), **e**) 24 h (1:100), **f**) 48 h (1:500), **g**) 48 h (1:100), **h**) 72 h (1:500), **i**) 72 h (1:100); **j**) Biotinylated Protein Ladder (9-200 kDa; Cell Signaling). All samples (10 µg of total protein) were subjected to SDS-PAGE on 12% polyacrylamide gels followed by immunoblotting with the rat monoclonal ABCG2 antibody BXP-53 (1:1,000).

The ratio of proteolytic degradation products (bands around 50 kDa) compared to the target ABCG2 protein at 63 kDa is nearly constant in the Sf9 membrane preparations, virtually irrespective of the infection time and the used dilution of the virus stock. However, membranes prepared 24 h after infection of the cell showed the lowest extent of proteolysis. Despite a lower expression level of the ABCG2 homolog in comparison to 48 h- and 72 h-preparations, these short-term infected membranes were preferred for the first ATPase experiments.

6.3.2.2   Glycosylation of the ABCG2 transporter

The ABCG2 transporter is a glycoprotein consisting of 655 amino acids with a predicted molecular weight of 72 kDa. As a 'half-transporter' it contains only one TMD forming a homodimer in the plasma membrane in order to function. The topology of human ABCG2 is displayed in **Figure 6.14**.
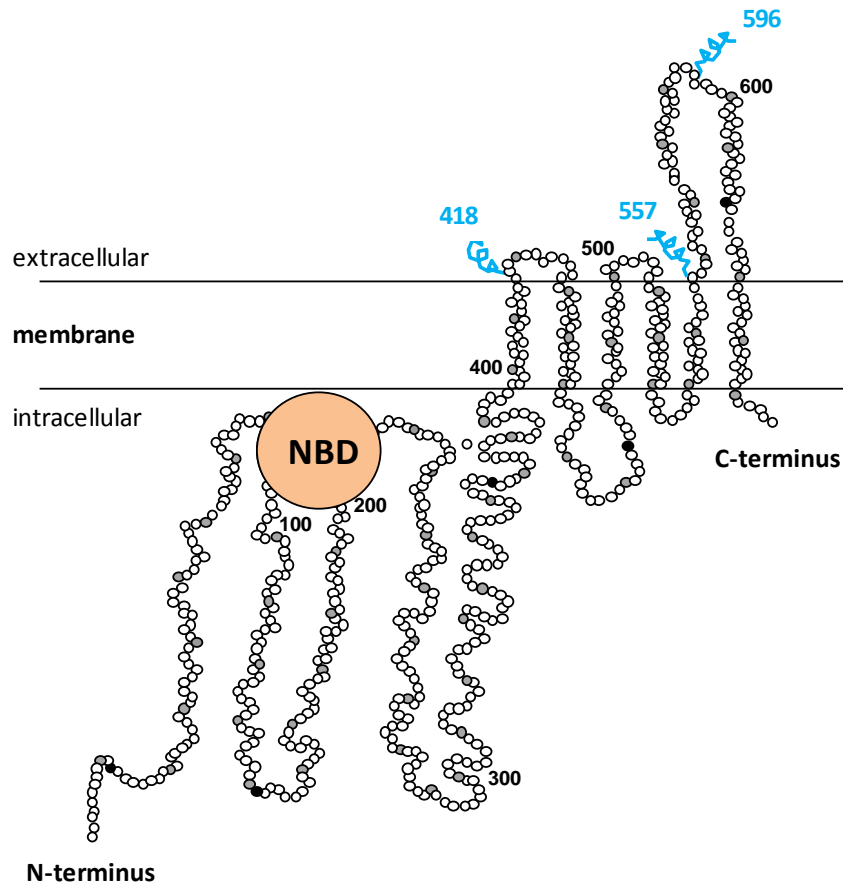
Figure 6.14: Topology model of the human ABCG2 half-size transporter consisting of 6 transmembrane domains and one nucleotide binding domain (NBD). Potential N-linked glycosylation sites at amino acid positions 418, 557 and 596 are displayed in blue (modified from [Ejendal and Hrycyna, 2002; Diop and Hrycyna, 2005]).

Diop and Hrycyna [Diop and Hrycyna, 2005] showed that stably expressed ABCG2 in membranes from human cells was only glycosylated at the N596 site, and treatment with endoglycosidase PNGase F (peptide-*N*-glycosidase F) reduced the molecular mass on SDS-PAGE gels to approximately 60 kDa. The phenomenon of a modified molecular weight due to deglycosylation has also been observed for ABCG2 expressed in MCF-7 cells upon treatment with PNGase F or the nucleoside antibiotic tunicamycin [Litman et al., 2002] as well as in Sf9 insect cells [Özvegy et al., 2001; Pozza et al., 2009; Jacobs, 2010] and yeast systems [Mao et al., 2004]. In mammalian systems, the ABCG2 transport protein is N-glycosylated. Yeasts and insect cells show a reduced glycosylation potential [Harrison and Jarvis, 2006] and the original human protein is therefore 'underglycosylated'.

It was reported that the disparity in the extent of glycosylation did not affect ATPase activity [Diop and Hrycyna, 2005; Pal et al., 2007] and the ABCG2 transporter was functionally active in ATPase assays using membrane preparations from Sf9 cells [Özvegy et al., 2001; Glavinas et al., 2007; Pozza et al., 2009].

6.3.3   Optimization, validation and application of the ABCG2 ATPase assay

6.3.3.1   Set-up of the ATPase assay for the human BCRP

Prior to any experiments, the instrumental set-up of the planned ATPase assay in the 96-well format had to be elucidated. Therefore, the optimal detection wavelength of the obtained blue colored phosphomolybdate complex (after reduction with ascorbic acid) was identified (**Figure 6.15**). Considering the spectral intensity of the arc-discharge xenon lamp of the plate reader, the detection wavelength was set to 830 nm.

In the concentration range from 0.05 to 2 mM the used NaH_2PO_4 standards show excellent linearity regarding absorbance at 830 nm (Interference filter 830-15/75; Eureca Messtechnik GmbH, Köln, Germany) after complexing and were therefore appropriate for the assay.
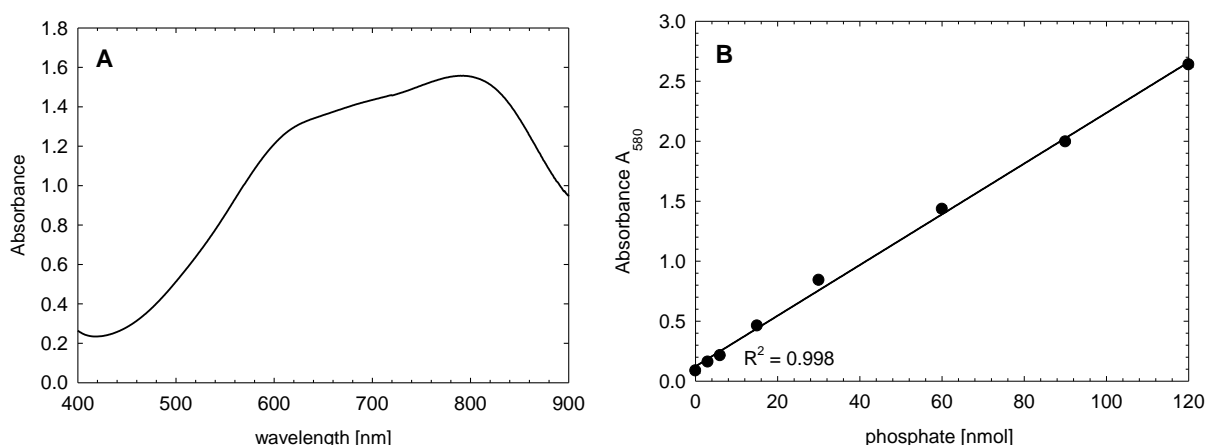
Figure 6.15: A) Absorbance spectrum of the reduced phosphomolybdate complex recorded with a Cary 100 UV-Vis spectrophotometer; **B**) Absorbance of the phosphate standards after complexation and reduction measured at the GENios Pro microplate reader at 830 nm.

Membrane preparations from Sf9 cells after an infection time of 24 h showed an ATPase activity of about 25 nmol P_i/min/mg protein when treated with 100 µM topotecan and prazosin, respectively. As shown in **Figure 6.16**, sodium orthovanadate at a concentration of 5 mM nearly completely inhibited vanadate-sensitive ATPase activity. The final concentration in the assay was set to 2 mM due to an unspecific color reaction of vanadate with the indicator solution at higher concentrations.

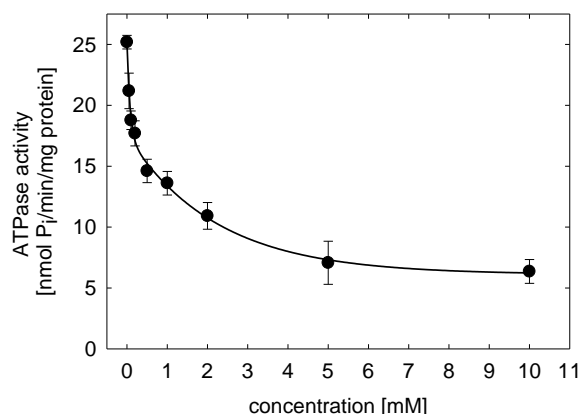**Figure 6.16:** ATPase activity of ABCG2-membranes (Infection: 24 h, 1:500) in the presence of different concentrations of sodium orthovanadate was reduced from 25 to 7 nmol P_i/min/mg protein (corresponding to vanadate-insensitive ATPase activity) when stimulated with topotecan [100 µM]. Data were obtained from two independent experiments.

First experiments on the ABCG2 ATPase activity, performed in the presence of the transporter substrates topotecan, mitoxantrone (**Figure 6.17**) or prazosin, using membrane preparations from Sf9 cells infected for 24 h, revealed a very high basal membrane ATPase activity. Under these conditions the sensitivity of the ATPase assay was substantially reduced, as the effects of the stimulatory drug relative to the negative control (2% (v/v) DMSO) were quite low. By reducing the final DMSO amount to a maximum of 1%, the
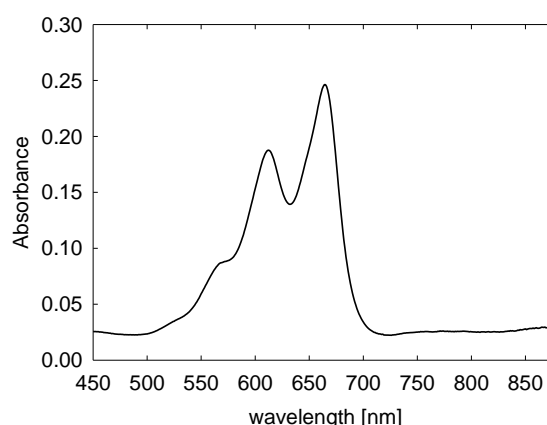

Figure 6.17: Absorbance spectrum of the ABCG2 substrate mitoxantrone with maxima at 612 and 664 nm. Mitoxantrone gives a dark-blue color which does not interfere with the detection of the molybdate complex in the ATPase assay at 830 nm.

difference between the negative (DMSO) control and topotecan could, indeed, be increased but was still insufficient (data not shown).

The molecular background of this high basal activity was extensively studied but is not known till now. It is speculated that the ABCG2 transporter is constitutively active, that is, the high basal activity may result from uncoupled (transport-independent) ATPase activity. The presence of unknown substrates in the membrane compartment [Sarkadi and Telbisz, 2013] and ineffective homodimerization of ABCG2 to a 'full transporter' have to be taken into account as well.

The problem of low sensitivity and a high basal activity of ATPase assays for the ABCG2 transporter has been described in literature [Özvegy et al., 2001; Özvegy et al., 2002; Mao et al., 2004] and different experiments have been conducted to solve the problem by preparing ABCG2 membranes with a fully active transporter protein to guarantee a high-sensitivity screening assay [Pal et al., 2007; Telbisz et al., 2007].

To exclude that the insensitivity of the assay has to be attributed to an insufficient expression level of the ABCG2 protein after 24 h of infection, additional experiments with membranes of cells with a longer infection time were performed in the presence of the ABCG2 substrates topotecan, prazosin and mitoxantrone and potent BCRP inhibitors including fumitremorgin C (FTC), Ko143 and different synthesized modulators (cf. Chapter 3). In fact, with ABCG2 overexpressing membranes of Sf9 cells with an infection time of 48 h, the difference between basal and substrate stimulated activity could be improved, but was still inadequate (**Figure 6.18**, bars **1-4**).

6.3.3.2   Mode of ATPase inhibition

There was a significant difference in vanadate-sensitive ATPase activity between substrate-treated and inhibitor-treated ABCG2 membranes (**Figure 6.18**). Topotecan-, mitoxantrone- and prazosin-stimulated ATPase activities (bars **2-4**) were reduced by about 30-40% from approximately 30 to 20 nmol P_i/min/mg protein with the addition of 5 µM fumtremorgin C (bars **6-8**). Compound **51** reduced the basal activity to the same extent, indicating that both FTC and **51** act as real ABCG2 inhibitors, not as substrates.
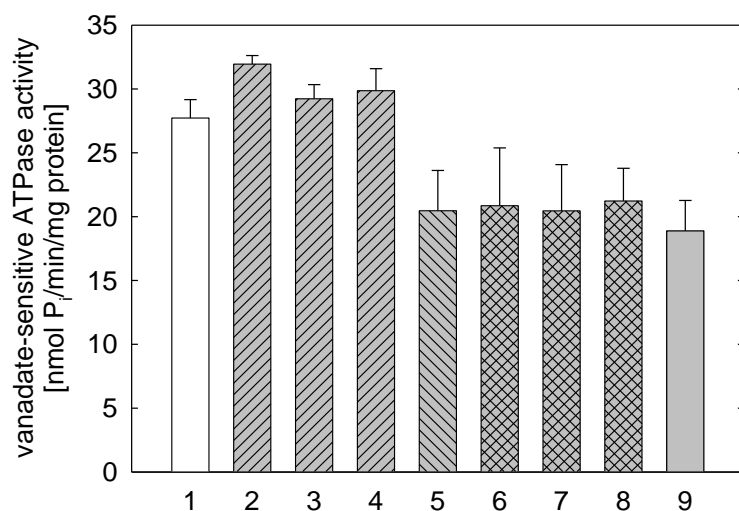

Figure 6.18: Vanadate-sensitive ATPase activity of ABCG2 membranes (48 h; 1:500) when treated with ABCG2 substrates, ABCG2 inhibitors or a combination of both:
1) Basal activity (DMSO 1%);
2) Topotecan [100 µM];
3) Mitoxantrone [5 µM];
4) Prazosin [5 µM];
5) FTC [5 µM];
6) Topotecan [100 µM] + FTC [5 µM];
7) Mitoxantrone [5 µM] + FTC [5 µM];
8) Prazosin [5 µM] + FTC [5 µM];
9) UR-MB108-4 (**51**) [10 µM].
Activity was calculated from 2-3 independent experiments.

A selection of synthesized modulators was investigated for concentration-dependent inhibition. Data are summarized in **Table 6.1**. The inhibitory effects obtained in the ATPase assay were not directly comparable to those in the Hoechst assay: The percental inhibition caused at the highest concentration tested in the ATPase assay refers to the drug-stimulated activity caused by 100 µM of topotecan, whereas the maximal inhibition in the Hoechst assay is referred to the inhibition caused by fumitremorgin C at 10 µM (100% inhibition). Nevertheless, data obtained in the two assay systems correlate quite well. IC_{50} values from the two assays are in a good correlation especially for highly potent compounds such as **3**, **32**, **51** and the standard compounds FTC and Ko143. Compounds with low efficiency in the Hoechst assay, for example **22**, also show reduced maximal effects in the ATPase

assay and vice versa (see compound **32**). As an example, the inhibitory effect of FTC and **51** in the ATPase assay is displayed in **Figure 6.19** in a concentration-dependent manner, giving reproducible sigmoidal concentration response curves. In general, the ATPase assay gave lower IC_{50} values than the Hoechst 33342 assay. This was particularly obvious for compounds **22** and **42**. Apperently, the (partial) proteolytic cleavage of the ABCG2 transporter when expressed in Sf9 cells (cf. section 6.3.2.1) does not affect the function of the membranes in the ATPase inhibition mode.
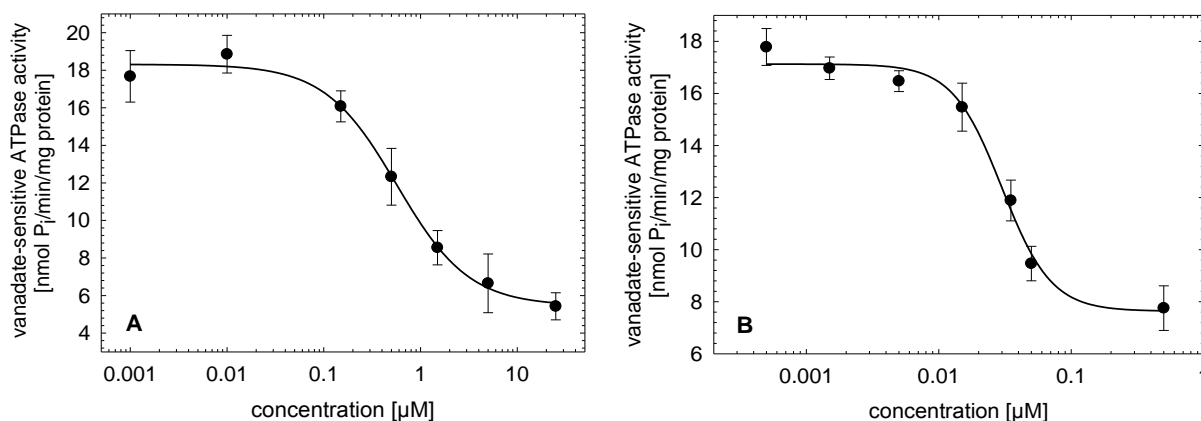

Figure 6.19: Vanadate-sensitive ATPase activity of ABCG2 membranes under the treatment of the potent BCRP inhibitors fumitremorgin C (**A**) and compound **51** (**B**).

Table 6.1: ABCG2 inhibition by selected compounds in the ATPase and the Hoechst 33342 assay.

Compound	ATPase assay[a]		Hoechst 33342 assay[b]	
	IC_{50} [nM][c]	Max. Inhibition (%)[d]	IC_{50} [nM]	Max. Inhibition (%)[e]
FTC	603 ± 161	62 ± 10	731 ± 92	100
Ko143	73 ± 14	71 ± 8	117 ± 5[f]	103 ± 7[f]
3 (UR-COP77)	65 ± 18	60 ± 8	183 ± 32[g]	83 ± 5[g]
7 (UR-COP145)	143 ± 40	57 ± 7	943 ± 79	87 ± 5
12 (UR-COP228)	178 ± 28	63 ± 5	591 ± 87	109 ± 8
22 (UR-COP238)	692 ± 74	35 ± 2	2,238 ± 202	22 ± 0
32 (UR-COP269)	37 ± 14	69 ± 5	59 ± 11	101 ± 5
42 (UR-QQS-2)	176 ± 59	59 ± 6	1,043 ± 53	107 ± 7
51 (UR-MB108-4)	23 ± 11	59 ± 4	64 ± 3	95 ± 3

[a] Data from inhibition of topotecan-stimulated [100 µM] ATPase activity on membranes of Sf9 cell infected for 48 h and 72 h, respectively (cholesterol-free); mean values ± SEM from two to three independent experiments performed in quadruplicate; [b] Hoechst 33342 microplate assay (ABCG2 overexpressing MCF-7/Topo cells); mean values ± SEM from two to three independent experiments performed in sextuplicate; [c] Respective concentration of the inhibitor required for half-maximal inhibition; [d] expressed as percental inhibition caused by the highest concentration of the test compound (reduced ATPase activity) relative to 100 µM topotecan (providing full ATPase activity); [e] Maximal inhibitory effects expressed as percental inhibition caused by the highest concentration of the compound tested relative to the reference compound FTC [10 µM] (100% inhibition); [f] [Kühnle, 2010]; [g] [Ochoa-Puentes et al., 2011]

The results revealed that the synthesized modulators inhibited the topotecan-stimulated ATPase activity, indicating that these compounds are not substrate of the ABCG2 transporters, but inhibitors. To confirm the mechanism of inhibition and the reliability of the assay, drugs working as inhibitors and poorly transported substrates should be included in the test series. With regard to investigations on competitive substrates/inhibitors in the ATPase assay, caution should be taken that an inhibitor of ABCG2 and its potency is dependent on the used substrate and the respective concentrations. Although competitive substrates have been identified for the ABCB1 transporter in drug accumulation studies [Scala et al. 1997], only few information is available about competitive ABCG2 substrates/inhibitors. Lately, imatinib mesylate, was shown to reverse BCRP-mediated resistance to topotecan and SN-38 (active metabolite of irinotecan) *in vitro* suggesting that it directly inhibits BCRP-mediated transport not being a competitive substrate [Houghton et al., 2004]. In contrast to that, Burger et. al. considered imatinib mesylate as a substrate of ABCG2 [Burger et al., 2004]. Furthermore, the inhibitory effect of the ABCG2 substrate flavopiridol on mitoxantrone efflux in ABCG2-overexpressing cells in high concentrations was attributed to competitive inhibition [Robey et al., 2001].

Despite low water solubility, the synthesized compounds worked well in this protein-free buffer system, although the ABCG2-ATPase activity was not completely inhibited. As the Hoechst 33342 assay was performed in the presence of FCS, the question arose whether albumin supplementation might increase the maximum effects of the compounds in the ATPase assay. The concentration-response curves of the ABCG2 inhibitor **12** on the ATPase activity in the presence and absence of 5% (m/v) BSA is shown in **Figure 6.20**. The addition of serum albumin did obviously not affect the ATPase inhibitory effect of **12** in this type of assay.
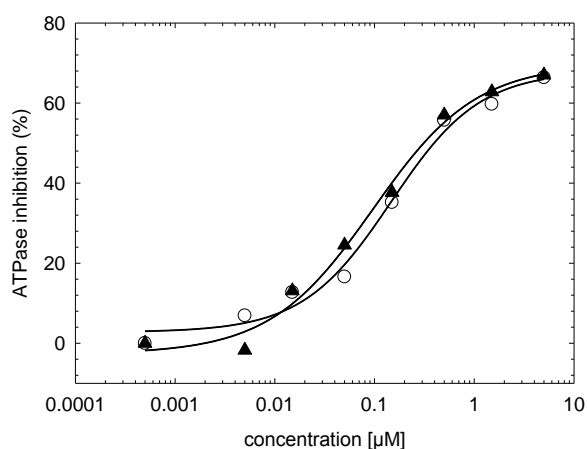

Figure 6.20: Effect of 5% (m/v) BSA (*triangles*) on the inhibition of ABCG2-ATPase activity by compound **12** in Sf9 membrane preparations; percental inhibition is determined as ratio of ATPase activity at the respective concentration referred to the topotecan-stimulated [100 µM] activity in absence of an inhibitor.

6.3.3.3 Cholesterol-loaded ABCG2 Sf9 membranes

It has been known for a long time that insects are unable to synthesize sterols *de novo* and require an exogenous supply of sterols [Clayton, 1964]. Cholesterol is the precursor of steroid hormones, for example cortisol in mammals and ecdysone in insects, and an essential constituent of membranes in animals [Ikekawa et al., 1993]. Cholesterol plays a crucial role in the function of membrane proteins. Previously, it was demonstrated that the cholesterol levels in insect cells are a limiting factor in the expression of the oxytocin receptor in the baculovirus/Sf9 system [Gimpl et al., 1995]. With the addition of cholesterol either to the insect cell culture medium or to membrane preparations, the specific binding of oxytocin to the oxytocin receptor was significantly increased in a concentration-dependent manner. Cholesterol-supplementation, however, produced controversial results regarding growth and morphology of insect cells, although lipids were shown to be essential for baculovirus infection and subsequent protein expression [Gimpl et al., 1995; Gilbert et al., 1996; Lua and Reid, 2005].

6.3.3.3.1 Effect of cholesterol on ATPase activity of ABCG2-Sf9 membrane preparations

By analogy with the above described results, Pal et al. observed a lack of ABCG2-ATPase activity stimulation by the BCRP substrates prazosin (**Figure 6.22**) and topotecan referred to the basal activity when expressed in Sf9 cell membranes, whereas ABCG2 overexpressing human cell membranes and cholesterol-loaded Sf9 membranes could be activated. The authors showed that the low cholesterol content of insect cells decisively influences ABCG2 stimulation, as cholesterol loading of membrane preparations significantly potentiates the stimulation of basal ABCG2 activity [Pal et al., 2007; Telbisz et al., 2007]. Therefore, membranes of Sf9 cells (48 h of infection) were thawed and incubated on ice for 20 min with a complex of randomly methylated-β-cyclodextrin (RAMEB) and cholesterol (final content: 5.4%) purchased from Cyclolab (Cyclodextrin Research and Development Laboratory; Budapest, Hungary) at a final concentration of 2.5 mg/mL. The membranes were centrifuged at 16,000 to remove residual cholesterol and, subsequently, resuspended in TMEP buffer (cf. 6.2.8.2). Wildtype ABCG2 membranes and cholesterol-loaded membranes were treated with ABCG2 substrates topotecan and prazosin, respectively, and the ATPase stimulation was compared. As shown in **Figure 6.21** the subsequent incubation with the RAMEB-cholesterol complex led to a 1.5-fold stimulation of basal activity for topotecan and prazosin, respectively, compared to 1.1 for wt membranes without cholesterol. The final ATPase stimulation in these membrane preparations is summarized in **Table 6.2**.
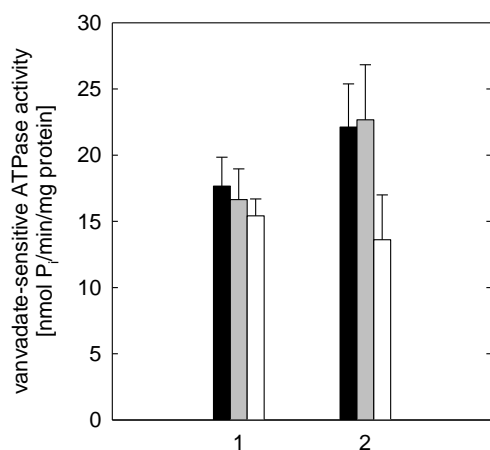
Figure 6.21: Vanadate-sensitive ATPase activity of ABCG2 Sf9 wt membranes (**1**) and cholesterol-loaded membranes (**2**) when incubated (1 h) with topotecan [100 μM] (*black bars*), prazosin [100 μM] (*grey bars*) and DMSO (=basal activity; *white bars*); results were obtained from 3 independent experiments each performed in quadruplicate.

Addition of cholesterol to ABCG2-Sf9 membranes significantly increased ATPase activity, suggesting that the low cholesterol content in Sf9 cells severely affected the activation of the ABCG2 transporter. It is difficult to decide whether cholesterol directly increases ABCG2-ATPase activity or has an indirect effect by altering the architecture and the fluidity of the phospholipid bilayer in the plasma membrane. Only a few studies addressing the effect of cholesterol on ABC transporters have been published so far, especially for the ABCB1 transporter [Garrigues et al., 2002; Arima et al., 2004]. Recently, it has been suggested that cholesterol is a substrate of ABCB1 [Le Goff et al., 2006]. This may also be taken into consideration in case of ABCG2 as other members of the ABCG subfamily were reported to be involved in cholesterol transport [Pal et al., 2007], e.g. ABCG5 and ABCG8 half transporters forming heterodimers for intestinal absorption and biliary excretion of cholesterol [Graf et al., 2003].

6.3.3.3.2   Modified membrane preparation protocol

Based on these encouraging results, the original membrane preparation protocol described in section 6.2.8.2 was slightly modified:

Prior to the last centrifugation step at 100,000 g, membranes were incubated with the RAMEB-cholesterol complex at a final concentration of 2.5 mg/mL for 20 min at 4 °C. After resuspension and protein quantification, membranes were subsequently aliquoted and stored at -80 °C until use.

6.3.3.4   Effect of CHAPS on basal and drug-stimulated ABCG2-ATPase activity

In a recently published patent by Sarkadi and Telbisz [Sarkadi and Telbisz, 2013], the difference between drug-stimulated and basal activity could be increased in the presence of CHAPS (3-[(3-cholamidopropyl)dimethylammonio]-1-propanesulfonate), a non-denaturing zwitterionic sulfobetaine detergent which is commonly used for protein solubilization and disruption of protein-protein interactions (**Figure 6.22**).
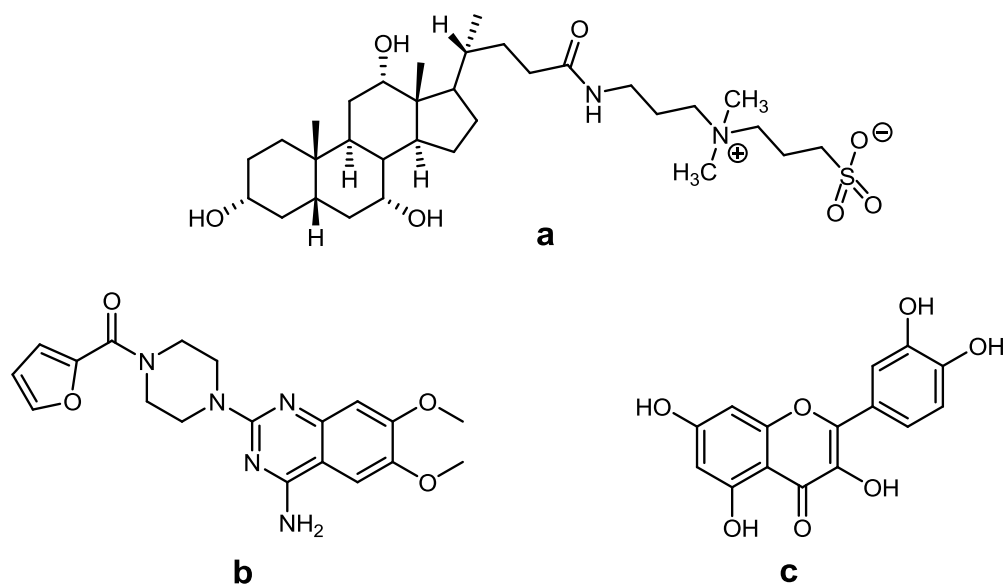
Figure 6.22: Chemical structures of the sulfobetaine-type zwitterionic *detergent* CHAPS (**a**) and the ABCG2 substrate prazosin (**b**). The flavonoid quercetin (**c**) was recently shown to be transported by ABCG2 [Sesink et al., 2005].

Cholesterol-loaded membranes (prepared as described in 6.3.3.3.2) were used for the ATPase assay in the presence and absence of prazosin [100 µM] under simultaneous treatment with different concentrations of CHAPS [0.1-2.0 mM] (**Figure 6.23**).
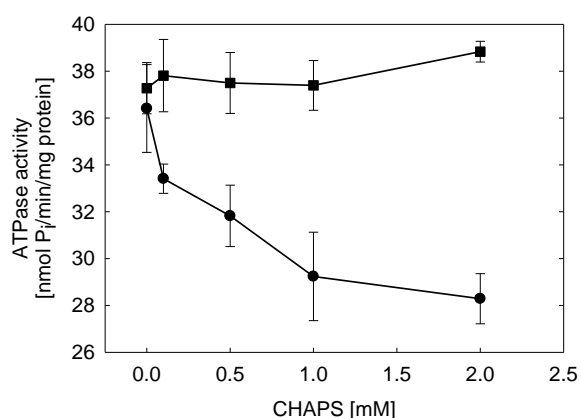
Figure 6.23: Effect of of CHAPS on the basal (*circles*) and prazosin-stimulated (*squares*) ABCG2-ATPase activity in cholesterol-loaded Sf9 membranes.

With the addition of CHAPS to the cholesterol-loaded membrane preparation the basal ATPase activity was significantly reduced about 25% whereas the drug-stimulated activity remained nearly unchanged. Accordingly, the protocol of the ATPase assay was modified: a final concentration of 1 mM CHAPS was added to the membrane preparations immediately prior to the experimental procedure.

The differences in topotecan-, quercetin- and prazosin-stimulated and FTC-inhibited ABCG2-ATPase activity using 'ABCG2 wildtype' and cholesterol-loaded membranes in the presence or absence of CHAPS become obvious from **Figure 6.24**.
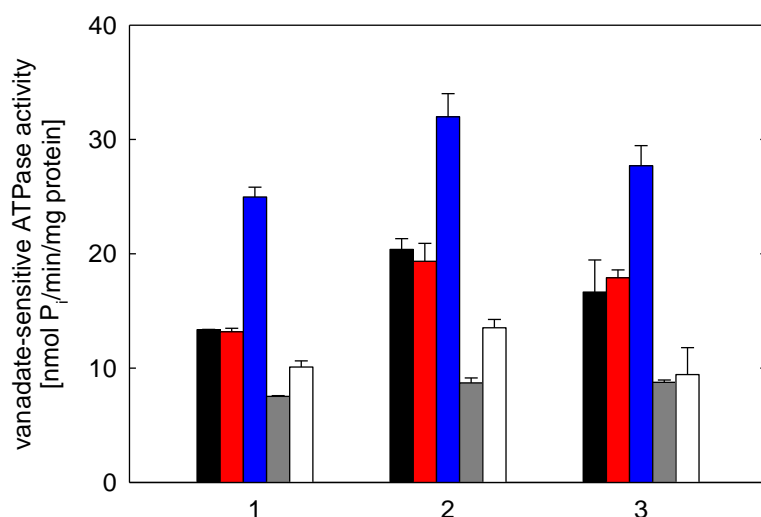
Figure 6.24:
Vanadate-sensitive ATPase activity of ABCG2 Sf9 wt (**1**), cholesterol-loaded (**2**) and cholesterol-loaded membranes modulated with CHAPS [1 mM] (**3**) when incubated with topotecan [100 μM] (*black*), prazosin [100 μM] (*red*), quercetin [10 μM] (*blue*), fumitremorgin C [10 μM] (*gray*) and DMSO (=basal activity; *white*), respectively; n = 3.

Table 6.2: Effect of cholesterol and CHAPS on the stimulation or inhibition of the ABCG2-ATPase in ABCG2 Sf9 membranes in presence of various ABCG2 modulating agents. Stimulation is expressed as the ratio of the drug-stimulated and the basal ATPase activity, inhibition is given as the percental reduction of the basal activity.

Compound	concentration [μM]	wt ABCG2 membranes	cholesterol-loaded ABCG2 membranes	cholesterol-loaded ABCG2 membranes + CHAPS [1 mM]
		fold stimulation	fold stimulation	fold stimulation
Topotecan	100	1.32	1.51	1.77
Prazosin	100	1.25	1.43	1.90
Quercetin	10	2.47	2.36	2.94
		Inhibition	**Inhibition**	**Inhibition**
Fumitremorgin C	10	25.4%	35.7%	7.2%

In summary, with the addition of cholesterol to the membrane preparation the ratio of stimulated and basal ATPase activity was significantly improved. The treatment with the modulation agent CHAPS led to an additional enhancement of sensitivity in the stimulation mode of the assay by reducing the basal ATPase activity. FTC was not able to further lower the reduced basal activity in presence of CHAPS suggesting that the minimum of basal activity is reached with the addition of the detergent.

Figure 6.25 shows the activation of basal ATPase activity by ABCG2 substrates topotecan, prazosin and quercetin in cholesterol-loaded (+ 1 mM CHAPS) and wt ABCG2 membranes in a concentration-dependent manner.
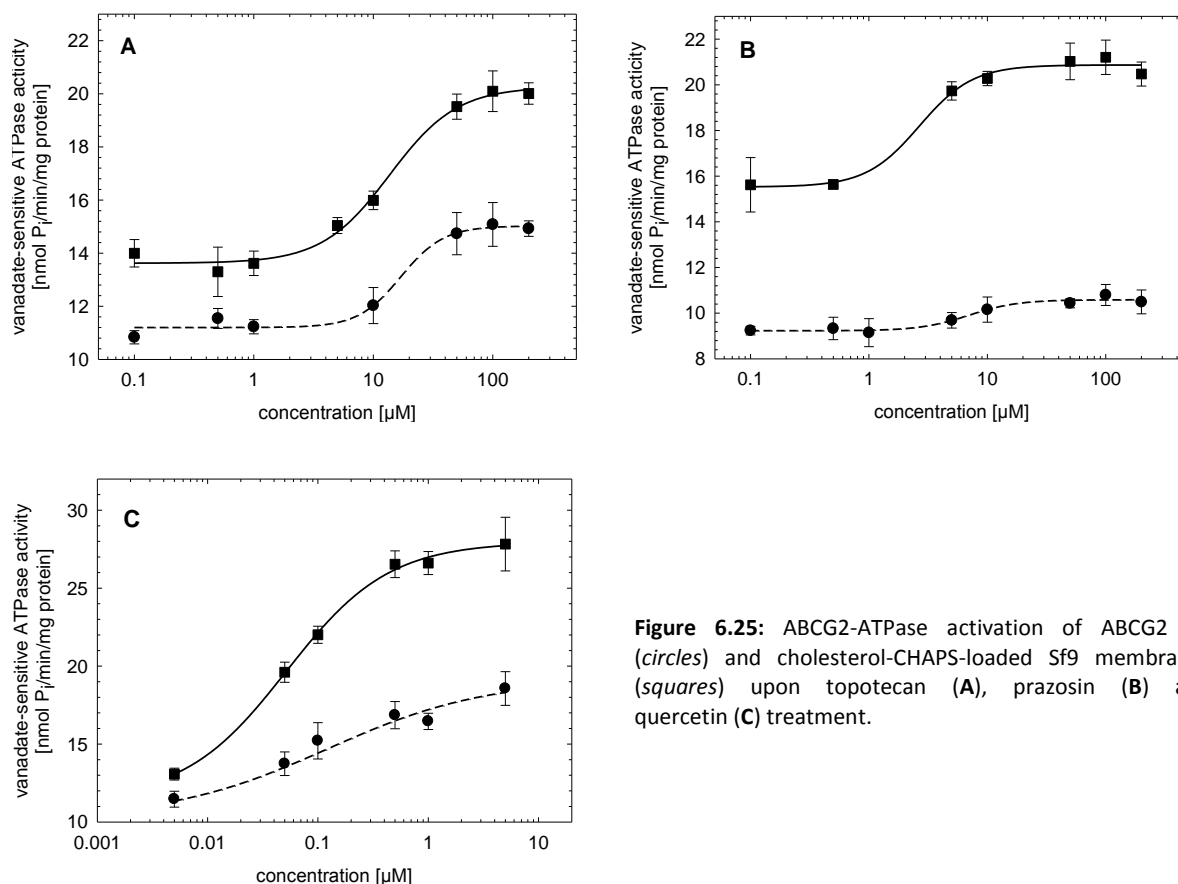
Figure 6.25: ABCG2-ATPase activation of ABCG2 wt (*circles*) and cholesterol-CHAPS-loaded Sf9 membranes (*squares*) upon topotecan (**A**), prazosin (**B**) and quercetin (**C**) treatment.

The comparison of ABCG2 wt and cholesterol-loaded membranes (without CHAPS) in the inhibition mode is exemplarily shown for compounds **32** and **52** in **Figure 6.26**. The use of cholesterol generally resulted in higher ATPase activities upon stimulation by topotecan, but did not influence potency and efficacy parameters to a noteworthy extent (**Table 6.3**).

Figure 6.26: Inhibition of ABCG2-ATPase by compound **32** (**A**) and **52** (**B**) after stimulation with topotecan [100 μM] in ABCG2 wt (*circles*) and cholesterol-loaded Sf9 membranes (*squares*).

In general, cholesterol-loaded membranes allowed for the construction of better reproducible sigmoidal concentration-response curves with higher amplitude, resulting in lower errors of the IC$_{50}$ values.

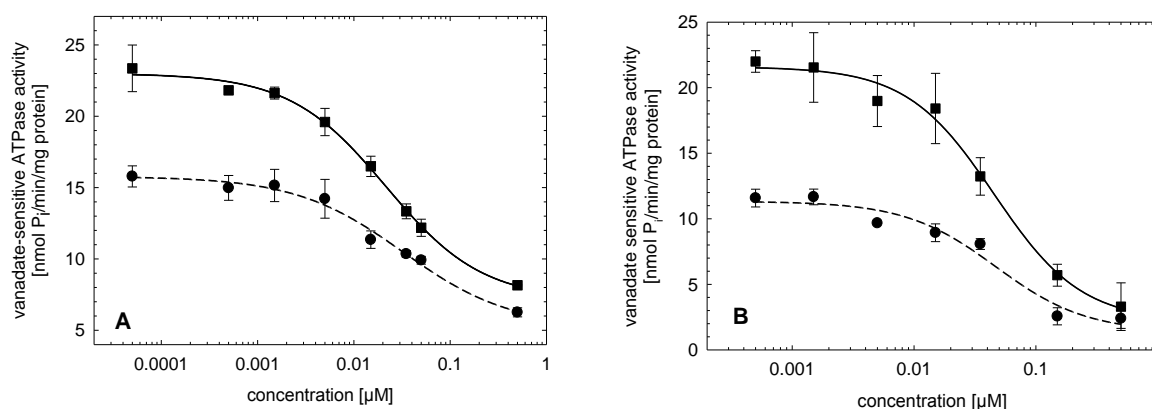**Table 6.3:** Inhibitory activities of selected ABCG2 modulators, determined in the ATPase assay on ABCG2 wt and cholesterol-loaded membranes [a]

Compound	wt ABCG2 membranes		cholesterol-loaded ABCG2 membranes	
	IC$_{50}$ [nM]	I$_{max}$ (%)	IC$_{50}$ [nM]	I$_{max}$ (%)
32	32 ± 11	60 ± 8	22 ± 3	65 ± 5
34	75 ± 13	79 ± 7	46 ± 12	75 ± 7
52	47 ± 25	79 ± 10	45 ± 11	85 ± 5

[a] Mean values ± SEM calculated from two independent experiments performed in quadruplicate.

6.4   Summary and conclusions

The ABCG2 template in combination with the signal peptide sequence for expression in Sf9 insect cells was successfully and error-free cloned into the pVL1392 vector. Recombinant baculoviruses encoding the ABCG2 transporter were generated and used for Sf9 cell infection. To achieve ABCG2 overexpression in Sf9 cell membranes, cells were infected for 48 h with high titer virus stocks despite a higher extent of proteolysis of the target ABCG2 protein when compared to cells infected for a period of 24 h.

In insect cells, the ABCG2 monomer was expressed at a lower molecular weight due to deglycosylation. However, the difference in the extent of glycosylation did not affect the ATPase activity of the transporter.

Very high basal activity severely compromised assay analysis. The low sensitivity caused high errors and an inacceptable signal-to-noise ratio. The narrow margin between basal and drug-stimulated ATPase activity of ABCG2 Sf9 membranes was significantly improved by incubating ABCG2-membranes with a cyclodextrin-cholesterol complex. The concomitant addition of CHAPS to cholesterol-loaded membrane preparations decreased the basal activity and led to a sufficient difference between basal and stimulated ABCG2-ATPase activity to establish an assay protocol. The ATPase inhibition mode produced slightly higher maximal effects when cholesterol was added to the membranes, but worked likewise with wildtype ABCG2 Sf9 membranes.

The results obtained from the ATPase assay demonstrated that the synthesized ABCG2 modulators described in Chapter 3 are inhibitors and not substrates. The established ATPase assay for the human ABCG2 transporter on Sf9 membrane preparations proved to be well-suited system to discriminate between ABCG2 substrates and inhibitors. In combination with other assays, the determination of ATPase activity harbors the potential of being used for the profiling of ABCG2 modulators to detect different mechanisms of drug-transporter interaction.

6.5   References

Arima, H., Yunomae, K., Morikawa, T., et al. Contribution of cholesterol and phospholipids to inhibitory effect of dimethyl-beta-cyclodextrin on efflux function of P-glycoprotein and multidrug resistance-associated protein 2 in vinblastine-resistant Caco-2 cell monolayers. *Pharm. Res.* **2004**, 21(4), 625-634.

Brunskole, I. Molecular and Cellular Analysis of Aminergic G Protein-Coupled Receptors: Histamine H2, H4 and β2-Adrenergic Receptors, a Scientific Paradigm. PhD Thesis, University of Regensburg, Germany, 2011.

Burger, H., van Tol, H., Boersma, A. W., et al. Imatinib mesylate (STI571) is a substrate for the breast cancer resistance protein (BCRP)/ABCG2 drug pump. *Blood* **2004**, 104(9), 2940-2942.

Chen, J., Sharma, S., Quiocho, F. A., et al. Trapping the transition state of an ATP-binding cassette transporter: evidence for a concerted mechanism of maltose transport. *Proc. Natl. Acad. Sci. U S A* **2001**, 98(4), 1525-1530.

Clayton, R. B. The Utilization of Sterols by Insects. *J. Lipid Res.* **1964**, 5, 3-19.

Diop, N. K. and Hrycyna, C. A. N-linked glycosylation of the human ABC transporter ABCG2 on asparagine 596 is not essential for expression, transport activity, or trafficking to the plasma membrane. *Biochemistry* **2005**, 44(14), 5420-5429.

Ejendal, K. F. and Hrycyna, C. A. Multidrug resistance and cancer: the role of the human ABC transporter ABCG2. *Curr. Protein Pept. Sci.* **2002**, 3(5), 503-511.

Garrigues, A., Escargueil, A. E. and Orlowski, S. The multidrug transporter, P-glycoprotein, actively mediates cholesterol redistribution in the cell membrane. *Proc. Natl. Acad. Sci. U S A* **2002**, 99(16), 10347-10352.

Germann, U. A., Willingham, M. C., Pastan, I., et al. Expression of the human multidrug transporter in insect cells by a recombinant baculovirus. *Biochemistry* **1990**, 29(9), 2295-2303.

Gilbert, R. S., Nagano, Y., Yokota, T., et al. Effect of lipids on insect cell growth and expression of recombinant proteins in serum-free medium. *Cytotechnology* **1996**, 22(1-3), 211-216.

Gimpl, G., Klein, U., Reilander, H., et al. Expression of the human oxytocin receptor in baculovirus-infected insect cells: high-affinity binding is induced by a cholesterol-cyclodextrin complex. *Biochemistry* **1995**, 34(42), 13794-13801.

Glavinas, H., Kis, E., Pal, A., et al. ABCG2 (breast cancer resistance protein/mitoxantrone resistance-associated protein) ATPase assay: a useful tool to detect drug-transporter interactions. *Drug. Metab. Dispos.* **2007**, 35(9), 1533-1542.

Gotoh, T., Miyazaki, Y., Sato, W., et al. Proteolytic activity and recombinant protein production in virus-infected Sf-9 insect cell cultures supplemented with carboxyl and cysteine protease inhibitors. *J. Biosci. Bioeng.* **2001**, 92(3), 248-255.

Graf, G. A., Yu, L., Li, W. P., et al. ABCG5 and ABCG8 are obligate heterodimers for protein trafficking and biliary cholesterol excretion. *J. Biol. Chem.* **2003**, 278(48), 48275-48282.

Harrison, R. L. and Jarvis, D. L. Protein N-glycosylation in the baculovirus-insect cell expression system and engineering of insect cells to produce "mammalianized" recombinant glycoproteins. *Adv. Virus Res.* **2006**, 68, 159-191.

Houghton, P. J., Germain, G. S., Harwood, F. C., et al. Imatinib mesylate is a potent inhibitor of the ABCG2 (BCRP) transporter and reverses resistance to topotecan and SN-38 in vitro. *Cancer Res.* **2004**, 64(7), 2333-2337.

Ikekawa, N., Morisaki, M. and Fujimoto, Y. Sterol-Metabolism in Insects - Dealkylation of Phytosterol to Cholesterol. *Accounts Chem. Res.* **1993**, 26(4), 139-146.

Jacobs, A. Expression, Aufreinigung und funktionelle Untersuchungen der ABC-Transporter ABCB1 und ABCG2. PhD thesis, Rheinische Friedrich-Wilhelms Universität Bonn, Germany, 2010.

Kühnle, M. Experimental therapy and detection of glioblastoma: investigation of nanoparticles, ABCG2 modulators and optical imaging of intracerebral xenografts. PhD thesis, University of Regensburg, Germany, 2010.

Le Goff, W., Settle, M., Greene, D. J., et al. Reevaluation of the role of the multidrug-resistant P-glycoprotein in cellular cholesterol homeostasis. *J. Lipid Res.* **2006**, 47(1), 51-58.

Litman, T., Brangi, M., Hudson, E., et al. The multidrug-resistant phenotype associated with overexpression of the new ABC half-transporter, MXR (ABCG2). *J. Cell Sci.* **2000**, 113 (Pt 11), 2011-2021.

Litman, T., Jensen, U., Hansen, A., et al. Use of peptide antibodies to probe for the mitoxantrone resistance-associated protein MXR/BCRP/ABCP/ABCG2. *Biochim. Biophys. Acta.* **2002**, 1565(1), 6-16.

Lua, L. H. L. and Reid, S. *The importance of cholesterol for insect cell growth and baculovirus production*. Animal Cell Technology Meets Genomics. Dordrecht, Netherlands, Springer. 2005, 565-568.

Mao, Q., Conseil, G., Gupta, A., et al. Functional expression of the human breast cancer resistance protein in Pichia pastoris. *Biochem. Biophys. Res. Commun.* **2004**, 320(3), 730-737.

Ochoa-Puentes, C., Höcherl, P., Kühnle, M., et al. Solid phase synthesis of tariquidar-related modulators of ABC transporters preferring breast cancer resistance protein (ABCG2). *Bioorg. Med. Chem. Lett.* **2011**, 21(12), 3654-3657.

Özvegy, C., Litman, T., Szakacs, G., et al. Functional characterization of the human multidrug transporter, ABCG2, expressed in insect cells. *Biochem. Biophys. Res. Commun.* **2001**, 285(1), 111-117.

Özvegy, C., Varadi, A. and Sarkadi, B. Characterization of drug transport, ATP hydrolysis, and nucleotide trapping by the human ABCG2 multidrug transporter. Modulation of substrate specificity by a point mutation. *J. Biol. Chem.* **2002**, 277(50), 47980-47990.

Pal, A., Mehn, D., Molnar, E., et al. Cholesterol potentiates ABCG2 activity in a heterologous expression system: improved in vitro model to study function of human ABCG2. *J. Pharmacol. Exp. Ther.* **2007**, 321(3), 1085-1094.

Pop, N. Development of functional assays for human neuropeptide Y (Y1,2,4,5) receptors exploiting GTPase activity and (bio)luminescence as readout. PhD thesis, University of Regensburg, Germany, 2010.

Pozza, A., Perez-Victoria, J. M. and Di Pietro, A. Overexpression of homogeneous and active ABCG2 in insect cells. *Protein Expr. Purif.* **2009**, 63(2), 75-83.

Pozza, A., Perez-Victoria, J. M., Sardo, A., et al. Purification of breast cancer resistance protein ABCG2 and role of arginine-482. *Cell. Mol. Life Sci.* **2006**, 63(16), 1912-1922.

Rendic, D., Wilson, I. B. H. and Paschinger, K. The glycosylation capacity of insect cells. *Croat. Chem. Acta* **2008**, 81(1), 7-21.

Robey, R. W., Medina-Perez, W. Y., Nishiyama, K., et al. Overexpression of the ATP-binding cassette half-transporter, ABCG2 (Mxr/BCrp/ABCP1), in flavopiridol-resistant human breast cancer cells. *Clin. Cancer Res.* **2001**, 7(1), 145-152.

Saito, H., Hirano, H., Nakagawa, H., et al. A new strategy of high-speed screening and quantitative structure-activity relationship analysis to evaluate human ATP-binding cassette transporter ABCG2-drug interactions. *J. Pharmacol. Exp. Ther.* **2006**, 317(3), 1114-1124.

Saito, H., Osumi, M., Hirano, H., et al. Technical pitfalls and improvements for high-speed screening and QSAR analysis to predict inhibitors of the human bile salt export pump (ABCB11/BSEP). *AAPS J.* **2009**, 11(3), 581-589.

Sarkadi, B., Price, E. M., Boucher, R. C., et al. Expression of the human multidrug resistance cDNA in insect cells generates a high activity drug-stimulated membrane ATPase. *J. Biol. Chem.* **1992**, 267(7), 4854-4858.

Sarkadi, B. and Telbisz, A. ABCG2 transporter assay. WO/2013/128217 A1 (PCT/HU2013/000021), **2013**.

Scala, S., Akhmed, N., Rao, U. S., et al. P-glycoprotein substrates and antagonists cluster into two distinct groups. *Mol. Pharmacol.* **1997**, 51(6), 1024-1033.

Senior, A. E., al-Shawi, M. K. and Urbatsch, I. L. The catalytic cycle of P-glycoprotein. *FEBS. Lett.* **1995**, 377(3), 285-289.

Sesink, A. L., Arts, I. C., de Boer, V. C., et al. Breast cancer resistance protein (Bcrp1/Abcg2) limits net intestinal uptake of quercetin in rats by facilitating apical efflux of glucuronides. *Mol. Pharmacol.* **2005**, 67(6), 1999-2006.

Telbisz, A., Muller, M., Özvegy-Laczka, C., et al. Membrane cholesterol selectively modulates the activity of the human ABCG2 multidrug transporter. *Biochim. Biophys. Acta.* **2007**, 1768(11), 2698-2713.

Chapter 7

7   Summary

Multidrug transporter proteins such as ABCB1, ABCC1 and ABCG2 are known to contribute the chemoresistance of malignant tumors. Expression of these transporters by cancer cells leads to an efflux of anticancer drugs. The inhibition of efflux pumps, namely ABCB1 (p-glycoprotein), has been explored in clinical trials as an approach to overcome ABC transporter mediated drug resistance in cancer patients, but did not lead to a drug approval. The limitations of this approach can be explained by multiple resistance mechanisms including the contribution of ABC transporters other than ABCB1. The relevance of ABCG2 inhibition has not been adequately explored.

Apart from chemoresistance in cancer, ABC transporters play a major role as efflux pumps expressed in epithelia and endothelial cells, influencing the bioavailability, tissue distribution, access to the brain, and the excretion of drugs. In particular, modulation of ABC transporters at the blood brain barrier (BBB) may considerably increase the entry of drugs into the central nervous system (CNS) and enhance the effectiveness of pharmacotherapy, including the chemotherapy of malignancies in the CNS, as demonstrated in a proof-of-concept study in mice with paclitaxel in combination with the ABCB1 modulator valspodar. This strategy should even be more effective in case of inhibition of ABCG2, as this transporter is considered to be the most important efflux transporter at the BBB. To prove this hypothesis, potent and selective ABCG2 modulators are required.

This doctoral project was pursued in collaboration with Prof. Dr. B. König (Institute of Organic Chemistry, University of Regensburg), aiming at the development of selective ABCG2 modulators. Previously reported quinoline carboxamide-type compounds from our laboratory such as UR-ME22-1 were highly potent and selective ABCG2 modulators, but revealed unfavourable physico-chemical properties, mainly due to poor solubility and rapid enzymatic cleavage of a central benzamide bond. Next generation inhibitors, synthesized in the Institute of Organic Chemistry, were characterized in various functional cellular assays (Hoechst 33342, calcein-AM, pheophorbide a, flow cytometric mitoxantrone assay, kinetic cytotoxicity assay) available in our laboratory. Additional *in vitro* models for the characterization of the transporter inhibitors were established (mitoxantrone microplate

assay for ABCG2, calcein ABCC1 assay, ATPase assay for ABCG2 using Sf9 membranes), the selectivity for ABCG2 compared to ABCB1 and ABCC1 was determined, and (bio)analytical studies (plasma protein binding by ultrafiltration, equilibrium dialysis, isothermal titration calorimetry and HPLC; stability in buffer and against enzymatic cleavage) were performed. Preliminary preclinical studies in nude mice bearing orthotopically implanted genetically modified human glioblastoma enabling optical *in vivo* imaging, proved that U-87MG xenografts grow rapidly in the brain. However, these tumors were too aggressive to perform therapeutic studies. Therefore, in search for a more appropriate tumor entity, three malignant human brain tumor cell lines (Daoy, LN-18 and SW 1783) were characterized *in vitro* regarding growth kinetics, chemosensitivity against several anti-cancer drugs, and ABC transporter expression as well as *in vivo* for tumorigenicity in a subcutaneous tumor model in nude mice.

Bioisosteric replacement of the central amide core of the first and second generation of ABCG2 inhibitors by a biphenyl, quinoline, indol or a triazole moiety resulted in chemically more stable compounds, and the introduction of triethyleneglcyol residues increased solubility. In the new compound libraries dual ABCB1/ABCG2 and ABCG2-selective modulators were identified which are among the most potent BCRP inhibitors reported so far.

Selected ABCG2 modulators were additionally investigated in an *in vitro* model of the BBB (porcine brain capillary endothelial cell layers, expressing ABCG2; cooperation with Prof. H. J. Galla, University of Münster) to get closer to the physiological situation and to predict the influence of the compounds on the penetration of co-administered drugs into the brain of nude mice bearing orthotopically growing xenografts. Surprisingly, in the BBB model the investigated inhibitors were much more potent than in the fluorescence based cellular assays.

The reduced transport of a substrate used to determine ABCG2 activity in the presence of a modulator may result from different modes of action: competition of the test compound with the indicator as a substrate or inhibition of the transport mechanism. To discriminate between the mechanisms of modulation, a colorimetric ATPase assay in the microplate format was established using membrane preparations from baculovirus-infected Sf9 cells expressing the human ABCG2 protein. All tested compounds turned out to be 'true' ABCG2 inhibitors, capable of inhibiting substrate-induced ATPase activity.

In summary, the new ABCG2 modulators were highly potent and selective inhibitors, but showed poor water solubility and very high plasma protein binding (almost 100%). The drug-like properties of these compounds have to be further improved in view of *in vivo* studies.

*A*ppendix

A   Expression of ABCG2 at the murine blood-brain barrier - immunohistochemical investigations

A.1   Introduction

Immunohistochemical (IHC) investigations were performed to study the expression of the Abcg2 protein (murine ortholog of the human ABCG2 transporter) at the blood-brain barrier of nude NMRI (nu/nu) mice using paraffin embedded brain tissue sections. According to an indirect method for the detection of the transporter protein, an unlabeled primary antibody and a horseradish peroxidase (HRP)-conjugated secondary antibody were used.

Principle of peroxidase immunohistochemical staining:

The protein of interest is targeted by an antibody that is conjugated with a peroxidase enzyme (e.g. HRP). The antibody or target protein is visualized via a peroxidase-catalyzed reaction in the presence of hydrogen peroxide. The substrate 3,3'-diaminobenzidine (DAB) is thereby oxidized giving a brown precipitate:

$$\text{Peroxidase} + 2\ H_2O_2 \longrightarrow O_2 + 2\ H_2O$$

$$O_2 + \text{DAB} \longrightarrow \text{insoluble, black-brown precipitate.}$$
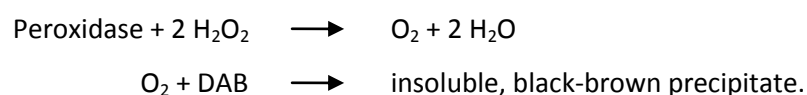
A.2   Materials and methods

A.2.1   Drugs and chemicals

Antibodies were obtained from Santa Cruz Biotechnology (Heidelberg, Germany) unless otherwise stated. 0.1% PBS-T buffer was made by diluting 1000 µL Triton X-100 (Sigma, Munich, Germany) in 1000 mL of PBS.

Nuclear fast red solution (0.1% (m/v); also known as 'Kernechtrot') was prepared by dissolving nuclear fast red (Sigma, Munich, Germany) in a 5% (m/v) aluminum sulfate solution. The solution was heated (80 °C) and filtrated through a paper filter when cooled down.

All other chemicals were purchased from Merck (Darmstadt, Germany) in p.a. quality if not otherwise stated. Millipore water was used.

A.2.2   Paraffin embedding and sectioning

In order to investigate the extent of Abcg2 transporter expression at the BBB after tumor implantation, a nude NMRI (nu/nu) mouse bearing intracerebral U-87 MG Luc2/Katushka_Clone 15 xenografts was killed by cervical dislocation (U-87 MG Luc2/Katushka co-transfectants were obtained as described elsewhere [Kühnle, 2010]) .

The brain was excised, fixed in Bouin´s solution (saturated picric acid/ formaldehyde/ glacial acetic acid 15:5:1) for one day and embedded in paraffin according to a standard procedure described elsewhere [Müller, 2007]. Serial coronal sections (6 µm) were cut every 200 µm using a Leica RM2255 microtome (Leica; Bensheim, Germany) and mounted on microscope slides.

A.2.3   Immunoperoxidase staining

For IHC investigations, paraffin tissue sections were deparaffinized with xylene (2 x 10 min) and rehydrated in graded isopropyl alcohol (iPrOH) followed by two washing steps (10 min) with PBS-T buffer. Unspecific binding of the primary antibody was blocked by incubation of the tissue sections in 3% nonfat dry milk in PBS-T (blocking solution) for one hour. Thereafter, the sections were incubated with different concentrations of the primary AB in blocking solution over night at 4 °C in Quadriperm lux-multiplates (Greiner, Frickenhausen, Germany). Wet filter paper was added to the Quadriperm chambers to create a humid atmosphere. To avoid wasting of the antibodies, the area around the tissue samples was encircled with a wax pen (PAP PEN; Kisker Biotech, Steinfurt, Germany) giving a water-repellent circle. In controls, the respective solution was added without primary AB to test the protocol and the specificity of the antibody used.

The next day, the secondary AB was added after three washing steps (10 min) with PBS-T, and samples were stored for 1-2 hours in the dark. After additional three washing steps with PBS-T, the tissue sections were stained via the peroxidase-diaminobenzidine reaction using a DAB Substrate Kit for Peroxidase (Vector Laboratories; Burlingame, CA) according to the instructions for IHC staining. In brief: immediately before use, the substrate solution was prepared by adding 2 drops of buffer stock solution to 5 mL of distilled water. Afterwards, 4 drops of DAB stock solution and 2 drops of the hydrogen peroxide solution were added and mixed. To obtain a gray-black stain 2 drops of nickel solution were added to the mixture and the tissue sections were incubated with the substrate solution at room temperature for 7-10 min. After washing in water for 5 min, nuclei were counterstained by mounting the samples for 8 min in a 0.1% nuclear fast red solution and washed thoroughly another three times with Millipore water. The wax pen marker was carefully removed using xylene. After dehydration in an ascending iPrOH series and xylene, sections were mounted with DePeX (EMS; Hatfield, PA). Stained tissue samples were analyzed with a BH-2 microscope (Olympus, Hamburg, Germany).

Two different antibody-combinations were used for IHC:

1. primary AB: ABCG2 (BXP-53); 1:50 and 1:100

   secondary AB: HRP-conjugated goat anti-rat IgG, 1:750

2. primary AB: rabbit polyclonal BCRP/ABCG2 antibody (orb10178), Biorbyt Ltd.
   (Cambridge,   UK), 1:100 and 1:500

   secondary AB: HRP-conjugated donkey anti-rabbit IgG, 1:1,000

A.3   Results

The visualization of Abcg2 at the BBB of a nude mouse, bearing an intracerebral U-87 MG Luc2/Katushka_Clone 15 tumor, using the ABCG2 (BXP-53) antibody from Santa Cruz Biotechnology (recommended for the detection of ABCG2 of mouse and human origin) was not successful. After immunoperoxidase staining with the DAB Substrate Kit from Vector Laboratories, only erythrocytes and blood constituents were positive, whereas Abcg2 expression was not detected at the murine brain capillaries (**Figure A.1**).
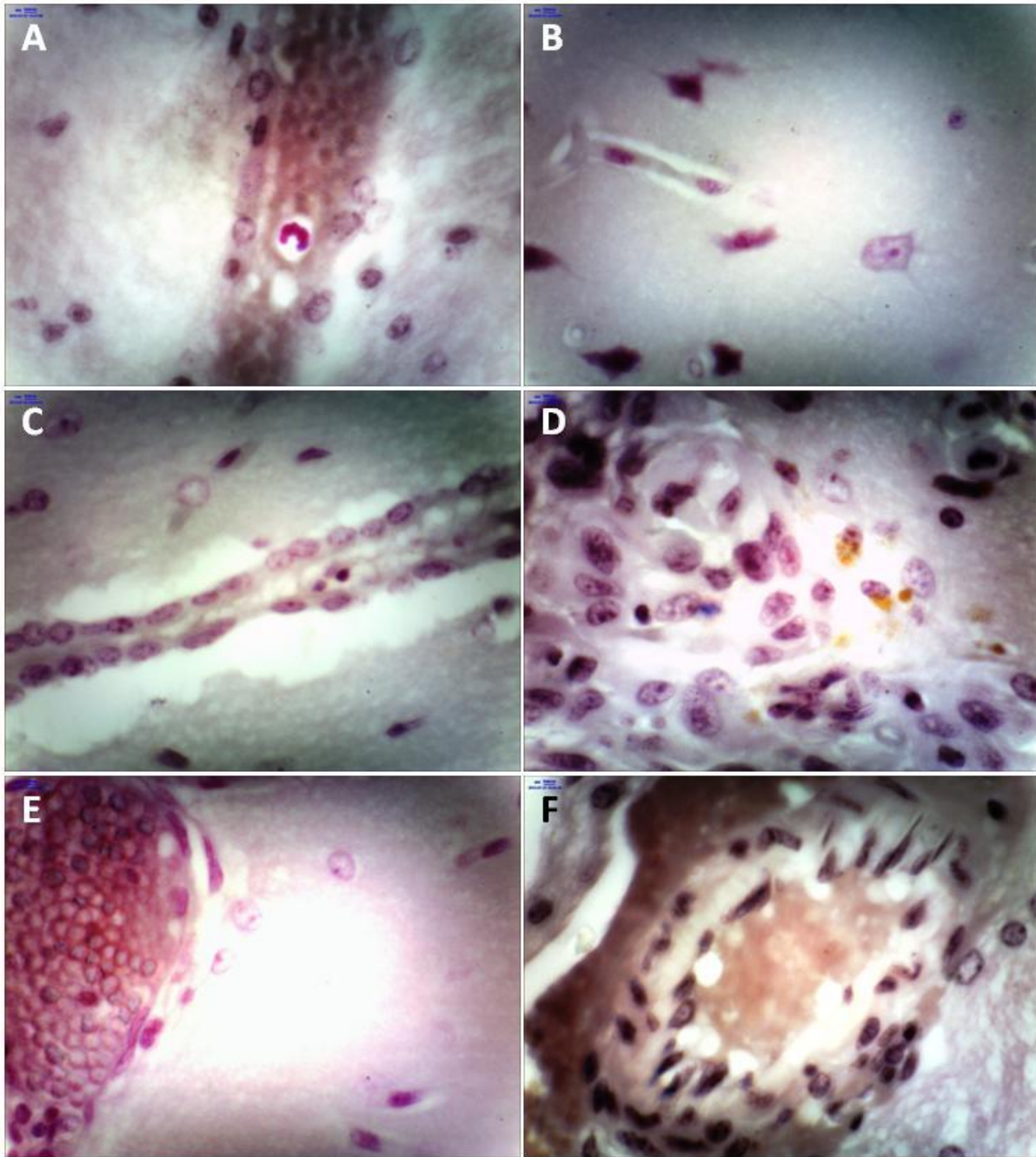
Figure A.1: Immunohistochemical peroxidase staining of brain tissue section of nude NMRI (nu/nu) mice bearing intracerebral U-87 MG Luc2/Katushka_Clone 15 xenografts using ABCG2 (BXP-53) antibody from Santa Cruz Biotechnology. **A**: Brain capillary with a clearly visible monocyte; **B**, **C**: Logitudinal section through a brain capillary; **D**: Unspecific staining of constituents in the tumor brain area; **E**: Blood vessel; **F**: Transverse section through a murine brain capillary.

To exclude that the failure of Abcg2 detection is antibody-dependent, the same experiment was performed with a rabbit polyclonal anti-BCRP primary antibody from Biorbyt Ltd. (Cambridge, UK), suitable for the detection of ABCG2 of human, mouse and rat origin, in combination with a secondary HRP-conjugated donkey anti-rabbit AB from Santa Cruz.

Unfortunately, the detection of Abcg2 transporter expression in brain capillaries of nude NMRI (nu/nu) also failed. In accordance to the immunohistochemical staining performed with the AB from Santa Cruz, only unspecifically stained erythrocytes became visible (results not shown).

A.4   Summary and conclusions

Although the presence of Abcg2 at the BBB of CF-1 mice was demonstrated previously by Real-Time quantitative RT-PCR [Cisternino et al., 2004], the Abcg2 transporter was not detectable at the mouse BBB of nude NMRI (nu/nu) mice by immunohistochemistry using two different antibodies, suggesting that either Abcg2 is not expressed in the brain of nude mice or the used antibodies do not react with the murine ABCG2 ortholog.

A.5   References

Cisternino, S., Mercier, C., Bourasset, F., et al. Expression, up-regulation, and transport activity of the multidrug-resistance protein Abcg2 at the mouse blood-brain barrier. *Cancer Res.* **2004**, 64(9), 3296-3301.

Kühnle, M. Experimental therapy and detection of glioblastoma: investigation of nanoparticles, ABCG2 modulators and optical imaging of intracerebral xenografts. PhD thesis, University of Regensburg, Germany, 2010.

Müller, C. New approaches to the therapy of glioblastoma: investigations on RNA interference, kinesin Eg5 and ABCB1/ABCG2 inhibition. PhD thesis, University of Regensburg, Germany, 2007.

Ich erkläre hiermit an Eides statt, dass ich die vorliegende Arbeit ohne unzulässige Hilfe Dritter und ohne Benutzung anderer als der angegebenen Hilfsmittel angefertigt habe; die aus anderen Quellen direkt oder indirekt übernommenen Daten und Konzepte sind unter Angabe des Literaturzitats gekennzeichnet.

Weitere Personen waren an der inhaltlich-materiellen Herstellung der vorliegenden Arbeit nicht beteiligt. Insbesondere habe ich hierfür nicht die entgeltliche Hilfe eines Promotionsberaters oder anderer Personen in Anspruch genommen. Niemand hat von mir weder unmittelbar noch mittelbar geldwerte Leistungen für Arbeiten erhalten, die im Zusammenhang mit dem Inhalt der vorgelegten Dissertation stehen.

Die Arbeit wurde bisher weder im In- noch im Ausland in gleicher oder ähnlicher Form einer anderen Prüfungsbehörde vorgelegt.

Regensburg, ...
Stefanie Bauer